



RESEARCHS REGARDING THE QUALITY OF THE STEEL USED FOR MAKING ROLLING STOCK COMPONENTS

^{1,3} UNIVERSITY POLITEHNICA OF TIMISOARA, FACULTY OF ENGINEERING - HUNEDOARA

² ROMANIAN MINISTRY OF TRANSPORTS

ABSTRACT:

The work presents the manner of settlement of the specific problems of steel ingot cast in a smooth cylinder format and its use as semi-finished product, compatible with the manufacturing of monoblock wheels, under the quality conditions thereof imposed by the manufacturing regulations. By means of the proposed research and experiments we intend to get to know the specific characteristics of the ingot and the optimization thereof in order to satisfy the quality requirements imposed on the products (monoblock wheels). During the manufacturing of wheels the chemical composition and the gas content (hydrogen, nitrogen, oxygen) are to a large extent the decisive elements regarding the obtaining of the main characteristics of the wheels corroborated with the hot deformation of the cast semi-finished product and the adequate thermal treatment. The main physical and mechanical characteristics established for the wheels are: resistance to rupture; yield point; elastic limit; elongation; rupture resistance or energy upon shock bending; strength; K1C tenacity.

KEYWORDS:

steel, quality, monoblock wheel, rolling stock

1. INTRODUCTION

Various flow sheets are used, around the world, for the manufacturing of monoblock railroad wheels, which use as raw material semi-finished goods cut from ingots or blooms.

The casting process for the steel wheels is constantly improved, which ensures an increase of the quality and efficiency of their production.

In Romania the manufacturing of monoblock railroad wheels is 35 years old in the former Factory of Axles and Bogies of Balș, which is currently called SC Subansambluri de Material Rulant – SA.

For the manufacturing of monoblock railroad wheels we have the following main technological processes: the obtaining of the starting semi-finished product which includes – the manufacturing of the steel, the casting of the ingots, the potential rolling of the blooms, the division of the ingots or blooms; the forging of the wheels which includes: the heating of the bars resulting from the division of the ingots or blooms, the actual forging with its stages (stamping, rolling, forming – calibration, perforation of the central hole in the hub), the cooling of the forged wheels; the thermal treatment of the wheels; the mechanical processing of the wheels which is usually performed in most of the cases in two stages, namely before and after the thermal treatment of the wheels.

2. METHODOLOGY AND DISCUSSION

Starting from the obtaining of the starting semi-finished product, we can very well say that until the manufacturing of an almost ideal semi-finished product, obtained by computer assisted development in duplex or triplex system continuously cast conjugate aggregates, certain improvements can be obtained even with the current equipment: a chemical and structural

homogeneity of the ingots; advanced purity regarding the non-metallic inclusions as well as the gases; economic format of semi-finished product.

The following shortcomings must be noted regarding the manufacturing of the liquid steel and the casting of the ingots: the full development of the steel in electric-arc furnaces is uneconomical, and the quality of the steel is not fully satisfying, due to the chemical and thermal inhomogeneity, the high content of endogenous inclusions and gas.

For the performed researches, objectives were established which could harmonize the influences of certain ingot technological manufacturing – casting factors upon the behavior of the semi-finished obtained product in the process of plastic deformation and upon the physical – mechanical characteristics of the manufactured wheels.

For the manufacturing of the monoblock railroad wheels high quality carbon steels are used and only in few cases attempts have been made regarding the use of alloy construction steels.

During the manufacturing of wheels the chemical composition and the gas content (hydrogen, nitrogen, oxygen) are to a large extent the decisive elements regarding the obtaining of the main characteristics of the wheels corroborated with the hot deformation of the cast semi-finished product and the adequate thermal treatment. The main physical and mechanical characteristics established for the wheels are: resistance to rupture; yield point; elastic limit; elongation; rupture resistance or energy upon shock bending; strength; K1C tenacity.

Experimental data obtained on the influence of chemical composition on the characteristics of resistance were processed in MATLAB computer program results are presented in graphical and analytical.

Regression equations are hyper surfaces:

$$R_{p02} = -2182,1605 \cdot C^2 + 1683,4169 \cdot Mn^2 - 810861,048 \cdot P^2 - 3686,2945 \cdot C \cdot Mn - 43612,0459 \cdot Mn \cdot P + 182628,5699 \cdot P \cdot C + 2189,3056 \cdot C + 426,6009 \cdot Mn - 47302,4451 \cdot P - 346,8306; \quad R^2 = 0,8753 \quad (1)$$

$$R_m = -1058,2742 \cdot C^2 + 517,8169 \cdot Mn^2 - 212838,9859 \cdot P^2 - 851,711 \cdot C \cdot Mn - 15326,9006 \cdot Mn \cdot P + 54597,7285 \cdot P \cdot C + 985,0177 \cdot C - 17,1633 \cdot Mn - 13266,2739 \cdot P - 89,5498; \quad R^2 = 0,8307 \quad (2)$$

Because these hyper surfaces can be represented in space with four dimensions, was used to replace, in succession, independent variables with each of its average value. Surface regression obtained and the contour lines are shown in Fig.1-6.

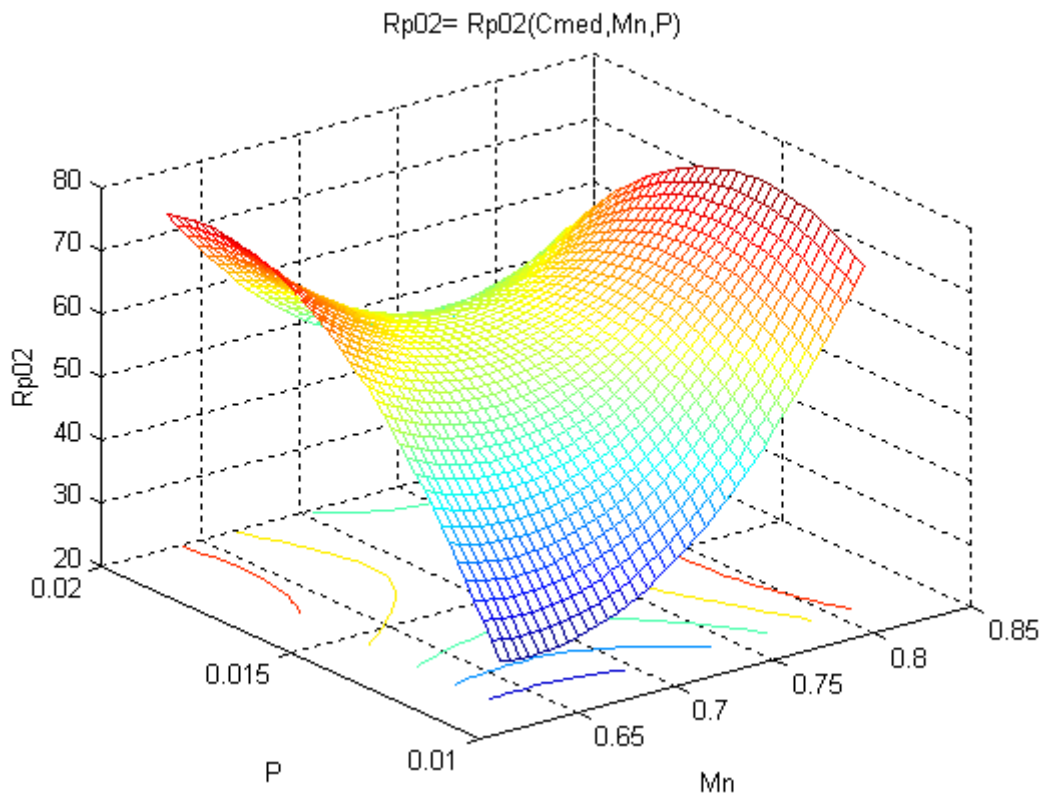


Fig.1. $R_{p0,2} = f(C_{med}, Mn, P)$

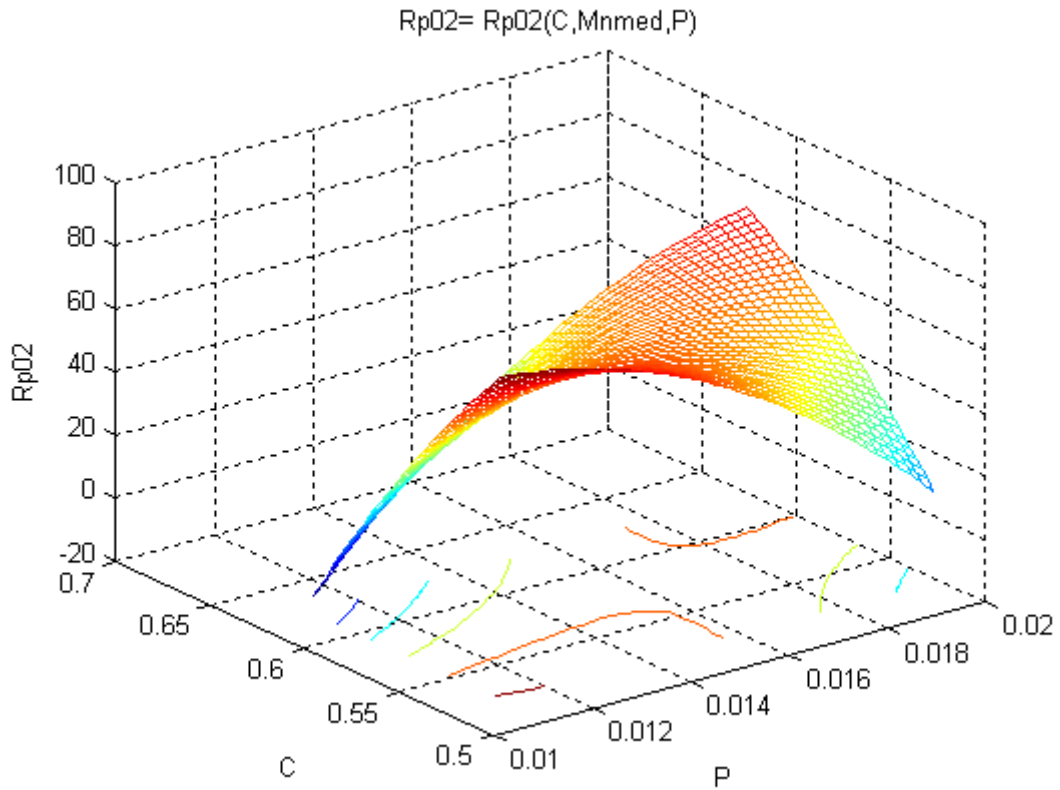


Fig.2. $R_{p0,2} = f(C, Mn_{med}, P)$

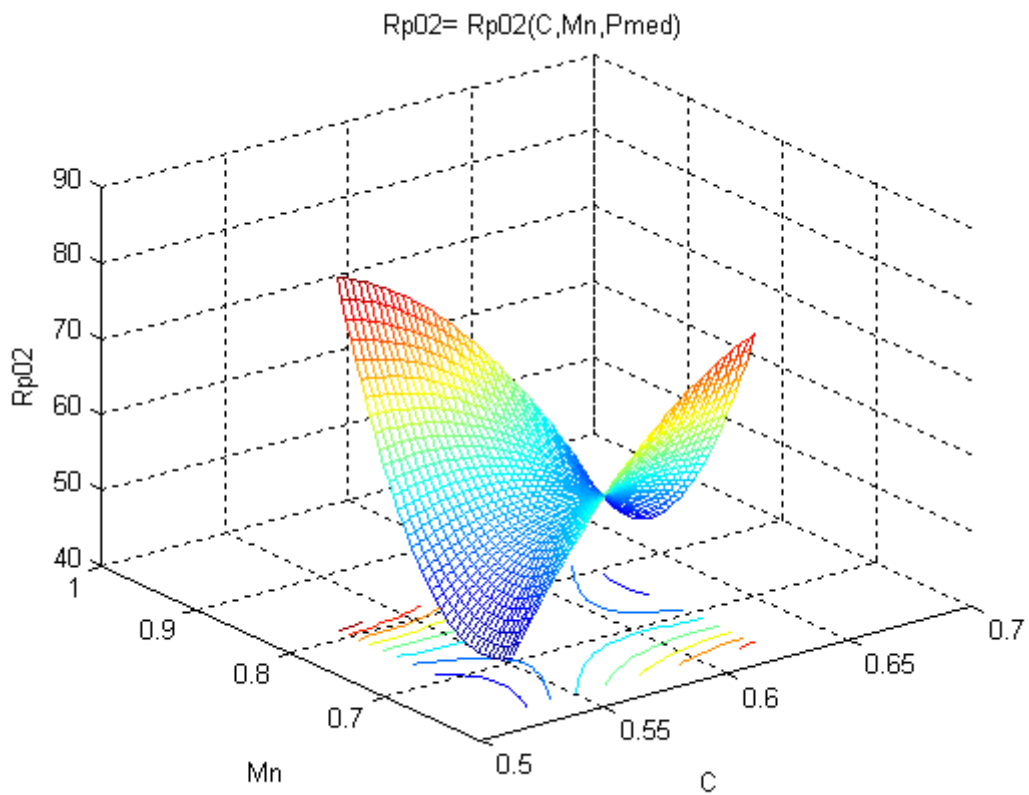


Fig.3. $R_{p0,2} = f(C, Mn, P_{med})$

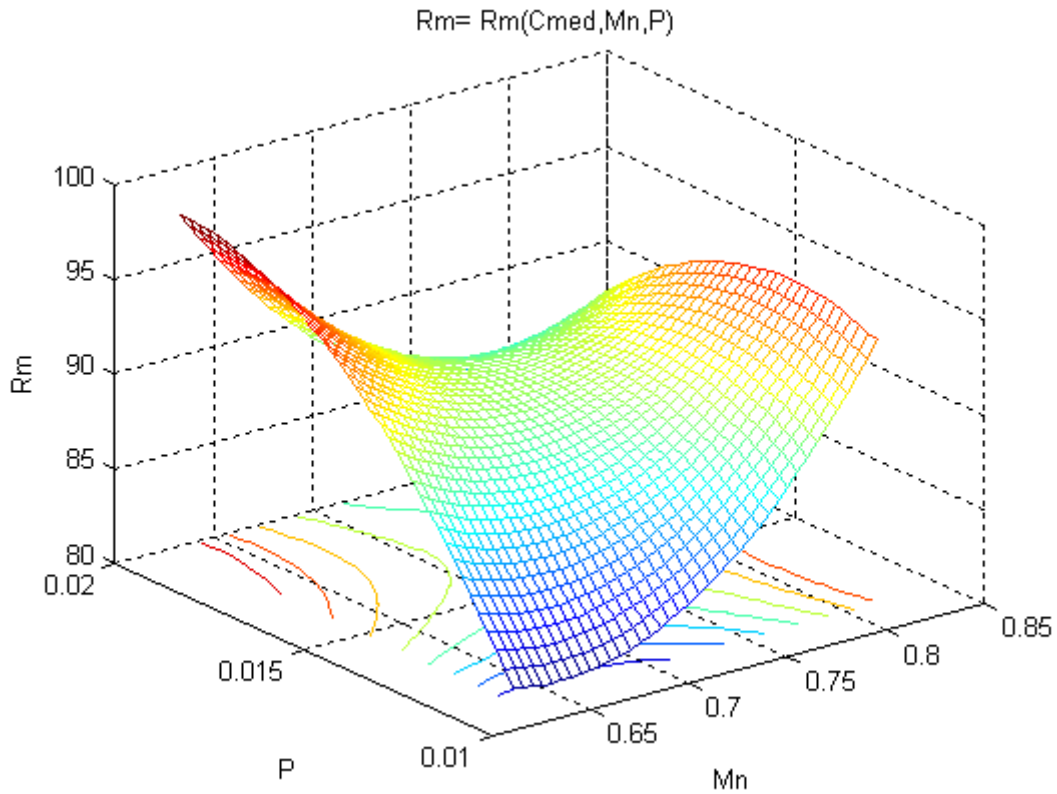


Fig.4. $R_m = f(C_{med}, Mn, P)$

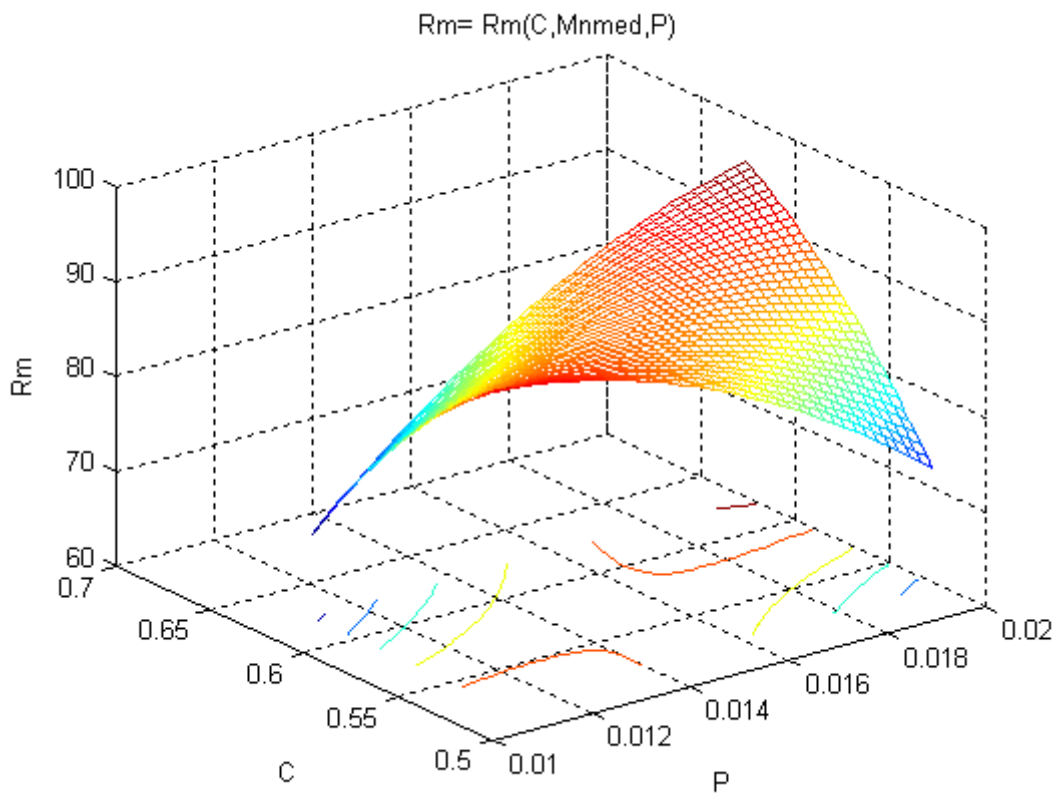


Fig.5. $R_m = f(C, Mn_{med}, P)$

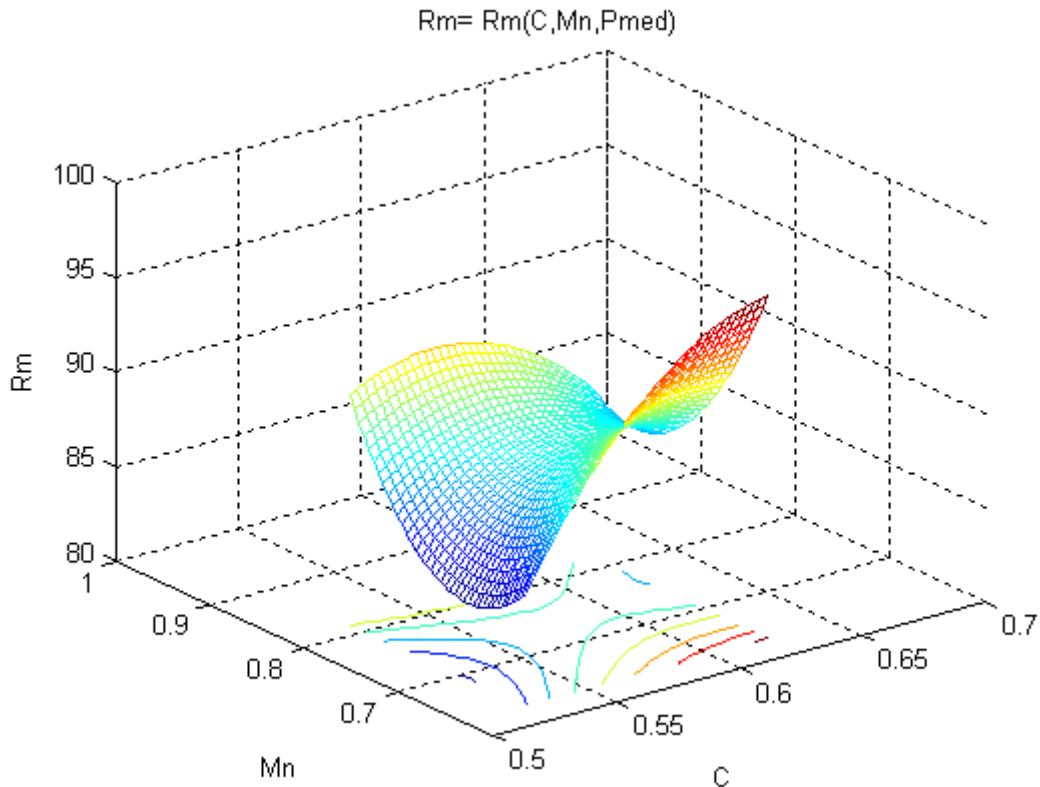


Fig.6. $R_m = f(C, Mn, P_{med})$

Surface regression equations for the mechanical strength are:

$$R_{p02}C_{med} = 1683,4169 \cdot Mn^2 - 810861,048 \cdot P^2 - 43612,0459 \cdot Mn \cdot P - 1698,0452 \cdot Mn + 57958,0215 \cdot P + 190,1026 \quad (3)$$

$$R_{p02}Mn_{med} = - 810861,048 \cdot P^2 - 2182,1605 \cdot C^2 + 182628,5699 \cdot P \cdot C - 79040,1203 \cdot P - 493,3114 \cdot C + 855,1341 \quad (4)$$

$$R_{p02}P_{med} = - 2182,1605 \cdot C^2 + 1683,4169 \cdot Mn^2 - 3686,2945 \cdot C \cdot Mn + 5177,7731 \cdot C - 287,0508 \cdot Mn - 1337,9938 \quad (5)$$

$$R_mC_{med} = 517,8169 \cdot Mn^2 - 212838,9859 \cdot P^2 - 15326,9006 \cdot Mn \cdot P - 508,0585 \cdot Mn + 18201,8715 \cdot P + 126,6252 \quad (6)$$

$$R_mMn_{med} = - 212838,9859 \cdot P^2 - 1058,2742 \cdot C^2 + 54597,7285 \cdot P \cdot C - 24420,0774 \cdot P + 365,2044 \cdot C + 172,1891 \quad (7)$$

$$R_mP_{med} = - 1058,2742 \cdot C^2 + 517,8169 \cdot Mn^2 - 851,711 \cdot C \cdot Mn + 1878,4351 \cdot C - 267,9671 \cdot Mn - 363,6258 \quad (8)$$

3. CONCLUSIONS

From the analysis of the data processed in a graphic and analytical form a series of conclusions can be drawn:

- ❖ the increase of the resistance to traction and of the yield point with the increase of the carbon content is due on the one hand to the increase of the pearlite ratio in the structure, constituent with superior values for these characteristics, and on the other hand due to the favorable action of the carbon upon the deoxidation and desulphuration process;
- ❖ manganese as element which is present in almost all steels dissolves in iron and forms solid solutions increasing their resistance. On the other hand, the manganese from the steel also has

a deoxidation and desulphuration role, which can be noticed in the improved resistance characteristics;

- ❖ regarding the silicon, it dissolves in ferrite increasing its resistance and toughness. At the same time, the silicon is also a deoxidizing agent with a great deoxidation power having the capacity to calm the steel completely and as a consequence decreases progressively the oxygen content of the steel, element which has a negative influence upon quality;
- ❖ in the analyzed steels phosphorous is present in very small concentrations and therefore it causes no negative effects, on the contrary when dissolved in iron it leads to the formation of mixed crystals which in their turn determine an increase of the toughness of the steel. The existing phosphorous content of the analyzed steel does not create the risk of the formation of a ternary eutectic $Fe_3P - Fe - C$ with a melting temperature of $953^{\circ}C$ which would cause the cracking of the ingot upon its processing due to the plastic deformation;
- ❖ regarding the sulphur content a decrease of the values for resistance to concentrations of more than 0.018% was found. Regarding the range of 0.011-0.018% we can say that its negative influence is insignificant. We believe that for values between 0.018 and 0.022% an inhomogeneity may exist regarding the distribution of the sulphur in the structure of the ingot, which may influence its characteristics;

Further research shall be performed in order to establish certain complex dependence relations, namely the data will be processed with the Matlab software by analyzing the influence of three independent factors (C, Mn, Si) upon the independent parameters (tensile resistance, yield point etc) and based on the obtained results we will be able to establish an optimal chemical composition. Moreover, we will also have in view the establishing of the dependence relations for other characteristics: toughness, resilience, elongation, as well as the gases content of the steel (a very important aspect for the steels destined for the manufacturing of rolling stock components).

REFERENCES

- [1.] BUTNARU, I., GEANTĂ, V., Tehnologii speciale de elaborare și rafinare a oțelurilor, Bucharest Polytechnic University Lithography, 1993.
- [2.] VACU, S., ș.a., Elaborarea oțelurilor aliate, vol.I and vol II, Tehnică Publishing House, Bucharest, 1980.
- [3.] NICA, GHE., SOCALICI, A., ARDELEAN, E., HEDUȚ, T., Tehnologii pentru îmbunătățirea calității oțelului, Mirton Publishing House, Timisoara, 2003.





RESEARCH REGARDING THE PHYSICAL AND CHEMICAL CHARACTERISTICS OF PRE-REDUCED IRON ORES AND THE ANALYSIS OF THE POSSIBILITIES OF THEIR USE IN THE IRON AND STEEL ELABORATING PROCESS

^{1, 2, 3} UNIVERSITY "POLITEHNICA" OF BUCHAREST, ROMANIA

ABSTRACT:

Taking into consideration the complexity of the traditional iron and steel elaborating methods that demand the existence of ore preparation plants, cookery, etc. moreover the deficit of coking coals and iron scrap it is necessary to search new possibilities of modifying the existent technologies or replacing them by new methods. One option regarding this way represents the use of sponge iron obtained by direct reduction of iron ores or prepared into the iron and steel elaborating process.

Considering the high materials and energy consumption and environment pollution in the traditional iron and steel elaborating methods our paper's aim is to analyze the opportunity and the possibilities of obtaining the iron and steel by non-conventional technologies.

Our paper presents the results obtained from direct reducing of iron ores and our conclusions resulted from statistic analysis of obtained data by correlating the initial characteristics of the ores and qualitative characteristics of the pre-reduced product.

KEYWORDS:

pre-reduced iron ores, iron sponge

1. INTRODUCTION

Taking into consideration the complexity of the traditional iron and steel elaborating methods that demand the existence of ore preparation plants, cookery, etc. moreover the deficit of coking coals and iron scrap it is necessary to search new possibilities of modifying the existent technologies or replacing them by new methods. One option this way represents the use of sponge iron obtained by direct reduction of iron ores or prepared into the iron and steel elaborating process.

Considering the high materials and energy consumption and environment pollution in the traditional iron and steel elaborating methods our paper's aim is to analyse the opportunity and the possibilities of obtaining the iron and steel by non-conventional technologies.

Our paper presents the results obtained from direct reducing of iron ores and our conclusions result from statistic analysis of obtained data by correlating the initial characteristics of the ores and qualitative characteristics of the pre-reduced product.

2. OBTAINING PRE-REDUCED MATERIALS AND THEIR PHYSICAL AND CHEMICAL CHARACTERISTICS RESEARCH

We conducted the research in the laboratories of University "Politehnica" of Bucharest, the Ferrous Department. We established the experiments conditions starting from the initial granule size and composition of the ores, agglomerates and pellets. For the pre-reduced product, we established the reducing degree, the softening and melting temperature, the mechanical resistance and we found the correlation between the initial physical and chemical characteristics of the ores and the final characteristics of the pre-reduced material.

The ore's reduction is made in a reactor pipe with 140 mm diameter and 1000 mm length, made from stainless steel, which has in its inferior half chamotte spheres in order to heat the reducing gas. The ore sample is introduced into a net wire cylinder with the capacity of 1-3 kg of iron ore. The reactor pipe's heating is realized into a furnace having vertical bars 95) that can assure temperatures of about 80-100°C (the transformer's power is 25 kVA). The reducing gas (H₂-99,5%) flows from the cylinder through the purifying vessels filled with mineral cotton, H₂SO₄ and CaCl₂. The hydrogen flow is measured and registered.

The determination of the removed oxygen quantity is made by continuous weighting of the reactor cylinder with the scales, and the temperature is measured with a platinum-platinum-rhodium couple. The methodology of the experiments is: the sample weigh: 1 kg, the sample's granule size, varies between 5 and 30 mm, temperature: 800-900°C, the process period: 45 min, the specific H₂ flow: 0,7 l/min. g O₂ in the sample.

The pre-reduced material is mainly characterized by the following parameters:

- the reducing degree – represents the percentage of oxygen from the iron oxides being removed in reducing process:

$$RD = \frac{O_{2\text{removed}}}{O_{2\text{initial}}} \cdot 100[\%], \quad (1)$$

- the reducing velocity – represents the medium velocity of the oxygen removal from the iron oxides:

$$RV = \frac{O_{2\text{removed}}}{\text{proc. period}} [\% / \text{min.}], \quad (2)$$

The pre-reduced sample (0, 5 kg and granule size over 5 mm) is maintained inside for 3 minutes (90 rotations). The crushed material is then screened on 5 mm and 1 mm screens, establishing the following parameters:

- the crushing index (C) – represents the 1-5 mm fraction (in percents);
 - the dusting index (DI) – represents the 0-1 mm fraction (in percents);
 - the degradation index (D) – represents the ratio between the crushing index for the material after (C_{a.r.}) and before (C_{b.r.}) reduction : D = C_{a.r.}/ C_{b.r.}

In Table 1 we present the experiment conditions and the results obtained at the pre-reduction of 10 sorts of iron ores previously agglomerated.

Table 1. Ore reduction experiments

Sampl. no.	Ore characteristics				Experiment conditions			Reduction characteristics		Resistance in hollow roll	
	Fe (%)	FeO (%)	CaO/SiO ₂	Granule Size (mm)	Time (min)	H ₂ flow (l H ₂ /min)	Temp. (° C)	RD (%)	RV (%O /min)	Re duced	Not re duced
1	51.75	8.4	1.26	5-10	45	0.0690	825	49.42	1.10	61	82
2	49.82	8.85	1.41	5-10	45	0.0698	810	63.82	1.42	53	65
3	51.79	13.18	1.20	5-10	45	0.0713	840	43.41	1.96	69	94
4	53.09	7.49	1.32	10-20	45	0.0699	835	57.02	1.28	56	76
5	52.48	12.74	1.23	10-20	45	0.0701	840	45.07	1.00	71	91
6	53.59	10.54	1.71	10-20	45	0.0698	825	64.23	1.43	46	88
7	53.01	10.37	1.02	5-20	45	0.0700	835	39.41	0.83	79	94
8	54.68	8.30	1.12	5-20	45	0.0700	840	42.20	0.94	73	92
9	53.27	7.77	1.30	10-30	45	0.0698	840	59.18	1.32	66	80
10	43.50	8.60	1.80	10-30	45	0.0700	835	62.19	1.38	51	93
11	48.6	10.18	1.20	5-10	46	0.072	870	50.74	1.10	78	88
12	48.7	9.32	1.35	5-10	46	0.067	860	40.20	0.87	76	88
13	51.5	10.00	1.31	5-10	46	0.064	830	50.05	1.09	66	83.8
14	51.98	8.03	1.35	5-10	45	0.070	834	59.40	1.32	79.8	86.2
15	50.47	10.32	1.35	5-10	46	0.072	818	48.82	1.06	68	85.7
16	48.6	10.18	1.20	10-20	46	0.073	855	63.45	1.38	66	90
17	48.7	9.30	1.35	10-20	46	0.068	878	65.32	1.41	68	87
18	51.5	10.00	1.31	10-20	46	0.067	830	54.81	1.19	50	80
19	51.98	8.03	1.35	10-20	45	0.071	838	63.14	1.40	64	75.5
20	50.47	10.32	1.35	10-20	46	0.072	818	48.82	1.06	68	85.7
21	48.6	10.18	1.20	10-20	46	0.072	878	56.1	1.21	70	72
22	48.7	9.32	1.35	10-30	46	0.069	885	52.74	1.15	69	86
23	51.5	10.00	1.31	10-30	46	0.069	825	57.20	1.24	42	59.6
24	51.98	8.03	1.35	10-30	45	0.070	843	57.05	1.27	69	78.7
25	48.6	10.18	1.20	10-30	46	0.072	870	48.74	1.08	73	87
26	48.7	9.32	1.35	unsorted	46	0.072	888	38.74	0.84	71	87
27	51.98	8.03	1.35	unsorted	45	0.071	841	57.53	1.27	69	78
28	50.47	10.32	1.35	unsorted	46	0.069	815	56.14	1.22	44	73.9

Analyzing the data from Table 1 we can conclude:

- generally, an optimal reduction degree can be obtained from granule size of about 15 – 25 mm;
- the easiest reducible materials are the ferrous ones with the basicity.
- $B = \text{CaO}/\text{SiO}_2$ between 1.35 and 1.7; a medium reducibility is reached by the samples with $B = 1.2 - 1.35$ and the samples with $B \leq 1.2$ being more difficult to reduce;

The tests we made shown that the higher is the reduction degree the higher is the crushing degree. Because pre-reduced materials obtained by reducing the iron ores (crude or prepared) are used in the blast furnace or the electric arc furnace, replacing the iron scrap, it is very important to know the behavior of these materials during the heating – the correlation between the reducing degree and their melting and softening temperatures. That is why we tested the softening of these materials. The plant we used to run these tests is presented in Figure 1.

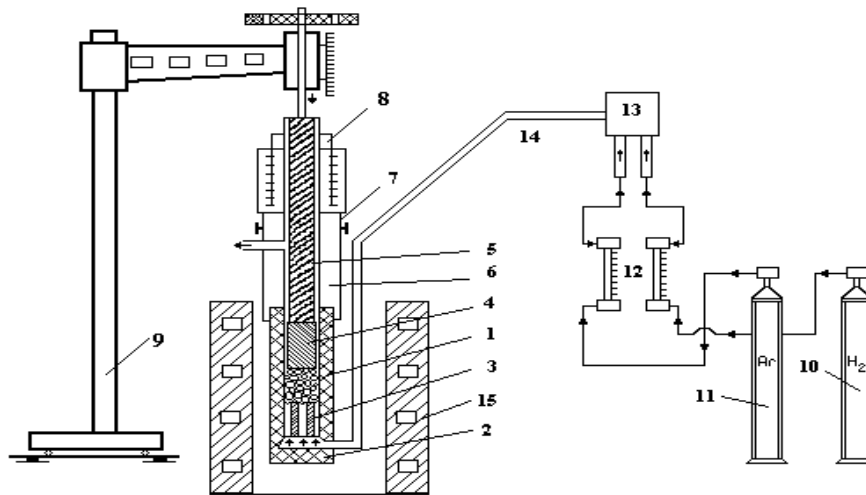


Figure 1. The experiment plant

1- graphite crucible; 2- gas distributor; 3- intermediary plate; 4 – piston; 5 – rod; 6 – graphite support; 7 – seal device; 8 – piston support; 9 – fixed support; 10 – H₂ cylinder; 11 – reducing gas cylinder; 12 – measuring device; 13 – gas mixer; 14 – gas pipe; 15 – induction electric furnace

Table 2. Data on the melting and softening characteristics of the agglomerates used in Romania

Sampl. no.	Chemical composition							Reduction degree (%)	Characteristics temperatures		
	FeO (%)	SiO ₂ (%)	CaO (%)	MgO (%)	Al ₂ O ₃ (%)	Fe (%)	B		T _{cz} (°C)	T _{mch} (°C)	ΔT (°C)
1	1.26	13.72	25.53	3.28	4.11	39.53	1.86	58.44	1010	1230	220
2	1.53	13.9	24.74	1.86	1.40	42.03	1.78	62.50	765	1240	475
3	3.11	13.75	24.71	1.29	2.16	41.18	1.79	70.00	1080	1320	240
4	6.59	10.28	26.16	3.72	0.28	43.65	2.54	68.00	1010	1330	220
5	8.52	10.60	24.73	3.40	1.76	43.13	2.33	69.80	1000	1330	330
6	7.40	11.05	23.56	5.45	1.96	43.18	2.13	70.35	980	1375	395
7	4.51	12.96	24.63	0.72	1.56	47.49	1.90	69.80	980	1210	230
8	10.56	12.64	24.11	2.80	3.06	44.26	1.90	53.60	1025	1240	215
9	3.64	11.10	24.37	4.74	1.89	44.94	2.10	54.64	1100	1270	170
10	3.94	10.08	24.72	2.49	0.21	44.98	2.45	58.50	1100	1250	150
11	8.60	10.38	20.35	1.57	0.31	46.81	1.95	56.51	1020	1240	220
12	8.20	9.52	17.12	2.75	3.49	48.77	1.79	50.57	1100	1360	260
13	19.90	7.00	14.43	3.00	1.90	51.79	2.06	60.84	1190	1365	175
14	16.24	8.08	16.25	2.15	3.64	52.36	2.01	50.53	1180	1295	115
15	19.93	7.93	16.00	0.87	4.72	49.84	2.01	58.00	960	1090	130
16	25.93	6.43	11.60	2.96	0.86	58.51	1.78	78.80	1170	1380	210
17	8.20	9.52	17.18	2.75	3.49	48.77	1.79	68.92	1155	1330	175
18	8.26	7.70	11.86	2.25	6.62	53.72	1.54	75.77	1160	1420	260

The experiment results are presented in Table 2. The experiments consisted of:

- ❖ from the crushed and screened material, we took a 3-5 mm fraction in samples of 240-310g;
- ❖ we heated the sample with 50-60°/minute;
- ❖ starting at 750°C we blew argon with 6.5-7.5 l/min., and at 900°C we blew hydrogen with 8 l/min. For 8 minutes, so we could reach reducing degrees of about 50-78%;
- ❖ we measured the temperatures every 3 min. and since the piston moved every 2 minutes;
- ❖ we determined the softening temperature when the piston moved firstly and the melting temperature when the piston movement as half the sample's height.

3. ECONOMICAL AND TECHNOLOGICAL CONSIDERATIONS ON THE USE OF PRE-REDUCED PRODUCTS IN IRON AND STEEL ELABORATING PROCESS

The pre-reduced materials obtained from solid reduction of iron ores (crude or prepared) can be used as raw material in the blast furnace charge with important economic effects.

Economies that can be obtained by using 1000 kg pre-reduced ore vary between 1 and 34 Euros for a pre-reducing degree of about 70%.

Pre-reducing the materials before using them in the furnace is a method that permits also the amelioration of the structure of the used combustibles (coke, etc.).

The economy obtained at the blast furnace, even in conditions of high energy consumption, covers completely the expenses from the pre-reducing process.

To study the possibilities of using the pre-reduced materials in electric arc furnace as iron sponge with different metallization degrees we made experiments on a 500 kg furnace in which the iron sponge was used 33, 55, and 79,100% of the charge.

We found out that using of iron sponge leads to a reduction of about 20% of the elaborating period and considerable diminish of manufacturing expenses.

4. CONCLUSIONS

Because they are very important we will mention these conclusions:

- ❖ the agglomerate's granule size doesn't have a notable influence on the "cohesive zone", that's why the recommended granule size (15-20 mm) which can assure a good permeability, can also assure the forming of an appropriate "cohesive zone";
- ❖ the chemical composition of the agglomerate influences the position and especially the width of "cohesive zone".

So, the rise of the MgO contents determines the rise of melting and softening temperatures and a lower position of the "cohesive zone" (i.e. positive influence). Also the rise of the MgO contents determines a higher difference between the melting and softening temperatures and rise the width of the "cohesive zone" (i.e. negative influence).

The necessary value for this parameter can be established following the influence of B on the "cohesive zone" and on charge's permeability in the granular zone. An optional value for B has to assure a goon mechanical resistance and an appropriate reducibility of the pre-reduced agglomerate.

From the experiments conducted on this last subject we conclude that the optimal value for B is 1.5 – 1.6. This value also assures a favorable influence on the "cohesive zone" that permits us to recommend the use of agglomerate with $B = 1.5 - 1.6$ in the blast furnace charge.

The laboratory research conducted on a large number of samples leaded us to the conclusion that the reduction degree of the iron oxides has the most important influence on the softening and melting of the agglomerate.

This influence due to the forming in the agglomerate granules of the metallic iron structures that assures a high permeability of the agglomerate layer in plastic state.

We can observe that the melting temperatures rise for a reduction degree over 58%. The same influence but less important manifests on the softening temperature.

REFERENCES

- [1.] N. CONSTANTIN, "Intensificarea proceselor din furnale prin perfectionarea circulatiei gazelor in vederea cresterii productivitatii si a economiei de coacs metalurgic si energie", Doctor Thesis, Bucharest, 1994.
- [2.] N. CONSTANTIN, "Ingineria producerii fontei in furnal", Ed. PRINTECH ", Bucharest, 2002.
- [3.] N. CONSTANTIN, C. PREDESCU, and M. JURA, "Cercetari pe model matematic asupra zonei coezive la furnale" International conference -Hunedoara 12-13 oct. 1995, pag. 18-26.
- [4.] N. CONSTANTIN, C. PREDESCU, and M. JURA, "Informatising management of blast furnace processes."București - International Symposium - "Traditions and perspectives in Romanian school of metallurgy." 25 - 26 oct. 1996, pag. 328-336.





¹. Violeta OANCEA, ². Nicolae CONSTANTIN, ³. Cristian DOBRESCU

RESEARCH ON THE POSSIBILITIES OF IMPROVING THE PRODUCTIN OF CAST IRON IN THE FIRST MERGER BY IMPROVING FLOW GAS PHASE IN THE BLAST FURNACE

^{1, 2, 3}. UNIVERSITY "POLITEHNICA" OF BUCHAREST, ROMANIA

ABSTRACT:

Because the cast iron-making blast furnace is a complex process of mass and energy transfer between solid and gas phase with reduced character, improving operating parameters can be achieved by improving gas flow in the blast furnace.

Obtaining an optimal permeability of the column of materials allow optimum circulation of a gaseous phase, using its entire reducing potential.

It is thus possible to increase utilization efficiency of useful volume thus increasing productivity.

This paper aims to study the permeability of different mixtures which can form the blast furnace load and propose optimal ratio between their weights.

KEYWORDS:

blast furnace, optimal permeability, mass and energy transfer

1. INTRODUCTION

Many research works as well as the practical operation of the blast furnaces have shown close correlation between the regime of operation of furnace and gas flow through solid materials in the tank column.

Thus the conclusion reached that gas can flow through the furnace in unit time through unit area of section, substantially influence the blast furnace productivity.

The blast furnace productivity decreases proportionally with increasing unevenness degree in the flow of gas, also an increase in specific consumption of coke due to improper use the reduction character of gaseous phase.

So it can't achieve an economic function of blast furnace without achieving optimal distribution of gas tank and consequently good contact of phases which are entering in reaction physics-chemical processes occurring in the blast furnace.

This favorable distribution of gases can be achieved by measures taken at the charge part of the blast furnace (the unit load size, the load schedule, the load level).

2. METHODOLOGY

In a column of infinite load as expanse volumes it can obtain a uniform distribution of the gases regardless of the size filling bodies particles. Instead in a limited load column as dimensions, the gases flowing depends on the ratio between (d) diameter of granules that are forming the load and (D) diameter of column, at high values of ratio d / D ascertaining a powerful peripheral gas circulation due to the higher value of the voids volume near the column walls.

But in a blast furnace, the flow of gas is influenced by the movement of cargo particles which facilitates the appearance of free spaces between these.

The tendency to form free spaces is larger to loads composed by large irregularly shaped pieces. From geometrical a reason at the spherical particles is accomplished the best possibility of charge particles movement.

In terms of the reduction process, small pieces behave better. Therefore it is seen mostly a better performance of the blast furnace when the pieces of agglomerate ores are smaller or when using pellets.

This leads on the one hand to a better performance of the blast furnace due to the gases uniform distribution on section by free spaces uniformly distributed without preferred corridors, but also may lead to a higher pressure loss to the equal flow of gases which are crossing the blast furnace because the pressure loss increases with decreasing of the particles diameter

The pressure loss per unit length depends on the gas flow speeds, the physical characteristics of these, the shape, the size and the settlement method of the filling bodies.

For dimensionless representation of the pressure loss it is used the relation between the dimensionless resistance coefficient ψ and Reynolds number: $\psi = f(Re)$

These two indices have been defined by M. Brauer as follows:

$$\Psi = \frac{\varepsilon^3}{1 - \varepsilon} \cdot \frac{d}{\rho w^2} \cdot \frac{\Delta p}{H}, \quad \text{and} \quad Re = \frac{1}{1 - \varepsilon} \cdot \frac{w \cdot d}{\nu}$$

where: ε - the goals factor in the column load; d - the diameter of filling bodies [m]; ρ - the gases density that flows through the load [kg/m³]; ν - the kinematic viscosity of gases [m²/s]; w - the speed of gases flow in the empty column [m/s]; H - the height column of load [m];

The loss of pressure has already been measured in a variety of materials. Most researches have been limited to the monogranulare materials and only few bigranulare materials such as the type of materials introduced into the blast furnace.

3. ANALYSES/ RESULTS

This paper aims to present the results and conclusions drawn for experiments with components materials of blast furnaces load from Romania.

The experiments dealt with determining the permeability of columns consisting of coke material, agglomerated, pellets but for comparison term and artificial load consisting by glass beads with diameter close to the pellets.

It has been followed the possibility of obtaining an optimum permeability for a column with similar load to that of cargo tank blast furnace, with the ultimate goal of increasing the intensity of operation by improving the gases flow through the blast furnace tank.

Experiments were conducted in the laboratory of Metallurgy of Cast Iron, Siderurgy Department from University "Politehnica" of Bucharest. The experimental installation is shown schematically in Figure 1.

The installation comprises a cylindrical container (1) with the height of 1.35 m and 0.35 m in diameter, provided at the top with a state gas valve for measuring the gas pressure after it passes through the granular load from the column (2). The cylinder is closed with a conical cap fitted with a gas discharge pipe (3). In the lower area there is a filler cap for draining of installation (4). Under the filling area is another one of pressure equalization (5). It consists of a cylindrical tube provided at both ends with flares of extending and tightens. Here there is a flare connected to measure the gases pressure in the entry of column load (6). The cylinder is fed with gas (air) through a pipe fitted with a valve for regulating the gas flow (7). The flow measurement is made with a measurement diaphragm (8). Gas supply (air) is made through a motor-blower group.

The experimental dates and a series of mathematical results of statistical processing are presented in Tables 1 and 2.

In the table 2 there are presented the linear correlations between pressure loss $y = \Delta p$ in [mmH₂O] and flow of air blown into the column $x = Q_a$ in [m³/h] of the form $y = f(x)$. For all 19th experiments were drawn simple linear correlations which can be accepted considering the correlation of coefficient values y_{xy} higher than 0.9. Grouping favorable studied cases and drawing lines in the same rectangular coordinates some important conclusions are obtained.

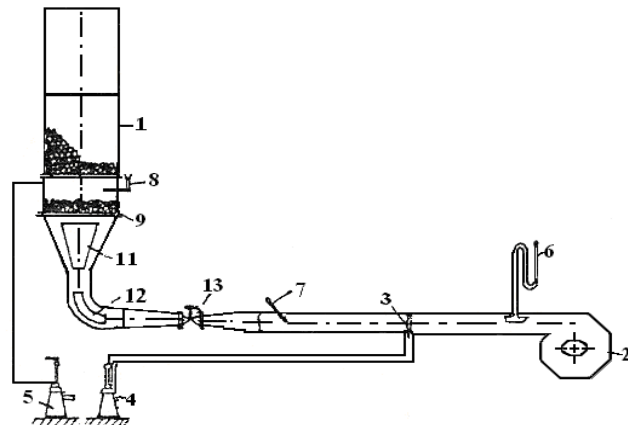


Figure 1. The experimental installation

Table 1.

Exp No	Load	Type of load	Average diameter[m]	Equivalent diameter[m]	Goals coefficient(ϵ)
1	1/1 balls	layer	0.019	0.019	0.371
2	1/1 pellets	layer	0.012	0.012	0.387
3	1/1 agglomerates	layer	0.03	0.03	0.417
4	1/1 coke	layer	0.04	0.04	0.478
5	1/3 balls+2/3 aggl.	mixture	-	0.022	0.380
6	1/3 balls+2/3 aggl.	layer	0.19/0.03	0.022	0.371/0.417
7	2/3 balls+1/3 aggl.	mixture	-	0.0179	0.378
8	2/3 balls+1/3 aggl.	layer	0.19/0.03	0.0179	0.371/0.417
9	1/3 pellets+2/3 balls	mixture	-	0.0158	0.35
10	1/3 pellets+2/3 balls	layer	0.012/0.019	0.0158	0.387/0.371
11	2/3 pellets+1/3 balls	mixture	-	0.0168	0.27
12	2/3 pellets+1/3 balls	layer	0.012/0.019	0.0168	0.387/0.371
13	1/3 balls+2/3 coke	mixture	-	0.029	0.40
14	1/3 balls+2/3 coke	layer	0.019/0.04	0.029	0.371/0.478
15	2/3 balls+1/3 coke	mixture	-	0.023	0.39
16	1/3 coke+2/3 aggl.	mixture	-	0.0186	0.39
17	1/3 coke+2/3 aggl.	layer	0.045/0.016	0.0186	0.478/0.395
18	1/3 coke+2/3 aggl.	mixture	-	0.0248	0.40
19	1/3 coke+2/3 aggl.	layer	0.04/0.021	0.0248	0.465/0.405

The dependences $\Delta p = f(Q_a)$, $y = f(x)$

Table 2.

Exp No	Eq $\Delta p=f(Q_a)$	Y_{xy}	The slope of line
1	$Y=1.542X-74.10$	0.970	57.03
2	$Y=1.570x-39.15$	0.976	57.50
3	$Y=0.887x-39.15$	0.966	41.57
4	$Y=1.208x-64.21$	0.969	50.38
5	$Y=1.134x-56.26$	0.960	48.59
6	$Y=1.035x-52.95$	0.965	45.98
7	$Y=1.614x-73.78$	0.978	58.12
8	$Y=1.294x-55.42$	0.981	52.30
9	$Y=2.188x-80.46$	0.975	65.43
10	$Y=2.474x-116.84$	0.965	67.99
11	$Y=2.577x-121.48$	0.968	68.79
12	$Y=2.010x-85.52$	0.969	63.54
13	$Y=1.442x-75.012$	0.969	55.26
14	$Y=1.396x-79.75$	0.966	54.38
15	$Y=1.596x-75.59$	0.969	57.93
16	$Y=1.151x-53.03$	0.970	41.73
17	$Y=0.892x-40.12$	0.977	49.01
18	$Y=1.027x-50.449$	0.951	45.76
19	$Y=0.789x-36.97$	0.945	38.27

4. CONCLUSIONS

Among the conclusions of the conducted research can be mentioned:

- ❖ The loads consisting of two granules size with small diameter d_k and large diameter d_g can represent the conditions from modern blast furnaces in which the load basically consists of agglomerates and coke, well grinded and loaded in granulate limits prescribed. In the case of loads formed by granules with two dimensions, the permeability varies according to how the load is made of in distinct layers or homogenous mixtures.
- ❖ confirming the experiments of Fomas, the coefficient of goals mixture (ϵ_m) passes through a minimum at about 28-30% large granules in mixture, the values of ϵ_m decrease in the same time with the diameters ratio d_k/d_g ;
- ❖ it is observed that regardless of the blowing air speed in the column, the pressure loss is greater at homogeneous mixtures than at loads in separate layers;
- ❖ the value of medium goals coefficient (ϵ_m) decreases proportionally with the size difference between the diameters of components (this value is best shown by these experiments (16 and 18));
- ❖ the coefficient values of goals for monogranular loads are different by the type of material. It can be noticed that at the same mixture of two different diameters the goals coefficient is not the same for different proportion participation of those two types of granules, (exp 9, 11).

- ❖ looking at the correlations $y = f(x)$ that means $\Delta p = f(Q)$, presented in Table 2, it can be observed the increase of Δp with Q_a for all experimental situations;
- ❖ for the mixtures made of the same type of granules the increasing of Δp with Q_a is more emphasized by the time the increasing of small granules proportion in the load (which is visible following the lines slope α in Table 2;
- ❖ for the same type of bigranulare loads the increase of Δp with Q_a is more emphasized for mixtures than for loads in separate layers;
- ❖ for the monogranulare loads the increase of Δp with Q_a is faster for loads with a smaller coefficient of goals.

As the gas flow through the furnace load, uniform and without fault in the descending column of material, requires minimal pressure loss, indicates that the upper area of the furnace (the granular area) there are advantageous to use the loads of granules of equal size between them, and the charging to be done in layers, each layer comprising granules of the same diameter.

From the technological point of view regarding the behavior of materials from the blast furnace load and in the other areas of the blast furnace it is necessary the existence of a certain ratio different from the value 1 between areas of agglomerate granulation and of the coke, the value of this ratio being 0.35 to 0.40.

REFERENCES:

- [1.] N. Constantin, "Intensificarea proceselor din furnale prin perfectionarea circulatiei gazelor in vederea cresterii productivitatii si a economiei de cocs metalurgic si energie", Doctor Thesis, Bucharest, 1994.
- [2.] N. Constantin, "Ingineria producerii fontei in furnal", Ed. PRINTECH", Bucharest, 2002.
- [3.] Nicolae CONSTANTIN: "Tratat de stiinta si Ingineria Materialelor vol 2 "Bazele teoretice si ingineria obtinerii materialelor metalice" Editura AGIR 2007,cap 5, pag.642-757 , ISBN 978-973-720-064-0, ISBN-978-973-720-162-1.
- [4.] Cezar NECȘULESCU, Edmond BERCEANU, Nicolae CONSTANTIN: "Îndrumar de prelucrare a datelor experimentale utilizând teoria probabilităților și statistica matematică" - tipărit Universitatea "Politehnica" București, 1993
- [5.] Nicolae CONSTANTIN, Victor GEANTĂ, Bogdan NICULAE, Radu ȘTEFĂNOIU: "Modelarea matematică și conducerea informatizată a proceselor din metalurgia extractivă feroasă." - tipărit Universitatea "Politehnica" București, 1997





¹ Ioan MILOSAN

STUDIES AND RESEARCHES ON THE DETERMINATION OF KINETIC AND THERMODYNAMIC PARAMETERS OF AN ADI

¹ TRANSILVANIA UNIVERSITY OF BRASOV, ROMANIA

ABSTRACT:

The paper presents an application for calculating the kinetics and thermodynamics parameters in the case of a phase transformation in solid state in A.D.I. S.G. grade. It is pointed out the influence of some factors (the temperature and the maintained time at the isothermal level) on the phase transformation and properties in the studied cast iron.

KEYWORDS:

A.D.I., phase transformation, kinetics, thermodynamics

1. INTRODUCTION

A wide range of properties can be obtained in these material components owing to changes in proportions of the major phases present in the microstructure: bainitic ferrite, high carbon austenite and graphite nodules. Martensite, ferrite, iron carbides and other alloy carbides may also be present.

Spheroidal graphite cast iron can be heat treated to produce Austempered Ductile Iron (A.D.I.). Recent studies have shown that, this material have excellent mechanical properties. The combination of high strength and high toughness achieved by A.D.I. suggests the engineering use of this material will continue to expand [1, 2].

The kinetics of austenitization of S.G. Cast Iron, was described by the Johnson-Mehl-Avrami equation and for the determination of the activation energy "Q", it was used the Arrhenius equation.

2. METHODOLOGY

The studied cast iron has the following chemical composition (% in weight): 3.85% C; 2.16% Si; 0.42 % Mn; 0.012%P; 0.0036%S; 0.076%Mg; 0.40% Ni; 0.39%Cu.

This cast iron was made in an induction furnace. Nodular changes were obtained with the "In mold" methods, with the help of prealloy FeSiCuMg.

The parameters of the heat treatment done were the following: the austenizing temperature, $T_A = 900$ [°C]; the maintained time at austenizing temperature, $\tau_A = 30$ [min]; the temperature at isothermal level, $T_{iz} = 380$ and 400 [°C]; the maintained time at the isothermal level, $\tau_{iz} = 1; 2; 5; 10; 20; 30; 40$ and 50 [min].

All these 2 experimental lots A ($T_{iz} = 380^\circ$ C) and B ($T_{iz} = 400^\circ$ C) were performed at isothermal maintenance in salt-bath, being the cooling after the isothermal maintenance was done in air.

From this material, 15 typical HB test specimens was done ($\phi 20 \times 50$ mm) and after the heat treating, it was determined the results of HB. The aim of the experiments is to determine the hardness (HB) at the isothermal temperature.

3. RESULTS

For the study of the phase transformation kinetics, it was used the first stage of the bainitic reaction [3]:

$$\gamma \rightarrow (\alpha) + (\gamma) \quad (1)$$

where: γ - metastable austenite; (α) - bainitic ferrite; (γ) - austenite enriched in carbon

In this researches work it was used the methods of the variation's hardness analyse function of the time at the isothermal level (τ_{iz}), considering that this values are depended from the proportion of the transformed fraction " $X_{(t)}$ ". It was utilised the expression:

$$X_{(t)} = \frac{H_0 - H_{(t)}}{H_0 - H_f}, [\%] \quad (2)$$

where: $X_{(t)}$ – the transformed fraction;

H_0 – initial hardness, corresponding $\tau_{iz} = 1$ min;

H_t – hardness obtained after a maintaining time (t) at the isothermal level, [%];

H_f – final hardness, corresponding at the maintaining time at the isothermal level, which are considered as a final time for the first stage of transformation of the bainitic reaction.

The experimental values of the hardness are presented in table 1.

Table 1. The experimental values of hardness, for various T_{iz} and τ_{iz}

T_{iz} , [°C]	τ_{iz} , [min]	Hardness, [HB]		
		H_0	H_f	$H_{(t)}$
380	1	493	302	493
	2			464
	5			415
	10			375
	20			363
	30			354
	40			325
	50			302
400	1	438	295	438
	2			393
	5			354
	10			333
	20			325
	30			311
	40			295

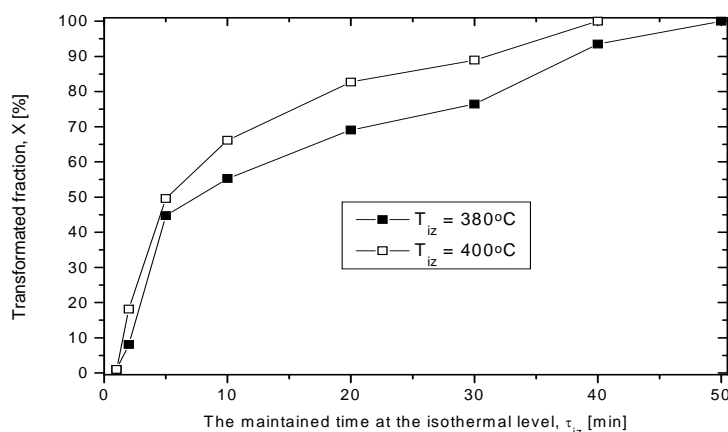


Fig. 1 Transformed fraction curves at $T_{iz} = 380$ and 400°C , for different maintaining time, τ_{iz} , at the isothermal level.

In order to determine "k" and "n", the natural logarithmic expression was used:

$$\log [-\log (1-X)] = (n \log k + \log \log e) + n \log t \quad (4)$$

The plot of " $\log [-\log (1-X)]$ " against " $\log t$ " in the isothermal temperature range $380-400^\circ\text{C}$ [3], for the isothermal maintaining time range 1 – 40 minutes, is shown in figure 2 and 3.

The obtained equations from the linear regression adjustment are:

$$Y_{380} = -4.32559 + 1.33043 \cdot X, R^2 = 0.95; \quad (5)$$

$$Y_{400} = -4.27583 + 1.37189 \cdot X, R^2 = 0.95; \quad (6)$$

Values of "n" and "k" determined from the slopes and intercepts of the linear regression lines are listed in table 2.

In figure 1 is represented the sigmoidal solid curves of the austenitic transformation during the bainite reaction.

Like the transformation fraction curves have sigmoidal shape, it was used the "Johnson-Mehl-Avrami" equation n [3]:

$$X(t) = 1 - \exp(-k t^n) \quad (3)$$

where:

$X(t)$ - the transformed fraction;

k - rate constant dependent on temperature;

n - exponent of the reaction.

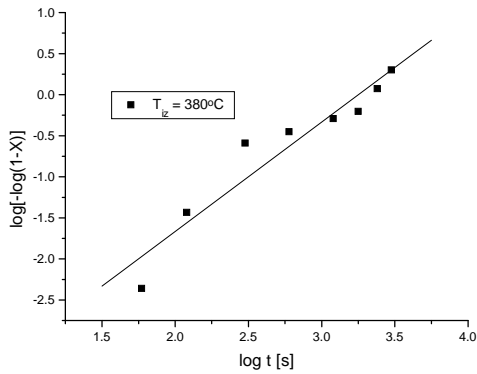


Fig. 2 The plot of “log[-log(1-X)] against “log t” in the isothermal temperature 380°C.

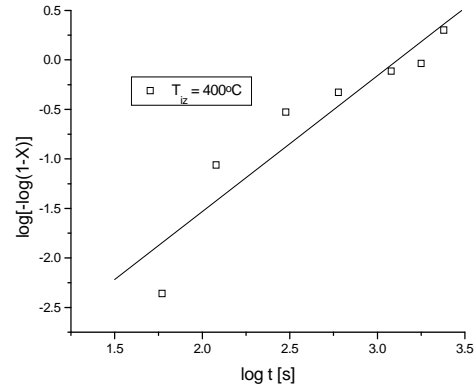


Fig. 3 The plot of “log[-log(1-X)] against “log t” in the isothermal temperature 400°C.

Table 2: Values of “n” and “k” for the formation of bainite

Lot	T _{iz} [°C]	n	k [1 / s]
A	380	1.33	1.05 x 10 ⁻³
B	400	1.37	1.40 x 10 ⁻³

According to Liu [3], if the “n” exponent is between 1 and 2.3 the transformation is interfacial controlled.

At the same maintaining time in the isothermal level, the transformation process is different in the each maintaining isothermal temperatures. The bainitic reaction rate “k” increases when the isothermal temperature increases from 380 to 400° C.

For the determination of the activation energy “Q”, it was used the Arrhenius equation:

$$k = A e^{-Q/RT}; [1/min] \quad (7)$$

where: k - constant rate dependent on temperature [1/s];

Q - activation energy [J /mol];

T - temperature [K]

R - gas constant 8.31 [J/mol.K]

A - constant dependent on frequency[1/s].

In order to determine “Q” and “A”, the natural logarithmic expression of eqn. (7) was used:

$$\log k = - \log e \frac{Q}{R} \frac{1}{T} + \log A \quad (8)$$

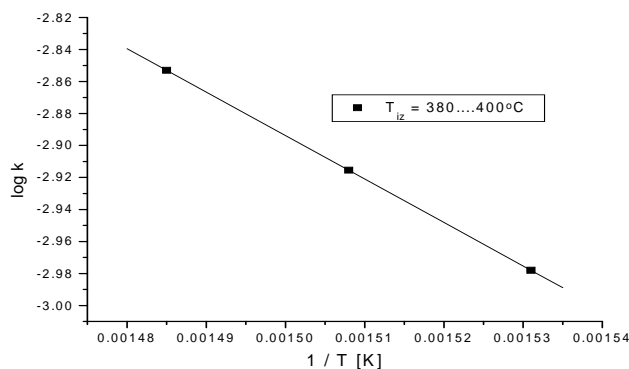


Fig. 4 Linear transform of the Arrhenius equation for the studied S.G. cast iron for T_{iz} = 380 and 400°C.

The plot of “log k” against “1/T” in the isothermal temperature range 380 - 400°C, for the isothermal maintaining time range 1 – 50 minutes, is shown in figure 4.

The equation of the linear regression is:

$$Y_{380-400} = - 1.18233 - 2717.3913 \cdot X, \quad R^2 = - 0.99; \quad (9)$$

Values of “Q” and “A” determined from the slope and intercept of the linear regression line are:

$$Q = 52029.891 [J/mol] \text{ and}$$

$$A = 0.0065 [1/s]$$

The activation energy of isothermal transformation are the same numerical

order like the values obtained in the technical specialty literature [2, 3].

From the linear regression, it was observed that the value of activation energy increases with the increasing of the maintaining temperature, from 380 to 400° C.

4. CONCLUSION

The isothermal bainitic transformation in a Ni-Cu S.G. cast iron was studied in the temperature range of 380-400° C and with maintaining time between 1-50 minutes. The main results are summarized as follows:

- a) The kinetics of austenitization of S.G. cast iron, can be described by an Johnson-Mehl-Avrami equation.
- b) The reaction exponent “n”= 1.33 – 1.37 and the transformation is interface controlled.
- c) The bainitic reaction rate "k" increases with increasing isothermal temperature from 380 to 400°C.
- d) The activation energy of isothermal transformation was 52030 [J/mol]
- e) The constant dependent on frequency was: 0.0065 [1/s]

REFERENCES

- [1.] D. Simon: ADI- a new material for the automotive engineer, Foundry Trade J., No. 2, p. 66-67, 1996.
- [2.] I. Miloşan: Some Aspects About Mo-Ni-Cu Low-Alloy S.G. Cast Iron Type A.D.I, Metalurgia International, No. 4, p. 54-55, 2008.
- [3.] Y.C. Liu, J.M. Schissler, J.P. Chabout, H. Vettters: Study of The Structural Evolution of Austempered Ductile Iron (ADI) during Tempering at 360°C”, Metallurgical Science & Tech. No. 13 p. 12-16, 1995



¹Maria NICOLAE, ²Irina VÎLCIU, ³Emanuela-Daniela STOICA

RESEARCH ON THE MECHANISM OF DAMAGE LINE BRICKS IN THE SLAG LF

^{1,3} POLITEHNICA UNIVERSITY BUCHAREST, ROMANIA

² ECOLOGICAL UNIVERSITY OF BUCHAREST, ROMANIA

ABSTRACT:

This paper proposed to analyze, based on fundamental known, the slag influence generated on LF process on the ladle refractory. In this purpose were studied the refractory destruction mechanisms used on LF, the slag quality, quality refractory and the slag influence on refractory especially because of the interactions between them, definitely elements for steel quality and also for the refractory endurance.

KEYWORDS:

refractory, interaction slag-refractory

1. INTRODUCTION

The main wear mechanisms of the refractory ladle slag line are chemical corrosion and mechanical erosion due to stirring of the steel bath. Chemical potential difference between the refractory and the slag under high temperature conditions is driving force for chemical wear mechanism. Destruction process depends on many variables: temperature, refractory composition, slag thickness, slag composition and stirring degree.

The objective of this paper is to analysis of the interaction between LF bricks steel ladle in contact with slag. In this purpose were determined the slag characteristics on the hot face brick, the slag and the refractory interaction carried out by optical and electronic microscopy (SEM) and X-ray diffraction.

2. THE STUDY

The study was carried out on scrapped brick from LF installation from Calarasi, the brick is part of the steel ladle refractory lining slag level. Determined proprieties for the studied brick are in the following table 1.

Tabel 1. Properties of bricks used at slag level

Apparent density (g/cm ³)	2,95
Apparent porosity (%)	4,8
Apparent density after heating at 1150 °C	2,87
Apparent porosity after heating at 1150 °C	11,2
Mechanical strength (MPa)	30

The slag deposited thickness on the refractory brick varies between 3-6 mm (fig.1).

The bricks appearance is shown in Figure 1 and in figure 2 is presented the bricks appearance after removal of an important part of slag layer deposited.

Tabel.2. LF slag chemical composition deposited on hot face brick

CaO	MgO	Al ₂ O ₃	SiO ₂	SO ₃	Fe ₂ O ₃	CoO	TiO ₂	MnO	Cr ₂ O ₃	P ₂ O ₅
30,14	29,54	10,43	2,95	1,31	0,16	0,33	0,12	0,08	0,05	0,05
Ca	Mg	Al	Si	S	Fe	Co	Ti	Mn	Cr	
25,64	15,45	5,14	1,36	0,59	1,06	0,34	0,01	0,08	0,05	



Fig.1. Deposited slag on brick after its used in LF



Fig.2. Interface between slag layer and brick

Tabelul 3.LF slag chemical composition

CaO	Al ₂ O ₃	SiO ₂	MgO	FeO	MnO	Cr ₂ O ₃	P ₂ O ₅	TiO ₂	S	K ₂ O	Na ₂ O
56,47	30,92	6,47	3,73	0,62	0,11	0	0,02	0,34	1,2	0,02	0,07
57,03	32,03	4,92	3,83	0,52	0,08	0	0,01	0,26	1,2	0,02	0,06
58,28	31,13	4,44	4,08	0,39	0,06	0	0,02	0,38	1,2	0,01	0,06

The removed slag was analyzed chemical and structural. The results are in table 3. Slag layer shows pores and two different layers (Fig. 3). These layers contain phases and micro structural aspects of different chemical compositions.

- ❖ First layer has 2.2 mm thickness and it is composed from dendrites crystals of magnesium oxide, iron oxide, iron and calcium aluminates and calcium silico-aluminates. All these are immersed in a matrix of calcium aluminates.
- ❖ The second layer has 3 mm thickness and it is composed of magnesium crystals damaged by iron and manganese alumino-silicates crystals with different contents of calcium, iron and titanium, calcium aluminates - magnesium - iron and calcium silicate crystals.



Fig.3. Two of slag layers

3. INTERACTION SLAG AND BRICK GRAIN

At the interface between slag and brick MgO grains were found torn from brick and immersed in slag. Distribution of elements in this area is shown in Figure 4. Corrosion can be observed due to the interaction between the iron grains oxide and magnesium oxide. Slag penetrates the silicate sinters grains network and melt intragranular silicates. This interaction speeds the lower temperature phase formed and facilitates separation from crystal.

Slag- brick martix

Micro structural analysis reveals the decarburization process of the brick matrix in contact with slag (Fig. 5). Interface slag-brick is shown in Figure 6. In the brick matrix there are formed spinal crystals. Also, crystals were identified calcium silicate in the brick matrix.

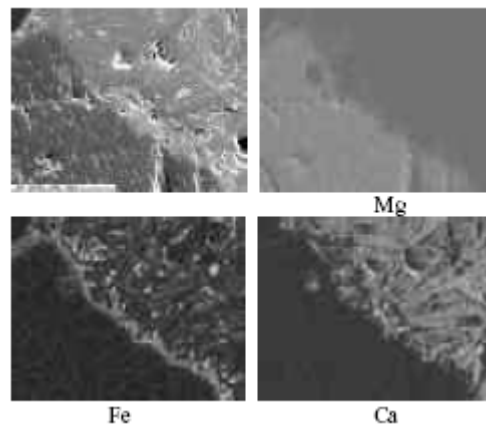


Fig.4. Indirectly Corrosion of MgO grains

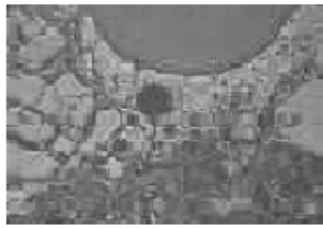


Fig. 5. Decarburization slag matrix and interface

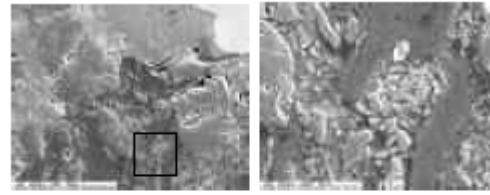
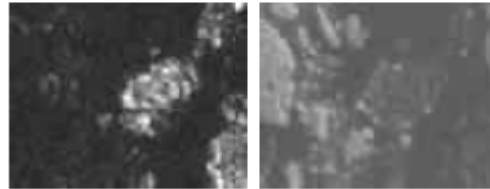


Fig. 6. Distribution of elements in hot brick surface



3. ANALISES, DISCUSSIONS, APPROCHES and INTERPRETATIONS

The first slag layer is composed on calcium aluminates matrix with melting temperature at 1400 °C and different crystals:

- ❖ calcium alumina and iron alumina, with softening temperature at 1336 °C (equilibrium phase diagram for the system $Al_2O_3 - CaO - FeO$);
- ❖ Calcium and aluminum silicates with softening temperature of 1380 oC (equilibrium phase diagram for the system $Al_2O_3 - CaO - SiO_2$ Fig. 7);
- ❖ MgO dendrites.

The chemical composition of the first slag layer is shown in Figure 6. This chart show that the slag is completely liquid at 1600 °C, and therefore, it is not saturated endanger. First layer of liquid slag is not saturated with MgO and at 1600 oC.



Fig. 7. Phase equilibrium diagram of the system $Al_2O_3-CaO-SiO_2$

The second layer is composed from adhered slag stickled to the brick, this layer contains a higher level than the first layer of iron oxide slag. He probably comes mainly from the pot slag before the LF treatment. Also, the second slag layer has a lower content of calcium oxide than the first layer of slag. The second layer of slag is composed of calcium aluminates matrix and different types of crystals:

- ❖ calcium, titanium, and iron silicates and aluminum with different contents of these elements with melting point at 1400-1500 °C;
- ❖ calcium silicates and aluminum with melting temperature at 1450 °C (fig. 7 diagram of phase equilibrium in the system $Al_2O_3 - CaO - SiO_2$);
- ❖ different contents alumina of calcium, magnesium and iron;
- ❖ MgO crystals attacked with iron oxide first and then the manganese oxide and calcium oxide.

This mechanism is the result of iron elements, manganese and calcium existing in the slag that runs the fastest in the refractory material to form the corresponding reaction products. The chemical composition of the second layer is shown in Figure 8. This slag is saturated with magnesium oxide at 1600 °C.

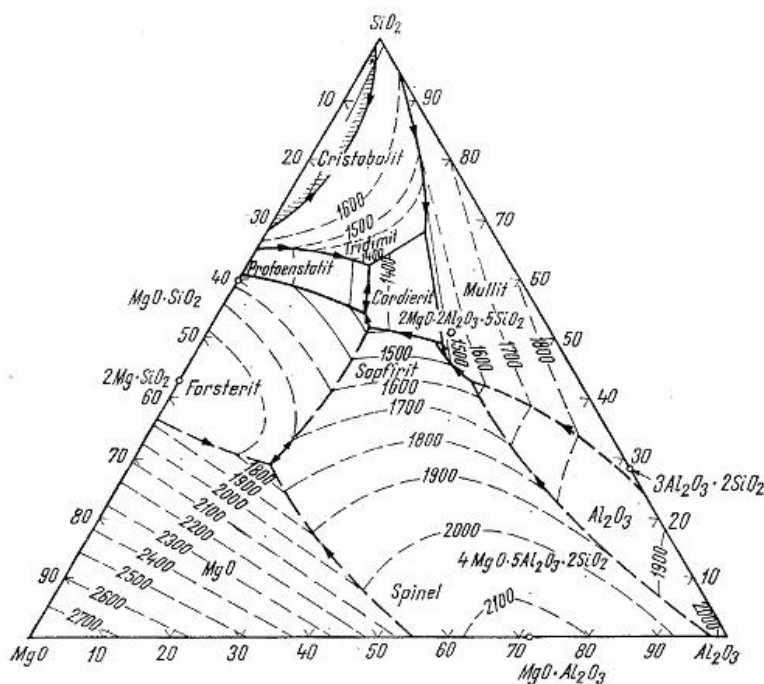
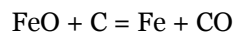


Fig. 8. Phase equilibrium diagram of the system $MgO-SiO_2-Al_2O_3$ temperature. It is well known that this conditions are the main cause of corrosions and bricklayer destructions;

- ❖ The second slag layer is saturated with MgO but contains a high level of iron content. This oxide in growth the slag fluidity-broke the silicate network from the brick and allow the matrix decarburization , thus :



Graphite oxidation growths bricks porosity, allowing slag penetration in the system, following periclase grains dispersion in slag. Review mechanisms identified are: graphite oxidation, slag penetration into matrix and around MgO grains and finally MgO grains dissolution into slag. More over, iron spread in MgO grain and allows MgO slag molder. This new phase decrease the MgO grains refractory and also delay speed destroy of refractory material. This mechanism leads indirect MgO grain dissolution.

REFERENCES

- [1.] A. Nicolae s.a. - Materiale ceramice refractare pentru instalații termotehnologice, Ed. Fair Parteners, București, 1999.
- [2.] P. Bartha et.al. – Heavy ceramic shaped materials, process for the production thereof and the thereof, United States Patent , nr. 4,775,648 oct.4.1988.
- [3.] G. Yuasa, et.al. - Refining Practice and Application of the Ladle Furnace (LF) Process în Japan, Transactions of the Iron and Steel Institute of Japan, vol, 24, no.5(1984), pp 412-418.
- [4.] P.G. Jonsson, L. Jonsson, D. Sicheđ – Viscosities of LF slag and their impact on ladle refining, ISIJ International, 1997, vol.37, no.5, pp 484-491.
- [5.] Z. Adolf, i. Husar, P. Suchanez - Investigation of the influence of the melt slag regime in a ladle furnace on the cleanliness of the steel, Materiali in tehnologije / Materials and technology 41 (2007) 4, 185–188
- [6.] L.Mihok, K. Seilerova, M. Frohlichova - Influence of Steel Cleanliness by Ladle Furnace Processes, Materials Science, vol. 11, no. 4. 2005,pp 320-323.
- [7.] P..S. Fredriksson - Thermodynamic studies of FeO-containing slags and their impact on ladle refining process. VII International Conference on Molten Slags Fluxes and Salts, The South African Institute of Mining and Metallurgy, 2004, pp 285-292.
- [8.] K.C. Mills, E.D. Hondros, L.Yushu - Interfacial phenomena in high temperature processes, Journal of materials Science 40, 2005, pp 2403-2409.
- [9.] Silvia Camelli, Marcelo Labadie-Analysis of the wear mechanism of $MgO-C$ slag line bricks for seel ladles.49. Internationales Feuerfest-Kolloquium 2006, pp 30-34.

4.CONCLUSIONS

The study of brick out off used was carried out through optical and electronic microscopy (SEM) and EDS analysis, allowed identification of slag- brick adherence characteristics, refractory wear mechanism and the microstructural changes inside the brick.

The slag on the brick hot face is composed of two different layers.. Aceste straturi conțin aspecte microstructurale distincte și faze cu compoziții chimice diferite. Both layers are agressive to the refractory material lining.

- ❖ The first slag layer is not saturated with magnesium oxide and it is completely liquid at the process

¹Victor BUDĂU, ²Sebastian DUMA

HARDNESS AND STRUCTURAL ASPECTS OF THE HEAT – TREATED HS 18-0-1 STEEL

¹⁻². UNIVERSITY "POLITEHNICA" OF TIMIȘOARA, FACULTY OF MECHANICS, TIMIȘOARA, ROMANIA

ABSTRACT:

High speed machining requires tools from special materials (rich alloyed steel, cermet materials etc.). In the category of high alloyed tool steels the important are high-speed steels. To obtain the corresponding operating characteristics they must be heat treated to show comparative features with ordinary steel. The paper presents the heat treatment and the structural characteristics and hardness analysis of HS 18-0-1 high-speed steel used to manufacture tools for cutting with high speed.

KEYWORDS:

HS 18-0-1 steel, annealing, quenching, tempering, ferroxylation, X-rays diffraction

1. INTRODUCTION

It's known that for cutting with high speed tools from high-speed steel are used. Compared with other tool steels these allow increased cutting speed of 2-4 times and ensure an increase of 10-30 times tool durability owing to high heat stability up to 600 – 620 °C [1, 4].

Achieving these performance is possible only after secondary quenching heat treatment followed by tempering which shows some features of carbon tool steels.

Based on these considerations, in the paper, the features of heat treatment and structural characteristics and hardness analysis of HS 18-0-1 high-speed steel are shown.

2. PREPARATION OF SAMPLES AND APPLIED HEAT TREATMENT

HS 18-0-1 steel (symbolization as EN ISO 4957) is a rich alloyed steel for tools, from high-speed steel category (symbolization as STAS with Rp3). Chemical composition of this steel is: C = 0.7 – 0.8 %; W = 17.5 – 18.5 %; Mo = max 0.6 %, V = 1 – 1.2 %; Cr = 3.8 – 4.5 %.

Φ 20 x 15 mm specimens were made from forged bars, and were subjected to heat treatment. The heat treatment cyclogram is shown in figure 1.

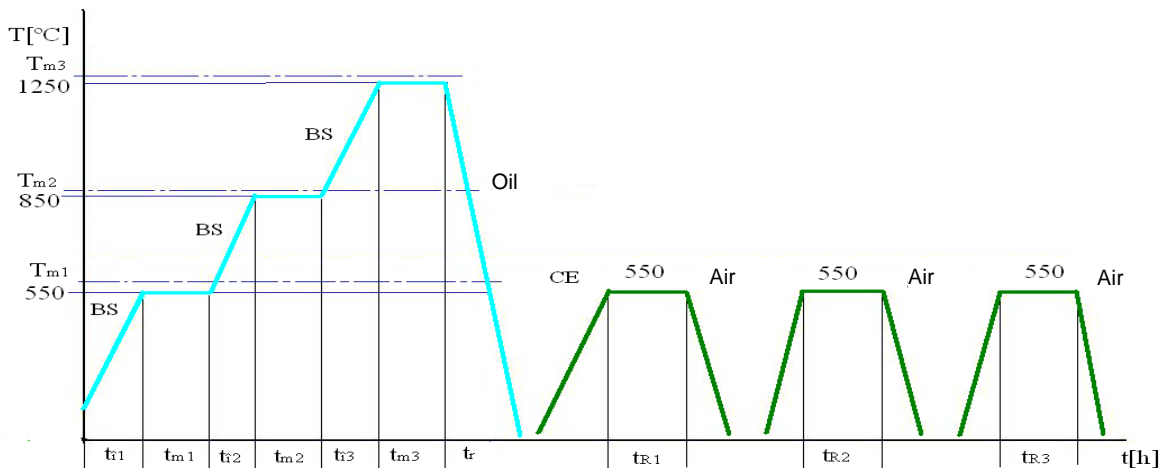


Figure 1. The cyclogram of the secondary heat treatment applied on the HS 18-0-1 steel

The transformations suffered by the material are as follows:

HEATING TRANSFORMATIONS

The heating for austenitization in order to quench high speed steels is made at high temperatures (1200- 1300°C). This ensures that a large quantity of carbides are decomposed and dissolved in austenite enriching it, and after cooling enriching the martensite [2,4].

These temperatures are much higher than the eutectoid temperatures of carbon steel used for tools. The components of the alloy (which are α -gene) increase the temperatures of critical points A_{c1} and A_{c3} forming carbides and reducing the susceptibility of overheating the austenite, reflected by its granulation (the susceptibility of overheating the austenite increases with the increase of dissolved carbon).

QUENCHING TRANSFORMATIONS

Because of the high austeniting temperatures, carbon and alloy components that lower the martensitic transformation point M_s , the austenite becomes stable and exists for a longer time, preventing it from fully transforming into martensite, leading to residual austenite. Thus, quenched high speed steels contain residual austenite, un-dissolved carbides and a small quantity of martensite. The presence of residual austenite in the structure prevents the reaching of a maximum hardness after quenching.

TEMPERING TRANSFORMATIONS

During the tempering process the diffusion intensifies because of the heating, resulting in a loss of hardness at about 300°C after carbon separation. Continuing with the heating process the diffusion of the iron and alloy components is favoured resulting in the precipitation of granular carbides that endow the structure with greater hardness. Thus, the austenite has a lower concentration of carbon and alloy elements, leading to an increase of temperature for martensitic transformation points, enabling the transformation of residual austenite in tempering martensite connected with an increase in hardness. The maximum hardness is obtained at 550°C and is called “secondary hardness” [1,2,3,4].

3. METALLOGRAPHIC, OPTICAL, ELECTRON, WITH X-RAY DIFFRACTION ANALYSIS AND HARDNESS MEASUREMENTS

After secondary heat treatment (as figure 1), the specimens were metallographic prepared and analysed by optical, electron microscopy and with X-ray, using equipment existing in the Chair of Materials Science and Welding - Timisoara (UPT – Mechanical Faculty).

In figure 1 is shown the microstructure (optical microscopy) of the specimen, which is in forged and annealed state, and in figure 3 is the corresponding X-ray diffraction spectrum.

It is noted that the structure in annealed state is formed by fine sorbite that includes primary and secondary carbides. The arrangement of carbides in strings is due to the forging.

In figure 4 is shown the microstructure (optical microscopy) of the specimen which is in quenched state. It is noted that the structure in quenched state is formed by austenite (polyhedral shape), undissolved carbides with a quantity of martensite. The diffractogram of this specimen (figure 5) confirms the microscopic analysis.

If the aim is to reduce the quantity of residual austenite before the high tempering treatment, the application of treatment at negative temperatures is required. [1],[4].

To draw attention of transformations from tempering process at 550 °C, especially the precipitations of fine carbides with globular shape, the quenching and tempering specimen at 550 °C was examined by electron microscopy (X 4000).

In figure 6 is shown the microstructure (electron microscopy) of the quenching and tempering specimen in three rounds of one hour at 550°C, and in figure 7 shows the resulting diffractogram.

It is noted that the structure is formed by fine martensite (Hardenită tempering martensite) and fine carbides.

Thus, the residual austenite that exists in a very low percentage even in annealed status grows in quenched status and totally transforms after tempering 2.

In order to ensure corrosion protection recommended application of thermochemical ferroxated treatment.

Ferroxation was performed after the second tempering by introducing the specimen into a retort at a temperature of 350°C for 20 minutes. Steam was then introduced at a pressure of 1,2 atm continuing up to 550°C and one hour in the presence of steam. The opening of the retort follows and the cooling of the specimen at 100 °C and after this, the final cooling in oil at 50 °C.

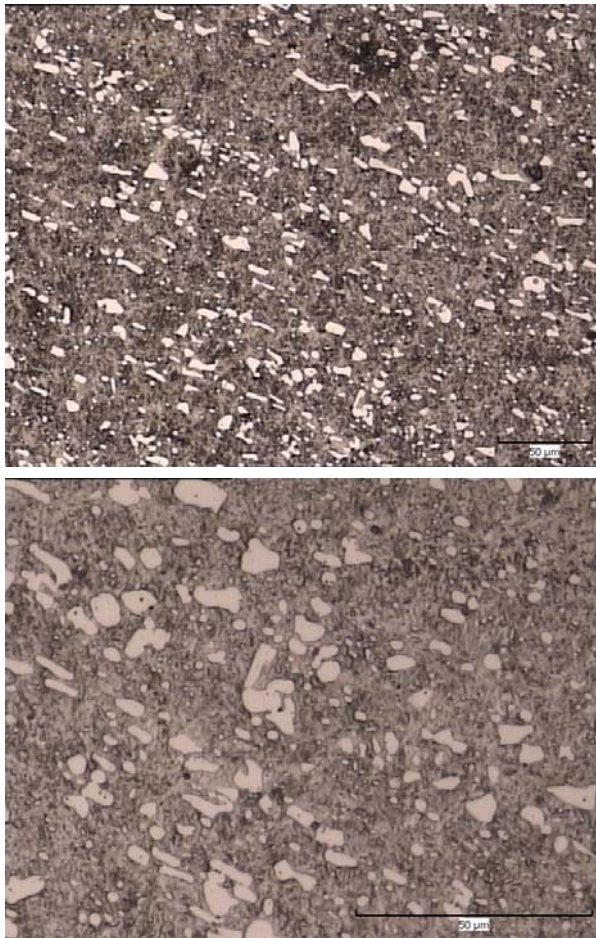


Figure 2. . HS 18 – o – 1 steel – forged + annealed (Sorbite and, primary and secondary carbides)

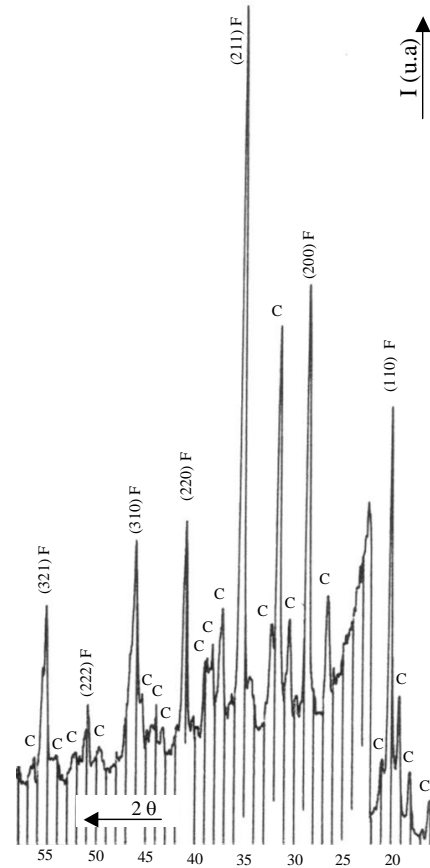


Figure 3: The diffractogram of the annealed status. (F-ferrite, C - Fe_3W_3C carbides).

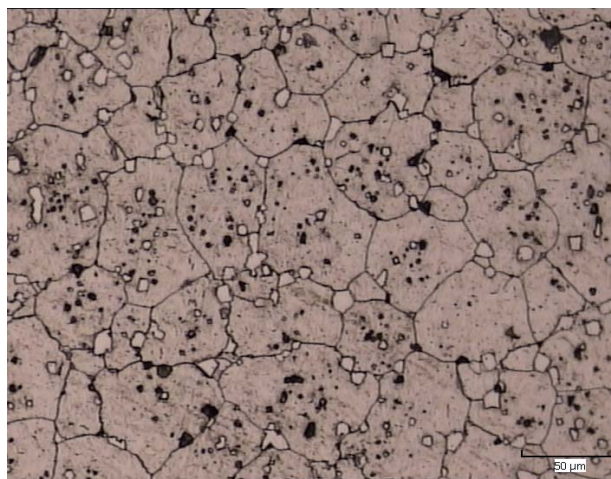


Figure 4. HS 18-0-1 steel - quenched

Figure 8 presents the diffractogram of the ferroxated state. Structure is formed out of tempering martensite, Fe_3W_3C carbides and iron oxides Fe_3O_4 majoritary and Fe_2O_3 minority.

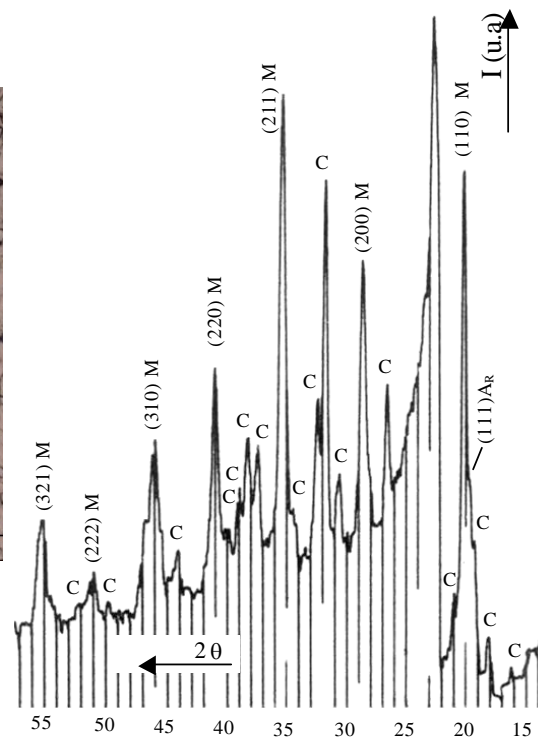


Figure 5: The diffractogram of the quenched status (M-quenching martensite, A_R - residue austenite, C- Fe_3W_3C carbides).

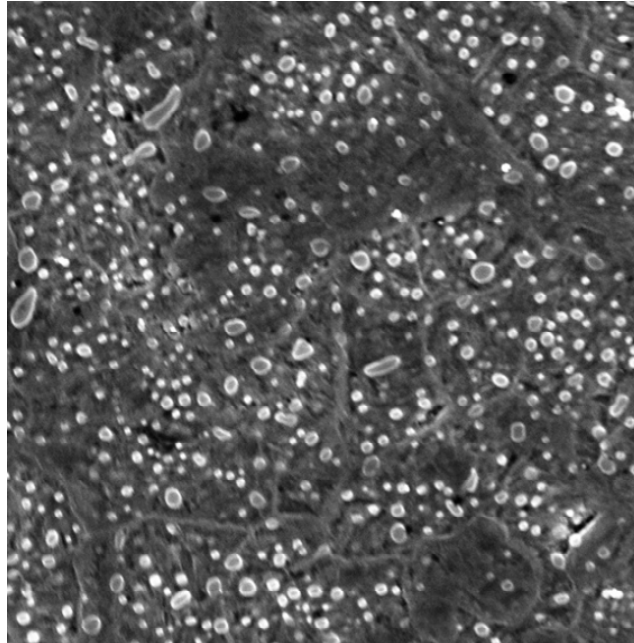


Figure 6. HS 18-0-1 quenched and tempered at 550 °C (x4000)

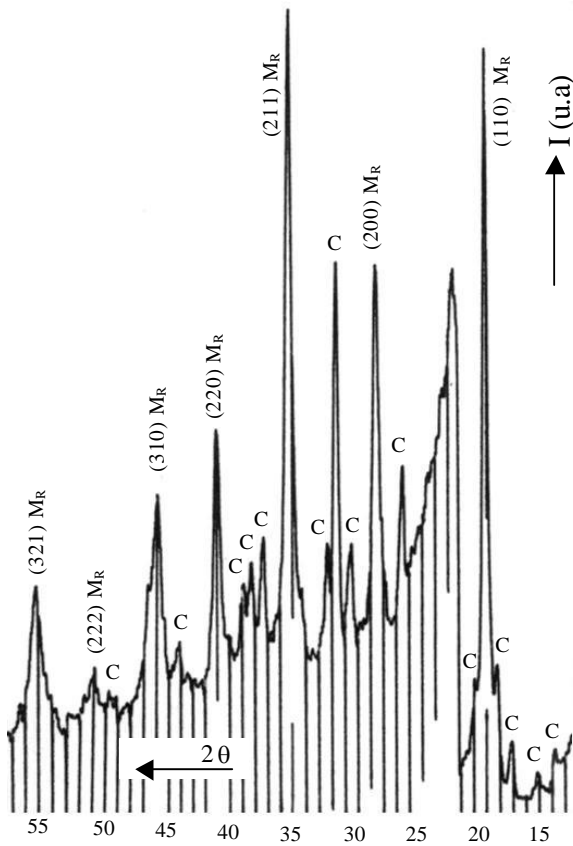


Figure 7: The diffractogram of the status, after tempering₃ (M_R tempering martensite, C - Fe_3W_3C carbides).

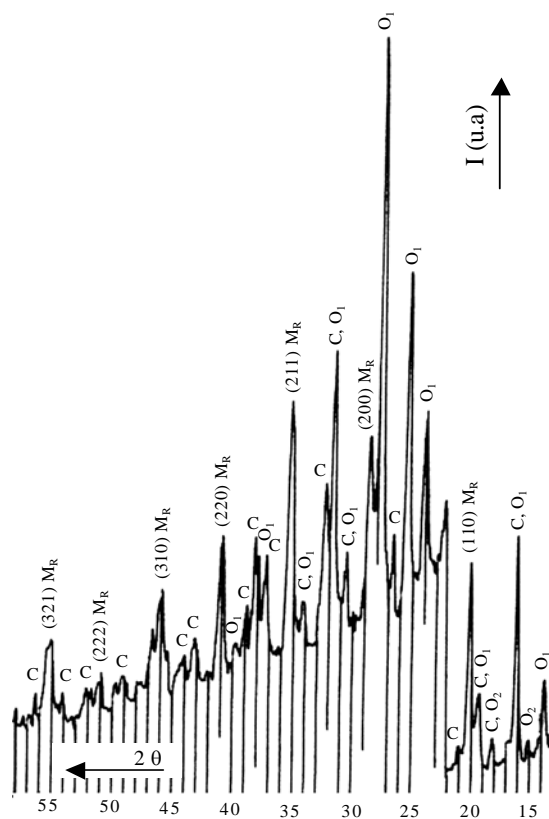


Figure 8: The diffractogram of the ferroxidated state (M_R tempering martensite, C - Fe_3W_3C carbides, O_1 - Fe_3O_4 oxide, O_2 - Fe_2O_3 oxide).

For all specimens hardness measurements was performed (Rockwell Method HRC) and the obtained values were presented in Table 1. It is noted that the hardness values are in close correlation with microscopic analysis and certifies the previously presented phenomena. Hardness after multiple tempering is higher than the quenching, phenomenon known as secondary hardness and this must be exploited when using high-speed steel to manufacture cutting tools.

Table 1. Hardness measurements

No.	Material	Status of thermal treatment	HRC hardness in 3 points	HRC hardness, average
1	HS 18-0-1	Forged + annealed	32, 35, 31	32,66
2	HS 18-0-1	Quenched	61, 62, 61.5	61,66
3	HS 18-0-1	Quenched and tempered at 550 °C	62.5, 64, 63	63,16
4	HS 18-0-1	Quenched + tempered at 550 °C and ferroxated	65, 63, 62.7	63,56

4. CONCLUSIONS

- ❖ HS 18-0-1 heat-treated steel by step-quenching (salts bath), with oil cooling and tempering in three rounds of one hour at 550 °C, ensure an uniform, hard and very thermally stable structure formed by fine tempering martensite and carbides of alloys elements.
- ❖ For aggressive environments, cutting tools executed from HS 18-0-1 high-speed steel, a final corrosion protection treatment is recommended.
- ❖ In special situations, when the active elements of the high-speed steel tool are strongly requested, for prolonging their service life up to three times, a coating with titanium nitride may be used.

REFERENCES

- [1.] Budău, V., Crăciunescu, C.M.: Studiul Materialelor. Ghid individual pentru lucrări de laborator. Editura Mirton, Timișoara, 1998
- [2.] Duma, S., Popescu, M.: The influence of thermic and thermochemical treatment on the structural characteristics and hardness on drills fabricated from HS 18-0-1 steel, Proceedings, Annual Session of Scientific Papers, "IMT Oradea – 2010", pp. 3.37, ISBN: 978-606-10-0128-6
- [3.] Liță, M.: Metode de investigație în știința materialelor, Editura Politehnica, 2009, ISBN 978-606-554-023-1
- [4.] Mitelea, I., Budau, V.: Studiul metalelor, Indreptar tehnic, Editura Facla, Timișoara 1987
- [5.] *** Metals Handbook, Ninth Edition, Vol. 9., Metallography and Microstructures, 1985







WAYS OF INCREASING THE PURITY OF THE STEELS THROUGH SLAGS, IN THE ELABORATION OF THE AGGREGATE

^{1,3,4} UNIVERSITY POLITEHNICA OF TIMISOARA, FACULTY OF ENGINEERING FROM HUNEDOARA

² ARCELORMITTAL SA HUNEDOARA, ROMANIA

ABSTRACT:

The purity of the steels, respectively the increase in their quality begins in the elaboration of the aggregate when, in addition to an appropriate load, the production should flow properly. This requires respecting the steel making technology, taking into account the specificity of the elaboration of the aggregate, the steel brand and the purity requirements required in the standards and / or by the beneficiary. The paper presents some correlations between the slag characteristics at the end of the melting process and the content of harmful elements (P, S).

KEYWORDS:

Steel, melting slag, EBT electric arc furnace, purity, dephosphoration, desulphuration

1. INTRODUCTION

Slag is a secondary product in the process of making steel, but the quality of the steel depends on the slag quality, because all the development processes depend on exchanges between metal bath and slag and between the atmosphere and metal bath through slag. If slag supplies the bath with the oxygen for purification processes and is able to retain the reaction products leaving the metal bath, if there are reactions in the slag that favors the reduction of oxides of alloying elements (Cr, Mn, etc.) then the steel will be of superior quality.

The slag, being at the steel surface, can be easily processed during development, so one should act on its characteristics to lead the process in the desired direction.

To do this, one should know the composition, liquid slag structure, physical properties and their physicochemical properties as well as the operational methods by which they may change during the production of steel. [1,2]

2. METHODOLOGY AND DISCUSSION

To analyze the influence of the slag on the steel purity, we analyzed the chemical composition of melting slags which result in the development of the pipe steel, the production taking place in an electric arc furnace EBT type of 100t capacity, data are presented in Table 1.

With these data we calculated the index of basicity (using equation 1 [2.3]), slag viscosity (according to the relation 2 [2.3]) and distribution reports of undesirable elements P and S:

$L_p = \frac{(P_2 O_5)}{[P]}$, respectively $L_s = \frac{(S)}{[S]}$ [3,4] the data being presented in tab.2.

$$p = \frac{(CaO)}{(SiO_2)} \quad (1)$$

$$\eta = -0,0509 \cdot (SiO_2) + 0,0178 \cdot (CaO) - 0,022 \cdot (MnO) - 0,0455 \cdot (Al_2O_3) - 0,0165 \cdot (FeO) + 0,0322 \cdot (Fe_2O_3) + 0,0201 \cdot (MgO) - 23,2 \cdot (S) + 1,17 \cdot (P_2O_5) + 1,88 \quad (2)$$

Table 1. Slags chemical composition, [%]

	Elements, [%]											
	S	Al ₂ O ₃	CaO	Cr ₂ O ₃	Fe ₂ O ₃	K ₂ O	MgO	MnO	Na ₂ O	P ₂ O ₅	SiO ₂	TiO ₂
1	0.133	2.53	31.36	1.19	33.07	0.004	7.52	8.56	0.084	0.589	13.11	0.25
2	0.134	5.06	34.03	1.02	27.92	0.002	7.13	9.24	0.076	0.509	13.36	0.25
3	0.153	4.27	33.48	1.02	26.21	0.001	7.97	9.19	0.072	0.537	15.21	0.27
4	0.107	3.18	32.70	1.31	34.97	0.002	7.06	7.78	0.082	0.476	11.72	0.21
5	0.098	2.95	29.55	1.09	43.37	0.001	7.00	6.47	0.091	0.372	8.72	0.17
6	0.159	3.66	36.95	1.12	29.28	0.001	7.83	7.24	0.069	0.460	11.26	0.22
7	0.145	4.14	31.78	1.26	31.35	0.008	7.58	8.75	0.091	0.513	14.28	0.27
8	0.072	1.98	23.52	1.12	46.82	0.009	8.39	7.01	0.121	0.324	11.01	0.18
9	0.168	3.20	30.52	1.15	36.13	0.004	6.46	8.05	0.095	0.430	14.05	0.25
10	0.089	2.99	30.24	1.11	35.38	0.006	7.34	7.75	0.096	0.445	13.83	0.24
11	0.069	3.43	30.71	0.90	32.58	0.001	9.53	7.50	0.079	0.417	13.28	0.24
12	0.092	2.27	32.37	0.99	33.48	0.001	8.48	7.86	0.085	0.440	13.12	0.25
13	0.098	2.28	30.39	0.96	37.95	0.007	7.06	6.94	0.092	0.435	12.63	0.26
14	0.116	3.52	29.25	0.97	41.92	0.006	6.57	6.46	0.086	0.410	10.64	0.23
15	0.072	3.99	29.98	1.00	35.31	0.003	7.48	8.14	0.085	0.423	13.00	0.26
16	0.133	4.59	34.13	0.93	27.55	0.007	7.41	8.75	0.074	0.427	14.39	0.31
17	0.065	1.53	24.92	0.93	49.32	0.004	5.92	6.31	0.102	0.349	10.63	0.19
18	0.097	2.37	32.48	1.07	33.90	0.004	9.11	7.08	0.071	0.453	13.02	0.26
19	0.089	2.08	30.06	0.99	36.99	0.002	8.69	6.86	0.080	0.446	11.80	0.26
20	0.045	3.07	23.87	1.48	43.85	0.005	9.52	7.39	0.106	0.468	9.78	0.24
21	0.061	3.59	28.64	1.47	33.73	0.010	8.48	7.97	0.085	0.561	12.20	0.27
22	0.053	3.58	27.23	1.34	33.44	0.009	8.54	7.77	0.092	0.558	12.51	0.29
23	0.051	2.50	27.45	1.42	36.54	0.006	11.60	7.87	0.086	0.540	11.97	0.27
24	0.048	3.43	24.65	1.26	41.55	0.017	8.81	7.03	0.107	0.467	11.82	0.25
25	0.047	2.09	27.05	1.53	35.12	0.016	12.07	8.26	0.094	0.473	13.14	0.27

Table 2. Indicators calculated based on the chemical composition of slag.

No.	$L_P = \frac{(P_2O_5)}{[P]}$	$L_S = \frac{(S)}{[S]}$	$p = \frac{(CaO)}{(SiO_2)}$	η
1	39.30	1.74	2.26	1.61
2	41.10	2.13	1.72	1.65
3	51.44	2.91	3.26	0.49
4	49.78	2.69	3.48	0.62
5	57.38	3.61	2.88	0.75
6	52.00	2.56	3.40	0.69
7	54.33	2.12	2.78	0.57
8	32.20	1.67	1.99	1.66
9	46.00	2.05	1.82	1.20
10	45.22	3.00	3.21	0.76
11	41.50	2.26	2.25	1.15
12	41.10	1.75	1.97	1.58
13	34.20	1.82	2.28	1.29
14	51.22	2.79	2.28	1.12
15	33.40	1.36	1.76	1.78
16	49.56	2.35	2.06	0.68
17	36.60	1.89	2.23	1.51
18	43.80	2.21	2.38	0.90
19	34.60	1.56	2.43	0.63
20	51.00	1.93	1.88	1.34
21	33.00	1.28	1.88	2.15
22	37.46	1.58	2.11	0.95
23	52.90	2.50	1.84	0.62
24	62.70	3.67	3.62	0.22
25	36.00	1.10	1.60	2.40

- With these data we performed the following dependency graphs and analysis, as follows:
- ❖ in figure 1 the histogram of the variation of slag basicity is shown. It can be seen that in 64% of data the basicity is more than two, which means that there are concerns from the oven to ensure optimal conditions of dephosphoration and prevents the absorption of the hydrogen in the metal bath;

- ❖ the variation of the slag viscosity is shown in figure 2, depending on the temperature of melting metal bath. The dependence is similar to that shown in figure 1 (inversely);
- ❖ the same dependency is shown in figure 3 – the variation of the slag viscosity depending on its basicity;
- ❖ instead, analyzing the dependencies between the distribution reports for P, respectively S depending on the bath temperature it can be observed that the dependence is directly proportional, the removal of these elements being driven by rising the temperature. The difference lies in the value of the distribution reports: to report the distribution of P values were calculated between $L_P = 32.2$ to 62.7 (figure 4) but to report the distribution of S the values were calculated much lower: $L_S = 1.1$ to 3.67 (figure 5).

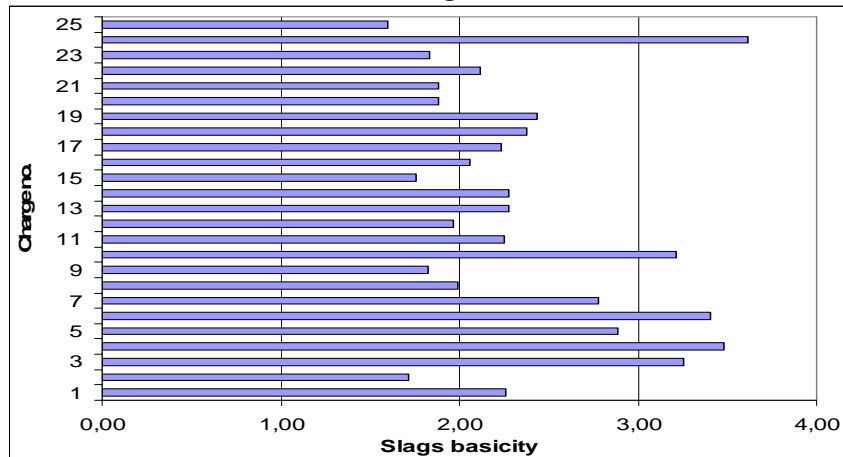


Fig.1. The basicity of the steel plants slag.

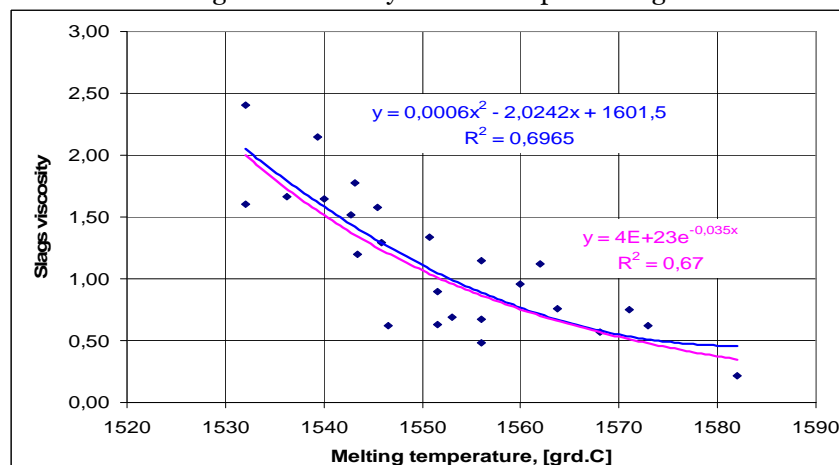


Fig.2. The dependence between the slag viscosity and the temperature of the metal bath.

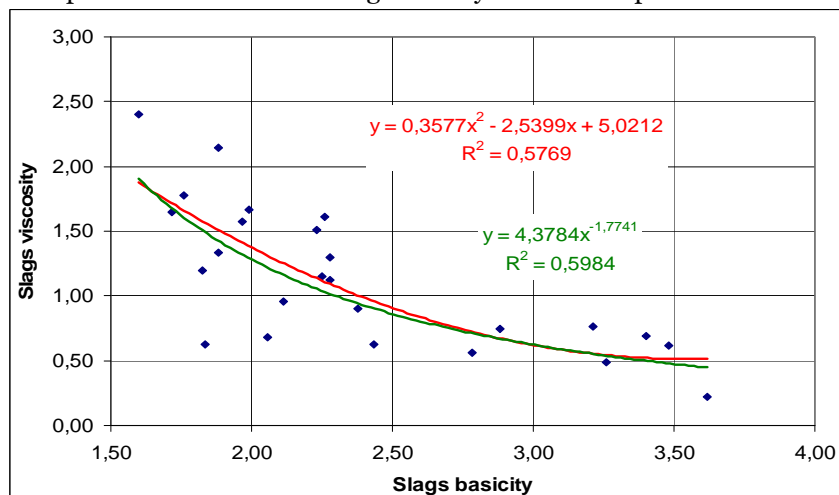


Fig.3. The variation of the viscosity depending on the slag basicity.

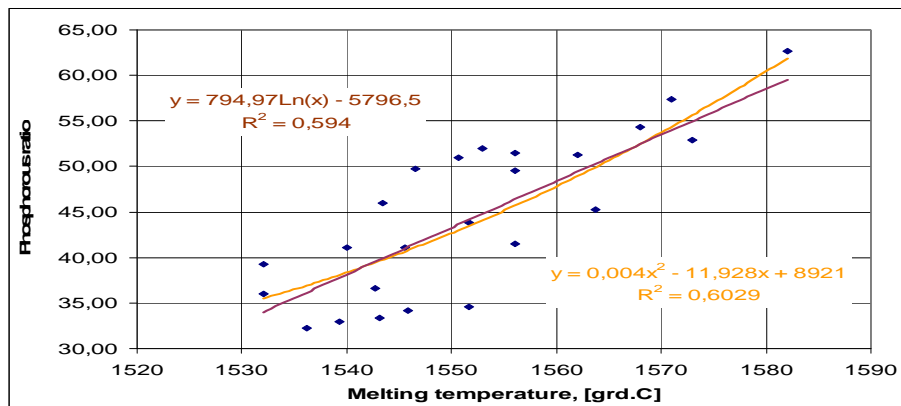


Fig 4. The dependence between the distribution report of the phosphorus between the slag and the metal bath and respectively the temperature of the bath.

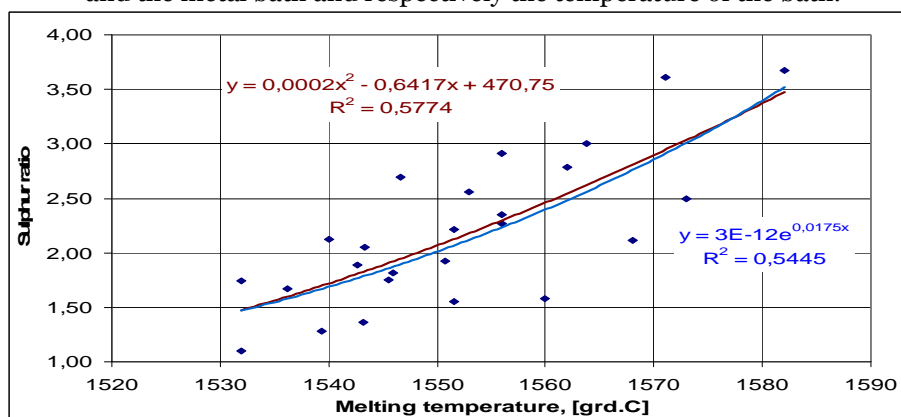


Fig 5. The dependence between the distribution report of the sulfur between the slag and the metal bath and respectively the temperature of the bath.

3. CONCLUSIONS

As a result of analyzing the literature and data from industrial practice, the following conclusions were presented:

- ❖ to increase the quality of the steel, the quality of the load should be the appropriate one;
- ❖ in what concerns the unwanted elements in the P it is known that the dephosphoration occurs at the end of the melting process. In industrial practice, P removal from the oven (by slag) is a continuous and constant over the last melting tip loading. At the end of melting, P contents are within the limits required by standards;
- ❖ S content decreases only at higher than 1620°C temperatures. We can observe an increase of S content compared to the sample in the melting process, due to melting of the amount of iron brought in the load (which places in the oven a high content of S) or by introducing petroleum coke (also with high S). Advanced desulphuration is achieved in the ladle during secondary treatment;
- ❖ In terms of hydrogen content at slag basicity $P > 2.1$, it is not absorbed into the metal bath. In industrial practice, basicity is adjusted by introducing lime calcined lumps containing approx. 98% CaO, dolomite reduction (by approx. 40% MgO and 58% CaO). Not to be neglected is the crushed magnesite inserted into the last tipper (1000 - 1100 kg/charge) for both protection of the refractory masonry and for basicity correction.

REFERENCES

- [1.] Geantă, V., Pumnea, C., Tehnologii speciale de elaborare și rafinare a oțelului, Ed. Universității Politehnice București, 1993.
- [2.] Oprea, F., Taloi, D., Constantin, I., Roman, R., Teoria proceselor metalurgice, Editura Didactică și Pedagogică, București, 1978.
- [3.] Tripșa, I., Pumnea C., Retopirea și rafinarea oțelurilor, Editura Tehnică, București, 1984.
- [4.] Nica, Ghe., Socalici, A., Ardelean, E., Heput. T., Tehnologii pentru îmbunătățirea calității oțelului, Ed. Mirton, Timișoara, 2003.



MATHEMATICAL MODEL ON THE CORRELATION OF THE COMBUSTION`S ZONE PARAMETERS IN CASE OF USING DIFFERENT AUXILIARY COMBUSTIBLES

^{1, 2, 3} UNIVERSITY "POLITEHNICA" OF BUCHAREST, ROMANIA

ABSTRACT:

The physical and chemical processes that are developing in the combustion zone of the blast furnace depend on many physical and metallurgical parameters, such as: blast air flow, oxygen content in blast air, humidity, pressure and blast air flow temperature.

The presented mathematical model establishes the correlation between blow parameters mentioned before and a performance function that is set to reflect precisely the development of the physical and chemical processes in the combustion zone of the blast furnace in case of using various auxiliary combustibles. This performance function is the theoretical temperature of the oxidant zone.

The establishment of the model equations was made starting from the functional real data of 1000 m³ blast furnaces.

KEYWORDS:

using different auxiliary combustibles

1. INTRODUCTION

The mathematical models established by many scientific research works make possible the computers assisted management of some stages of the pig iron manufacturing processes in blast furnace. They establish the correlation between the important parameters of processes and the choice performance functions selected to show the development of physical and chemical processes from blast furnace in the case of using auxiliary combustibles. This performance function for the presented model is the theoretical temperature of oxidant zone in blast furnace.

The establishment of the mathematical model starts from the presented model is the theoretical temperature of oxidant zone in blast furnace.

The mathematical model uses as enter variable or resulting variable the specifically consumption of the metallurgical coke (the physical coke – "without water coke").

A basis of the model is represented by the combustion zone thermal balance.

For an optimal function of blast furnace the theoretical temperature in this zone is accepted to be 1800...2000°C.

2. THE THEORETICAL AND CALCULATION PRESUMPTIONS OF THE MATHEMATICAL MODEL

The mathematical model proposed in the present scientific research work supposes the establishment of some correlations between the blow air parameters.

These parameters could enter or exit variables the other entire dependent.

The establishment of the mathematical models equations has been made starting up from the real function data of blast furnaces. As starting data for the calculation was proposed the following specifically consumptions:

- ❖ the metallurgical physical coke (the technical coke - "without water coke") - K_{ti} - as enter variable of the model with 400...600 kg/t values and K_{etr} as exit variable;
- ❖ the tar - D_t - as enter variable of the model with 0...5000 kg/h values and D_{et} as exit variable;

- ❖ the methane gas – M_{gi} – as enter variable of the model with 0...9000 Nm³/h values and M_{ge} as exit variable;
- ❖ the pitch liquid fuel – D_{pl} – as enter variable of the model with 0...5000 kg/h values and D_{epl} as exit variable.

Concerning the practical manage of pig iron manufacturing for tar methane gas and pitch liquid fuels it operates with hour flow and the mathematical model uses as enter variables the values of D_t , M_{gj} , and D_{pl} . In the same time, the mathematical model gives the relations to transform the hour flows in specifically consumption T_i , M_j , P_{li} . The exit variables of the mathematical model expressed in hour flows in specifically consumption T_i , M_j , P_{li} . The exit variables of the mathematical model expressed in hour flows are in this case the following: T_e , M_e , P_{le} .

The theoretical temperature from combustion zone T_{tez} is initially presented in mathematical model as exit variable, but after that it serves as enter variable with technological optimal value 2123K.

The values for specifically heat of the constant pressure by blow air and water vapors of blow air (h_a , h_w) are known, and for the specifically heat of the obtained gas in combustion zone (h_g) can be used in the initial calculation the value 0, 35. For other calculations the value is:

$$h_g = 0,311 + 0,208 T_{tez} \cdot 10^{-4}, \text{ [kcal/kg}\cdot\text{K]}, \quad (1)$$

The chemical composition used in calculation for the tar is:

$$C_{free} = 55\%, C_{(CS_2)} = 0, 2\%, C_{total} = 55, 2\%, CH_4 = 13, 6\%, C_2H_2 = 28, 8\%, W = 5\% \text{ (among } 5...20\%).$$

The chemical composition used in calculation for the pitch liquid fuel is:

$$C_{free} = 43\%, C_{(CS_2)} = 0, 2\%, C_{total} = 43, 2\%, CH_4 = 15\%, C_2H_2 = 16\%, W = 5\% \text{ (among } 5...20\%).$$

For the substitution index of coke by methane gas is used in calculation the value $I_{kmg} = 1$, obtained by pig iron making real data in blast furnace with 1000 m³ volume in different periods.

For the substitution index of coke by tar and pitch liquid fuel in concordance with data on specialty studies [1, 2] are used the values $I_{kt} = 0, 87$ and $I_{kpl} = 1, 04$.

The adopted values for this index can be modified by the subsequent functionally data of blast furnace.

3. THE MATHEMATICAL MODELS EQUATIONS

3.1. The hour production of pig iron

$$P_{hp} = \frac{Q_p \cdot n_{bu}}{24}, \text{ [pig iron t/h]}, \quad (2)$$

3.2. The specific consumption of the tar, methane gas and pitch liquid fuel

$$T_i = \frac{D_t}{P_{hp}}, \text{ [Kg/t]}, \quad (3)$$

$$M_i = \frac{M_{gij}}{P_{hp}}, \text{ [Nm}^3\text{ CH}_4\text{/t]}, \quad (4)$$

$$P_{li} = \frac{D_{pl}}{P_{hp}}, \text{ [kg/t]}, \quad (5)$$

3.3. The specific consumption of the technical coke

$$K_{th} = K_t \cdot P_{hp}, \text{ [kg/h]}, \quad (6)$$

3.4. The technical coke substituted by auxiliary combustibles

To determine the substitution index of coke by the tar is used the relation:

$$I_{kt} = 1,184 - 0,0191W_{tr} - 0,577 \cdot 10^{-3}S_{tr} + 0, 56 \cdot 10^{-5}W_t \cdot S_t, \text{ [kg/kg]}, \quad (7)$$

For substitution index of the coke by methane gas and pitch liquid fuel are used the values $I_{km} = 1$, $I_{kpl} = 1, 04$.

The substituted quantity of the technical coke by auxiliary combustibles is:

$$K_{ts} = I_{kt} \cdot T_i + M_i + 1,04P_{li}, \text{ [kg/t]}, \quad (8)$$

3.5. The technical coke specific consumption

In case of using auxiliary combustibles T_i , M_j , P_{li} the technical coke consumption will be:

$$K_{tr} = K_{ti} - K_{ts}, \text{ [kg/B.U]}, \quad (9)$$

3.6. The technical coke quantity in burden unity

$$K_{tbu} = K_{tr} \cdot Q_p, \text{ [kg/B.U]}, \quad (10)$$

3.7. The technological coke quantity in burden unity

$$K_{thbu} = \frac{100 \cdot K_{tbu}}{100 - W_{kt}}, \text{ [kg/B.U]}, \quad (11)$$

- W_{kt} represents the humidity of the technological coke.

Using the results given by the mathematical model of burden calculation the mass and the heat balances presented in other scientific research work [3] K_{ti} can be determined by the following mode:

$$K_{ti} = K_t + M, \text{ [kg/t]}, \quad (12)$$

A true correlation between the present mathematical model and [3] can lead to the equality:

$$K_{tbu} = K_{ti}, \quad (13)$$

3.8. The necessary combustion oxygen quantity

From the processing of the pig iron making real data in blast furnace with a volume of 1000 m³ and in correlation with the data presented by the specialty literature [4,5] it can be considered that approximately 68% of carbons coke burns in crucible (in front nozzle surface) will be:

$$C_b = 0,068 \cdot C_k \cdot K_{tr}, \text{ [kg/t]}, \quad (14)$$

- C_k represents the percentage content of free carbon out of coke.

The carbon quantity burnt in front nozzle surface in one hour time is:

$$C_{bh} = C_b \cdot P_{hp}, \text{ [kg/h]}, \quad (15)$$

The auxiliary combustible quantities burnt in one hour time in crucible reported at 1 kg C_{bh} are:

$$T_{rc} = \frac{D_t}{C_{bh}}, \text{ [kg tar/kg C]}, \quad (16)$$

$$M_{rc} = \frac{M_{gl}}{C_{bh}}, \text{ [Nm}^3 \text{ CH}_4\text{/kg C]}, \quad (17)$$

$$P_{lrc} = \frac{D_{pl}}{C_{bh}}, \text{ [kg pl/kg C]}, \quad (18)$$

The necessary oxygen for burning in front nozzle surface in case of using the quantities T_{rc} , M_{rc} , P_{lrc} is:

$$Q_{2nec} = 0,933 + 0,85T_{rc} + 0,5M_{rc} + 0,61P_{lrc}, \text{ [Nm}^3 \text{ O}_2\text{/kg C]}, \quad (19)$$

Considering the percentage content of oxygen in blow air O_2 among 21...30%, the necessary volume of blow air for burning will be:

$$V_a = 1,15 \cdot \frac{100 \cdot O_{2nec}}{O_2}, \text{ [Nm}^3 \text{ air/kg C]}, \quad (20)$$

The blow air hour flows necessary for burning 1 kg C out of coke:

$$Q_a = V_a \cdot C_{bh}, \text{ [Nm}^3 \text{ air/h]}, \quad (21)$$

This quantity represents the theoretical necessary of blow air for burning in blast furnace crucible and the quantity differs from the real quantity that considers all the casualties in air transport network.

3.9. The obtained quantity of gas in the combustion zone

The obtained carbon monoxide volume in combustion zone:

$$V_{CO} = 1,867 + M_{rc} + 1,75T_{rc} + 1,28P_{lrc}, \text{ [Nm}^3 \text{ CO/kg C]}, \quad (22)$$

The obtained hydrogen volume in combustion zone:

$$V_{H_2} = 0,01V_a + 2M_{rc} + 0,62T_{rc} + 0,52P_{lrc}, \text{ [Nm}^3 \text{ H}_2\text{/kg C]}, \quad (23)$$

The obtained nitrogen volume in combustion zone:

$$V_{N_2} = V_a \cdot (0,99 - 0,01O_2), \text{ [Nm}^3 \text{ N}_2\text{/kg C]}, \quad (24)$$

The obtained gas volume in combustion zone:

$$V_g = V_{CO} + V_{H_2} + V_{N_2}, \text{ [Nm}^3\text{/Kg C]}, \quad (25)$$

The obtained hour gas quantity in combustion zone:

$$v_{gh} = V_g \cdot C_{bh}, \text{ [Nm}^3\text{/h]}, \quad (26)$$

3.10. Objective function of present model and correlation between the blows parameters

“The theoretical temperature of combustion zone”: using the heat zone balance (heat balance at combustion zone of blast furnace) is obtained the following relation for the objective function of the present mathematical model:

$$T_{tez(e)} = \{2340 + 1583, 24T_{rc} + 439M_{rc} + 1120, 94P_{lrc} + v_a [(h_a + 0, 01\varphi \cdot h_w) \cdot t_a - 25, 8\varphi]\} / (h_g \cdot v_g), \text{ [}^\circ\text{C]}, \quad (27)$$

- φ , t_a represents the humidity and the temperature of blow air in [%] and [$^\circ\text{C}$].

“Correlation between blow parameters in crucible of the blast furnace”:

- Correlation $K_{eth} = f$ (other blow parameters):

$$K_{eth} = \{v_{gh} \cdot T_{tez} \cdot h_g - 1583, 24Dt - 439M_{gj} - 1150, 94Dpl - Q_a [(h_a + 0, 01\varphi \cdot h_w) \cdot t_a - 25, 8\varphi]\} / (15, 91 \cdot C_k), \text{ [kg/h]}, \quad (28)$$

- Specific consumption of technical coke:

$$K_{etr} = \frac{K_{th}}{P_{hp}}, [\text{kg/t}], \quad (29)$$

- Correlation $D_{et} = f$ (other blow parameters):

$$D_{et} = \{v_{gh} \cdot T_{tez} \cdot h_g - 15,91C_k \cdot K_{th} \cdot P_{hp} - 439M_{gi} - 1120, 94D_{pl} - Q_a [(h_a + 0, 01\varphi \cdot h_w) \cdot t_a - 25, 8\varphi]\} / 1583, 24, [\text{kg/h}], \quad (30)$$

- Correlation $D_{epI} = f$ (other blow parameters):

$$D_{epI} = \{v_{gh} \cdot T_{tez} \cdot h_g - 15,91C_k \cdot K_{th} \cdot P_{hp} - 439M_{gi} - 1583, 24D_t - Q_a [(h_a + 0, 01\varphi \cdot h_w) \cdot t_a - 25, 8\varphi]\} / 1120, 94, [\text{kg/h}], \quad (31)$$

- Correlation $M_{ge} = f$ (other blow parameters):

$$M_{ge} = \{v_{gh} \cdot T_{tez} \cdot h_g - 15,91C_k \cdot K_{th} \cdot P_{hp} - 1583D_{dt} - 1120, 94D_{pl} - Q_a [(h_a + 0, 01\varphi \cdot h_w) \cdot t_a - 25, 8\varphi]\} / 439, [\text{Nm}^3/\text{h}], \quad (32)$$

- Correlation $Q_{ea} = f$ (other blow parameters):

$$Q_{ea} = \{v_{gh} \cdot T_{tez} \cdot h_g - 15,91C_k \cdot K_{th} \cdot P_{hp} - 1583D_{dt} - 1120, 94D_{pl} - 439M_{gi}\} / (h_a + 0, 01\varphi \cdot h_w) \cdot t_a - 25, 8\varphi, [\text{Nm}^3/\text{h}], \quad (33)$$

- Correlation $D_{eO_2} = f$ (other blow parameters):

$$D_{eO_2} = 0,0135Q_a \cdot O_2 - 0,284Q_a, [\text{Nm}^3/\text{h}], \quad (34)$$

$$O_{2(e)} = \frac{100 - O_{2nec} \cdot C_{bh}}{Q_a}, [\%], \quad (35)$$

Correlation $t_{a(e)} = f$ (other blow parameters):

$$t_{a(e)} = (v_g \cdot T_{tez} \cdot h_g - 15,91C_k \cdot K_{th} \cdot P_{hp} - 1583D_t - 1120, 94D_{pl} - 439M_{gi} + 25,8\varphi \cdot Q_a) / (h_a + 0,01\varphi \cdot h_w) \cdot Q_a, [^\circ\text{C}], \quad (36)$$

4. CONCLUSIONS

The mathematical model presented in this scientific research work can use for the computers assisted management for all processes that are developed in the blast furnace crucible combustion zone in case of using varied auxiliary combustibles.

For this reason, first of all the process simulation has been made using this model.

During the process simulation are obtained results that can be confirmed by the blast furnace real function. In certain real situations, the results of the mathematical model are not totally confirmed, in that case the models equations must being improved by adoption at the real pig iron making conditions (for these are introduce the corrections index).

It is obtained a mathematical model that shows obviously the carry on of all the processes in the blast furnace combustion zone. It can be obtained the automatically manage of the pig iron making and remarkable material and energy economy.

REFERENCES:

- [1.] N. CONSTANTIN, D. IONIȚĂ, A. SEMENESCU, C. V. SEMENESCU: „Analytical methods for blast furnace ironmaking optimization by optimal correlation of coke rate with blowing parameters in the raceway”, *Metalurgia* nr.6/2003, pag. 5 – 12.
- [2.] N. CONSTANTIN: „Blast furnace process intensification by gas circulation improvement, in order to ensure productivity growth and energy and metallurgical coke economy”, Doctor Thesis, Bucharest, 1994
- [3.] N. CONSTANTIN, D. IONIȚĂ, A. SEMENESCU, C. V. SEMENESCU, M. COSTACHE: „Efficiency of blast furnace making by computer-assisted of this process”, *Metalurgia*, nr.7, 2003, pag. 17 – 28
- [4.] N. CONSTANTIN: „Nonconventional process for production of ferrous materials”, “PRINTECH” Publishing House, Bucharest, 2002
- [5.] N. CONSTANTIN: „Blast furnace iron making engineering”, “PRINTECH” Publishing House, Bucharest, 2002
- [6.] N. CONSTANTIN: „Replacement of natural gas in the blast furnace by injected steam in the raceway area”, *Metalurgia*, nr.11 - 12, 1991, Romania





ALTERNATIVE IRON MAKING TECHNOLOGIES

^{1, 2, 3} UNIVERSITY "POLITEHNICA" OF BUCHAREST, ROMANIA

ABSTRACT:

The paper presents few aspects concerning the implementation of alternative iron making technologies in Romania. A few reasons are analyzed for the apparition and development of such technologies in the world steel market competition. The presence of alternative iron making technologies will be a benefit for metallurgic, economic, social and environmental reasons and a plus for EU adhesion.

The preliminary researches made using wastes from chemical and metallurgical industries are encouraging for developing alternative iron making pilot plants.

KEYWORDS:

alternative iron making technologies

1. INTRODUCTION

The steel industry has been greatly restructured, is much more competitive and is going through a technological revolution driven by capital requirements, shortages in raw materials such as coke and low residual scrap, environmental concerns and very important customer demands. It is very important to know if production technologies are still appropriate in present and which are the new processes that have to be developed in order to meet the future needs of steel market 1, 2, 3 and 4. The steel manufacturing process is highly capital intensive in relationship to the added value to the input materials. Direct iron making using coals and iron ores directly will eliminate the need for coking coals, coke making and agglomeration and address the need to reduce capital and environmental concerns 2, 3.

Society continues to press the industry to reduce emissions and recycle more waste materials. Consequently, processes that recycle blast furnace and steel making dust and have lower emissions than conventional coke making and sintering must be developed.

Customers will continue to require improved properties and quicker and more reliable delivery of steel at a good value relative to competitive materials. Development of a technique allowing coal and ore to be directly transformed into base iron solid/liquid products will enhance the flexibility and reliability of steel industry in order to maintain its competitive position. For industrialized areas such as the US, Japan and Europe a coal based and low capital cost process must be developed 1 and 4.

2. IRON MAKING ALTERNATIVE TECHNOLOGIES

It is well known that the quality of the main raw materials for EAF plants – scrap – has deteriorated during recent years. Scrap becomes more and more polluted by metallic tramp elements and organic compounds; this requires improved cleaning and sorting of scrap, by physical and chemical treatments. If the scrap quality is insufficient for achieving the required steel properties, virgin iron has to be added to the metallic charge. This addition can be hot metal, cold pig iron or direct reduced iron in order to improve the quality of products because they are tramp elements free 1, 4. Another reason for developing iron making alternative technologies is the possibility of wastes recycling as raw materials. Waste recycling processes will reduce the environmental impact of waste disposal. Minimizing plant waste/by-products (by in-works recycling) and valorizing them (by the use of slag in agriculture or civil engineering) are other important objectives including the ecological one.

In recent years, many alternative iron making processes have been proposed and developed to replace the conventional iron making process – the blast furnace process. Blast furnaces have played a major part in pig iron production because of their high heat and gas utilization efficiency, mass production. In present blast furnace processes have some unavoidable problems, environmental pollution by the coke plants, lower production flexibility and high degree of raw materials preparations.

The alternative iron making process may be required to satisfy the criteria such as the use of different coals, simplified material preparation, metal with little impurities, independent process steps, closed energy system, efficient pollution control and no waste generation. They also may have a higher productivity per unit volume than a blast furnace and the capital cost seems to be significantly lower than the conventional process 1, 2 and 4.

Until now, the Corex process was the most fully developed, which uses lump ore, pellets or sinter, as well as lumpy coal as raw materials, producing 300,000 tons of pig iron annually without any problems. In this process, coal is charged into the melter- gasifier reactor and is combusted to CO and H₂ to produce the heat to melt the iron pellets. Then the off-gas is used to reduce iron ore to more than 90% metallization in the shaft-type prereduce. The other smelting reduction processes presently under development throughout the world use ore fines and coal fines as feedstock in order to avoid as well the coking operation and the agglomeration of iron ores. They generally consist of two superposed reactors: a prereduction vessel and a smelting vessel. None of these processes (Hismelt, Dios, CCF and Circofer) has out passed the pilot and demonstration stage in spite of the considerable amount of research funds already invested. In view of the risks and costs inherent to developments it is questionable when they will reach industrial maturity 1, 4.

The direct reduction processes which today are in commercial use - Midrex, Hyl, Fior – produce about 20-25 million tones DRI (direct reduced iron) per annum, which is a rather small amount compared to the roughly 200-220 million tones of steel per annum produced by the EAF in the world.

3. FERROUS WASTES – RAW MATERIALS FOR ALTERNATIVE IRON MAKING

An efficient way to decrease the cost of raw materials and to meet the environmental requirements is to use alternative technologies for iron and steel making. For the alternative technologies the costs of raw materials and preparation is not so high especially if they are by-products from own or related industries. The environment protection is double, directly because the waste will be recycled in-works and not land filled and indirectly because the natural resources will be preserved.

In the world ferrous metallurgy around 75-80% of wastes are recycled. Unfortunately in the same time in Romania only 40-45 % of them are recycled. There are a lot of problems concerning collection, transportation, storage and recycling of all kinds of wastes from metallurgical and chemical industries. Subsequent problems with maintenance and extension of landfills are expected 1, 3 and 4.

In ferrous metallurgy an important part of the wastes are from blast furnaces (flue dust and sludge), sinter plants (dust and fines) and from EAF's and LD converters (dust and slurry). These kinds of wastes are very fine dusts from electrical dust collectors, wet gas cleaner secondary dedusting system.

Another category of by-products are cinder, mill scales, oily sludge, grinding swarfs. All this iron sources and moreover cheapest iron ore which is not suitable for blast furnace can be used for alternative iron making processes. Pyrite ashes are chemical by-products form sulphuric acid fabrication which could have great importance for ferrous metallurgy because of their high content in iron.

In Romania these kinds of wastes were land filled and the environment was damaged in that area (Valea Călugărească, Turnu Măgurele and Năvodari). The pyrite ashes are very light and in dust presentation (average diameter is 50µm). Land filling with this waste has lead to severe environmental impact on air, soil and surface and underground water in extended areas than landfills. It is creating a much polluted environment in plant proximity and affects also their own equipments and control devices, moreover agricultural areas are unproductive.

All types of low cost carbon bearing materials such as medium and low volatile coals, coke fines, coke breeze, graphite, pet coke, ground electrodes and toner can be used as reductants.

Taking into account the above mentioned reasons and the existence of such kind of wastes suitable for recycling Romania has to initiate projects in the alternative iron making area. This will be a good step for both steel industry and the environment.

Moreover, it will enhance the level of integration in the European Union.

4. EXPERIMENTS

Direct reduction processes are widely known alternatives for the blast furnace route to iron manufacture. In direct reduction rotary kilns, the solid reductant serves the purpose of both fuels and reducing agent.

In order to make estimation about using pyrite ashes and blast furnace dust like raw materials for a direct reduction process some preliminary experiments have been conducted.

For direct reduction experimental heats a lab scale rotary furnace with 2kW electrical resistance was used (figure 1). Internal space has a cylindrical shape with 200mm diameter and 350mm length. The raw materials chemical compositions used for the experimental heats are presented in table 1. The reduction and combustion agent was fine coal (87,5% carbon, 1% sulphur, 11% ash, 1,5% volatile) with dimension between 0 - 5mm.



Figure 1. Rotary furnace for direct reduction

(figure 1). Internal space has a cylindrical shape with 200mm diameter and 350mm length. The raw materials chemical compositions used for the experimental heats are presented in table 1. The reduction and combustion agent was fine coal (87,5% carbon, 1% sulphur, 11% ash, 1,5% volatile) with dimension between 0 - 5mm.

Table 1. Chemical composition of raw materials (%)

Raw material	Fe	Mn	SiO ₂	CaO	MgO	Cu	Pb	Zn	K	As	Al ₂ O ₃
Blast furnace dust	41,2	1,03	9,28	9,76	1,8	0,01	0,2	0,86	0,14	-	0,05
Pyrite ash Valea Călugărească 1	51,4	-	6,8	-	-	0,46	0,53	1,13	-	0,01	-
Pyrite ash Valea Călugărească 2	53,5	-	7,0	-	-	0,5	0,5	1,1	-	0,6	-
Pyrite ash Turnu Măgurele	51	-	6	-	-	0,35	0,25	0,4	-	0,25	-
Pyrite ash Năvodari	53	-	5	-	-	0,5	0,3	1,1	-	0,4	-

The raw materials (dusts and coal fines) were introduced in the rotary furnace together with a dispersion agent. This agent consists in 10-12 mm diameter wear resistant ceramic balls. Around 1, 5 kg ceramic balls were introduced. The role of the dispersion agent was to mix the charge increasing the reaction area, initiating the direct reduction process and preventing floating of coal on the raw materials. The types of charge and experimental conditions are depicted in table 2. The temperature was measured with a Pt/Pt-10%Rh thermocouple coupled with a digitally display device. In order to melt the obtained iron base powder a Tammann furnace was used. The samples of iron base powder from each charge were melted at 1700°C in 10-15 minutes, in reductive atmosphere in graphite or alumina crucibles.

Table 2. Experimental conditions

Sample	Charge	Temp., °C	Reaction time (min)
1	1 Kg, blast furnace dust + 0,3 Kg coal fines	900	30
2	1Kg pyrite ash Valea Călugărească 1+ 0,3 Kg coal fines	920	30
3	1 Kg pyrite ash Valea Călugărească 2 + 0,3Kg coal fines	940	30
4	1 Kg pyrite ash Turnu Măgurele + 0,3 Kg coal fines	820	30
5	1 Kg, pyrite ash Năvodari + 0,3 Kg coal fines	880	30

5. RESULTS

The products resulted from direct reduction process were: iron base powder, combustion gas, sterile. The iron base powder was separated from sterile with a permanent magnet. The analysis of combustion gases shown that they contain around 70-75% CO.

The resulted iron base powders from each charge were chemically analyzed. For iron base powder the metallization degree was establish with this formula:

$$M = \frac{Fe_{met}}{Fe_{tot}} \cdot 100 ,$$

Fe_{met} – metallic iron%, Fe_{tot} – total iron%

The results are depicted in table 3.

After melting iron base powder in a Tammann furnace, the crucibles were quenched and the slag and the metal phases were separated, weighted and analyzed. The results for the metallic phase are depicted in table 4.

Table 3. Chemical composition of iron base powder

Sample	Fe total	Fe metal	M, %	Cu	Pb	Zn	As
1	56,08	50,55	90,1				
2	61,8	55,87	90,4	0,37	0,18	2,05	0,09
3	60,55	56,3	93	0,32	0,72	0,97	0,09
4	55,97	41,4	74	0,31	0,07	0,86	0,07
5	63,29	55	86,9	0,34	0,06	2,08	0,05

Table 4 – Chemical composition of metallic phase

Nr	Metallic sample from:	C %	Mn %	Si %	S %	P %	Fe %
1	Blast furnace dust	4,00	0,62	2,30	0,074	0,135	92,87
2	Pyrite ash Valea Călugărească 1	3,25	0,60	2,75	0,054	0,141	
3	Pyrite ash Valea Călugărească 2	3,30	0,55	2,84	0,047	0,148	
4	Pyrite ash Turnu Măgurele	3,40	0,25	3,04	0,0281	0,146	93,13
5	Pyrite ash Năvodari	2,90	0,22	1,89	0,0136	0,108	94,86

After the melting of the obtained powder bath it is rich in iron, around 85-95%, and also with carbon that is necessary to eliminating the gases and nonmetallic inclusions. The contents of sulphur and phosphorus are not bigger than an usual pig iron as well as those of mangan and silicium.

6. COMMENTS

The iron base powder resulted from direct reduction can be used in steel making (powder injection in EAF, after briquetting as scrap substitute in LD, induction furnace, EAF), or raw material for ductile cast iron or other cast iron qualities.

The sensible heat of directly reduced iron can be utilized by hot charging in the above mentioned melting facility in order to increase the efficiency of the method.

The forecast of the authors to obtain a metallization degree of 85-90% was reached. But, the scale of the rotary lab furnace had a negative influence on direct reduction processes. For industrial scale we predict a metallization degree of 95% in 1/2 hour.

The forecast for energy consumption in industrial scale plant is around 2,2 Gcal/tFe under the present values 3,5-3,9 Gcal/tFe in other direct reduction processes. Future work has to take into account the recovery of other wastes (EAF, LD, and mill scale etc) and poor iron ore. Moreover topics concerning for example influence of raw material average diameter on reduction degree, slag basicity after melting, removal of sulphur and phosphorous, avoidance of ash sticking on the refractory walls and dispersion agent (balls) should be analyzed. In order to enhance the level of research and to propose a new alternative efficient direct reduction technique is necessary also to improve the experimental device: charge-discharge technique, gas energy recovery, pollution control and continuity of the process.

Efficient recycling metallurgical and chemical industries wastes and waste management are important topics in the European Union.

Taking into account the quantities of these kinds of wastes Romania should solve the problem by developing projects in the alternative iron making and steel making area. According to preliminary researches carried out this is very possible without big financial efforts.

The advantages of direct reduction processes are: using of waste from chemical and metallurgical industry and unmaking coal, small quantities of electrical energy, easy preparation of raw materials, small plants very flexible for different raw materials, high level of environment protection, minimization of land filling of wastes/by-products, saving natural raw materials utilizations.

Implementing at large scale this kind of technologies offers the steel industry flexibility and a chance to decrease the costs of products in the frame of environmental friendly processes.

REFERENCES

- [1.] N Constantin: „Procedee neconvenționale de obtinere a materialelor metalice feroase.” tipărit Editura PRINTECH București, 2002
- [2.] N. Constantin, M. Nicolae, V. Geantă and I. Butnariu: „Procese și tehnologii alternative în siderurgie.” Ed. Fundația Metalurgia Română, 1997, ISBN 973-98314-0-0
- [3.] N. Constantin, V. Geantă, M. Nicolae: „Procedee neconvenționale de reducere a minereurilor feroase.” tipărit Universitatea "Politehnica" București, 1995
- [4.] N. Constantin, V. Geantă, B. Niculae, R. Ștefănoiu: „Modelarea matematică și conducerea informatizată a proceselor din metalurgia extractivă feroasă.” - tipărit Universitatea "Politehnica" București, 1997



¹: Alina MIHAIU, ²: Claudiu CONSTANTIN, ³: Cristian DOBRESCU

SOME COMPUTATIONS REGARDING THE DIRECT REDUCTION OF THE IRON ORES

^{1, 2, 3}: UNIVERSITY "POLITEHNICA" OF BUCHAREST, ROMANIA

ABSTRACT:

In this paper, we present a technological solution to reduce the iron ores and specifically the zunder, broken in small pieces, in fluidized bed, where the energetically source and simultaneously, reducing thermal agent, is coal, eventually associated to another gaseous or liquid fuel, without use of technical oxygen; the forming of CO and heat are obtained by the oxidation of the coal and hydrogen from the fuel, by making use of the oxygen contained in the initial raw material.

KEYWORDS:

iron ores, zunder, small pieces, fluidised bed

1. INTRODUCTION

The nowadays technologies of cast obtaining starting from coal ores, subdued, before being introduced into the blast furnace, to some agglomeration and coking operations, use the furnace as the main elaboration aggregate. It is well known that in Romania the furnace departments are endowed with medium and big blast furnaces, having 1000...3500 m³.

Because of the lower demand of cast into the internal consumption, a series of furnaces has been closed, and those which still run are forced to work very slowly, registering small productivities, big materials and energy consumptions, resulting implicitly big production costs for the elaborated cast.

Because of the binding coal deficit and of the iron ores of a good metallurgical quality, the first fusion cast quantities necessary to the steel elaboration or to the cast pieces moulding are more and more difficult to ensure. Corroborated to the scrap iron deficit, this problem creates considerable difficulties to the steel producers. Thus, it imposes an alternative technology which allows the obtaining of the unconventional energo - technological resources from ferrous and coals wastes with small granulation which will be used as scrap iron substitute into the steel elaboration aggregates.

All over the world, the industrial implemented technologies allow the iron sponge obtaining from ball ore, reduced at Fe by a decelerator, usually gaseous (Hyl, Midrex, Wiberg, Purofer methods), from small ores reduced in layer fluidized by a gaseous decelerator (H₂, CO, H₂+CO) (Novalfer, Nu-Yron, H-Yron) or from balls ores and balls solid decelerator into circular furnaces (SLRN, Krupp - Renn).

The cast is directly obtained from coal and ores as a result of some alternative technologies (Corex, Kawasaki and Midrex) which suppose investments costs heavily supported by the economic agents from Romania, even in the conditions of some eventual associations.

Those being the conditions, the unconventional technology proposed by this research works allows the iron sponge obtaining with a high metallization degree, and afterwards, by its melting, the cast obtaining directly from small iron ores and from small coal into a main aggregate as a rotary tube furnace type where the dispensor mass, the thermic agent and the heat changer are represented by metallic or ceramic granules heated beforehand at about 1300°C into an aggregate which uses as an energetically fluid a re-circulated gas from its own process of fabrication.

Through the processes efficient leading they can obtain unconventional energo-technological resources having a high metallization degree used as scrap iron substitute by the steel producers.

It is necessary to mention that in Romania this technology is 100% original. So far there are no research units having such kind of preoccupations.

The proposed technology realizes with minimum technological and economical costs a very good scrap iron substitute, starting with the capitalization of some fine ferrous sub-products found as stored wastes.

2. EXPERIMENTS

2.1. Some theoretical considerations

One considers a raw material, formed by: 76 % FeO, 17 % Fe₃O₄, 2 % Fe₂O₃ and 5 % SiO₂. The content of Fe in the raw material will be: $76 \frac{56}{56+16} + 17 \frac{3 \cdot 56}{3 \cdot 56 + 4 \cdot 16} + 2 \frac{2 \cdot 56}{2 \cdot 56 + 3 \cdot 16} = 59.1 + 12.3 + 1.4 = 72.8\%$.

The oxygen extracted by a complete reduction is: $76 \frac{16}{72} + 17 \frac{64}{232} + 2 \frac{48}{160} = 16.9 + 4.7 + 0.6 = 22.2\%$ (SiO₂ is not reduced).

The consumption of raw material is: $\frac{1}{0.728} = 1.374$ t / t Fe, from which one extract 1.374 x 0.222 = 0.305 t O₂/t Fe, theoretically refound, at 1050°C, in 73.1 % CO and 26.9% CO₂, and practically in 75 % CO and 25 % CO₂. 1Nm³ from this mixture contains 0.75 x 0.5 + 0.25 x 1.0 = 0.625 Nm³ O₂/Nm³ = $0.625 \frac{32}{22.414} = 0.8923$ kg O₂/Nm³ and $\frac{12}{22.414} = 0.5354$ kgC/Nm³.

From reduction, it will result 305/0.8923 = 342 Nm³/tFe and one consume 342 x 0.5354 = 183.1 kgC/t Fe.

The heat ceded by the carbon refound in the gaseous mixture is: 0.25 x 8.140 + 0.75 x 2.452 = 3.874 kcal / kg C = 0.7093 Gcal/t Fe.

The consumption of heat for the ore reduction is 0.76 x 1150.5 + 0.17 x 1583 + 0.02 x 1758 = 1178.7 kcal/kg Fe = 1.179 Gcal/t Fe. The carbon necessary to deoxidations has an energetic share of 183.1 x 8140 x 10⁻⁶ = 1.490 Gcal/t Fe.

The surplus is equal to 1.490 – 1.179 = 0.311 Gcal/tFe and it is consumed in the heat dissipations, in the drying of raw material (with 5 % water) and the coal drying (with 15 % water) and in the evacuation of the substances emerged with some sensible heat.

The burning of the reducing gaseous combustible fuel is made with 1.1 x 0.75 x 0.5 / 0.21 = 1.964 Nm³ air/Nm³ mixture (with air excess of 10 %) and yields 1.000 (CO₂) + 0.79 x 1.964 (N₂) + 1.964 x 0.21 – 0.75 x 0.5 (O₂) = 2.589 Nm³ burning gas for any Nm³ gaseous mixture, with 38.6 % CO₂, 59.9 % N₂ and 1.5 % O₂.

In the focus-tubes, the gaseous mixture cedes 8.140 - 3.874 = 4.266 kcal/kg C = 4.266 x 0.5354 kcal / Nm³_n mixt. = 2.283 kcal / Nm³ gas.mixt. (= 0.75 x 68.220 / 22.414, as control).

For the gaseous mixture (75% CO și 25 % CO₂), at 1050°C, C_p = 0.75 x 0.339 + 0.25 x 0.530 = 0.387 kcal / Nm³K, and at 950°C, C_p = 0.75 x 0.336 + 0.25 x 0.522 = 0.382.

The gas of complete burning, with 10% air excess, have C_p at 1200°C, which represents the temperature at the emergence from the focus-tubes, of 0.386 x 0.541 + 0.599 x 0.339 + 0.015 x 0.358 = 0.417 kcal/Nm³K, and at 150°C (at the evacuation from exchangers), of 0.386 x 0.416 + 0.500 x 0.311 + 0.015 x 0.317 = 0.352 kcal/ Nm³K.

In order to avoid the gluing of the iron particles and faillit between them, at 1050°C= the temperature in the reactor in fluidised bed, one recirculates in reactor a mass of dust (silica, alumina, silicium carbide etc.), with a relatively high refractoritaty and such that, associated with the sterile from the ore and with the coal ash, totalize about 50% massic și 120% volumic in comparison with the iron.

2.2. A short description of the proposed solution

The raw material and the coal, both at a granulation under 1...2 mm, are introduced in a reactor with fluidised bed, at a flow of gas formed at 600...1050°C, recirculated in the proportion required by bed; the energy necessary for the continuity of the endothermic processes of the deoxidation is assured by the focus-tubes, where the gaseous fuel, coming from the space of reduction, is burnt with air preheated at 1000°C by the combustion gas collected from the focus-tubes.

The temperature in reactor is about 1050°C, in the case of use of coal only and sensibly diminished if this is associated with the gaseous fuel; the reactor operates at a pressure up to 10 bars (limited by the pressure of the gaseous fuel). If the raw material is particularly FeO, as in the case of zunder, considered in subchapter 2. 1, then one gets an excedent of gas, greater if less coal is used.

Due to the reduction of the iron ore in solid phase, the iron carburation is less than 0.8 %, much better than in the case of the liquid pig iron. In the case of iron ores having much sterile, the iron and sterile evacuation are made under the Curie point, thus allowing the sterile elimination by magnetic separation. As advantages of the technology, one mention: the possibility of iron ore reduction with inferior coal and waste coke, the consumption of fuel being smaller in comparison with the actual technologies, including the COREX procedure, diminishing the production of the „ gas export”.

Another important point is that no technical oxygen is used, being enough the oxygen from raw material. Due to the intensification of the heat and mass transfer, the plants applying the technology will be compact and cheap.

In what follows, we present as an example, the main components of a plant which yields 3 t/h iron, from the raw material initially considered, in subchapter 2. 1.

The iron ore from a silo enters the plant, being mixed up with coal; the mixture enters a preheater, then a reactor, organized as fluidised bed, where it takes place the reduction of the oxides from ore, with C, CO, H₂; in order to proceed the endothermic reactions, the heat consumption is recovered by burning gaseous fuel in the focus-tubes.

The reactor has a cylindrical construction, with a vertical axle, having the interior diameter about 3000 mm and the interior height of the fluidised bed of 1700 mm and that total of 3000 m, with walls in refractory concrete, plating with corindonic plates for max. 1300°C. The focus-tubes will have the diameter 120 mm, the length 2400 mm and the wall thickness about 10 mm, being carried-out of vibrated casting alumina.

The ore heater is vertical and has as a shape of truncated cone, with 9 fluidised beds in series, with a total height of about 3000 mm and the inferior diameter 1100 mm and that superior 2500 mm; the maximum interior pressure is 0.8 manometric bars at the inferior part, the construction of the heater being carried-out of usual materials for 900°C. The deoxidated ore is evacuated by a hook-up and cooled.

The ore cooler is similar to the ore heater, having the pressure at the inferior part of 1.5 manometric bars and at the superior one of 0.8 manometric bars, for max. 1100°C.

The circulation of nitrogen (in fact air with the oxygen retained by a small share of carbon), with the flow of 4200 Nm³ /h, is assured by a compressor with a flow 1.7 m³/s which compress it at 1.6 bars, by consuming max. 100 kW.

The plant also includes a compressor which compresses 0.8 m³/s gaseous combustible mixture at max. 80°C, from 3 to 3, 5 manometric bars and is mounted in a metallic precinct, where a pressure of 3 bars is setting up; the consumed power is only 5 kW. There also is an air ventilator for 800 m³ / h and 150 mm water spout (CA), trained by a motor of 1 kW; one also needs an exhaustor for the burning gas, for 1300 m³ /h at max. 200°C and 200 mm water spout, trained by a motor having an installed power of 3 kW (that consumed being of 1.2 kW).

The plant also includes two metallic silos, each 50 m², one for ore and another for coal, raised at about 14 m height.

The specific consumption of heat is about 1.55 Gcal / t Fe and it is recovered exclusively by the carbon from coal; one can also use of small coke, coke dust or coke of oil with an acceptable content of sulphur. One can also use any liquid or gaseous fuel , replacing partially or even totally the coal , remarking that , on a hand , the temperature of reduction decreases and , on the other hand , the production of excedentary gaseous combustible increases.

In order to avoid any glueings of the particles of iron ore in evolution, we have above underlined some sure measures and cautions.

The plant is highly ecological: indeed, the component CO circulates by airtight pipes only, the gas evacuated in atmosphere result after a complete combustion, without CO, NO_x or dioxins (by an air excess 20 % and by burning at favourable temperatures).

The plant can be carried-out with materials of current use.

3. RESULTS

In order to simplify the thermic and mass balances, one considers that the dried raw material and the coal (only dried C) are introduced in the plant together with 500 kg sterile per any tone of iron. One admits that the drying of the iron ore and coal takes place in the reactor (water is benefic, by the dissociation and reassociation in reactor, with the catalytic effects of the transient H₂, which proceed from some water molecules and is reformed in others; in fact, H₂ and H₂O spreads through the ore easier than CO and CO₂). The temperature of reduction descends towards 800°C, with a metallization degree over 99 % and, by replacing the coal with liquid and/ or gaseous fuel, which massively generates H₂ in reactor, the temperature could descend to 570°C. But one

encounters the disadvantage of producing some excedentary gaseous combustibile, which cannot be available in the plant and must be exported.

In what follows, we present the thermic balance and the mass balance on the components of a plant which produces 1 t iron, under the above mentioned hypothesis:

Component	kg	Nm ³	°C	kcal
1. COOLER OF REDUCED ORE				
Inputs				
- Reduced ore=iron +sterile	1069	-	1050	199796
- Ash + sterile	431	-	1050	126714
- Nitrogen	-	965	100	30012
TOTAL				356522
Outputs				
- Reduced ore	1069	-	200	29290
- Ash + sterile	431	-	200	17240
- Nitrogen	-	965	950	304361
- Dissipations				5631
TOTAL				356522
2. PREHEATER OF THE COMBURENT AIR				
Inputs				
- Burning gases	-	569	1200	284728
- Air	-	672	0	0
TOTAL				284728
Outputs				
- Air	-	672	1100	251328
- Burning gases	-	569	150	30043
- Dissipations				3357
TOTAL				284728
3. PREHEATER OF NITROGEN WITH BURNING GASES				
Inputs				
- Burning gases	-	316	1200	158126
- Nitrogen	-	413	100	12844
TOTAL				170970
Outputs				
- Burning gases	-	316	200	22752
- Nitrogen	-	413	1050	145273
- Dissipations				2945
TOTAL				170970
4. PREHEATER OF ORE AND COAL				
Inputs				
- Nitrogen from 1	-	965	950	304361
- Nitrogen from 3	-	413	1050	145273
- Ore	1374	-	0	0
- Carbon	183.1	-	0	0
- Ash	150	-	0	0
- Recirculated sterile	281	-	200	11240
TOTAL				460874
Outputs				
- Nitrogen	-	1378	100	42856
- Iron ore	1374	-	880	263588
- Coal	183.1	-	880	53172
- Ash + recirc.sterile	431	-	880	92924
- Dissipations				8334
TOTAL				460874
5. THE PLANT OF REDUCTION (REACTOR)				
Inputs				
- Iron ore	1374	-	880	263588
- Coal – sensible heat	183.1	-	880	53172
- Coal- potential energy	(183.1)	-	880	1490434
- Ash + recirc.sterile	431	-	880	92924
- Gas. mixt. –sensible heat	-	283	1050	113511
- Gas. mixt. – potent.heat	-	(283)		646089
- Preheated air	-	672	1100	251328
TOTAL				2911046

	Outputs			
- Heat for reduction	-	-	1050	1179000
- Reduced ore	1069	-		
- Ash + sterile	431	-	1050	199796
- Gas. mixt. – sensible heat	heat -	342	1050	126714
- Gas. mixt. potent heat	-	342		137176
- Supplem. cooling of the recirc. gas. mixture	-	700		780786
- Burning gases	-	885	1200	23450
- Dissipations				21270
TOTAL				2911046

4. DISCUSSION

The nitrogen from the system of ore heating - cooling is formed in some minutes after the air introduction, which loses the oxygen retained by a part of the carbon from the heater of ore and coal.

The carbon imposed by deoxidations brings more heat than the plant consumes and this implies the production of that excedentary gaseous combustible (59 % Nm³/t Fe = 0.16 Gcal / t Fe, hence over 10 % of the coal contribution), however about 10 times less than the COREX technology. One also mentions that the final iron will contain only 0.5 % = 5 kg C / t Fe, due to the ore reduction in solid phase (in liquid phase this content would be at least 4 %).

From the above balances, it follows that the specific consumption of carbon is 183.1 kg / t Fe, imposed by the deoxidations, but including the production of the excedentary gaseous combustible; adding the carburization of the final iron, all lead to a specific consumption of 1.52 Gcal / t Fe = 6.36 GJ / t Fe. The above mentioned excedent is less than 60 Nm³/ t Fe.

The total energy entered the plant is:

$$E = 183.1 \times 8140 \text{ kcal} = 1490434 \text{ kcal} \approx 6240 \text{ MJ} .$$

The dissipations of all 5 components included in the above balances cumulate: $\delta = 5631 + 3357 + 2945 + 8334 + 21270 = 41537 \text{ kcal} \approx 174 \text{ MJ}$ (representing about 3% of E).

Other losses are, according the above balances the following: the supplementary cooling (from the component 5 – the reactor): 23450 kcal; the burning gas (from 2): 30043 kcal; the burning gas (from 3): 22752 kcal; the ash+ sterile (from 1): 17240 kcal; the reduced ore (= iron + sterile from 1): 29290 kcal and finally, the excedent of sensible heat (from 5): 137176 – 113511 = 23665 kcal. All these totalize:

$$\lambda = 146440 \text{ kcal} \approx 613 \text{ MJ} \text{ (representing about 10 \% of E).}$$

The energetic efficiency of the plant is:

$$1 - (\delta + \lambda) / E = 1 - (174 + 613) / 6240 \approx 0.874 = 87.4 \text{ \%} .$$

This is superior to many similar technologies. Moreover, the above presented technology could be improved in many points: the useful cooling of the excedentary gaseous combustible (for instance, to heat the raw material and the coal), the sell of this excedent, the use of the sensible heat to produce hot water.

5. CONCLUSIONS

The implementation at the industrial level of the unconventional technology proposed by the present research paper, offers new and profitable adaptation possibilities without high costs of the Romanian metallurgy to the international economic situation imperatives.

From the multiple offered advantages it mentions the following:

- ❖ the reduction of the un-oxidization processes lasting from at least 20 hours to 0,5 hours;
- ❖ the direct utilization of the ore powder, eliminating the granulation;
- ❖ the capitalization of the pyretic ashes and the dusty ores;
- ❖ the capitalization of the waste chalk obtaining an acceptable quality lime and a carbon dioxide of high purity having multiple utilizations;
- ❖ the cheapness under 70% of the obtained iron, provided in granules;
- ❖ the utilization of the non-binding coal instead of the coke;
- ❖ there is no necessary another type of energy;
- ❖ the charge preparation is not so expensive as in blast-furnaces case;
- ❖ small units of production permit the easy adaptation at diverse requests.

REFERENCES:

- [1.] COREX, a revolution in iron making, Voest Alpine Industrie, 2001.
- [2.] C.STĂNĂȘILĂ, N. CONSTANTIN, O. STĂNĂȘILĂ – O posibilitate de reducere directă a minereurilor de fier, Conf. Naț. de Metalurgie , 2006.
- [3.] C. STĂNĂȘILĂ, N. CONSTANTIN, O. STĂNĂȘILĂ – New technology on coal drying, Metal. Intern, vol.11, nr. 1, 34-38, 2006.





¹Vasile PUȚAN, ²Adriana PUȚAN

DESULPHURATION OF STEEL WITH SYNTHETIC SLAG WITH ADDITION OF TITANIUM OXIDE

^{1,2} UNIVERSITY "POLITEHNICA" TIMIȘOARA, FACULTY OF ENGINEERING OF HUNEDOARA, ROMANIA

ABSTRACT:

In the practice of deoxidation with synthetic slag, we usually use the slag from the binary systems: CaO-Al₂O₃, CaO-TiO₂ and CaO-CaF₂ or from the ternary systems: CaO-SiO₂-Al₂O₃ and CaO-CaF₂-Al₂O₃. According to the literature, the best results were obtained with synthetic slag from the binary system CaO-Al₂O₃ (50-52% CaO and 38-42% Al₂O₃).

The paper presents the results of laboratory experiments on steel desulphurisation with slag from the system CaO-SiO₂-TiO₂.

To determine the influence, on the desulphurisation process, of the titanium oxide added in calcium aluminate slag, we experimented, in the laboratory phase, the steel treatment with a mechanical mixture consisting of lime, aluminous slag and slag obtained from the titanium making process through the aluminothermic technology.

During the research, we aimed to establish correlation equations between the sulphur distribution coefficient and the slag components (CaO, Al₂O₃, TiO₂, FeO, MgO and MnO). The data obtained in the experiments were processed in Excel and MATLAB programs, resulting simple or multiple correlation equations, which allowed the elucidation of some physical-chemical phenomena specific to the desulphurisation processes.

KEYWORDS:

steel, deoxidation, desulphuration, synthetic slag

1. GENERAL CONSIDERATIONS

In case of electric steel works, the sulphur reaches in the steel bay from the metallic charge and from adding's. Because the sulphur content of these sources cannot be lowered below certain limits, the elaboration process must be so developed to perform an advanced desulphuration, both in the oven and in the casting ladle. During the last years, it is more and more manifested the tendency to perform the desulphuration outside the elaboration aggregates (desulphuration with synthetic cinders under vacuum, with reactive powders injection), obtaining this way important energy saving, deoxidizers and desulphurants, as well as an productivity increase [1,2].

The steel refining with liquid slag or various powder mixtures of synthetic slag is based on the intensification of the unwanted impurities (sulphur, non-metallic suspensions & oxygen) passage from the liquid steel in the slag, mainly by diffusion, or partly through the entrainment of some suspensions by settling the synthetic slag particles found in the treated steel bath. The synthetic slag can be also obtained by adding mechanical mixture directly in the casting ladle; in this case, for compensating the cooling of the steel in the casting ladle due to the addition of materials (melting and superheating), the steel temperature should be at least 20-40°C higher than the normal one. In the practice of deoxidation with synthetic slag, we usually use slag that correspond to the binary systems CaO-Al₂O₃, CaO-TiO₂ and CaO-CaF₂, or to the ternary systems CaO-SiO₂-Al₂O₃ and CaO-CaF₂-Al₂O₃. According to the literature, the best results were obtained with synthetic slag that corresponds to the binary system CaO-Al₂O₃, containing 50-52% CaO and 38-42% Al₂O₃.

The viscosity of the synthetic slag has significant influence on the development of physical and chemical processes during the treatment of the liquid steel, interfering with significant weight on the emulsifying capacity of slag. The increase of the slag viscosity from 0.15 to 0.45 Ns/m² (from

1.5 to 4.5 Poise) determines the decrease with approx. 30% of the steel-slag interaction surface. Such increasing of the calcium aluminate slag viscosity can be seen when its temperature is decreasing (for example, from 1600°C to 1470°C). Therefore, it is very important to ensure, during processing the steel with liquid slag, the optimum thermal regime specific to the chosen slag type and to realise its convenient fluidity (viscosity).

The viscosity of the synthetic slag is also influenced by other components; it increases significantly with the increasing of the SiO₂ content, while MgO contents up to 8% are favourable. At temperatures higher than 1500°C, the viscosity is slightly decreasing when adding TiO₂ in the calcium aluminate slag.

2. LABORATORY EXPERIMENTS

To determine the influence, on the desulphurisation process, of the addition of titanium oxide in the calcium aluminate slag, we performed laboratory experiments, i.e. we treated the slag with liquid synthetic slag obtained by melting the mixture consisting of limestone, aluminate slag and slag obtained from the titanium making process through the aluminothermic technology.

The steel melting was carried out in an induction furnace of 10 kg capacity and the slag melting was carried out in a crucible furnace, both existent in the "METALLIC MELTS" laboratory of the Engineering Faculty of Hunedoara.

The charge to be melted consisted of steel samples (samples of steel for tubes, taken from the casting ladle before the LF treatment, i.e. before introducing the steel in the LF).

To form the liquid synthetic slag, we melted in the crucible furnace a mechanical mixture consisting of limestone, calcium aluminate slag (from melting the aluminium scrap) and slag obtained from the titanium making process through the aluminothermic technology. The steel quantity obtained was 10 kg/heat, and the addition of liquid slag was 3% (300 g/heat). The synthetic slag was added directly in the casting ladle; so, the slag reached the ladle before the steel, ensuring a good mix between the two melts. To determine the sulphur distribution coefficient, we took steel and slag samples before and after the treatment, to find the sulphur content and the chemical composition. We also measured the steel and slag temperature before and after the treatment.

3. RESULTS OBTAINED FROM PROCESSING THE EXPERIMENTAL DATA

By processing the data obtained in the laboratory phase, we obtained equations of correlation between the chemical composition of the synthetic slag and the sulphur distribution coefficient (L.S). The data were processed in Excel and MATLAB programs, the results being presented hereunder, in graphical and analytical forms.

In Fig. 1, we can see that a TiO₂ content increase up to 5-6% leads to the increasing of the L.S., fact explicable, from a technological point of view, through to the positive influence of the titanium oxide on the slag fluidity, especially at temperatures above 1500°C. Therefore, we recommend contents of 3-6% TiO₂ in the refining slag.

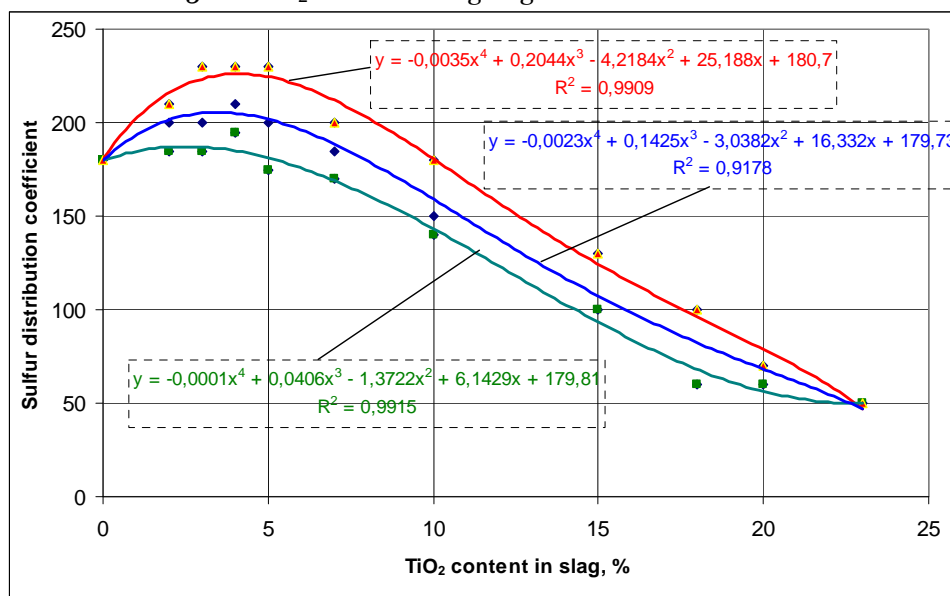


Fig.1 The variation of the sulphur distribution coefficient versus the TiO₂ content in slag

The graphical representation presented in Fig. 1 shows that the higher values for the L.S. (230-250) were obtained for a CaO content of 52 -54%. According to the data presented in the literature [2] the minimum viscosity of the slag that corresponds to the CaO – Al₂O₃ system is obtained for contents of approx. 56% CaO, which confirms the results obtained for the slag used in our experiments. The CaO contents higher than 55%, determine the decreasing of the L.S. values, because the slag viscosity is increasing. Having in view that, in industrial conditions, there are frequent deviations from the above mentioned range of chemical composition, we recommend contents of 52-56% CaO.

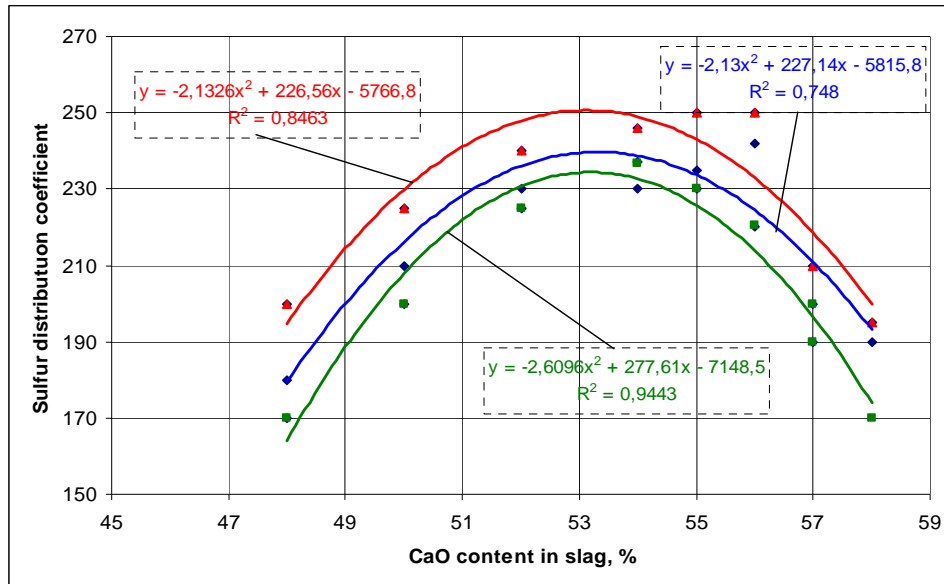


Fig.2 The variation of the sulphur distribution coefficient versus the CaO content in slag

Analysing the graphical representation presented in Fig.3, we can see a variation in the L.S. depending on the Al₂O₃ content, similar to the variation depending on the CaO content in slag. The maximum L.S. value was obtained at 34–37% Al₂O₃. The increasing of the aluminium oxide content up to values that vary between the above mentioned limits is due to the decreasing of the slag viscosity and, in consequence, the intensification of the sulphur diffusion in the slag bath. The increasing of the Al₂O₃ content beyond the above mentioned limits determines the decreasing of the L.S. values, as a consequence of the slag viscosity increasing. We recommend contents of 33-37% Al₂O₃ in slag.

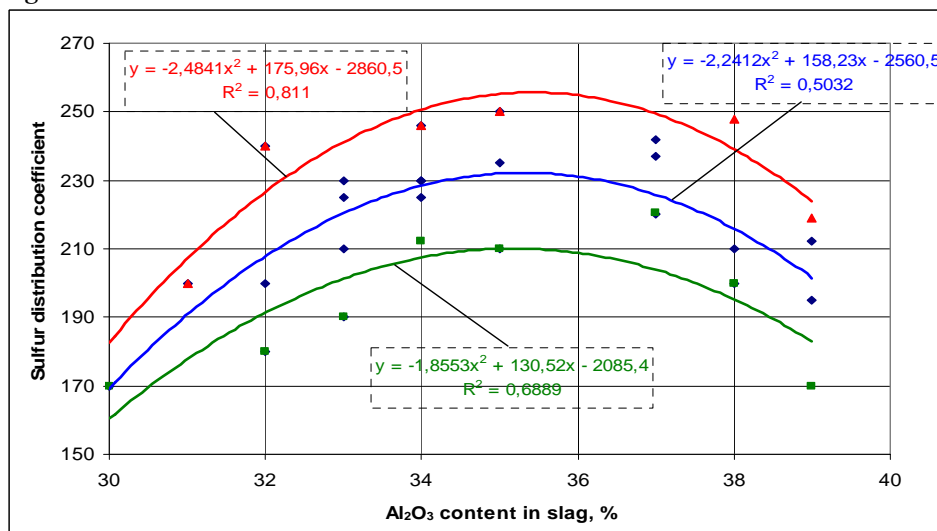
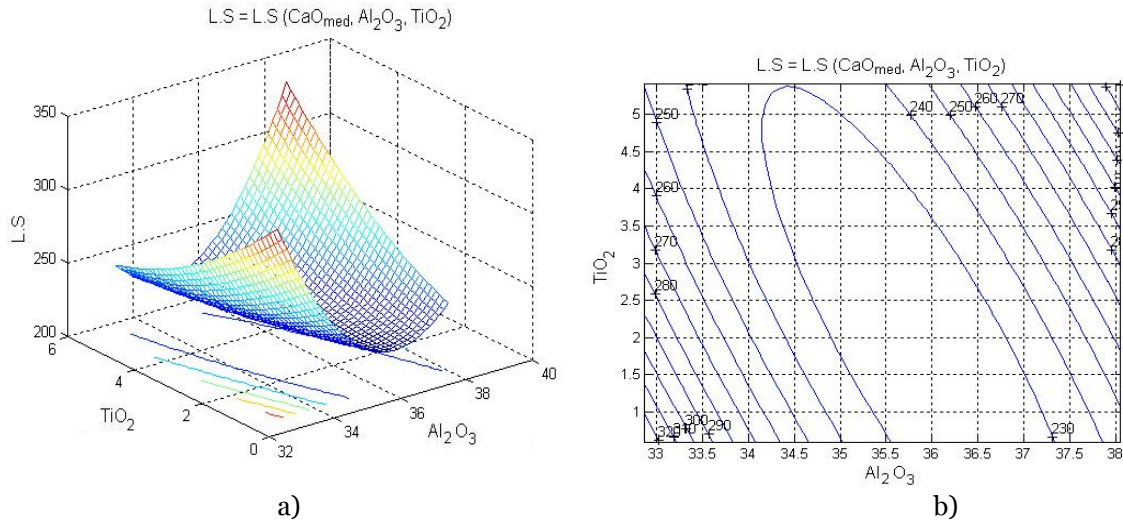
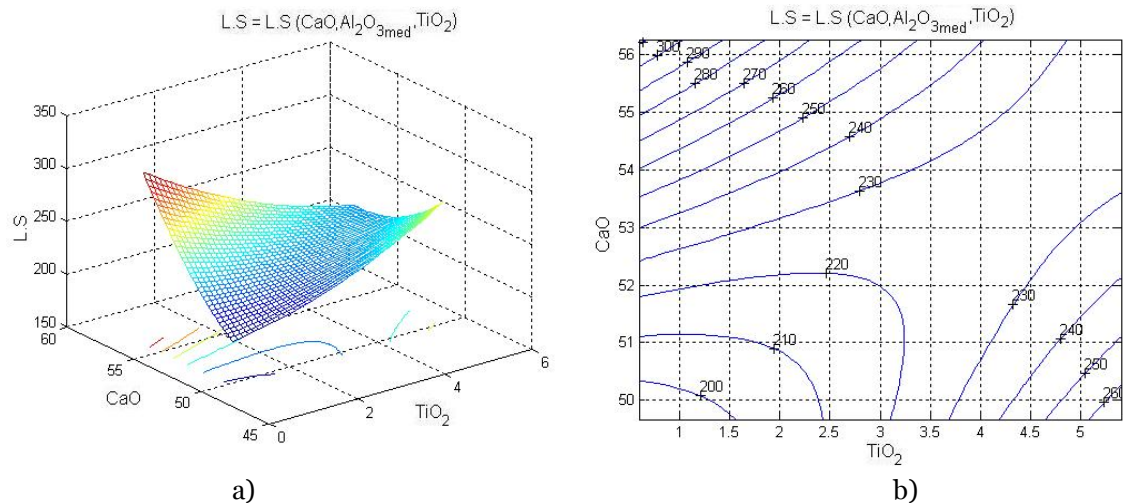


Fig.3 The variation of the sulphur distribution coefficient versus the Al₂O₃ content in slag

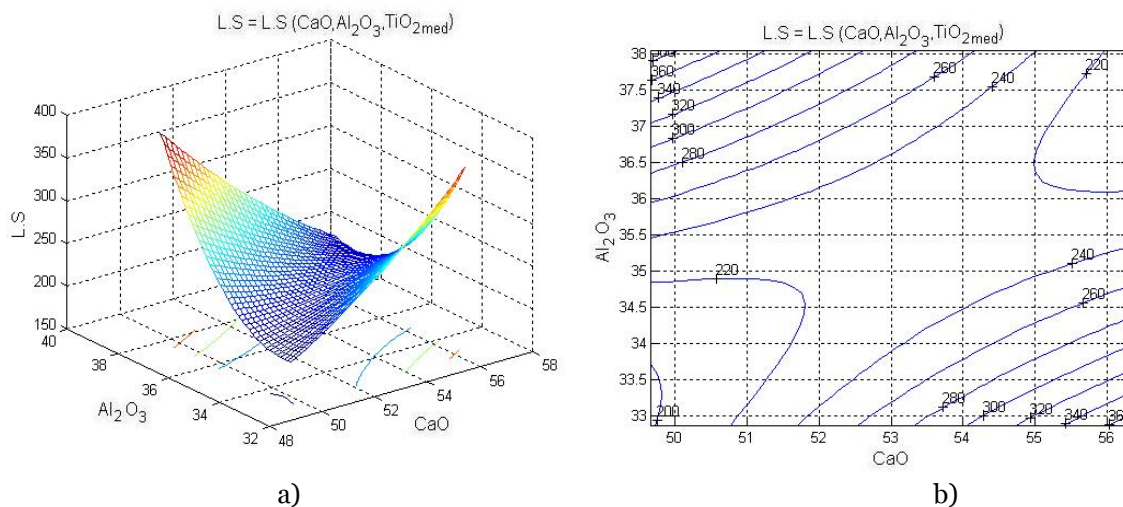
By processing the data in the MATLAB program, we obtained multiple correlation equations and, by graphically represented them, we obtained the correlation surfaces. To establish the optimum chemical composition range, we analysed the regression surfaces for finding the value of the L.S., desirable above the average value obtained from the data afferent to the analysed heats.



a) b)
 Fig.4 The variation of the sulphur distribution coefficient (L.S) versus the TiO_2 and Al_2O_3 content in slag: a) surface; b) contour lines



a) b)
 Fig.5 The variation of the sulphur distribution coefficient (L.S) versus the TiO_2 and CaO content in slag: a) surface; b) contour lines



a) b)
 Fig.6 The variation of the sulphur distribution coefficient (L.S) versus the CaO and Al_2O_3 content in slag: a) surface; b) contour lines

4. CONCLUSIONS

Based on the experiments, on the results obtained from data processing and on the technical analysis of these data, we concluded the followings:

- From a technological point of view, the slag types used in our experiments met our needs, mainly due to their adequate fluidity;
- The chemical composition of the slag has a significant influence on the L.S., either indirectly, due to the viscosity, or directly, due to the affinity of the oxide cautions to the sulphur anions;
- We consider that it is possible to obtain very good results in the desulphurisation process by using synthetic slag having the following chemical composition: $\text{CaO} = 48 - 55\%$; $\text{Al}_2\text{O}_3 = 40 - 45\%$; $\text{SiO}_2 = \text{maximum } 3.0\%$; $\text{MgO} = \text{maximum } 3\%$ and $\text{FeO} = \text{maximum } 1\%$
- Based on the results obtained during the laboratory phase, we believe that good results can be achieved under industrial conditions, too. So, we propose to perform such experiments in a future stage.

REFERENCES:

- [1.] VACU, S., ș.a., Elaborarea oțelurilor aliate vol. I, Ed. Tehnică, București, 1980.
- [2.] VACU, S., ș.a., Elaborarea oțelurilor aliate vol. II, Ed. Tehnică, București, 1980.
- [3.] TRIPȘA, I. PUMNEA, C., Dezoxidarea oțelurilor, Ed. Tehnică, București, 1981.
- [4.] HEPUȚ, T., ARDELEAN, E., KISS, I., Some influence of the viscosity of synthetic slags used in continuous steel casting. Revista de Metalurgia 41(3), Madrid, 2005.
- [5.] HEPUȚ, T., ARDELEAN, E., SOCALICI, A., MAKSAY, ST. GĂVĂNESCU, A., Steel desulphurization with synthetic slag, Revista de Metalurgia 43(3), Madrid, 2007.







¹Mihaela FLORI, ²Bernard GRUZZA, ²Luc BIDEUX, ²Guillaume MONIER,
²Christine ROBERT-GOUMET, ³Jean-Pierre CHERRE, ¹Daniela MILOȘTEAN

INFLUENCE OF MICROSTRUCTURE DEFECTS ON THE PROPERTIES OF 42CrMo4 NITRIDED STEEL

¹"POLITEHNICA" UNIVERSITY OF TIMISOARA, FACULTY OF ENGINEERING HUNEDOARA, ROMANIA

²LASMEA, UMR CNRS 6602, BLAISE PASCAL UNIVERSITY, CLERMONT-FERRAND, FRANCE

³LABORATOIRE DE GENIE CHIMIQUE ET BIOCHIMIQUE, BLAISE PASCAL UNIVERSITY, FRANCE

ABSTRACT:

Metallographic and chemical analyses were done in order to determine the influence of microstructure defects on the hardness of 42CrMo4 steel plasma nitrided in industrial conditions. By means of light microscopy carried out after Picral reagent etching it was revealed the steel sample microstructure presenting defects as segregation bands, probably formed during the elaboration stage of the steel. The Electron Probe MicroAnalysis (EPMA) technique was used for nitrogen and iron concentrations measurements, while HV_{0.3} hardness tests were done for the steel properties determination. Tests were made as vertical profiles and as individual measurements in the nitrided layer and in zones presenting defects, respectively.

KEYWORDS: Plasma nitriding; 42CrMo4 steel; Segregation bands; Picral etching; Light microscopy; Electron Probe MicroAnalysis (EPMA); Hardness measurements

1. INTRODUCTION

Although the behavior of quenched and tempered structural steels treated through plasma nitriding is much discussed in the literature, one may notice that the nitrided layer analysis concerns mainly the resistance to fatigue [1-3], to corrosion [4] or to wear [5]. Also, the microstructural analysis of the nitrided layer is turned on its thickness and nature of the constituent phases obtained by varying the treatment conditions (proportion and nature of the nitriding gases, treatment duration and temperature) [6]. However, there are not well delineated the studies on the defects existing in bulk material (i.e. segregation bands resulted in the solidification stage of the steel ingot) and their influence on the structure and mechanical properties of the nitrided structural steels.

It is known that all elements accompanying iron in low alloyed steels (chromium, manganese, sulfur, phosphorus) participates more or less to dendritic segregation during solidification, this phenomenon being more intense as the steel is rich in carbon. These elements influence the steel structure by forming longitudinal heterogeneities (named "segregation bands" or "microstructural banding"). In references [7, 8] are presented detailed reviews concerning the origins of the chemical segregation, its effects on the solidification structure and its influence on the properties of carbon and alloy steels. Also, reference [9] contains a literature overview on the microsegregation models which describe the alloys solidification phenomenon. The characteristic features of microstructural banding may be observed better by light microscopy after etching with Picral metallographic reagent [10, 11]. After etching, the steel structure appears as adjacent light and dark bands which are oriented in the rolling or forging direction. The non-uniform distribution of some of the alloying elements in the steel structure depends mostly on the austenite grain size and on the cooling rate during solidification [12].

The aim of this article is to study the influence of the banded structure on the mechanical properties of 42CrMo4 steel, plasma nitrided in industrial conditions. In order to evaluate the banded structure we have etched the steel sample with 4% Picral reagent and observed it by light microscopy. In completion with hardness measurements, EPMA chemical analysis and imaging are used.

2. EXPERIMENTAL AND ANALYSIS DETAILS

2.1. SAMPLE PREPARATION

In this study we have used a cylindrical piece (~25 mm diameter and ~10 mm thickness) of 42CrMo4 steel grade whose chemical composition (in wt%) was identified by spark spectroscopy as: 0.43%C, 0.33%Si, 0.78%Mn, 1.02%Cr, 0.17%Mo, 0.1%Cu, 0.11%Ni, 0.02%P and 0.02%S.

In order to obtain the martensitic structure needed for nitriding, the piece was subjected to a heat treatment consisting in: austenitization at 850 °C during 30 min. then water quenching and tempering at 650 °C for 30 min. with further slow cooling in air. Next, the piece was degreased with trichlorethylene and introduced in a Nitron-10 industrial furnace for a conventional plasma nitriding treatment. The working parameters were: pressure of 10^{-2} mbar, applied voltage of 750 V, temperature of 530 °C and maintenance duration of 10 h. The nitriding atmosphere was obtained by ammonia thermal dissociation in 75% H_2 and 25% N_2 , this mixture being introduced in the furnace with a debit of about 20 l/h. At the end of the treatment, the piece was furnace cooled.

Further, the nitrided piece was cut along a diameter into two samples, so all the analyses could be made in the cross-section. After mounting in resin, the two samples were subjected to a metallographic preparation consisted in grinding with SiC papers (having different granulations from 120 to 2500), followed by polishing with diamond (3 μ m size) and finally by fine polishing with an alumina suspension (0.05 μ m size).

One sample (sample A) was used for microstructure observations and hardness measurements, while the other one (sample B) was used for the EPMA analysis. Sample A was etched with the Picral reagent, prepared with 4% picric acid in etilic alcohol and a few drops of benzalkonium chloride. Immersion was made at room temperature for 30 s, followed by ethanol rinsing and drying with hot air. As observed by light microscopy, etching with this metallographic reagent revealed very well the microstructure by differential color etching: the carbides and the metallurgical segregations were darkened, while the iron nitrides remained white.

2.2. DETAILS OF THE ANALYSIS TECHNIQUES

Microstructure observations were done with an Olympus BX60M light microscope.

The hardness was determined with a Mitutoyo Vickers instrument using a ~3 N force ($HV_{0.3}$). Results were obtained as a vertical profile with depth and as individual point measurements in the zones where it was observed the presence of defects (segregation bands).

The chemical analysis was made with a Cameca SX100 electron probe microanalyser (EPMA) employing five wavelength-dispersive spectrometers. Before being analyzed the sample was plated with a graphite layer under vacuum. The experiments were done with the following parameters of the incident electron beam: intensity of 15 nA and accelerating voltage of 10 kV. As standard samples for Fe and N concentration determinations it was used pure iron and BN, respectively.

Also, the EPMA technique permits, besides the chemical analysis, the imaging of the sample surface, so one may better interpret the experimental results. In an EPMA image the brightness (or contrast) of an area is proportional to the backscattered electrons intensity (of the incident beam) depending on the atomic number of the elements present in the sample. So, atoms having high atomic number backscatter the incident electrons strongly and give a bright area in the EPMA image, while atoms with low atomic number give a dark one [13]. Thus, in metallurgical research, using the EPMA technique to study the segregation phenomenon in steels is probably the most important application [13].

3. RESULTS AND DISCUSSIONS

3.1. METALLOGRAPHIC EXAMINATION

The light micrographs obtained in the cross-section of the steel sample plasma nitrided at 530 °C during 10 h are shown in Fig.1.a-d. For the metallographic etching it was used 4% Picral reagent. At low magnification (Fig.1.a) one may observe very well the banded structure. The bands that were etched darkly indicate a zone rich in alloying elements as Mn and Cr [14]. The distance between two successive segregation bands was estimated at about 50 μ m.

Also, etching with Picral reagent permitted identification of the diffusion zone which is formed by two regions: one, situated immediately under the surface, which was darkened and another one which was colored in lighter shades, being positioned under the first one (Fig.1.a). The thickness of the diffusion zone is estimated at about 0.3 mm.

The compound layer (“white layer”) formed on the surface of the steel sample during nitriding may be observed at higher magnification in Fig.1.b. This layer has a thickness of ~3.8 μ m.

In the diffusion zone the nitride precipitations appear as white dots at the grain boundaries (some are marked by the arrows in Fig.1.c). Also, in steel bulk one may recognize the tempered martensite features (Fig.1.d). Immediately after the microstructure observations, the sample was used for the hardness measurements and observed once more by light microscopy.

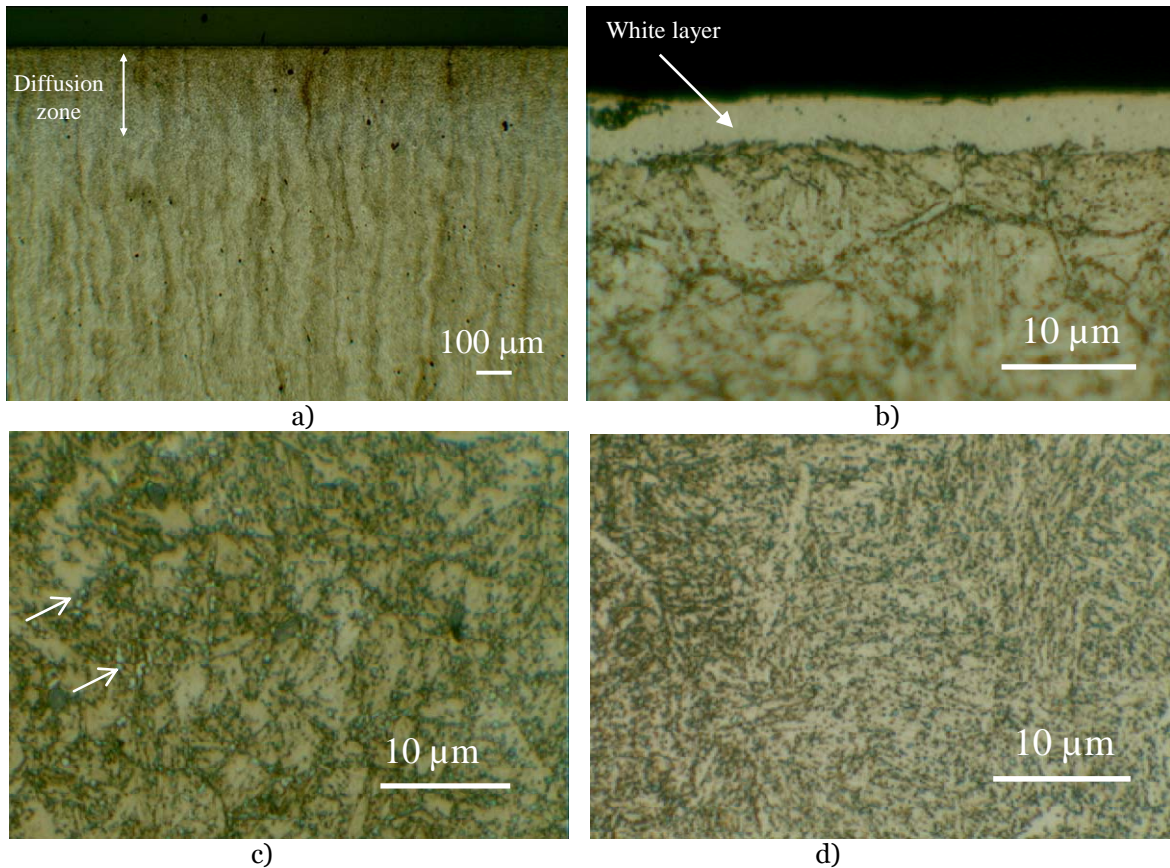


Figure 1. Cross-section micrographs of the nitrided steel sample after 4% Picral etching: low (a) and high magnification, near surface (b), in the diffusion zone (c) and in bulk (d).

3.2. HARDNESS MEASUREMENTS

A vertical hardness profile was measured in the cross-section of the nitrided sample on a length of about 1 mm. The distance between prints was kept approximately constant at 0.1 mm. A light micrograph of the analyzed zone is presented in Fig.2.a, and the variation of the hardness with depth (corresponding to the profile from Fig.2.a), is presented in Fig.2.b.

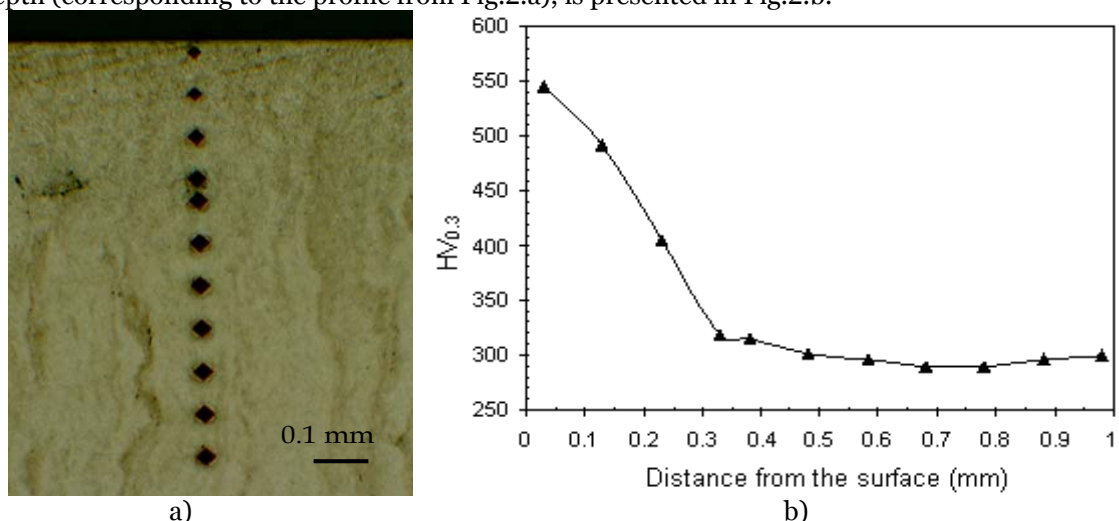


Figure 2. Light micrograph of the hardness prints distribution – 4% Picral etching (a) and the variation of the obtained values with depth (b).

As a general view, the $HV_{0.3}$ measured values taken in depth indicate a continuous decrease, which is characteristic to a nitrided structure. The uniformity of the values suggests that in vertical direction the segregations have not a great influence on the hardness probably because the experiments were done in a zone between two segregation bands (the diagonal of the prints being estimated at about $30 \mu\text{m}$).

By nitriding the steel sample surface hardness has increased by ~1.8 times with respect to the bulk, up to ~550 HV (Fig.2.b). From Fig.2.b one may estimate the diffusion zone thickness at about 0.32 mm, value close to that identified by the light microscopy observations (see Fig.1.a). Next, up to 1 mm in depth, the hardness values are maintained in a constant range around 300 HV (the bulk hardness). In the diffusion zone, the hardness is increased due to nitrogen incorporation which may be found as dissolved in the solid solution and as nitride precipitations [15]. It is known that only 0.1 wt% of nitrogen dissolved in the steel ferritic matrix during nitriding gives an important increase of hardness [15].

Moreover, to complete this study we have done nine punctual hardness measurements in the zones with (prints 3 up to 7) and without segregations (prints 1, 2, 8 and 9) in the bulk of the steel sample. Micrographs of the prints are shown in Fig.3.a-c, while in Tab.1 are given the print diagonals and the corresponding HV_{0.3} values.

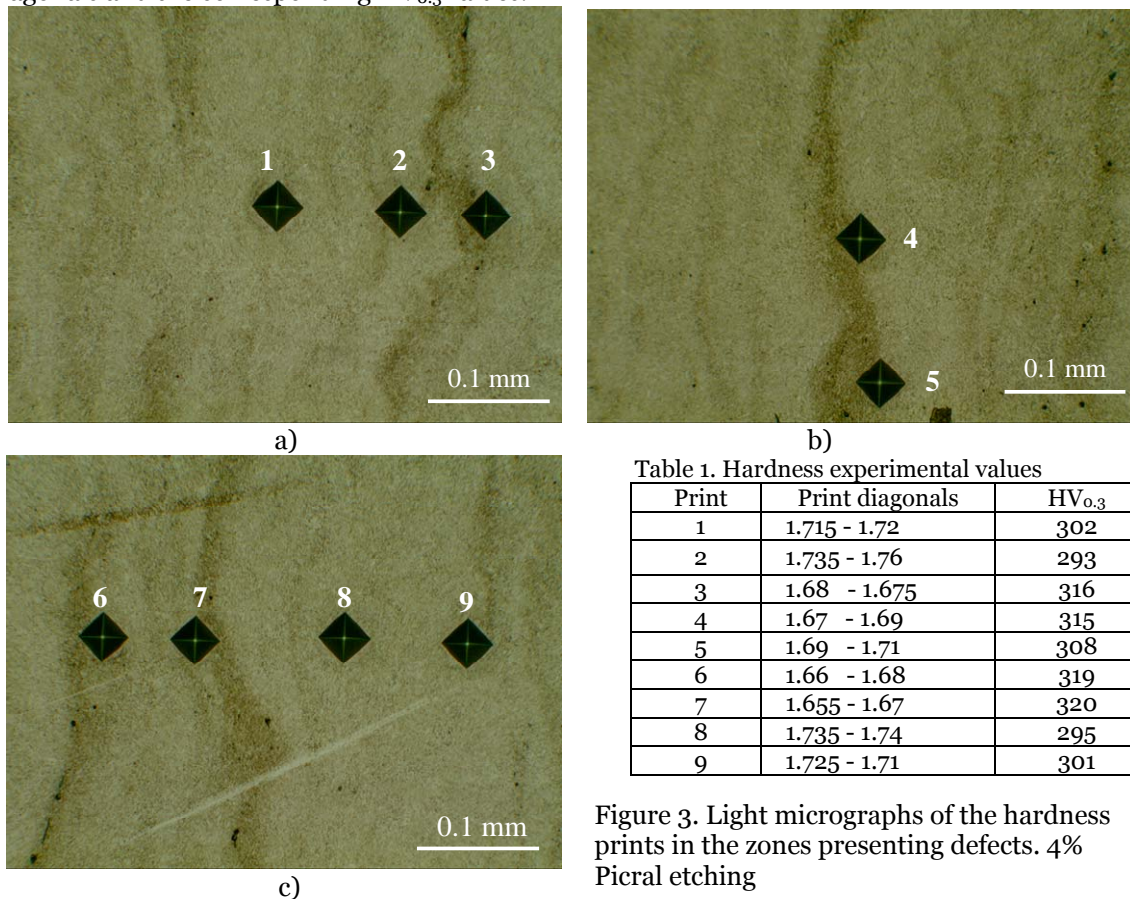


Figure 3. Light micrographs of the hardness prints in the zones presenting defects. 4% Picral etching

It is obvious a correlation between the presence of segregations and the hardness values. So, in the zones presenting defects (prints 3 up to 7), the average hardness is 315.6 HV_{0.3}, while in the others zones (prints 1, 2, 8 and 9), the average value of the hardness is 297.7 HV_{0.3}.

3.3. EPMA RESULTS

In Fig.4. are given: an EPMA image showing the path of incident electron beam in the analyzed area (indicated by the arrow in Fig.4.a) and the obtained atomic concentrations with depth (Fig.4.b). The nitrogen and iron concentration profiles in depth were determined from the surface of the sample through the compound layer and the transition zone to the diffusion layer, on a length of ~15 μm. As estimated from the EPMA image (Fig.4.a), in the analyzed zone the compound layer has a thickness of about 4.8 μm, but on the average this layer has a thickness close to 3.6 μm.

At the steel sample surface, in the compound layer, the presence of about 20% nitrogen and 80% iron suggest the presence of the γ'-Fe₄N nitride (Fig.4.b). In depth, up to ~5 μm, these proportions are changing toward lesser nitrogen but much iron content. The iron surplus is detected probably from the steel sample structure, this indicating a discontinuity (mixture) in the compound layer.

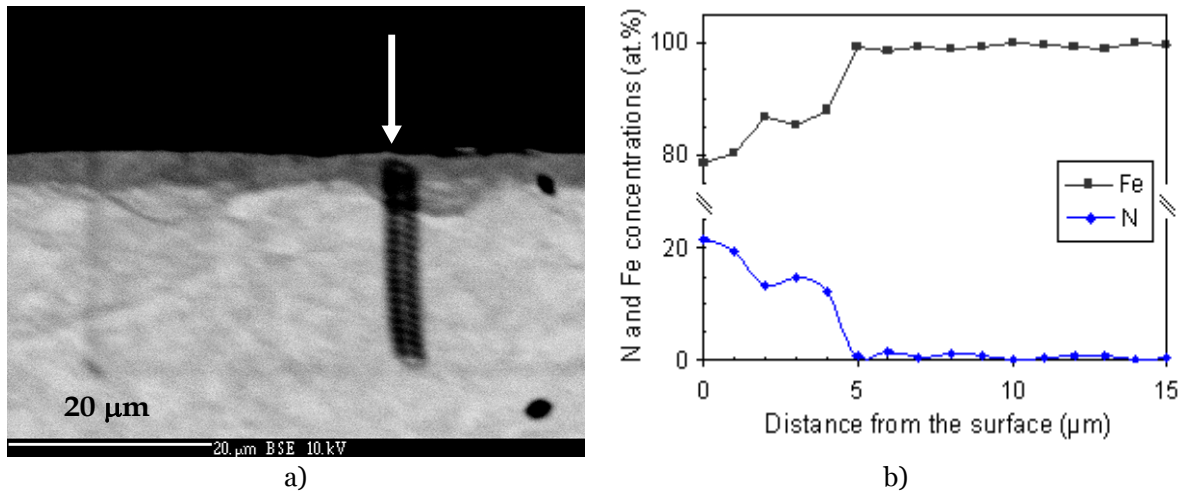


Figure 4. EPMA image showing the path of incident electron beam in the compound and diffusion layers (a) and the obtained atomic concentrations with depth (b).

Also, as shown in the EPMA image presented Fig.5 and taken in the diffusion layer, the nitrided steel sample structure appears inhomogeneous (with zones of different contrast). So, by the brightness, the analyzed area may be divided into two zones, a bright and a dark one (Zone A and B, respectively in Fig.5), bounded by a white dot line.

Further, we have measured the nitrogen and iron concentrations (in at.%) in different points in the analyzed zone, the results being presented in Tab.2. The three experimental points (from 1 to 3) where marked on the EPMA image during the measurements by the apparatus (Fig.5). The first experimental point (1) is situated at about 15 μm from surface and the position of the other points (2 and 3) was arbitrary chosen by the contrast of the zone. Thus, experiments 1 and 3 were done in the bright zone, while experiment 2, in the dark one.

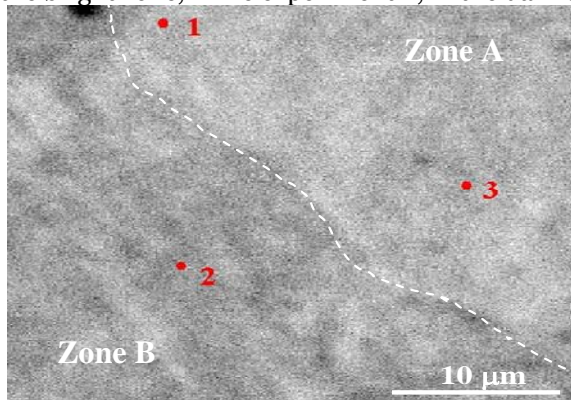


Table 2. Atomic concentrations determined in different points in the diffusion layer

Point	N (at.%)	Fe (at.%)	Zone
1	2.0795	97.9205	A - bright
2	0.8707	99.1293	B - dark
3	1.7101	98.2899	A - bright
4*	0.2799	99.7201	bright, at ~50 μm from surface
5*	0	100	bright, at ~350 μm from surface

*Not marked in Fig. 5.

Figure 5. EPMA image showing three experimental points taken in the diffusion layer

If the sample structure heterogeneity would be due to the nitriding treatment, in Zone A one would expect a nitrogen poor zone, while in Zone B, a nitrogen rich zone. Analyzing the experimental values from Tab.2 one may conclude that this assumption is not sustained because of the lesser nitrogen content obtained in experiment 2 versus experiments 1 and 3. So, the steel sample structure heterogeneity was formed before nitriding, probably during its solidification stage and the limit between Zone A and B may be probably assigned to a segregation band limit.

In Zone A, the nitrogen content maybe detected from the nitride precipitates, whose presence was already identified in the diffusion layer by the light microscopy (Fig.1.c). In Zone B the contrast is probably due to the presence of elements such as chromium, manganese, sulfur and phosphorus which have a smaller atomic number than iron and which segregate at the grain boundaries during the solidification period of the steel [14-16]. Also, in the bright zones situated more in depth (experiments 4 and 5- Tab.2), the nitrogen content decrease up to 0 because here the nitriding treatment effects are not visible.

4. CONCLUSIONS

A 42CrMo4 steel sample plasma nitrided in industrial conditions was used to study the correlation between the microstructure defects and the mechanical properties. The microstructural defects (i.e. segregations bands resulted in the solidification stage of the steel) were revealed by

light microscopy after 4% Picral reagent etching. The distance between two successive segregation bands was estimated at about 50 μm .

Also, the hardness measurements ($\text{HV}_{0.3}$) and the EPMA chemical analysis performed both in the nitrated layer and in the zones with defects, showed the following:

- ❖ The hardness profile, taken with depth from the steel sample surface, correspond to a nitrated structure and the uniformity of the values suggests that in vertical direction the segregations have not a great influence probably because the experiments were done between two segregation bands;
- ❖ The difference between the average hardness values measured in the zones with and without segregations is of only $\sim 18 \text{ HV}_{0.3}$ points;
- ❖ The nitrogen and iron concentration profiles indicate the presence of the $\gamma\text{'-Fe}_4\text{N}$ nitride on the surface of the steel sample;
- ❖ The chemical analysis made in zones of the diffusion layer which appeared bright or dark in the EPMA backscattered electrons image showed an inhomogeneous structure due to the presence of segregations.

Acknowledgement

The authors would like to acknowledge Mr. Jean Luc DEVIDAL for the EPMA tests at "Magma et Volcan" Laboratory (UMR 6524), Blaise Pascal University, Clermont-Ferrand, France.

REFERENCES

- [1.] M.A. Terres, H. Sidhom, A.C. Larbi, H.P. Lieurade, Tenue en fatigue flexion d'un acier nitrure, *Ann. Chim. Sci. Mat.* 28 (2003) 25-41.
- [2.] K. Genel, M. Demirkol, T. Gulmez, Corrosion fatigue behaviour of ion nitrated AISI 4140 steel, *Mater. Sci. Eng. A* 288 (2000) 91-100.
- [3.] A. Celik, S. Karadeniz, Improvement of the fatigue strength of AISI 4140 steel by an ion nitriding process, *Surf. Coat. Technol.* 72 (1995) 169-173.
- [4.] A. Alasaran, F. Yildiz, A. Celik, Effects of post-aging on wear and corrosion properties of nitrated AISI 4140 steel, *Surf. Coat. Technol.* 201 (2006) 3147-3154.
- [5.] B. Podgornik, J. Vižintin, O. Wänstrand, M. Larsson, S. Hogmark, H. Ronkainen, K. Holmberg, Tribological properties of plasma nitrated and hard coated AISI 4140 steel, *Wear* 249 (2001) 254-259.
- [6.] P. Corengia, T.G. Ybarra, C. Moinaa, A. Cabo, E. Broitman, Microstructural and topographical studies of DC-pulsed plasma nitrated AISI 4140 low-alloy steel, *Surf. Coat. Technol.* 200 (2005) 2391-2397.
- [7.] G. Krauss, Solidification, Segregation, and Banding in Carbon and Alloy Steels, *Metall. Mater. Trans. B* 34/6 (2003) 781-792.
- [8.] J.D. Verhoeven, A Review of Microsegregation Induced Banding Phenomena in Steels, *J. Mat. Eng. Perf. JMEPEG* 9 (2000) 286-296.
- [9.] X. Tong, C. Beckermann, A diffusion boundary layer model of microsegregation, *J. Crystal Growth* 187 (1998) 289-302.
- [10.] L.E. Samuels, *Light Microscopy of Carbon Steels*, ASM International, Materials Park, OH, ISBN 0-87170-655-5, 1999.
- [11.] B.L. Bramfitt, A. O. Benscoter, *Metallographer's guide: practices and procedures for irons and steels*, ASM International (OH), ISBN-13: 9780871707482, 2002.
- [12.] D. Chae, D.A. Koss, A.L. Wilson, P.R. Howell, The effect of microstructural banding on failure initiation of HY-100 steel, *Metall. Mater. Trans. A* 31 (2000) 995-1005.
- [13.] J.A. Belk, A.L. Davidies, *Electron Microscopy and Microanalysis of Metals*, Elsevier Publishing Co. Ltd., London, 1968, pp. 151 and pp. 219.
- [14.] Z. Sterjovski, D.P. Dunne, D.G. Carr, S. Ambrose, The Effect of Cold Work and Fracture Surface Splitting on the Charpy Impact Toughness of Quenched and Tempered Steels, *ISIJ International* 44/6 (2004) 1114-1120.
- [15.] S.R. Hosseini, F. Ashrafizadeh, Accurate measurement and evaluation of the nitrogen depth profile in plasma nitrated iron, *Vacuum* 83 (2009) 1174-1178.
- [16.] T.F. Majka, D. K. Matlock, G. Krauss, Development of microstructural banding in low-alloy steel with simulated Mn segregation, *Metall. Mater. Trans. A* 33 (2002) 1627-1637
- [17.] A.C. Stauffer, D.A. Koss, J.B. McKirgan, Microstructural banding and failure of a stainless steel, *Metall. Mater. Trans. A* 35 (2004) 1317-1324





¹: Moniĳa Eriĳa POPA

RESEARCH AND SIMULATION OF THE SOLIDIFICATION FRONT AT THE CONTINUOUS CAST HALF-FINISHED PRODUCT

¹: UNIVERSITY POLITEHNICA OF TIMISOARA, FACULTY OF ENGINEERING FROM HUNEDOARA, ROMANIA

ABSTRACT:

This section is divided with discreet element structure. Using these experiments is made graphical dependents of temperature in some different point from surface crust to center of half-product, and also solidification speed for S235. Primordial method for the decrease of the superheat of the steel of the crystallizer, consist in the introduction of consumable micro-coolers, which can be exterior or internal. The mathematical molding of the solidification and cooling phenomenon of continuously cast half-products, presented the in afterwards, is based on the mathematical description of phenomenon.

KEYWORDS: steel, micro-coolers addition, continuous casting, experiments, simulations

1. INTRODUCTION

The main task of the continuous cast is improved of continuous cast steel quality. In order to assured the solidification conditions imposed by the steel chemical composition must be synchronize a numerous technological factors the most important be the steel chemical composition, the casting temperature and speed of drawing. Primordial method for the decrease of the superheat of the steel of the crystallizer, consist in the introduction of consumable micro-coolers, which can be exterior or internal. The exterior micro-coolers can be prepared out of the system and entered the crystallizer, and the internal micro-coolers are constituted from steels crusts, immediate format in the core of the half-products, on the water cooled surfaces. The outside micro-coolers can be entered in the liquid steel below different forms: small shots, granules or particles, draw-bars, wire, tube, etc.

The addition of micro-coolers in crystallizer drives to the growth of the zone of the echi-axial crystals, diminish the degree of superheat and reduce the axial porosity. The mathematical molding of the solidification and cooling phenomenon of the solidification and cooling phenomenon of continuously cast half-products, presented the in afterward, is based on the mathematical description of phenomenon. This solution problem is, practically, the heat solving equation in of nom-steady regime. For defined the heat conduction between half-product and crystallizer is necessary the cognition of initial conditions, the variation law of the heat flux between half-product – crystallizer – and the flux between crystallizer – cooling water. Some conditions are can easy schematized, other only that drive to systems of which equations can be solved on analytic path.

2. METHODOLOGY

The computer program is written in C++ and works under Win32. For the graphic interface the program uses Microsoft Foundation Classes, a class library that encloses the functional character of the standard programming interface Windows API – Application Program Interface. The 3D graphs are realized with the Windows implementation of OpenGL specification (Open Graphics Library). For implementation of an algorithm of the above described model we need the following initial data: ambient temperature, casting temperature, initial temperature of the crystallizer, number of nodes from half-finished product and from crystallizer with respect to both

axes, values of thermal conductivity for steel and copper function of temperature, values of enthalpy for steel and copper function of temperature. In case of steel this functional dependence need to include fusion latent heat; tapping condition of half-finished product from equipment; stopping condition of the algorithm. This could be: manual stopping, after a given time period at a specified minimum, average, or maximum temperature of the half-finished product, maximum variation of enthalpy at an iteration.

3. DISCUSSION

The simulation is realized for a half-finished product $\Phi 270$ mm made of steel OL37-2K, according to the SREN 1025 standard. The data are: the ambient temperature 20 °C, the casting temperature 1550 °C, the convection constant $K=15$. For configuration of specific dates for every steel grade, using the main interface (figure 1).

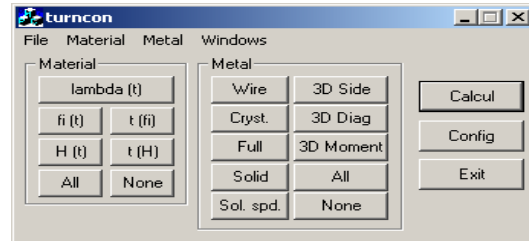


Figure 1. The main window of the program

The simulation of the continuously cast half-products is effectuated in the case of 1% consumable micro-coolers introduced in crystallizer. The simulation is effectuated just for the primary and secondary cooling and not for the entire line of cast installation. Thus is explained the great values of the temperature of steel in the interior of the half-products (the middle layers) but which we diminish the feather below the value of the temperature solidus up to the moment which in the half-products is uttered. With the number of knots of digitization in major (both the crystallizer and the half-products) and the maximum the variation of in an enthalpy in single iteration is less, the real time of simulation is major. The run of the program can be interrupted all moments, but with the mention as be start from same moment of time but must run the program from beginning. For illustrate the operation of the program, we accomplished captures of the screen to different moments of times, from which can obtain some information concerning the temperatures in the cast equipment, the real and simulated times.

The temperatures are indicated by the mean of a colored gradient, having the values: red for casting temperature, blue for ambient temperature and green for their average. Any intermediary temperature is a combination of these. A first obtained dependence is represented by temperature variation of the half-finished product function of time (figure 2). The distribution of the discredited points is also presented.

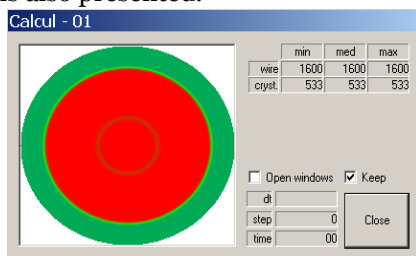


Figure 2. The dialog window at 1s (simulated time) at the moment of the micro-coolers introduces

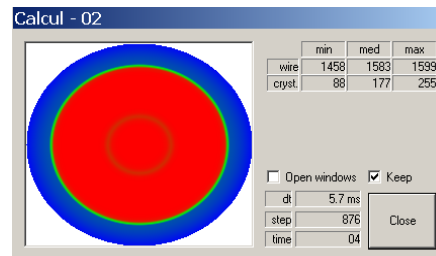


Figure 3. The dialog window at 2s

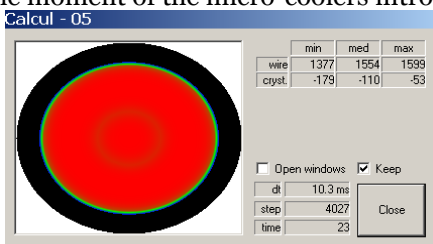


Figure 4. The dialog window at 5s

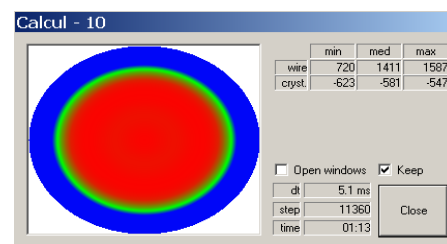


Figure 5. The dialog window at 10s

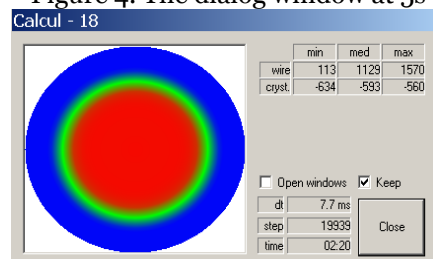


Figure 6. The dialog window at 18s

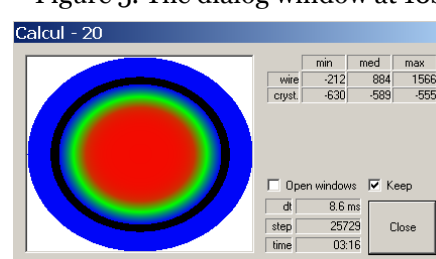


Figure 7. The dialog window at 20s

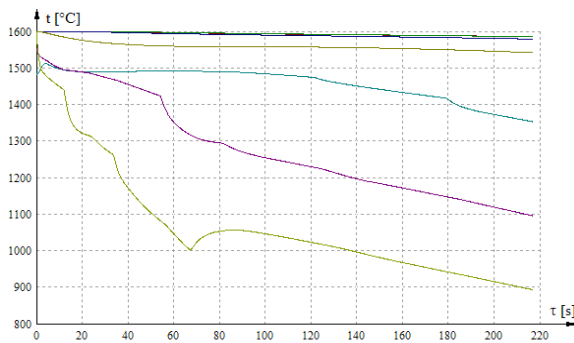


Figure 8. The temperature variation function of time (10%, 25% and 100% from the cast line)

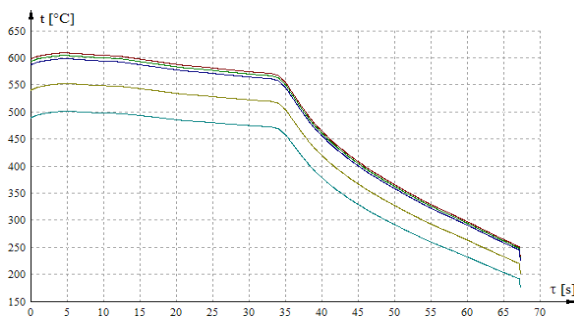


Figure 9. The temperature variation in the crystallizer, function of time (1%, 5%, 10%, 50% and 100% from crystallizer)

In figure 10 the cumulate diagram of the temperature are presented. It is observed the two cooling zone, respectively the primary cooling (when varied both the temperature in crystallizer and the cast line), and the secondary cooling (when only the cast line temperature is present). It was obtained variation type for the solidification speed function of time. It refers to a solidification speed calculated between two consecutive iterations, fact that partially explain the oscillating aspect of the curves (figure 11).

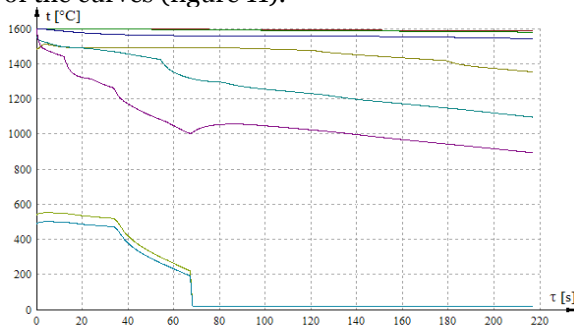


Figure 10. The temperature variation in the crystallizer and the cast line

At time moment, when it took place the driving out of considered surface from crystallizer, it took place an increasing of temperature in the superior layers of the half-finished product (with approximately 100 °C in the exterior and with 35...50 °C in different points of the surface). This increasing of the temperature is due to the lack of cooling of the wire immediately after the driving out from crystallizer to the first ring of secondary cooling. After this moment the cooling and the solidification of the wire took place normally, the recorded temperatures corresponding to the measured ones. It needs to be specified that the simulation was realized just for primary and secondary cooling not for the entire running of the wire in the equipment. This explains steel's high temperature values in the interior of the half-finished product (middle layers), but they are decreasing under the solidus temperature value until the cutting of the half-finished product.

As regards the temperatures distribution in the crystallizer (which take over the heat transferred by the half-finished product and transfer it to the cooling water), it is presented in figure 9. In this case to be presented also the position of the discredited points.

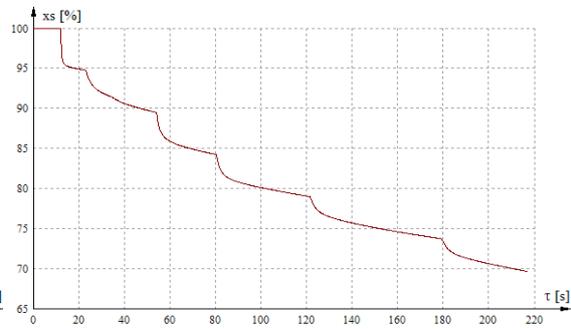


Figure 11. The solidification front (100%=surface of the cast line)

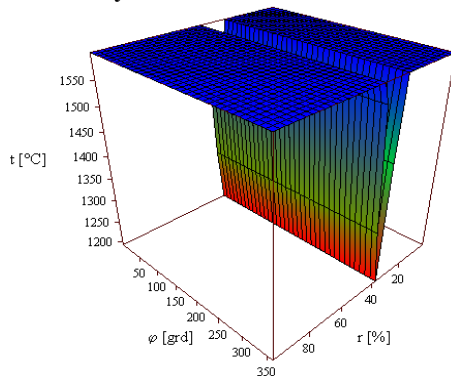


Figure 12. The thermal field at 1s after the micro-coolers addition

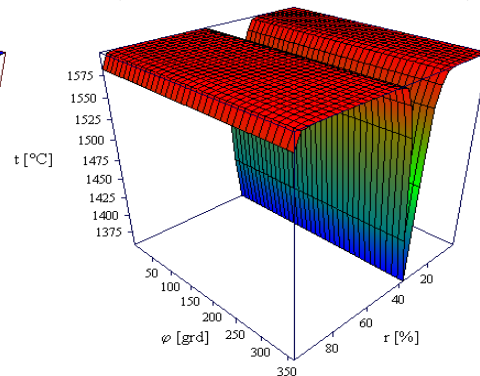


Figure 13. The thermal field at 2s after the micro-coolers addition

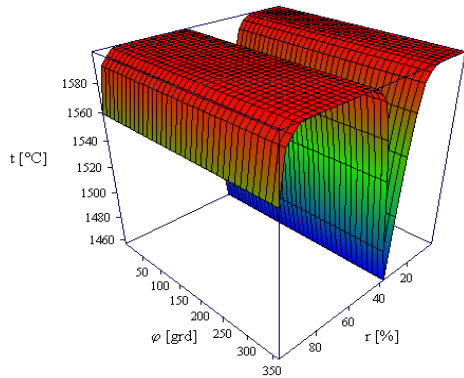


Figure 14. The thermal field at 5s after the micro-coolers addition

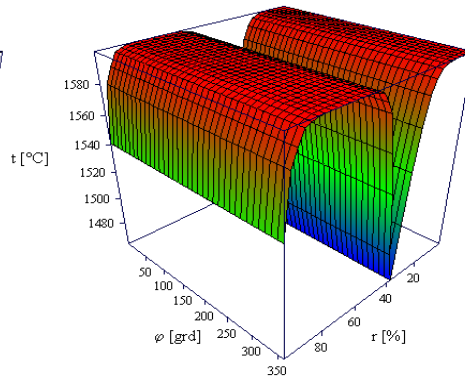


Figure 15. The thermal field at 10s after the micro-coolers addition

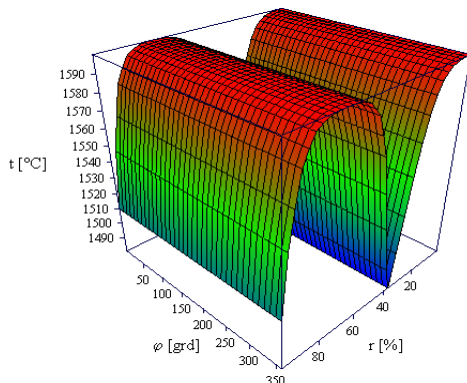


Figure 16. The thermal field at 18s after the micro-coolers addition

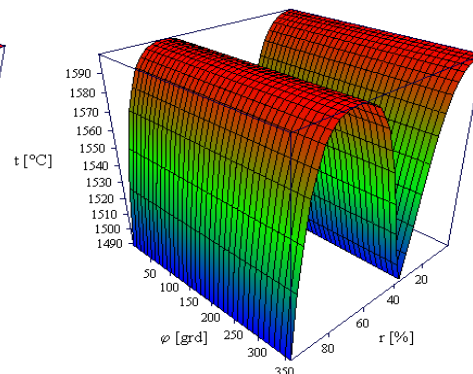


Figure 17. The thermal field at 20s after the micro-coolers addition

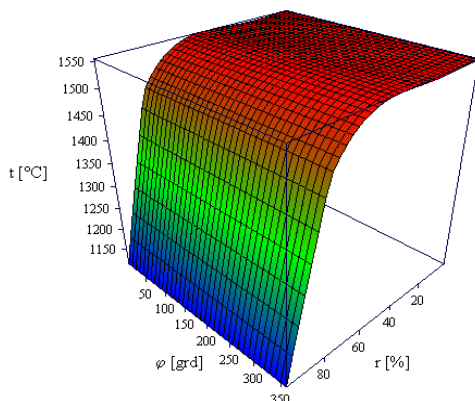


Figure 18. The thermal field in half-product ($\Phi 270$ mm), in time (at simulation's end)

Another type of temperature distribution, when the half-finished product is droved out from secondary cooling zone, it is presented in figure 12...figure 17, at 1s, 2s, 5s, 10s, 18s and 20s, after introduced the micro-coolers. The figure 18 presents the thermal field in the half-product in the end of the simulated time. The obtained regression surfaces corresponded from a quarter from the half-product section is like similarly of the other parts of the section. From the point of view of the temperature values, the half-product surface is the first cooled section, and the core is the most slowly cooled part.

4. CONCLUSIONS

Analyzing the graphical dependences from the performed researches, based on literature review data

and from own experimental work it results the following conclusions:

- ❖ The results obtained by simulation with presented program being similar with practical data;
- ❖ In every diagram there diagram there are observed a temperature leap or a solidification speed leap after approximately 60s from the beginning of the casting (from a totally 220s simulation time), respectively immediately after the driving out from the crystallizer of the considered section, leap caused by the impossibility of elimination of a heat flux from the half-finished product interior;
- ❖ It is observed a numerous crystallizing centers, uniform distributed;
- ❖ Also, it is observed an appreciate difference between the liquid steel temperature and the steel temperature from immediate proximity of micro-coolers;
- ❖ The indurations advances consisted standardized it a temperatures of first in of the minute after the administration of micro-coolers;
- ❖ After precinct a minute from the administration micro-coolers don't else notices significant differences what in looks the variation of the temperature of the in mass of steel;

- ❖ Through the addition of micro-coolers is obtained adjustment of the temperature of the in of the crystallizer depending on the quality and quantity of micro-coolers.

The chosen time interval represent the time in which the unsteady heat transfer process is approximate with a steady process. From this reasons as well as the characteristics of the real process are far from that of a steady one, the iteration period should be smaller. The proposed algorithm can be used for the analysis of both stationary and moving solidification problems in which phase change occurs at a specific temperature. An integrated understanding of heat transfer during solidification, friction/lubrication at solid-liquid interface, high temperature properties of the solidifying shell etc. is necessary to control the continuous casting process.

REFERENCES

- [1.] Popa Monika Erika – Cercetări privind procesele fizico-chimico-metalurgice ce au loc la interfețele cristalizor-zgură-oțel lichid asupra oțelului turnat continuu, Teza de doctorat, Ed. Politehnica 2009
- [2.] Hepuț T., Kiss I., Popa E., Ardelean E., Ardelean M. - Research and experiments regarding the quality of continuous cast steel- Scientific Conference Research And Development Of Mechanical Elements And Systems Jahorina – Irmes, Sarajevo, 2002, BOSNIA, Pp 349...354
- [3.] Popa E., Kiss I., Mihut G. - Researches regarding the quality of the continous cast semi-finished products- Management Of Manufacturing Systems MMS-2008 – 3rd Conference With International Participation, Presov, SLOVAKIA, 187...190 ISBN: 978 – 80 – 553 – 0069 – 6
- [4.] Popa E., Kiss I. -“ Mathematical modelling of the thermal regime in the continous casting process- Tinerii Si Cercetarea”, Al VII-Lea Simpozion International – Resita, 2005, ISSN 1453 – 7394
- [5.] Popa M. E., Kiss I., Danciu A. - The thermal regime in the continuous casting process– in mathematical interpretations - Annals of Faculty of Engineering Hunedoara, 2005, Tome III, Fasc 3, Pp 235...242, ISSN 1584 – 2673
- [6.] Popa E., Kiss I. - Mathematical Modelling Of The Thermal Regime In The Continous Casting Process - Analele Universității “Eftimie Murgu” Reșița, 2005, Pp 231-237, ISSN 1453 – 7394
- [7.] Popa E., Kiss I., Danciu A. - Research Of Experiments Regarding The Influence Of Casting Parameters Upon The Surface Temperature Of The Continous Caste Semiproduct. - Annals Of Oradea University, Fascicle Of Management And Technological Engineering, 2005, CD, ISSN 1583 – 0691



¹Simon JITIAN

OBTAINING THE ABSORPTION SPECTRA OF SILICON FROM THE IR REFLECTANCE SPECTRA RECORDED AT TWO ANGLES

¹UNIVERSITY „POLITEHNICA” OF TIMIȘOARA, FACULTY OF ENGINEERING HUNEDOARA, ROMANIA

ABSTRACT:

This paper presents an analytical method for obtaining optical constants \bar{n} and \bar{k} , which define the complex refractive index $\tilde{n} = \bar{n} - i\bar{k}$ of solid absorbent materials. From specular reflectance, IR spectra recorded at two different incidence angles φ_01 and φ_02 the reflectances R are measured, using unpolarized radiation. [1].

KEYWORDS:

optical constants, two angles IR reflectance spectra, refractive index spectra

1. INTRODUCTION

The reflection of a plane polarized monochromatic radiation on the boundary of two different optical media is expressed by the Fresnel complex reflection coefficient $\tilde{r} = r \cdot \exp(i\delta)$. Two reflection coefficients \tilde{r}_s and \tilde{r}_p are defined for two components of plane polarized radiation with the electric field vector located perpendicular and parallel to the plane of incidence, respectively.

The square modulus of the complex reflection coefficient is the reflectance (or the reflectivity) $R_s = \tilde{r}_s \cdot \tilde{r}_s^*$ or $R_p = \tilde{r}_p \cdot \tilde{r}_p^*$. In the first approximation we can consider the reflectance for natural radiation to be the arithmetic mean of the two components R_s and R_p :

$$R = \frac{R_s + R_p}{2} \quad (1)$$

If we consider that the two components in incident radiation do not have equal weight, we can introduce a parameter S whose value is between $S = 0$ for the radiation polarized parallel to the incidence plane ($R = R_p$) and $S = \infty$ for the radiation polarized perpendicular to the incidence plane ($R = R_s$) [2]. S is defined as the ratio between the intensity of light polarized perpendicular to the plane of incidence and the parallel polarized one reaching the detector:

$$S = \frac{R_s^o}{R_p^o} \quad (2)$$

where: R_s^o and R_p^o are the perpendicular and parallel components that were measured.

The reflectance can be expressed by:

$$R = \frac{S}{S+1} R_s + \frac{1}{S+1} R_p \quad (3)$$

The reflection coefficients \tilde{r} and the reflectance R depend on the relative complex refractive index of refractive and incidence medium, respectively:

$$\tilde{n} = \frac{\tilde{n}_1}{n_0} = \bar{n} - i\bar{k} \quad (4)$$

according to relations:

$$\tilde{r}_s = |\tilde{r}_s| \exp(i\theta_s) = \frac{\cos \varphi_o - \tilde{n} \cos \tilde{\varphi}}{\cos \varphi_o + \tilde{n} \cos \tilde{\varphi}} \quad (5)$$

$$\tilde{r}_p = |\tilde{r}_p| \exp(i\theta_p) = \frac{\tilde{n} \cos \varphi_o - \cos \tilde{\varphi}}{\tilde{n} \cos \varphi_o + \cos \tilde{\varphi}} = -\tilde{r}_s \frac{\tilde{n} \cos \tilde{\varphi} - \sin \varphi_o \tan^2 \varphi_o}{\tilde{n} \cos \tilde{\varphi} + \sin \varphi_o \tan^2 \varphi_o} \quad (6)$$

where $\tilde{\varphi}$ is the complex refractive angle, from Snell refraction law:

$$\sin \varphi_o = \tilde{n} \sin \tilde{\varphi} \quad (7)$$

A single measurement of the reflectance at a certain frequency is insufficient to determine the two optical constants \bar{n} and \bar{k} . Several methods that use at least two experimental values of measurable physical quantities corresponding to reflection [3] are known. Usually, they use graphical methods since the optical constants \bar{n} and \bar{k} can not be explicitly expressed from the reflectance expressions [4]

2. MODEL DETAILS

We present an analytical method, using some approximations, to obtain reflectance spectra $\bar{k} = f(\tilde{\nu})$ and $\bar{n} = f(\tilde{\nu})$ from the reflectance spectra $R = f(\tilde{\nu})$ recorded at two different incidence angles, using non-polarized radiation [5,6].

For two different incidence angles φ_{01} and φ_{02} the refraction law is written:

$$\sin \varphi_{01} = \tilde{n} \sin \tilde{\varphi}_1 \quad \text{and} \quad \sin \varphi_{02} = \tilde{n} \sin \tilde{\varphi}_2 \quad (8)$$

By writing equation (3) for the two angles of incidence, we obtain the system of equations:

$$S \cdot R_{s1} + R_{p1} - (S + 1) \cdot R_1 = 0 \quad (9)$$

$$S \cdot R_{s2} + R_{p2} - (S + 1) \cdot R_2 = 0 \quad (10)$$

If in relations (5) and (6) we introduce the notations:

$$\tilde{n} \cos \tilde{\varphi}_1 = X - i \cdot Y \quad \text{and} \quad \tilde{n} \cos \tilde{\varphi}_2 = U - i \cdot Z \quad (11)$$

then the reflectances for two polarization states corresponding to the two different incidence angles, are:

$$R_{s1} = \frac{(X - \cos \varphi_{01})^2 + Y^2}{(X + \cos \varphi_{01})^2 + Y^2} \quad \text{and} \quad R_{s2} = \frac{(U - \cos \varphi_{02})^2 + Z^2}{(U + \cos \varphi_{02})^2 + Z^2} \quad (12)$$

respectively:

$$R_{p1} = R_{s1} \frac{(X - \sin \varphi_{01} \tan \varphi_{01})^2 + Y^2}{(X + \sin \varphi_{01} \tan \varphi_{01})^2 + Y^2} \quad \text{and} \quad R_{p2} = R_{s2} \frac{(U - \sin \varphi_{02} \tan \varphi_{02})^2 + Z^2}{(U + \sin \varphi_{02} \tan \varphi_{02})^2 + Z^2} \quad (13)$$

X, Y, U and Z depend on the complex refractive index according to the relations:

$$\tilde{n}^2 = (X - i \cdot Y)^2 + \sin^2 \varphi_{01} \quad ; \quad \tilde{n}^2 = (U - i \cdot Z)^2 + \sin^2 \varphi_{02} \quad (14)$$

By equating the right side of each relationship (12) we get:

$$XY - UZ = 0 \quad (15)$$

$$X^2 + Z^2 - Y^2 - U^2 + \sin^2 \varphi_{01} - \sin^2 \varphi_{02} = 0 \quad (16)$$

The nonlinear system of equations (9), (10), (15) & (16) leads to optical constants \bar{n} and \bar{k} .

3. RESULTS AND DISCUSSION

To illustrate this method silicon was chosen. The refractive index values for this material are well known and stressed in the reference literature [9,10,11].

In order to obtain the optical constants \bar{n} and \bar{k} of silicon we used specular reflectance IR spectra. The spectra were recorded with a UR20 spectrograph, using non-polarized radiation. For IR radiation incident on the sample, the proportion of the plane polarized component, perpendicular to the plane of incidence, is 63% which corresponds to the parameter of equation (3) $S = 1.7$.

Figure 1 presents the IR reflectance specular spectra of silicon recorded at two incidence angles 20 and 55 degrees respectively.

To obtain optical constants \bar{n} and \bar{k} from reflectance spectra we used our own computer program in MATLAB language, calling a routine for solving systems of nonlinear equations. To do this, first we wrote the nonlinear system of equations (9), (10) (15) and (16) to canonical form.

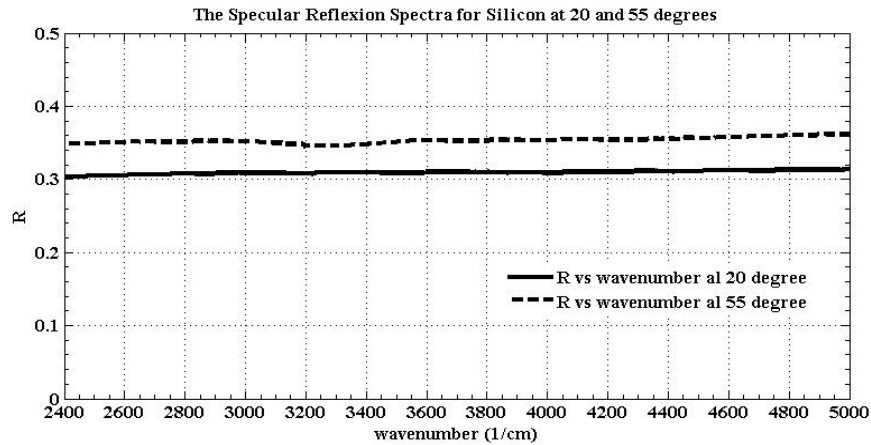


Fig. 1. The reflectance specular spectra of silicon recorded at two incidence angles, using non-polarized light

To find the solution of the nonlinear equations system it is very important to choose the correct test-solution to resolve the routine. For this, we started from the value $X = U = 3.4$ and $Y = Z = 0$ since it is known from reference literature that in the spectral range examined $n \cong 3.4$ and $k=0$ for silicon [9, 10, 11]. In (14) the contribution of the second term on the right is small, so $X = U = n = 3.4$ and $Y = Z = k = 0$.

The refractive index \tilde{n} and optical constants \bar{n} and \bar{k} respectively are calculated from equation (14) based on X and Y values obtained by solving the nonlinear equations system.

Figure 2 shows the refractive index spectrum of silicon obtained from specular reflectance spectra recorded at two incidence angles 20 and 55 degrees.

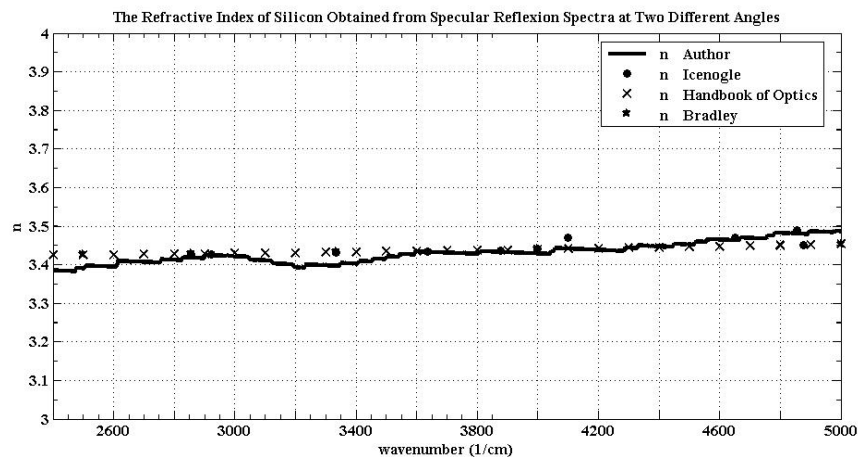


Fig. 2. The refractive index of silicon obtained from the specular reflectance spectra at two different incidence angles: 20° and 55°

The refractive index spectrum obtained by processing the silicon specular reflectance spectra are in very good agreement with the corresponding data from the reference literature, as can be noticed in Figure 2. The absorption index \bar{k} values are equal to zero over the whole spectral range analyzed, in agreement with literature data.

4. CONCLUSIONS

The specular external reflection spectra recorded at two or more different incidence angles can be used to determine the refractive index and absorption index spectra corresponding to solid materials.

When the radiation used to record the spectra is non-polarized or partially polarized it is important to know the contribution of the two components R_s and R_p in the incident radiation.

It is important to choose the correct initial solutions to start the routine for solving nonlinear equations system. The start solutions of the program for solving nonlinear equations system can be based on values of X and U close to $\bar{n} = 3.4$. The initial values of Y and Z should be close to $\bar{k} = 0$.

The values of the optical constants \bar{n} and \bar{k} obtained by the method are in agreement with the corresponding values reported in the reference literature.

REFERENCES

- [1.] S. Jitian și I. Bratu, Stud.Univ. Babeș-Bolyai, Phys., **31(2)**, p.30 (1986)
- [2.] Crawford Bryce Jr., „Measurements of Optical Constants in the Infrared by ATR”, in Advances in Infrared and Raman Spectroscopy, R.J.H. Clark and R.E. Hester eds., Heyden-London, (1978)
- [3.] E. Kawate, Measurement Science Review, **5 (3)**,(2005)
- [4.] A.Vasicek, „Tables of Determination of Optical Constants from the Intensities of Reflected Light”, Nakladatelstvi Ceskoslovenske Akademie Ved., Praga, (1964)
- [5.] S. Jitian, Teză de doctorat, Cluj-Napoca, (1987)
- [6.] S.Jitian, Analele Univ. Oradea, (1994), p. 74-78
- [7.] J. Fahrenfort, Spectrochim. Acta,**17**, p.698, (1961)
- [8.] W.R. Hunter, Journal of the Optical Society of America, **55**, (10), p.1197, (1965)
- [9.] - Handbook of Optics, 3rd edition, Vol. 4. McGraw-Hill, (2009)
- [10.] H. W. Icenogle, B. C. Platt, and W. L. Wolfe, "Refractive indexes and temperature coefficients of germanium and silicon" Appl. Opt. **15**(10), pp. 2348-2351, (1976),
- [11.] S. Khedim, A. Chiali, B. Benyoucef and N.E. Chabane Sari, Revue des Energies Renouvelables ICRES-07, Tlemcen, pp. 337 – 341, (2007)





¹Miriam MATÚŠOVÁ, ²Erika HRUŠKOVÁ, ³Angela JAVOROVÁ

MATERIAL FLOW STRATEGY BY SOFTWARE WITNESS

¹⁻³SLOVAK UNIVERSITY OF TECHNOLOGY IN BRATISLAVA, FACULTY OF MATERIALS SCIENCE AND TECHNOLOGY IN TRNAVA, INSTITUTE OF PRODUCTION SYSTEMS AND APPLIED MECHANICS, DEPARTMENT OF TECHNOLOGICAL DEVICES AND SYSTEMS, SLOVAKIA

ABSTRACT:

Resolving of material flows is actual term in present. It brings a lot of problems with layout of particular devices as elements of manufacturing process according to required and defined technology. In present time are suitable software tools for improving of transport, manipulation and storage systems. The simulation of these three systems relation is realized support CA systems to optimal whole technological processes. In this case this problem is solved by simulation software Witness used in Institute of Manufacturing Systems and Applied Mechanics of our faculty.

KEYWORDS:

production system, manufacturing, material flow, layout optimizing

1. INTRODUCTION

Predictive simulation technology is attracted of specialists in many fields. Competitiveness retention and raising the level of services required by organizations constantly change. It is necessary to verify the possibility of planned systems and find successful solutions under conditions of strict monitoring costs. Requirements to change technology or business processes, however, entail some risk.

2. SIMULATION

The simulation model is a dynamic model in which there are phenomena of the same order as the system modeling. Simulation methods obtain solutions to some transformation of values that have been learned from observing the model run (run program). The simulation model provides results based on information collected from the changes in the model over time.

Contribution of simulation methods in the field of operational research is particularly in facilitating the work of dynamic and complicated probability ties. As far as the achievement of the goal to create an analytically solvable model, it is necessary to prioritize. Such a model adequately reflects the essential reality site. This model is usually more general (simulation methods provide results only in numerical form) and to construct and less expensive solutions. In addition, simulation methods are appropriate for assessing the number option than to solve problems that lie in finding optimal solutions to large sets or even an infinite number of elements. With the growing complexity of systems that need to be rationally designed and managed will need to increase the use of simulation methods.

3. SIMULATION MODELS AS TOOL TO OPTIMIZE THE MATERIAL FLOW

There are mostly used in practice following types of simulation:

- ❖ dynamic simulation and physical systems (differential equations, finite element method, etc.)
- ❖ discrete event simulation systems (network theory front, etc.)
- ❖ simulation aimed at training people (air simulators and trainers, simulators and other operator).

Using simulation to solve the various proposals for optimization of production lines and several systems in different industries to track:

- ❖ verification of the new designed production line operations, a comparison of the old organization to the proposed production control system based on KANBAN,
- ❖ the design of optimal production batch subject to a lot of clock and production of products,
- ❖ the optimization of the number of workers in the system, the allocation of operations jobs.

4. PROCESS SIMULATION SOFTWARE

WITNESS - is successful program to simulate the production, maintenance and logistics processes. It is used for interactive model creation, creation of modular structures, interactive experimentation, working with CAD / CAM applications and information systems, creating a single optimization module, 3D visualization - virtual reality module. Other administration routes of the Witness:

- ❖ modern methods implementation of production management,
- ❖ the identification and removal of bottlenecks,
- ❖ optimal allocation of production and logistics units, material flow analysis,
- ❖ the prediction of the operational interventions consequences.

Application Witness simulation program can be realized in the order:

- ❖ the choice of components,
- ❖ manufacturing process technology,
- ❖ the choice of machines,
- ❖ making production variations,
- ❖ comparison of the designed variations,
- ❖ selecting of an acceptable variant.

Technological process of production

In the technological process of product manufacture is necessary to ensure selection of appropriate means of production, namely:

- ❖ products production and production volume,
- ❖ determination of the technological processing structures and methods,
- ❖ technology and organizational structure of production, especially mass, production specified, degree of automation and flexibility,
- ❖ technology equipment - machines and devices, tools and products,
- ❖ handling equipment,
- ❖ control equipment. [3]

The choice of machine

The most important factor in machines classification is a kind of manufacturing plant production. This classification determined the concept of machine technology and automation. [2]

Classification systems of production machines recognize:

- ❖ universal production machines,
- ❖ specialized production machinery,
- ❖ special-purpose ,
- ❖ numerically controlled machine,
- ❖ numerically controlled manufacturing centers,
- ❖ numerically controlled machines for automated manufacturing systems.[1, 4]

Development of production variants

At this stage, to shape the overall concept of technology production. Detail degree of technology depends on whether the choice of production facilities does:

- ❖ for the compilation of the existing technological process in production,
- ❖ technological solutions to project a new or upgraded, respectively modernized production,
- ❖ reconstruction of production facilities.

It is possible to proceed in various ways to create proposals for production. One is the analysis of material flow in production. In Fig. 1 shows the analysis of material flow through production line graphical display.

Different variants of the production lines can be designed using the following symbols, depending on the technological process of manufacturing the product. Comparison of original and newly proposed material flow in production:

Symbol	classification activities
○	technological operation
□	control
→	transport, handling of material
D	break, downtime sorting
▽	storage
X	loading, unloading
⊥	weighing
⬡	packaging

Fig. 1 Symbols illustrated activities

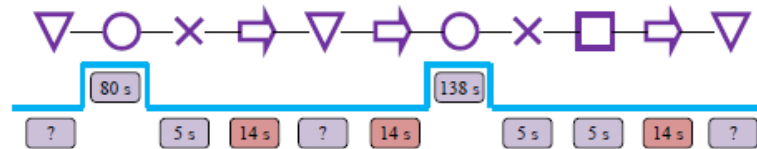


Fig.2 Production line variant by symbols

5. SIMULATION OF THE VARIANTS

Simulation of material flow production lines is shown in Fig. 3.

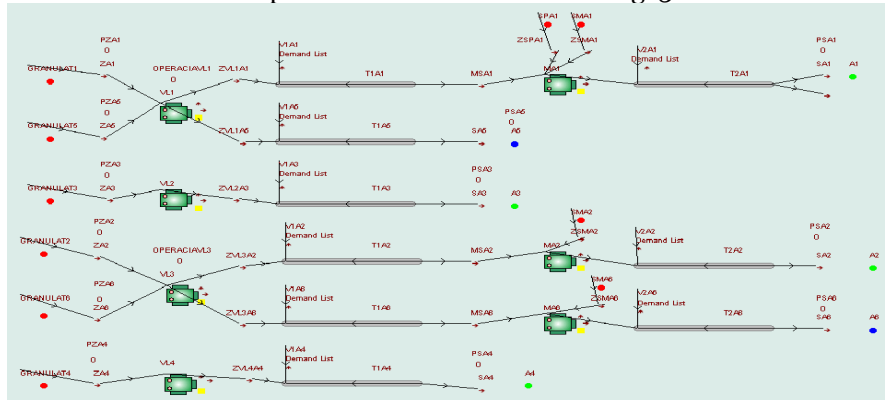


Fig. 3 Example of production lines simulation



Fig. 4 Graph operation of machines and devices during the simulation

6. GRAPHICAL SIMULATION OUTPUT OF MACHINERY AND DEVICES

The simulation software generates statistics on the performance of machines and devices after a simulation of the production line. In this case, the witness was used.

Based on the above chart it is possible to achieve productivity gains and to address the increasing efficiency of machines. The solution is to reduce downtime and streamlining manufacturing process technology for finishing. It is necessary to increase the number of inspectors who would ensure the continuity of material flow in quality control. This eliminates the accumulation of technology stocks.

7. CONCLUSION

Any proposal for a perfect relocation of production lines and the subsequent operation of the production system is still subject to further change. They are caused by innovation of products on the market, qualitative and quantitative requirements of the customer etc. Therefore, the production system in operation there may be changes in the parameters of the production system, which, depending on time may decrease, unchanged, or rise. Simulation of the production system is a tool to select from a large number of possible solutions. The simulation is to select the optimal variant. By choosing this option should be to optimize the production system. An appropriate choice of the optimal solution and the result of a rationalization of the project are dependent primarily on a thorough analysis of the production system and production program.

ACKNOWLEDGEMENT:

This paper was created thanks to project supported by European Union concrete Operational program RESEARCH and DEVELOPMENT (Appeal OPVaV-2009/2.2/03-SORO) named **Manufacture technical level and control effectiveness increase in the field of plastics component production**. Faculty of Material Science and Technology of Slovak University of Technology in Trnava is realized this project in cooperation with HANIL E-HWA AUTOMOTIVE SLOVAKIA s.r.o. in Považská Bystrica in Slovakia.

The main aim of cooperated project is increasing of manufacture technical level and of control effectiveness in the field of plastics component production with three specific project aims:

- ❖ Building of laboratory for construction and tool simulation for processing of plastics components,
- ❖ Material flow and production planning optimalization,
- ❖ Mechanisation and automation as a tooling for elimination of bad human factor influence to the manufacture quality.

This article was created with the support of the
OP Research and development for the project
**Manufacture technical level and control effectiveness increase in
the field of plastics component**
ITMS 26220220094,
co-financing from the resources of European Regional Development
Fund.



Support research activities
in Slovakia/
Project is co-financing
from resources EU



REFERENCES

- [1] Danišová, N., Zvolenský, R.: Intelligent manipulating and transport systems. In: International Doctoral Seminar 2007: Proceeding. 13-16 May, 2007, Smolenice. - Trnava : AlumniPress, 2007. - ISBN 978-80-8096-011-7. - pg. 34-38
- [2] Horváth, Štefan - Danišová, Nina: Power elements of flexible manufacturing and assembling systems. In: International Doctoral Seminar 2008 : Proceedings. Smolenice, May 18-20, 2008. - Trnava : AlumniPress, 2008. - ISBN 978-80-8096-058-2. - pg. 130-136
- [3] Horváth, Štefan - Javorová, Angela: Planning and design production system organizational structures and procedures. In: Annals of Faculty of Engineering Hunedoara - Journal of Engineering. - ISSN 1584-2673. - Tom VIII, Fasc 3 (2010), s. 331-335
- [4] Javorová, Angela - Matúšová, Miriam: Automated assembly system design with help of computer aided system. In: Annals of The Faculty of Engineering Hunedoara. - ISSN 1584-2665. - Tom VII, Fasc. 2 (2009), s. 43-48
- [5] Mudriková, Andrea - Hrušková, Erika - Velíšek, Karol: Logistics of material flow in flexible manufacturing and assembly cell. - registered in ISI Proceedings. In: Annals of DAAAM and Proceedings of DAAAM Symposium. - ISSN 1726-9679. - Vol. 19, No.1. Annals of DAAAM for 2008 & Proceedings of the 19th International DAAAM Symposium "Intelligent Manufacturing & Automation: Focus on Next Generation of Intelligent Systems and Solutions", 22-25th October 2008, Trnava, Slovakia. - Viedeň : DAAAM International Vienna, 2008. - ISBN 978-3-901509-68-1, s. 0919-0920
- [6] Mudriková, Andrea - Košťál, Peter - Velíšek, Karol: Material and information flow in flexible manufacturing cell. - registered in ISI Proceedings. In: Annals of DAAAM and Proceedings of DAAAM Symposium. - ISSN 1726-9679. - Vol. 18, No.1. Annals of DAAAM for 2007 & Proceedings of the 18th International DAAAM Symposium "Intelligent Manufacturing & Automation: Focus on Creativity, Responsibility, and Ethics of Engineers" : Croatia, Zadar 24-27th October 2007 (2007). - Viedeň : DAAAM International Vienna. - ISBN 3-901509-58-5, s. 485-486
- [7] Pecháček, František - Charbulová, Marcela: Stavebnicové upínacie systémy. Modular fixture systems. In: Strojárstvo - Strojírenství. - ISSN 1335-2938. - Roč. 12, č. 9 (2008), 191/5-192/5





STRUCTURAL PROPERTIES OF NANO- STEEL POWDERS PREPARED BY POWDER METALLURGY

¹ UNIVERSITY OF PANNONIA, EGYETEM U. 10, 8200 VESZPRÉM, HUNGARY

² RESEARCH INSTITUTE FOR TECHNICAL PHYSICS AND MATERIALS SCIENCE, HUNGARIAN ACADEMY OF SCIENCES, KONKOLY-THEGE M. ÚT 29-33, 1121 BUDAPEST, HUNGARY

ABSTRACT:

In this paper, the first results of preparation and structural characterization of the nanostructured strengthened steels are presented. The samples were prepared by powder technology. A high energy milling process at different parameters has been applied to strengthened steel powder production. The high efficient attrition mills are on the basis of this work assuring grains with nanostructure. Powder samples were investigated by scanning electron microscopy (SEM). The structural changes during milling steps have been described. It was demonstrated that 4 hours milling in wet atmosphere are enough to realize steel powders with nano dimensions.

KEYWORDS:

nanostructured strengthened steels, powder technology, scanning electron microscopy (SEM)

1. INTRODUCTION

Oxide dispersion strengthened (ODS) FMS are promising materials with a potential to be used at elevated temperatures due to the addition of extremely thermally stable oxide particle dispersion into the austenitic or martensitic matrix. ODS steels show high-strength at high-temperatures [1]. Oxide-dispersion-strengthened steels have attracted attention for advanced nuclear power plants applications such as fast and fusion reactors, because of their superior high temperature mechanical properties [2, 3]. ODS steels are being developed and investigated for nuclear fission and fusion applications in Japan [4, 5], Europe [6, 7] and the United States [8, 9].

Powder metallurgy of stainless steel (PM SS) components constitutes an important and growing segment of the PM industry. The PM processing provide a feasible and economic manu-facturing of au-stenitic stainless steels components with complex shape and advantages such as good dimensional precision, high surface finish and good mechanical properties [10 – 14]. The production of oxide dispersion- strengthened steel involves many processes, such as mechanical alloying, degassing, canning, hot extrusion, and heat treatments. In the procedures, the hot extrusion process strongly affects precipitation behavior of oxide particles and their dispersion. [15]. Fundamental studies concerning optimization of mechanical milling (MM) processing as well as effects of alloying elements on the high-temperature mechanical strength had been carried out in cooperation with fabrication vendors [16].

In this work, the structural and morphological properties of nanostructured ODS steel powders prepared by powder metallurgy methods are presented.

2. THE STUDY

An efficient dispersion of ODS steels will be achieved by employing a high efficient milling process, namely the attritor milling (Figure 1). In this paper the wet coating process of fine ceramic particles is proposed by the help of mechano-chemical processes assured by attrition milling. In the case of our model experiments, for some of the powder mixtures a high efficient attritor mill (DMQ-07 Union Process) was employed. This apparatus allowed a high rotation speed (2000-2800 rpm)

and a contamination free mixing process, because of stainless steel parts (tank, arm, balls) as in Figure 1.

Based on our former observations the attritor mill has more advantages to conventional planetary mill. In the wet process, the attritor may work at higher speeds as 3000 rpm in comparison to planetary mill, 500 rpm. The delta discs employed in the attritor, as well as the small media 0.1- 1 mm assure a very efficient dispersion. The commercial austenitic powder (Hoganas 316L) were milled by attritor for 1, 2, 3, 4 and 5 hours in propanol (wet milling).

Morphology and microstructure of the powder and sintered steels were studied by scanning electron microscope (Zeiss-SMT LEO 1540 XB and Jeol JSM-25-SIII).

3. ANALYSES, DISCUSSIONS, APPROACHES AND INTERPRETATIONS

Structural characterization of starting austenitic steel powder was performed by scanning electron microscopy (Figure 2). Austenitic sample consisted of globular particles. The average size of particles is 50 – 100 μm . The composition of starting austenitic powder is Fe and 0,02% C, 13% Ni, 16,8% Cr, 0,85% Si, 0,20%O, 0,04% N and 2,2% Mo.

The powder structure after 1 hour milling showed considerable differences to starting powder. The forms of austenitic particles are globular. Their average size is lower, about 80 μm (Figure 3a). The structural investigations demonstrated the existence of small grain in few micrometer ranges among globular grains (Figure 3b).

Figure 4 showed the morphology of austenitic sample after 2 hours milling time. The average size of globular particle is about 60 μm . 1 hour intensive high efficient milling decreased the particle size about 15 – 20 μm . The shape of grains has not changed.



Figure 1. Horizontal high efficient attritor mill

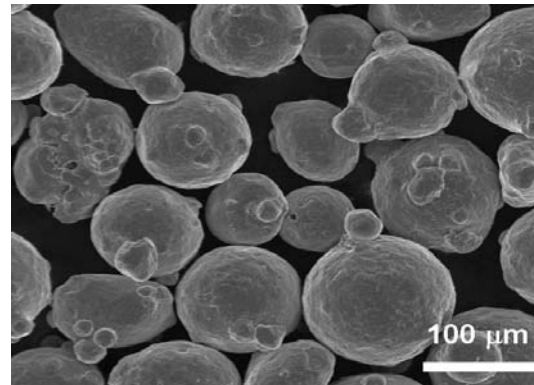
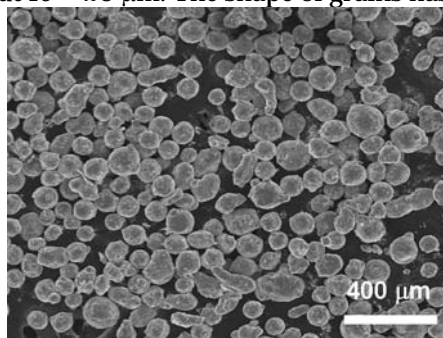
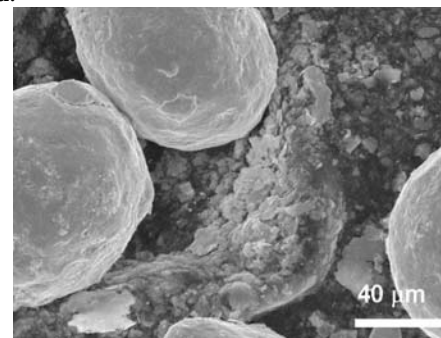


Figure 2. SEM image of starting commercial austenitic powder

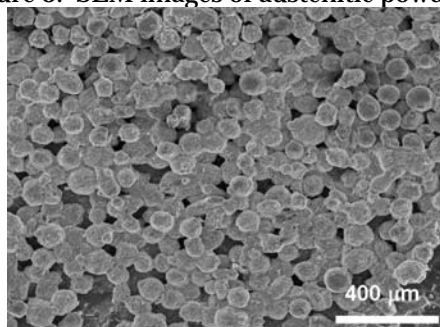


a)

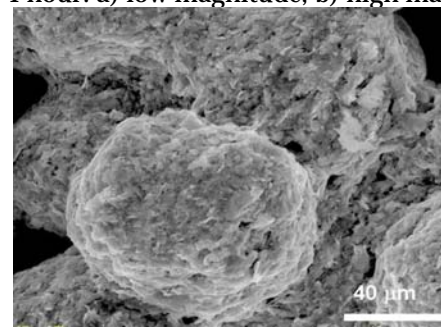


b)

Figure 3. SEM images of austenitic powder milled for 1 hour. a) low magnitude, b) high magnitude



a)



b)

Figure 4. SEM images of austenitic powder milled for 2 hour. a) low magnitude, b) high magnitude

The next 1 hour milling time (3 hours) decreased the particle size about $10\ \mu\text{m}$ as shown the Figure 5a. The parts of particles are globular, but the SEM investigation proved the developing of particles with rough surface (Figure 5b). This disintegration effect is on the basis of the evaluation of nanoparticles.

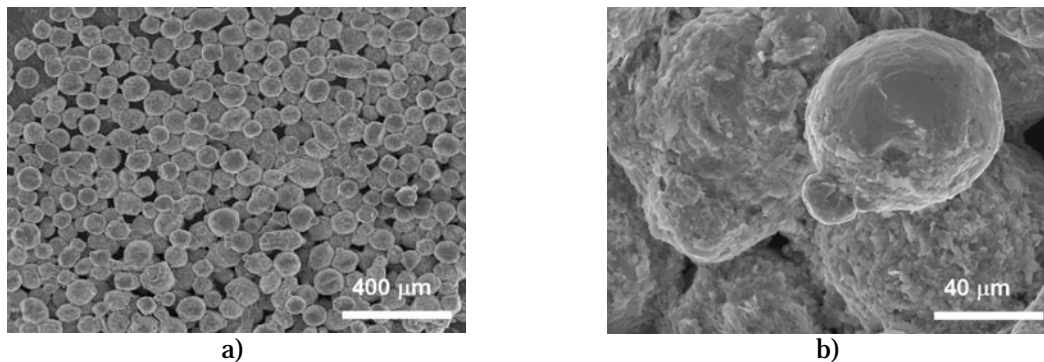


Figure 5. SEM images of austenitic powder milled for 3 hour. a) low magnitude, b) high magnitude

After 4 hours wet milling, the structure showed the drastically change in morphology. The sample consisted of very small austenitic grains with lamellar structure and of few $80\ \mu\text{m}$ size globular particles (Figure 6a). The average size of lamellar particles in one dimension is nanometer range, their length is few micrometers (Figure 6b).

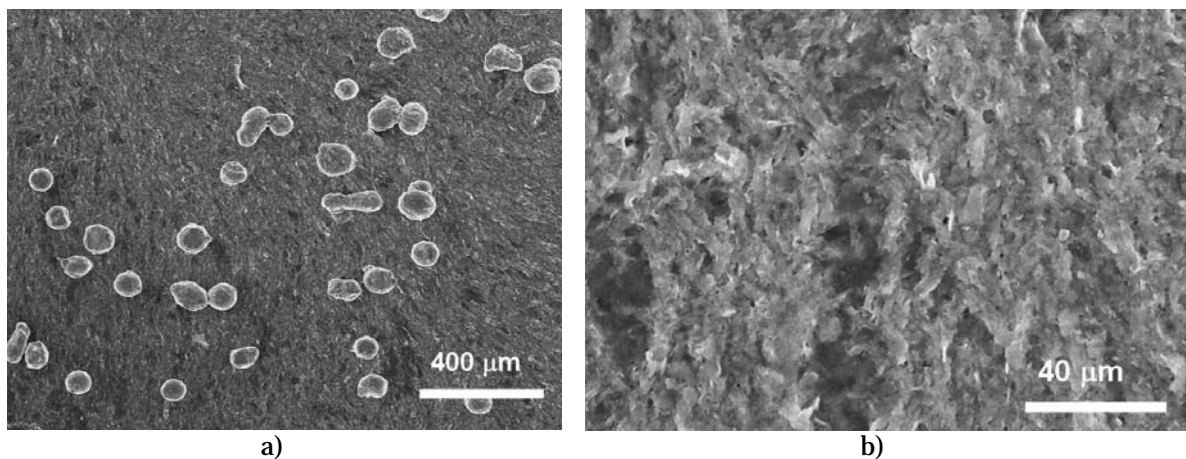


Figure 6. SEM images of austenitic powder milled for 4 hour. a) low magnitude, b) high magnitude

The final nanostructure was achieved after 5 hours milling time (Figure 7a). The sample consisted from very thin lamellar particles, the existing of larger grains is not shown. Figure 7b show the very fine austenitic structure.

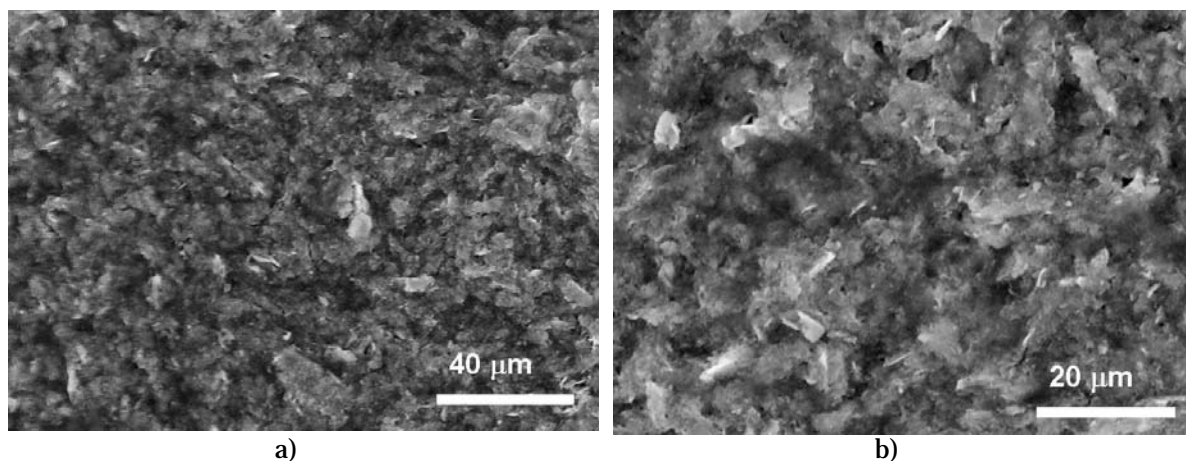


Figure 7. SEM images of austenitic powder milled for 5 hour. a) low magnitude, b) high magnitude

4. CONCLUSIONS

In this paper, the first results of preparation and structural characterization of the strengthened nanostructured steels prepared by the powder technology is presented. A high energy wet milling process in propanol for 1, 2, 3, 4 and 5 hours milling time has been applied to strengthened steel powder production. The structural changes have been observed. The average size of starting commercial austenitic powder was about 100 μm . The particle size of nanometer range in was achieved after 4 milling hours.

The help in the preparation of this work is gratefully acknowledged to Gy. Babócs, P., V. Varga, A. Petrik, L. Illés. Special thanks to Dr. Á. Horváth (AEKI). This work is supported by TÁMOP 4.2.2-08/1-2008-0016 project.

REFERENCES

- [1.] A. Kimura, T. Sawai, K. Shiba, et al. Nucl. Fusion 43 (2003) 1246.
- [2.] J.J. Huet, Powder Metall. 10 (1967) 208.
- [3.] J.J. Huet, V. Leroy, Nucl. Tech. 24 (November, 1974) 216.
- [4.] S. Ukai, T. Nishida, H. Okada, T. Okuda, et al., J. Nucl. Sci. Technol. 34 (1997) 256.
- [5.] S. Ukai, T. Yoshitake, S. Mizuta, et al., J. Nucl. Sci. Technol. 36 (1999) 710.
- [6.] A. Alamo, J. Decours, M. Pigoury, C. Foucher, Structural Applications of Mechanical Alloying, ASM International, Materials Park, OH, 1990.
- [7.] A. Alamo, H. Regle, G. Pons, L.L. Bechade, Mater. Sci. Forum 88–90 (1992) 183.
- [8.] D.K. Mukhopadhyay, F.H. Froes, D.S. Gelles, J. Nucl. Mater. 258–263 (1998) 1209.
- [9.] M.K. Miller, E.A. Kenik, K.F. Russell, et. al., Mater. Sci. Eng. A 353 (2003) 140
- [10.] F. Borgioli, E. Galvanetto, T. Bacci, et al., Surf. Coat. Technol. 149 (2002) 192–197.
- [11.] O. Sandberg, L. Jönson, Advances in Powder Metallurgy, Adv. Mater. Process. 12 (2003) 37–42.
- [12.] P. Lindskog, The future of ferrous PM in Europe, Powder Metall. 47 (2004) 6–9.
- [13.] Koszor O, Horváth A, Weber F, Balázsi K, Gillemot F, Horvath M, Fényi B, Balázsi Cs, KEY ENG MAT 409: pp. 237-243. (2009)
- [14.] H. Sakasegawa et al. / Journal of Alloys and Compounds 452 (2008) 2–6
- [15.] T. Okuda, S. Nomura, et al., Proc. Symp. Sponsored by the TMS Powder Metallurgy Committee, Indiana, 1989, p. 195.





¹ Martina KUSÁ, ² Miriam MATÚŠOVÁ, ³ Marcela CHARBULOVÁ

OPTIMALISATION METHOD OF MATERIAL FLOW AT MANUFACTURING PROCESS

¹⁻³ SLOVAK UNIVERSITY OF TECHNOLOGY, FACULTY OF MATERIALS SCIENCE AND TECHNOLOGY,
INSTITUTE OF PRODUCTION SYSTEMS AND APPLIED MECHANICS, TRNAVA, SLOVAKIA

ABSTRACT:

A today trend in manufacturing is characterized by production broadening, innovation cycle shortening, and products having new shape, material and functions. The production strategy focused to time needs change from traditional functional production structure to production by flexible manufacturing cells and lines. Production by automated manufacturing system (AMS) is a most important manufacturing philosophy in last years.

KEYWORDS:

production system, manufacturing, material flow, layout optimizing

1. INTRODUCTION

This paper was created thanks to project Operational program RESEARCH and DEVELOPMENT (OPVaV-2009/2.2/03-SORO) number ITMS 26220220094 named „Manufacture technical level and control effectiveness increase in the field of plastics component production“. Faculty of Material Science and Technology of Slovak University of Technology in Trnava is realized this project in cooperation with HANIL E-HWA AUTOMOTIVE SLOVAKIA s.r.o. in Považská Bystrica in Slovakia.

The main target of project is a manufacturing and control processes effectivity increasing at plastics parts production process. Goal of effectivity increasing is competitiveness increasing at automotive manufacturing market by knowledge and technology transfer and joined research and development activities between industrial and academic sphere.

This project is covered by the category of applied research. It is focused to planed research for new knowledges and skills acquirement for new plastic component development (tools for plastics molding), processes (new processes in manufacturing) and significant quality increasing of existing products (existing tools and processes optimizing).

Rationalization of production system allows elimination of negative influences on production costs and product price. Rationalization projects starts with data acquisition followed by analysis and evaluation of data. Once aims of rationalization are clearly defined a new production system or innovative production process is designed. Designed changes cannot be implemented during production of the factory, because effectiveness of proposed alternatives is not guaranteed. Due to this reason, simulation of proposed alternatives using various simulation computer programs gains on importance. Simulation is a suitable tool for elimination of imperfections in production process. Furthermore, it allows searching for possibilities of increasing effectiveness of production as well as for problems, which may interfere with continuous production cycle of a factory.

Main aim of rationalization projects is an improvement of production processes and prevention from losses and wasting of all possible kinds of production resources (material, energy, production area, production time, production facilities, etc.), this all from material purchase from supplier to dispatch of finalized products to customer at all workstations as in case of production preparation so as during production itself.

2. LAYOUT OPTIMIZATION

Principle of systematic application of logical thinking during solution of difficult issues and elimination of losses and wasting during production process is aimed predominately at 4 essential areas:

1. Minimization of stock size and supply and release of financial resources and also lowering the logistics expenditures for storage, manipulation, etc.
2. Constant improvement of all activities of logical chain: suppliers – product – customer (lowering the production costs, shortening the production time, improvement of work environment, etc.)
3. Concentrate attention at sites, which are decisive for quality, competitiveness, perspective, productivity, costs, etc.
4. Optimize system of material and information flows – eliminate losses, which may cause irregularity or overload of production, complexity of material flows, downtime caused by organization imperfections, etc..

Solving the optimization of production requires detailed information about whole production process. Because technological procedure of production is given, it is possible to adjust material and data flow. Fig. 1 shows former structure of material flow through production. Aim was to provide continuous production process in automotive area of Hanil company.

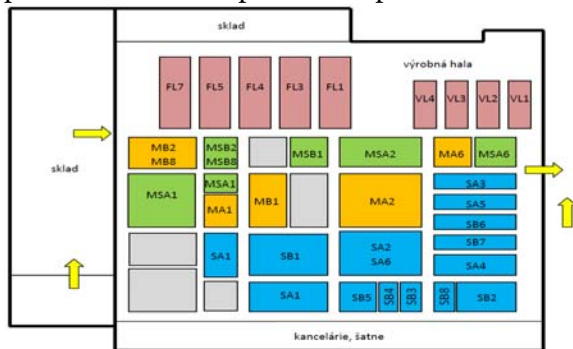


Fig. 1 Former layout of the company workshop

Wastage is present at each workshop, but it is possible to identify and solve it using 5S method, which is suitable for production and service oriented organizations. Applying the 5S method allows achieving an improvement and simplification of material flow, machine layout and stock.

Other benefits are:

- ❖ Quality, productivity and safety improvement
- ❖ Better company culture, people attitude, less apathy
- ❖ Improved work environment.

Method of 5S is under development and nowadays sixth S is also defined, know as safety. Reason is to realize all improvements at workplace in such manner, that employees are not endangered. Apart of this, it put emphasis on availability and unambiguous identification of all safety devices. The aim is to prevent from danger during work and limit occupational accident to a minimum possible.

The aim of material flow projection is solution of:

- ❖ Minimization of transport, manipulation and storage
- ❖ Simplification of system to minimum – minimum consumption of expenses and time □ solution of important relationships,
- ❖ Workplaces and capacities – incorrectly designed capacity causes unevenly distributed material flow, stock accumulation, necessity of inter-stocks and buffers and additional manipulation activities,
- ❖ Information flow and control system – correct control of inputs of production tasks, synchronization of purchase, production and dispatch, coordination of system of production control with transportation system,
- ❖ All components of the production system have to be designed in mutual relations and it is ideal if all are verified before installation using simulation model.

Solving the given material flow requires specification of the aim of innovation of a given material flow.

The proposal of the layout of production lines is solved as a combination of concerned layout (according to a number of products declared in PQ diagram) and technological layout (consideration of a technology of injection and technology of forming). In the frame of detailed design were relocated beginnings MT on production facilities in order to eliminate intersection of MT directly in front of production facilities. In fact this change counts only

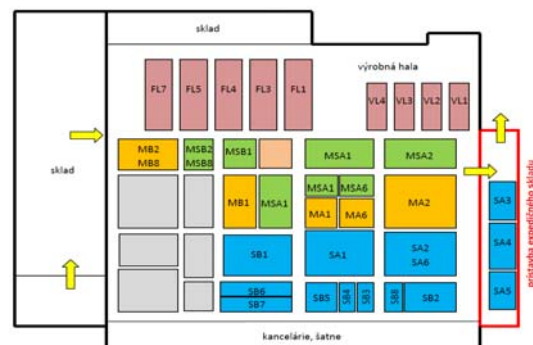


Fig.2 Innovation of the workshop

for location of the product, which undergoes technological operation. Combination of products in the frame of one production facility remains with respect to the available capacity unchanged. Respecting the MT proposal, the layout of stocks is realized close to dispatch, taking into account space required for expedition trolleys. Distribution of a part of trolleys with finalized products is realized in proposed annex building of dispatch stock with dimension of 10 × 70 meters.

Simulation of the proposed change is possible to avoid unavailing losses during ineffective trials related with application of innovations. During simulation is required to fulfill production plan, which is documented in the form of a table.

Fig. 3 shows production plan, which is compared with values of outputs after the simulation is completed.

SOFT TRIM				MAREC				ROK 2010								
sk. B	VÝROBOK	počet ks v aute	ED 5DV	ED WGN	ED 3DV	KM	EL	počet aut	celkom ks/mesiac	ED 5DV	ED WGN	ED 3DV	KM	EL	počet aut	celkom ks/rok
1.	LUGGAGE SIDE S	2	4 550	3 900	1 150			9 600	19200	50 600	43 400	12 300			106 300	212600
2.	FLOOR CARPET FRT	1	4 550	3 900	1 150	2 200		11 800	11800	50 600	43 400	12 300	33 700		140 000	140000
3.	LUGGAGE CVR MAT	1	4 550		1 150			5 700	5700	50 600		12 300			62 900	62900
4.	LUGGAGE CVR BORD	1	4 550		1 150			5 700	5700	50 600		12 300			62 900	62900
5.	C/SELF	1	4 550		1 150			5 700	5700	50 600		12 300			62 900	62900
6.	LUGGAGE CVR"G CTR	1		3 900				3 900	3900		43 400				43 400	43400
7.	LUGGAGE CVR"G FRT	1		3 900				3 900	3900		43 400				43 400	43400
8.	FLOOR CARPET RR	1				2 200		2 200	2200				33 700		33 700	33700

Fig. 3 Production plan

Figure 4 depicts simulation of SOFT TRIM component production in HANIL company and partial tables with outputs from simulation.

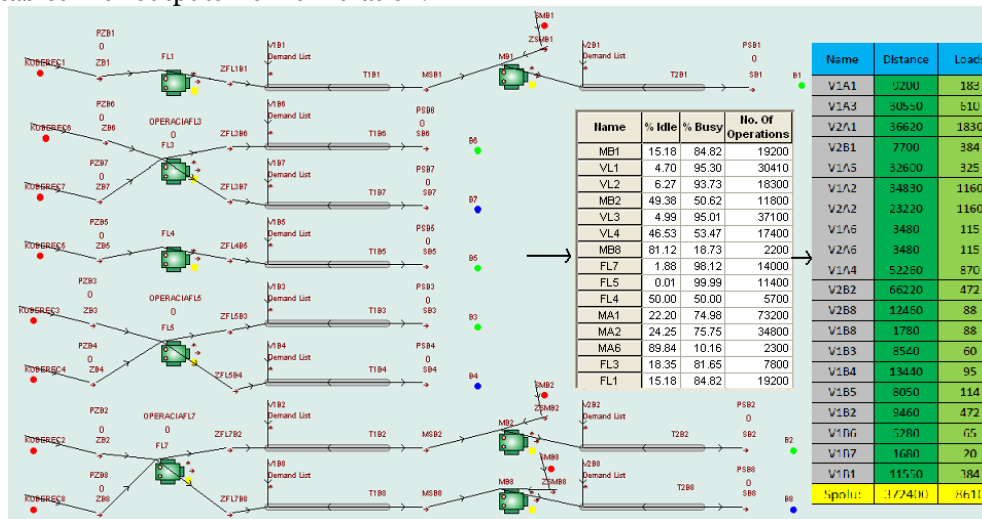


Fig.4 Simulation of innovation of workshop layout

3. CONCLUSIONS

Proposal of new layout of production lines is adjusted for current capacity of production with aim to optimize material flows. Application of proposed solution is in fact possible to realize during full production process, because it counts mostly for relocation of dispatch trolleys. Relocation of those trolleys would be effective after finishing the building of dispatch hall at current dispatch site. Building the dispatch hall would not affect production process, what is benefit of the proposed solution. Expected time required for building up the dispatch hall with dimensions of 10×70 meters is approximately one month. After finalizing the hall, zones required for different types of trolleys would be calculated and subsequently labeled zones for stock areas, service areas and transportation paths. After the trolleys relocation and clear out the spaces, workplaces for assembly would be relocated. This procedure would affect the production process significantly. This change would be implemented during weekends using internal employees of the company, predominately. Implementation of all changes is expected to last approximately two months. From economic point of view, most significant impact would have an investment into the new stock for distribution logistics. Expenses related with relocation of workplaces are negligible and could be realized also during full production. When comparing this investment with shortening transportation time between workplaces, return on investment is expected in few months. From the long term point of view and considering ambitions of the company, which are aimed at increasing volume of production, the investment into dispatch stock is in short term range necessity. Other advantage of building the dispatch stock is simplification of production process and establishment of space for dispatch trolleys with finalized products.

This article was created with the support of the
OP Research and development for the project
**Manufacture technical level and control effectiveness increase in
the field of plastics component**
ITMS 26220220094,
co-financing from the resources of European Regional Development
Fund.



Support research activities
in Slovakia/
Project is co-financing
from resources EU



REFERENCES

- [1] Danišová, N. - Zvolenský, R.: Intelligent manipulating and transport systems. In: International Doctoral Seminar 2007 : Proceeding. 13-16 May, 2007, Smolenice. - Trnava : AlumniPress, 2007. - ISBN 978-80-8096-011-7. - pg. 34-38
- [2] Horváth, Š. - Danišová, N.: Power elements of flexible manufacturing and assembling systems. In: International Doctoral Seminar 2008 : Proceedings. Smolenice, May 18-20, 2008. - Trnava : AlumniPress, 2008. - ISBN 978-80-8096-058-2. - pg. 130-136
- [3] Hrušková, Erika - Holubek, Radovan - Velíšek, Karol: The possibilities of increasing the flexibility of intelligent assembly cell. In: 10th Biennial Conference on Engineering Systems Design and Analysis (ESDA2010) : Turkey, Istanbul, July 12-14, 2010. - : ASME, 2010. - ISBN 978-0-7918-3877-8. - S. 1-10
- [4] Mudriková, Andrea - Hrušková, Erika - Velíšek, Karol: Logistics of material flow in flexible manufacturing and assembly cell. - registrovaný v ISI Proceedings. In: Annals of DAAAM and Proceedings of DAAAM Symposium. - ISSN 1726-9679. - Vol. 19, No.1. Annals of DAAAM for 2008 & Proceedings of the 19th International DAAAM Symposium "Intelligent Manufacturing & Automation: Focus on Next Generation of Intelligent Systems and Solutions", 22-25th October 2008, Trnava, Slovakia. - Viedeň : DAAAM International Vienna, 2008. - ISBN 978-3-901509-68-1, s. 0919-0920
- [5] Mudriková, Andrea - Košťál, Peter - Velíšek, Karol: Material and information flow in flexible manufacturing cell. - registrovaný v ISI Proceedings. In: Annals of DAAAM and Proceedings of DAAAM Symposium. - ISSN 1726-9679. - Vol. 18, No.1. Annals of DAAAM for 2007 & Proceedings of the 18th International DAAAM Symposium "Intelligent Manufacturing & Automation: Focus on Creativity, Responsibility, and Ethics of Engineers" : Croatia, Zadar 24-27th October 2007 (2007). - Viedeň : DAAAM International Vienna. - ISBN 3-901509-58-5, s. 485-486
- [6] Pecháček, F.; Charbulová, M.: Stavebnicové upínacie systémy. Modular fixture systems. In: Strojárstvo - Strojírenství. - ISSN 1335-2938. - Roč. 12, č. 9 (2008), 191/5-192/5
- [7] Velíšek, Karol - Javorová, Angela - Košťál, Peter: Flexible assembly and manufacturing cell. In: Academic Journal of Manufacturing Engineering. - ISSN 1583-7904. - Vol. 5, No. 2 (2007), s. 141-144





VIBRATION TECHNIQUE – AN IMPROVEMENT SOLUTION FOR QUALITY OF CAST METALLIC MATERIALS

¹⁻²UNIVERSITY POLITEHNICA BUCHAREST, ROMANIA

ABSTRACT:

The influence of purifying processes by metallic melts degassing and refinement it is not a recent technological news. The processes of local undercooling, nucleation, crystallization and solidification of metallic melts represent a future technical solution in quality increase of castings. The work presents the results of some reasearch experiments in this field.

KEYWORDS:

undercooling, nucleation, crystallization, metallic melts, castings

1. INTRODUCTION

High and low frequency mechanical oscillations, sonic and ultrasonic vibrations respectively, may form only in elastic continuous medium, and general acoustic laws are available also in the ultrasonic vibrations range.

Mechanical vibrations or sonic and ultrasonic vibrations convey by progressive particles movement of the medium, melt alloy respectively, and due to this particles will come back in the initial position.

Due to the inertia and elasticity of the liquid alloy, particles continue to oscillate around the equilibrium position, even after vibrations stop, but with a damped movement. If the oscillation direction of the particles is parallel with the propagation direction of the wave, waves are called longitudinal waves and the interference is made in the propagation direction, namely the particles movement $X(t)$ in the system which oscillate according to the harmonic oscillations, is parallel with normal \vec{n} to the waves surface.

Propagation speed of longitudinal elastic waves in solid medium is expressed by the square root of the elastic modulus and density ratio, with the Newton relation [1]:

$$v = \sqrt{\frac{E}{\rho}} \quad (1)$$

where: v is propagation speed of waves [m/s];

E – elastic modulus [N/mm²];

ρ – density of the medium [kg/m³].

If we considerate the fact that oscillations are produced adiabatically, namely the variation speed of pressure is so high that the heat exchange between the near layers can be neglect, the propagation speed of mechanical oscillations in elastic liquid mediums is given by the relation:

$$v = \sqrt{\frac{1}{\rho \cdot K}} \quad (2)$$

ρ is desity of the medium [kg/m³];

K – adiabatic compression of the medium.

$$K = \frac{1}{\chi \cdot p} \quad (3)$$

χ - specific heats ratio varying with number of atoms in the molecule;
 p - alloys pressure at a given moment [Pa].

For gases, elastic modulus has to be replaced with pressure. Because of rapid progressive dilatations and compressions, the local temperatures have variations which can not be balanced by heat exchanges. These compressions and dilatations have adiabatic feature.

If we multiply the pressure with the specific heats ratio, the propagation speed of longitudinal waves will be expressed by relation:

$$v = \sqrt{\frac{p}{\rho} \cdot \chi} \quad (4)$$

Knowing the value of $\chi = 1.66$ for monoatomic gases, 1.4 for biatomic gases and 1.33 for triatomic gases, thus we can calculate the speed v .

Relation (4) gives the possibility to calculate the speed, at a given temperature t , when temperature t_0 is known and pressure stays unchanged.

Knowing that density varies with temperature by the relation:

$$\rho_t = \frac{\rho_0}{1 + \alpha \cdot \Delta t} \quad (5)$$

results:

$$v = \sqrt{\frac{p \cdot (1 + \alpha \cdot \Delta t)}{\rho_0}} \cdot \chi \quad (6)$$

and thus:

$$v_t = v_0 \sqrt{1 + \alpha \Delta t} \quad (7)$$

In conclusion: speed of the elastic longitudinal waves for gases, increase proportionally with the square root of dilatation binomial [1].

In real conditions of solidification, pressures may reach values of dozens of atmospheres and may substantially influence on the reordering of the insoluble impurities and crystalline structure formation of metals.

Crystallization pressure p is the maximum possible for a given undercooling of the growing surface, calculable with relation:

$$p = - \frac{\Delta T \cdot L}{T \cdot V_0} \quad (8)$$

where: ΔT is alloy undercooling [K];

L – latent heat of alloy crystallization [J/kg];

T – absolute temperature [K];

V_0 – molecule volume in crystal lattice [m³/kmol].

At high undercoolings appear many centres of crystallization embedding all impurities. At low undercooling, crystals grow in dendritic form, and impurities are also embedded by the growth of branches I and II type.

Analysis of the thermophysical conditions of crystallization pressure development shows that it has a peculiar role in ingots and castings solidification. To identify the influence rate of different parameters on the movement process or impurities embedding, we will show how forces influence in the area of stranger particles for the alloy in solidification progress (fig.1).

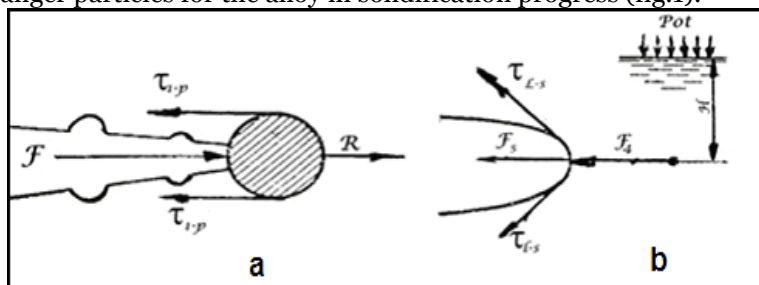


Fig.1. Representation of forces action in area of stranger particles in the liquid alloy
 a) interaction with particle; b) exceeding the ferrosstatic pressure

Force of crystallization pressure of the crystal acts on the particle being able to move in the alloy with crystallization speed. Forces of interphasic tensions inbetween impurities and liquid

alloy stand up to this movement ($\Gamma_{\sigma} = \pi \cdot r \cdot \sigma_{l-p}$), and movement hydrodynamical resistance of spherical surface in the alloy is:

$$\Gamma_s = C_r \cdot \rho \cdot \frac{v_{\text{crist}}^2}{2} \cdot \pi \cdot r^2 \quad (9)$$

Equilibrium conditions of forces are:

$$\frac{\Delta T \cdot L}{T \cdot V} = \pi \cdot r \cdot \sigma_{l-p} + C_r \cdot \rho \cdot \frac{v_{\text{crist}}^2}{2} \cdot \pi \cdot r^2 \quad (10)$$

where: C_r is the resistance coefficient.

Knowing the crystallization speed v_{crist} and ΔT we can determine the tolerable radius of the inclusion which is going to be separated by the crystallization pressure inside the casting, where after that it will be able to curdle and float to the surface.

It has been determined that during crystallization process of the alloy it may appear some ferrosstatic pressures same as alloy hydrodynamical resistance itself. This assumption is real, since the dendrites growth (according to the literature) it takes place with the speed $v_{\text{crist}} = 1000$ mm/min. In some conditions, the growth speed can be much more increased.

Analysing the scheme for this case in fig.1.b, it results that following forces acts on the growing crystal:

- 1) Force of ferrosstatic pressure

$$F_f = p_{\text{at}} + \gamma \cdot H \quad (11)$$

where: p_{at} is atmospheric pressure [N/m²];

H - height of metal layer above the crystal [m];

γ – alloy specific weight [N/m³].

- 2) Force of hydrodynamic resistance

$$F_s = C_f \cdot \rho \cdot \frac{R^2}{2} \cdot \pi \cdot r^2 \quad (12)$$

- 3) Capillary forces of moistening

$$F_{\sigma} = \pi \cdot \sigma_{l-s} \quad (13)$$

σ_{l-s} – interphasic force at alloy-crystal limit.

Based on these equations it might be assumed:

$F > F_f + F_s + F_{\sigma}$ crystal growth can take place;

$F < F_f + F_s + F_{\sigma}$ crystal growth is arrested or interrupted;

$F = F_f + F_s + F_{\sigma}$ it appears the optimum crystallization speed;

$$v_{\text{crist}} = \frac{1}{r} \cdot \sqrt{\frac{2}{C_f \cdot \pi \cdot \rho} \left(\frac{\Delta T \cdot L}{T \cdot V} - \pi \cdot r \cdot \sigma_{l-s} \right)} \quad (14)$$

Fact that at the liquid – mould contact at the beginning of crystallization, the undercooling ($\Delta T = 150 - 200^{\circ}\text{C}$) and real speed of crystallization doesn't exceed 25–30 mm/min in the first minute, leads to the idea that beside the thermophysical conditions, crystallization is also influenced by hydrodynamic ones. This fact is proven by lower dimensions of crystalline grains from the inferior levels of the ingot which solidify under the influence of some high ferrosstatic pressures.

2. METHODOLOGY

Greatest effects of ultrasonic cavitation are those observed in the metals crystallization process. The kinetics of this process it can be characterized by the nucleation rate (number of crystallization centers “n” which appears on the volume unit in the time unit) and linear growth speed “c” of crystals. More higher the nucleation speed and lower the growth speed is, more finer the grains structure will be.

Number of grains is determined by relation:

$$N = \sqrt{\frac{n^3}{c^3}} \quad (15)$$

Granular structure with fine grains randomly oriented with about same size in any direction, indicates a macroscopic isotropic and relatively homogeneous material, with good properties from

technological point of view. Undercooling degree influences both the kinetics of crystallization and structure, and formed crystals configuration. For high values of crystalline undercooling, crystals grow without attaining a regular shape and get a branched dendritic form, which reduces significantly the resistance of material.

The cavitation will appear in ultrasonic melts, if the acoustic pressure exceeds a specific value (table 1) feature to every metal. Usually, there are favoured the incipient conditions and cavitation bubbles in the melts, because they easily saturate with different gases, dissolved in melts volume, and their different solubility degree eases the formation of undissolved gas supply of nucleation centers of cavitation.

Cavitation process, generate shock waves of high intensity in the melts, nearby the crystallization front (if we consider the factors which produce the break of and dispersion of growing crystals, as a strong local perturbation source of homogeneity and melts thermodynamical equilibrium respectively).

Table 1. Values of P_t and P_c for some metallic materials

Material	Threshold power P_t [W]	Inceipient power of cavitation [W]
Aluminium	400	400
Bismuth	60	50
Cadmium	400	-
Lead	250	200
Antimony	300	300
Tin	350	250
Zinc	500	-

Effects role of cavitation in fine granular structure formation of metals appear when it exists a correlation between ultrasonic threshold power $P_{t \text{ required}}$ for important structure modifications and power P_c at which cavitation will start to appear into the melt. For cadmium and zinc cases, when cavitation appears at much more higher powers (over 400) given to that required for obtaining a fine structure, it results that cavitation has no effect for obtaining a fine granular structure.

Cavitation influence on crystallization process it can be explained by the fact that pulsatile cavitation bubbles appear in the melt, whose volumes suddenly increase in semiperiod of expansion and liquid evaporation takes place inside the bubble. Increase of evaporation and bubble volume leads to a decrease of temperature inside of it. If temperature reaches below the equilibrium one, melt gets into an undercooled state at bubble wall and it might appear a crystallization center. In the next stage, when bubble breakage takes place, the crystal just formed it detaches the bubble wall due to the difference between liquid speed and that of the solid phase, and shock wave generated by the implosion of bubble will throw the crystalline nucleus into the melt mass.

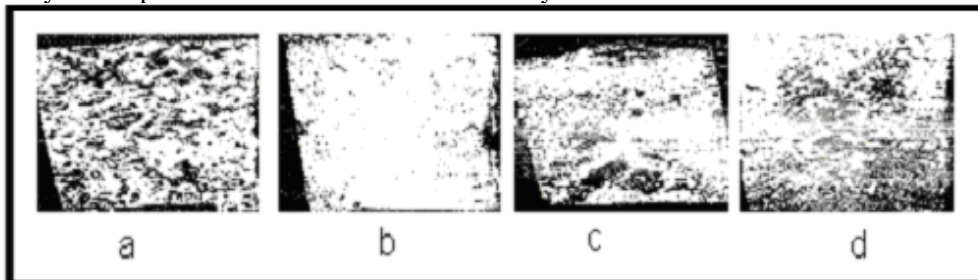


Fig.2. Structure of bismuth ultrasonic vacuum processed samples:

- a) reference ingot; b) processed ingot at atmospheric pressure; c) at pressure of 10^{-3} mmHg; d) at pressure of $1,5 \cdot 10^{-3}$ mmHg.

Another explication is based on shock wave generation during cavitation bubble breakage.

Efficiency of ultrasonic depends on the capacity of ultrasound to penetrate the melt volume and the capacity of crystallization process. Penetration of ultrasound into the melt is determined by the acoustic joint made between the acoustic radiator and melt, and in its turn, this joint is function of interfacial tension on the radiator – melt separation surface and the melt viscosity. Cavitation effects has a significant role, leading to the substantial improvement of mechanical and technological properties of materials.

Fluxes of metallic melt mass which move along the solidification limit with high speed and form low pressure areas, can generate hydrodynamic cavitation. By decreasing absolute pressure (below the critical one), in this area will appear gas bubbles or cavitation bubbles, filled with vapours. Their movement from low pressure areas leads to bubbles destruction (breakage), this

being accompanied by the immediate increase of pressure and temperature and destroys the solidification front.

Pressures reached in the moment of gas bubbles disintegration in liquid may be considerable (see table 2). Maximum cavitation pressure is in the center of bubble, and at a distance of $l = 2r$ it decreases with more than two times. Therefore, cavitation caverns in narrow bands form are close to the damaged solid surface.

Table 2. Pressure value in the moment of gas bubbles disintegration in liquid

Initial radius of the bubble r_0 [mm]	Radius in the breakage moment r [mm]	Maximum pressure in the breakage moment P_{max} [MPa]	Pressure at distance: $l = 2r$ [mm]
40	0.64	220	-
40	0.017	2500	200
40	0.006	25000	1000
1,27	0.012	6700	350
1,27	0.00371	58200	800

Cavitation caverns form in those discharged points of melt volume at solidification limit, where tensions stress which acts on the liquid, exceed bonding forces between its molecules. In this case, fracture strength reaches 150MPa as a result of the hydrophobic solid particles and insoluble gases presence into the melt.

Cavitation tendency is determined with dimensional criteria named critical number of cavitation:

$$Q_k = \frac{P - P_n}{\rho \cdot \frac{v}{2}} \quad (16)$$

unde: v flux speed [W/m^2]; ρ – density of molten mass [kg/m^3].

Cavitation develops in conditions when cavitation number $Q_k < 0,35 \dots 1$. Base parameter which influences the development process of cavitation is flux speed, which determines the value of static pressure at solidification limit. Its value is equal with the sum of surrounding static pressures, $P_0 = 0.1MPa$ and dynamic ones:

$$P = P_0 + \rho \frac{v^2}{2} \quad (17)$$

A.D.Pernik established the relationship between cavitation and Reynolds criteria value, relating to predominant influence on cavitation processes of kinetic speed of medium. Accepting the known condition that cavitation caverns form predominantly while crossing solid surfaces, he proposed the following function for cavitations number determination:

$$Q_k = 2 \cdot \frac{P - P_n}{\rho \cdot v^2} \approx Re^{0,282} \quad (18)$$

where: P is the absolute external pressure [N/m^2];

P_n – elasticity (pressure) of saturated vapours of liquid [N/m^2];

v – kinetic speed of liquid [m/s].

Cavitation centers are solid particles which exist in molten mass, gases bubbles, non-metallic inclusions. Cavitation bubbles appear more intensive close to the crystallization front surface, which has crystals peaks coming out from different caverns and cracks, filled with gas.

In the elastic forces field, two compression and dilatation zones can be distinguished (see fig.3) by longitudinal formed wave, with maximum values [1].

To obtain high cavitation pressures which determine crystals destruction, molten mass must have a smaller possible diameter of dispersed particles and gas bubbles. Usually, molten mass is subjected to degassing and refining during ultrasonic processing. Use of physical modelling for studying processes of cavitation caverns appearance allowed to obtain the following results:

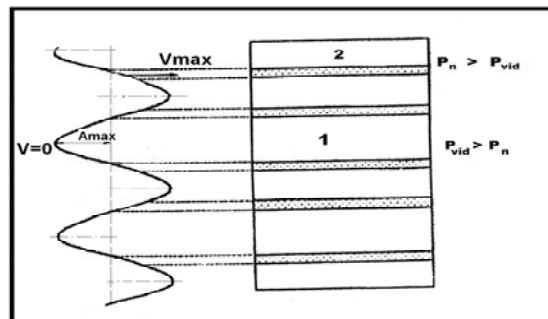


Fig. 3. Distribution of elastic wave in molten liquid mass: 1 – compression zone; 2 – dilatation zone

1. gas bubbles move inbetween growing crystal by alloy solidification without external actions;
2. for average and high speeds, the limit of solidification is covered by small gas bubbles which can form cavitation centers by superposition of elastic waves;
3. at temper crystallization speed and high gas content in alloy, big gas bubbles are emitted at solidification limit whose radius is bigger than critical one. These can generate centers for development of cavitational processes, but they remain in casting (as gas inclusions) or they leave the liquid mass.

Researching of a considerable quantity of crystalline structure obtained by high frequency vibrations, allowed to establish the influence of frequency and amplitude on solidification processes. Quantity of bubbles which appears in a second in 1cm³ of metal can be determined by I.R.Zeldovici equation:

$$J = A \cdot e^{-\frac{W}{RT}} \quad (19)$$

where: A is a constant equal for all liquids 10³¹[m³/s];

W – mechanical work required for bubble formation with radius r [J]

$$W = 4 \cdot \pi \cdot r^2 \cdot \sigma + \pi \cdot r^3 \cdot \gamma - \frac{4}{3} \pi \cdot r^3 \cdot P \quad (20)$$

P – pressure inside the bubble, equal in equilibrium existence of its external vibration pressure P_{vib} [N/m²].

From propagation theory of elastic waves it is known that vibration pressure value (without considering atmospheric pressure) depends on frequency and oscilations amplitude:

$$P_{vib} = \rho \cdot A \cdot \omega^2 \cdot \sin \omega \tau \quad (21)$$

Forces which determined formation and destruction of caverns at vibrations, represent continuous high frequency oscillations with high amplitude. So, it can be concluded that modidying the base parameters of elastic wave and vibrations regimes, it can control the crystalline structure of alloys.

In fig.4. it is presented schematically the movement of gas bubble (with the pressure inside equal with saturated vapours pressure P_n) along the peak of crystal. Its kinetic speed is equal with local speed of flux which depends on relief of solidification limit.

At undersonic speeds, calculated value of pressure for cavitation bubble destruction reaches 3·10⁵MPa (practically, these pressures reaches values of 220...400MPa).

At a relative low distance of the breakage center, this pressure decreases more than 10 times. Distance from breakage point to the destroyed surface of crystal depends on the initial dimension of gas bubble. More bigger it is, more time will take to break and transportation time of cavern to destruction surface [1].

After Relley data, breakage timp is:

$$\tau = 0,9146 \cdot r_0 \cdot \sqrt{\rho/P_\infty} \quad (22)$$

where: r₀ is initial radius of bubble [mm];

P_∞ – pressure into the flux of medium [N/m²];

ρ – density of medium [kg/m³].

The biggest caverns break close to the crystal surface.

Gas content has a great influence on saturated vapours pressure in cavitational medium. At a high gases content which diffuses into the cavern, the force of shock wave decreases at its disintegration. This is explained by that a part of the gas which is in cavern absorbs part of destruction energy, because it is consumed at gas compression.

3. DISCUSSIONS/RESULTS/ANALYSES

Waves propagate in a limited space and they always have two phases: of compression in waves maximum values (where amplitude has maximum value, and kinetic speed is zero) and

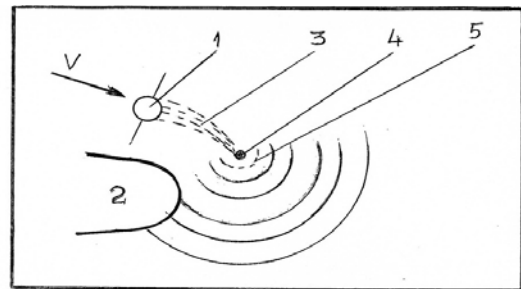


Fig. 4. Propagation scheme of shock wave obtained by cavitational bubble breakage close to the crystal peak: 1) bubble; 2) crystal; 3) pressure increase in flow direction; 4) breakage point; 5) shock wave determined by bubbles breakage

discharging in the center of oscillations (where the kinetic speed has maximum value, and wave deviation from average position is zero).

Kinetic speed of the medium is calculated by wave propagation:

$$v = A \cdot \omega \cdot \cos \omega \tau; v_{\max} = A \cdot \omega \quad (23)$$

where: v is kinetic speed of the medium [m/s];

A – amplitude of vibration [10^{-3} m];

ω – frequency of vibration [Hz];

τ – time of system to move from maximum value to the center position [s].

Limited use of vibration of metallic alloys work is explained by contradictory data about the vibration action mechanism on solidifying metal. Causes of vibration influence on crystalline structure are explained by different authors by following factors:

- 1) mechanical damage of crystallization front under the strong elastic waves action and generation of complementary crystallization centers;
- 2) appearance of undercoolings grown in periodical dilatation ranges of molten mass and increase of existent additions activity, by which are created the conditions to increase the appearance speed of crystallization centers;
- 3) surface tension reduction between phases and the viscosity of molten mass, which eases the movement process of atoms from liquid phase in solid one by crystallization centers formation;
- 4) acceleration of thermocapillary mass transportation of elements from the space between the dendrites ramifications.

Microstructure of the sample obtained without vibration is presented in fig.5.a. Characteristic elements can be observed: columnar and equiaxed crystal, shrinkage, inferior cone formed by individual crystals precipitation zones. Obtained sample by vibration action in crystallization period has a different macrostructure than the control sample fig.5.b.

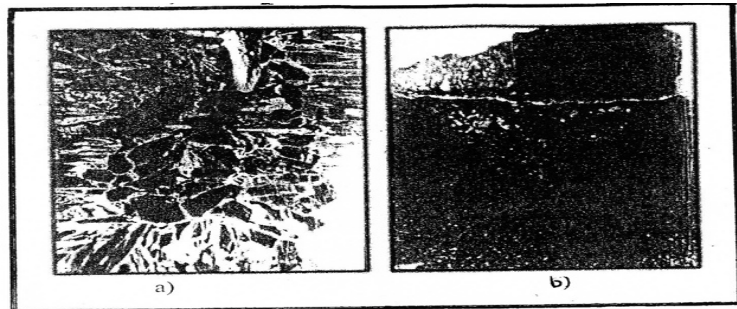


Fig. 5. Aspect of microstructure in a salol sample
 a) without vibration ; b) after vibration

Practically, the zone of columnar crystals disappeared and equiaxed crystals zone increased properly and determined a ragging of grains and increased concentration. This fact indicates a more compacted configuration of crystalline structure in the sample under elastic oscillation action.

In fig.6.a are presented the typical diagrams recorded during the crystallization process of samples without vibration, and fig.6.b shows the diagrams by vibration action with a frequency of 94Hz and amplitude 1mm. OA sector corresponds to the thermostatic period of molten mass, and AB corresponds to the cooling period. At the beginning moment of crystallization latent heat of phase transformation is released, and thus, it is explained the bounce of temperature of BC sector. CD sector corresponds to the cooling of solid phase.

Comparative analysis of crystallization process diagrams (thermograms) of ingot in control experiments and by the vibration action indicates that vibration in beginning state of process (AB sector) contributes to temperature equalization in the whole volume of sample. It influences the heat transfer rate from molten mass to cooled chamber. Vibration also influences maximum undercooling of molten mass, which can be seen from the placing of points B comparison (fig.6. a and b). It can be seen that rapidly increase of temperature starts simultaneous in the whole samples volume by vibration, and without vibration, the beginning of this increase of temperature it is unequal for different portions of molten mass. Following section explains the decrease of columnar zone thickness, which has been determined in practice. Temperature growth speed in portion BC (fig.6) is unequal without elastic oscillations application and by the vibration action.

By vibration, temperature reaches a certain minimum value, increase suddenly, and temperature increase takes place slower during control experiments, and when it reaches a certain value, it increases again (CD sector).

In fig.7. it is presented the dependence cooling rate of molten mass with vibration frequency. Increase of cooling rate in elastic oscillations field it is caused by intensive movements of molten mass in crystallization chamber and by the increase of heat transfer coefficient from the molten superheated mass to the wall of crystallizer. Its value it is proportional with kinetic speed of molten mass ($\alpha = A \cdot W^{0.8}$), and increase of oscillations frequency contributes to increase of this speed. In

fig.8. it's been highlighted the dependence of maximum undercooling with elastic oscilations frequency. It can be noticed that an oscilations frequency takes place, which leads to the decrease of maximum undercooling zone of molten mass (hatched section). In fig.9. appear the dependences of structural features (grains dimensions) of ingots with vibrations frequency at constant amplitude of oscilations equal with $10^{-3}m$. Maximum (1) and minimum (2) dimension decreases with the increase of frequency up to 40 Hz. Variation of frequency from 50 up to 4500 Hz didn't indicate any minimal differences in ingots structure.

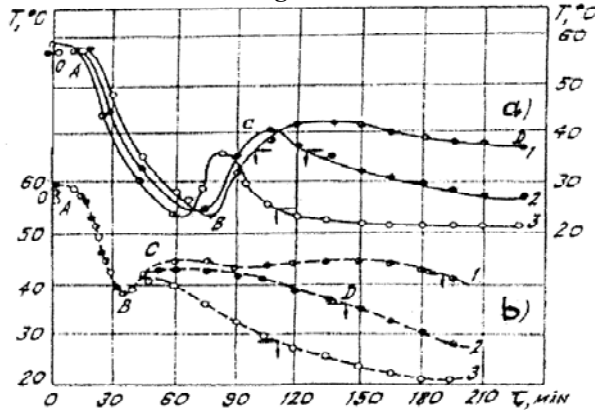


Fig.6. Diagrama solidificării probei de salol: a) fără vibrație; b) cu

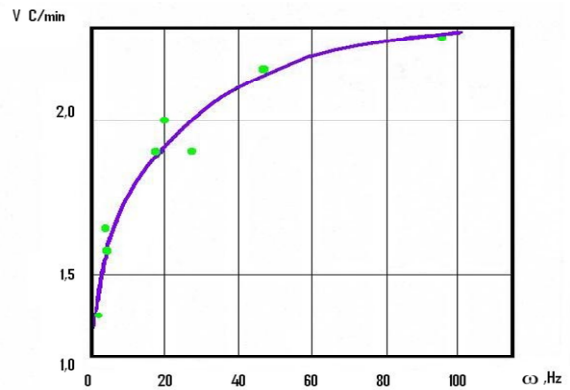


Fig.7. Dependența vitezei de răcire a masei topite funcție de frecvența vibrației

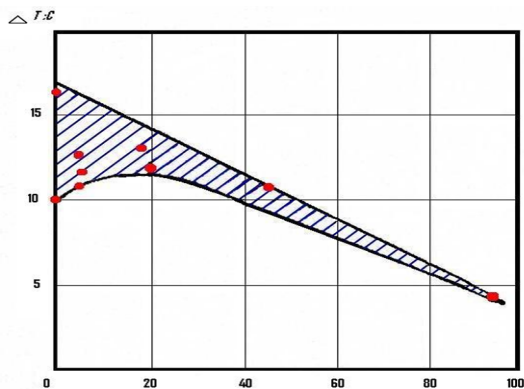


Fig.8. Dependence of molten mass undercooling with elastic oscilations frequency

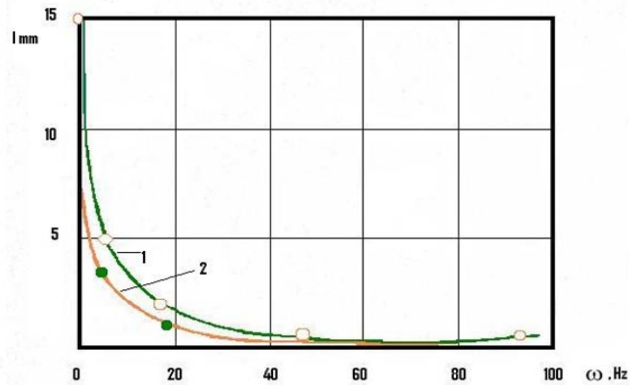


Fig.9. Dependence of crystalline grains dimensions with vibration frequency (at constant amplitude) : 1 – maximum dimension of grains ; 2 – minimum dimension of grains

4. CONCLUSIONS

Main effect of forced oscilations is the movement of waves by pressure and depression which alternates forcing the cyclic movement of alloy mass, with formation of extra crystallization centers and dendrites fragmentation.

Vibration leads to breakage of secondary branches of dendritic crystals. Increase of pressure by 105 times in liquid due to the cavitation carvens implosion, contributes to formation of new crystallization centers. Undissolved impurities may become sites for crystallization nuclei. The greatest finishing is given by vibration with circular amplitude in horizontal plan, but it can be used forms of different dimensions. Once frequency value increase, number of equiaxed grains increases and decreases the number of columnar crystals. At vibration with frequency of 100 Hz, the value of angle ω formed between surface of solidification front and vertical axe of casting has the value of $\omega > 120^\circ$, which means that it forms an open concentrated shrinkage, with small height, which can lead to a reduction of feeder by 50%.

Once the amplitude increases, it increases the proportion of equiaxed crystals and decrease the columnar ones. Alloy vibration during all the solidification time, leads to the decrease of grains by about three times. Influence of mechanical vibrations at metals casting are characterized by:

- ❖ increase of undercooling degree by increase of alloy - mould heat transfer;
- ❖ creating new nuclei for fragmentation of forming solid phase;
- ❖ activity of crystallization surfaces;

- ❖ at high solidification rates and small temperature gradient it appear nuclei in whole casting section, when the mould can continuously remove the crystallization latent heat;
- ❖ mechanical vibrations decrease the thermal gradient and increase the solidification rate favouring endogenous growth;
- ❖ the decrease of distance between dendritic branches leads to shorter time of homogenization thermal treatment;
- ❖ materials with fine grains are recommended as materials subjected to plastic deformation;
- ❖ improvement of properties results from the fine distribution of microporosity and secondary phases during blocking the dislocations at grains borders;
- ❖ columnar crystals zone can be eliminated for non-ferrous materials: Al, Cu, Sn, Zn, etc. And especially for their alloys (bronzes, brass);
- ❖ mechanical vibrations influence the interphase surface tension (solid – liquid) by decreasing it, which leads to the decrease of minimum radius of nuclei from which they can't melt anymore but develops.

REFERENCES

1. PĂRVULESCU C. - Cercetări privind influența vibrației asupra solidificării aliajelor turnate în piese; Teză de doctorat, UPB 2010.
2. ȘUȘU Cătălin - Contribuții la îmbunătățirea calității topiturilor unor aliaje de aluminiu destinate turnării pieselor. Teză de doctorat, Universitatea Tehnică din Cluj-Napoca, 2008.
3. CĂMUI C. - Studii și cercetări privind efectul acțiunilor fizice ale energiei vibrațiilor de joasă frecvență asupra cuprului în momentul turnării și solidificării în semifabricate; lucrare de absolvire cursuri post universitare, București 1991.
4. MĂRGINEAN L. - Studii și cercetări privitoare la realizarea unor compozite ceramo-metalice. Teză de doctorat, Universitatea Tehnică din Cluj-Napoca, 2007.
5. POP Alin Mihai - Cercetări asupra tehnologiilor și materialelor moderne pentru confecționarea garniturilor de model. Teză de doctorat, Universitatea TRANSILVANIA din Brașov , 2009.





¹Ioan ILCA

DEFFICIENCY OF SCIENCE AND TECHNIQUE ASSIMILATION

¹FACULTY OF ENGINEERING HUNEDOARA, ROMANIA
Member of ROMANIAN SCIENCE AND TECHNIQUE ACADEMY

ABSTRACT:

Assimilation in production of acquirement of science and new technique is the most important motor of development. Romania must improve step by step organizational systems, in view to develop the science, to improve the material basis, to grow the quality level and to increase the productivity in science researches, to reduce the gap in science, between our country and UE.

KEYWORDS:

acquirement of science, new technique, productivity, production, scientist

1. INTRODUCTION

Is very known that the main indicator of national economy progress is labor productivity and productivity increase is possible with implementation of technical progress and science conquest.

If the rate of productivity decrease, is necessary to cast about for deficiencies of science and technique assimilation.

Based on Romanian statistics, we can observe that in the past the labor productivity was around 13 %, after this was stagnation, and now is dramatically decrease. Is clear that the assimilation of science and technique are not properly and because of this I want to discuss the break down of new technique assimilation.

Is known, that in Romanian Industry, the assimilation of science and techniques novelties are very slow and difficult to be done. In Romanian language we use for it the word “introducere= introduction”; introduction of new technique, introduction of science realization, etc”. The word “introduction” in Romania language have the understanding of a difficult process take in place with environment resistance and we used this word for many years without observation of un careless condition of new technique assimilation. When we will pass from this to “acquirement of new technique” will be created the normal conditions for assimilation process.

2. CONDITIONS FOR NEW TECHNIQUE AND SCIENCE ASSIMILATION

My personal experiences for many years in this field show those are necessary to be fulfilling some conditions, we name those and will analyze the possibility to be fulfill.

First conditions: Assimilation of new technique – artless say, industry to learn to do what he never does until now.

This assimilation is necessary to grow into a learning process, mandatory sustain of pedagogical procedures used in case of new learning's. To want to learn, is the most important condition, when we communicate knowledge's to the students. In case of our Industry we have questions: Our industry wants all the times, willingly, get into new technique? Are we created conditions for convince our industry of needed new technical assimilation?

Admittedly, to appear this wish, we must create adequate material and ethic conditions. Our industry must create adequate conditions in which, our industry, our Commercial Companies, to be interested in new technologies, those must fill the necessity, and the profitableness, and that acquirement of new technologies represent progress.

The second condition: Satisfactoriness, basic level of knowledge's for learning peoples. We can't teach for example "Theory of Plastic Deformation in case of metallic materials" to the students who don't know "Superior Mathematics". Who learn new things must have a adequate technical preparation for clear understanding of new technique.

The third condition: very known in pedagogy is – Don't overload the student in learning process. Each Company, each industrial plant, can assimilate during an year, a limited quantity of new things, even the peoples are properly prepare and have the desire to improve. In Romania, happen frequently, when new companies start to manufacture some products, she starts to be overload with new tasks. Is important to don't forget that industry, like people, have a limited capacity to acquire the new.

The fourth condition: in learning process, must be created the adequate material conditions.

To educate, a person or a company, only with internal material resources, is not possible.

Higher education needs a proper material base, adequate at his purpose. Simple say: we must allotment sufficient of funds, for learning process.

The necessity of those four conditions, is easier to understand and make them happen is also easier.

The fifth condition not saw evident and considerable difficult to be achieve, is: in educational process is imperious necessary to have/ elaborate an analytical learning program.

Practical, for new science and technique acquirement is necessary to have a proper, detailed action plan in view to achieve the request results.

In our case, usual, the attention is low, and often the educational process is made haphazard, without thinking about the necessity of an even simple action plan.

There is a dilemma, when the action plan is made by scientist, inventor, or research institute, they don't take in consideration the particularities of production process. When the action plan is made by the companies are not taken in consideration specific tasks of new technologies. The result action plans contain a lot of imperfections. How to solve this dilemma? The life shows us that there are engineers with capabilities to cover both parts of the issue, they are not sowing many, and we must find and promote this kind of specialists in new science and technique acquires teams. As rule we must include the applicable idea that new science and technique acquires in practical, industrial process to be done based on a proper action plan.

The seventh and last condition, under my opinion is applied to the scientist. Where are students, is necessary to have teachers. If the new technique creators, is scientist, inventor, or research institute, must be directly interested in practical implementation of new technology. Are they? There is a link between the scientists and companies?

We will analyze now, only the case when the "teacher" is scientist.

Under our legislation, the teacher who is also scientist, concern oneself about implementation of new technology, is not pay for this. In Romania the collaboration between the teachers/scientist from Technical Universities and industrial sector is consider gratuitously activity.

Normally the teacher who is also scientist, make this work from his conviction, but is must to have an proper working environment, to be social recognize and the state must appreciate his cooperation with industrial activity. The State institutions, like Ministries', don't have a proper attitude in case of recognize of this special work and this are not good for the relations between students and teachers.

Many times are considered if a edict was emitted, in view to a technology assimilation, the process of acquirement of new technique was done. The acquirement of new technique and technology is not only an administrative activity, sure by administration activity is establish the amount, financing elements and number of peoples, but this important and special activity of acquirement of new technologies is based on the good communication between the magister and his disciple, on the interest of this in achievement of proper results and on a proper Action plan.

3. COMPARISON OF SCIENCE ACTIVITIES IN ROMANIA, EUROPEAN COMMUNITY AND THE WORLD

I want to open a new subject: Is sufficient the infusion bring by our science in national economy progress? The efficiency of scientist work is satisfactory?

To answer to this question is important to compare some of the elements of our scientific activities with similar activities from the states of European Community.

Research activity is one of the most actual points in political agenda of European Community. In accordance with EUROSTAT – European Statistics Office, in 2009, the allowance for Research and Development was 1.84% from GDP, in Europe, compare with 3.2 % in Japan and 2.7 % in USA.

Inside European Community the allowance have significant variations: for example in Sweden – was 3.82 % and Finland – 3.45 % from GDP, opposite was the allowance in Cyprus - 0.42 % and Bulgaria – 0.48 % from GDP.

In Romania the allowance in 2009 was 0.46 % from GDP, the most amount from public funds, $\frac{1}{4}$ from this amount was ensure by private sector, and Attention!, only 0.02 % from outside funds.

This was the situation in 2009, but now in 2010 the allowance for Research and Development in Romania is 0.19 % from GDP, we considered this” dangerous”, taken in consideration that European Union target is 3 % from GDP – part of Lisbon Strategy for economical and competitively enlargement.

Making a analysis of allowance for Research and Development in Japan, SUA and UE, we can see that a large part of this have the destination research for acquirement of science and new technique in production, or like we preferred to say “researches with applicative theme”.

In last 10 years, statistical based, in SUA was draw in more than 53000 scientists, most of them younger scientists, out of which 30000 engineers, 14000 physicians and 9000 other kind of scientists, that means more than 5000 specialists per year.

If we consider 500 younger graduates per year per University, that means that minimum 10 University from Europe prepare free of charge specialists for SUA, but the American’s take only the best elements – cream of 50 Universities. This situation alarmed the Royal British Society, who named a special committee to analyze the exodus of youngest scientist and propose action plans for stopped this impoverishment of British science. The conclusion was that England and Germany however, pay to their good scientist a big amount, American’s pay double. But the payment is not the only reason; the committee establishes that the most attractive is the science development conditions create in SUA.

We must say that in last period the gap in science, between our country and UE, increase, that means a big need to find solutions and funds for elimination of this gap. If in next future years the Romanian scientist productivity will not be improved, if we will not improved the acquirement of science and new technique in production, then the assignment to come up with the European developed states, will failed. But, if we used with determination and intelligence the experience we have in education organization, scientifically research and in industry, than the gap will means only a passing episode.

We must improve step by step organizational systems, in view to develop the science, to improve the material basis, to grow the quality level and to increase the productivity in science researches.

4. CONCLUSIONS

We, scientist from Romania, must be preoccupied with all seriousness about this new provocation. We are the avant-garde of Scientist Institution of the Country, and due to this we are responsible, more than other people, from development of our science and acquirement of science and new technique in production.

REFERENCES

- [1.] Irina, St. – Dezvoltarea infrastructurii de cercetare-dezvoltare (CD) a intreprinderilor cu sprijinul finantarilor europene, Tehnica si Tehnologie, Editura Tehnica Maria, nr. 6, 2009, Bucuresti
- [2.] EVZ Special – Cercetarea romaneasca are probleme de “marketing”, EVZ, nr. 5781, 2009, Bucuresti



¹Monika Erika POPA, ²Gabriela Cornelia MIHUT

EXPERIMENTS REGARDING THE THERMICAL REGIME IN THE CONTINUOUS CASTING PROCESS

¹⁻² UNIVERSITY POLITEHNICA OF TIMISOARA, FACULTY OF ENGINEERING FROM HUNEDOARA, ROMANIA

ABSTRACT:

Continuous casting is one of the prominent methods of production of casts. Effective design and operation of continuous casting machines needs complete analysis of the continuous casting process. In this paper the basic principles of continuous casting and its heat transfer analysis using the finite element method are presented. In the analysis phase change is assumed to take place at constant temperature. A front tracking algorithm has been developed to predict the position of the solidification front at each step. Finally, examples that are solved by the proposed algorithm are discussed. The results show that there is a good agreement between the method developed in this work and other previously reported works.

KEYWORDS:

steel, micro-coolers addition, continuous casting, experiments, simulations

1. INTRODUCTION

In the continuous casting process, illustrated in figure 1, molten metal is poured from the ladle into the tundish and then through a submerged entry nozzle into a mould cavity. The mould is water-cooled so that enough heat is extracted to solidify a shell of sufficient thickness.

The shell is withdrawn from the bottom of the mould at a "casting speed" that matches the inflow of metal, so that the process ideally operates at steady state. Below the mould, water is sprayed to further extract heat from the strand surface, and the strand eventually becomes fully solid when it reaches the "metallurgical length".

Solidification begins in the mould, and continues through the different zones of cooling while the strand is continuously withdrawn at the casting speed. Finally, the solidified strand is straightened, cut, and then discharged for intermediate storage or hot charged for finished rolling.

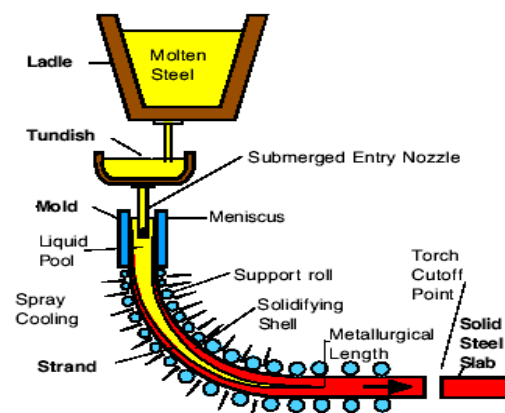
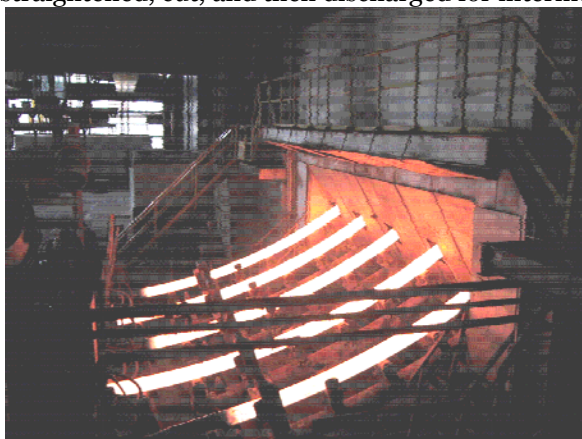


Figure 1. Schematic representation of the continuous casting process

To start a cast, the bottom of the mould is sealed by a steel dummy bar. This bar prevents liquid metal from flowing out of the mould and the solidifying shell until a fully solidified strand

section is obtained. The liquid poured into the mould is partially solidified in the mould, producing a strand with a solid outer shell and a liquid core. In this primary cooling area, once the steel shell has a sufficient thickness, the partially solidified strand will be withdrawn out of the mould along with the dummy bar at the casting speed. Liquid metal continues to pour into the mould to replenish the withdrawn metal at an equal rate. Upon exiting the mould, the strand enters a roller containment section and secondary cooling chamber in which the solidifying strand is sprayed with water, or a combination of water and air (referred to as "air-mist") to promote solidification. Once the strand is fully solidified and has passed through the straightened, the dummy bar is disconnected, removed and stored.

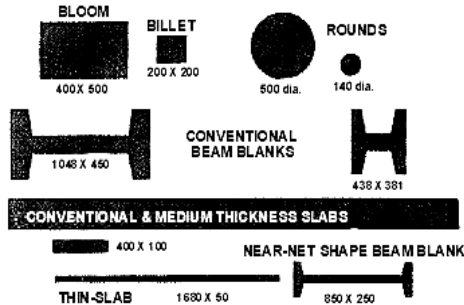


Figure 2. Continuously cast sections

Depending on the design of the casting machine, the as-cast products of the continuous cast process are slabs, blooms, billets, or beam blanks. The cross sections of these products are shown in Figure 2. Billets have cast section sizes up to about 200 mm square. Bloom section sizes typically range from approximately 200 mm to 400 mm by 600 mm. Round billets include diameters of approximately 140 mm to 500 mm. Slab castings range in thickness from 50 mm to 400 mm, and over 2500 mm wide. The aspect ratio (width-to-thickness ratio) is used to determine the dividing line between blooms and slabs. An aspect ratio of 2.5:1 or greater constitutes an as-cast product referred to as a slab.

2. METHODOLOGY

By its nature, continuous casting is primarily a heat-extraction process. The conversion molten metal into a solid semi-finished shape involves the removal of the following forms of heat: superheat from the liquid entering the mould from the tundish. The latent heat of fusion at the solidification front as liquid is transformed solid, and finally the sensible heat (cooling below the solidus temperature) from the solid shell.

These heats are extracted by a combination of the following heat-transfer mechanisms: convection in the liquid pool heat conduction down temperature gradients in the solid shell from the solidification front to the colder outside surface of the cast, and external heat transfer by radiation, conduction and convection to surroundings. Also not less important is heat transfer before the molten metal is poured into the mould. For instance, in the casting of steel, heat transfer is important before the steel enters the mould because control of superheat in the molten steel is vital to the attainment of a predominantly equiaxed structure and good internal quality. Thus, conduction of heat into ladle and tundish linings, the preheat of these vessels, convection of the molten steel and heat losses to the surroundings also play an important role in continuous casting.

Because heat transfer is the major phenomenon occurring in continuous casting, it is also the limiting factor in the operation of a casting machine. The distance from the meniscus to the cut-off stand should be greater than the metallurgical length, which is dependent on the rate of heat conduction through the solid shell and of heat extraction from the outside surface, in order to avoid cutting into a liquid core. Thus, the casting speed must be limited to allow sufficient time for the heat of solidification to be extracted from the strand.

Heat transfer not only limits maximum productivity but also profoundly influences cast quality, particularly with respect to the formation of surface and internal cracks. In part, this is because metals expand and contract during periods of heating or cooling. That is, sudden changes in the temperature gradient through the solid shell, resulting from abrupt changes in surface heat extraction, causes differential thermal expansion and the generation of tensile strains.

Depending on the magnitude of the strain relative to the strain-to-fracture of the metal and the proximity of the strain to the solidification front, cracks may form in the solid shell. The rate of heat extraction also influences the ability of the shell to withstand the bulging force due to the ferostatic pressure owing to the effect of temperature on the mechanical properties of the metal. Therefore, heat transfer analysis of the continuous casting process should not be overlooked in the design and operation of a continuous casting machine.

3. DISCUSSION

The importance of mathematical modeling of the continuous casting process can be seen in situations where the following are necessary.

- ❖ Simulation of an existing casting machine with a view to learning more about its operation;

- ❖ Prediction of effects of a change in a casting parameter on the performance of an operating caster;
- ❖ Design of new casting machines.

In particular, most process engineers are probably interested in the effect of increasing the casting speed on machine operation as higher output is sought to match planned or existing production capacity. Do changes then need to be made to the mould length, spray system, and position of the cut-off strand? Another area of interest to the process engineer is the minimization of internal cracks such as halfway or centerline cracks. These points are discussed in this section to show the importance of a mathematical model, based on heat-transfer principles, in adjusting casting conditions and improving overall machine performance.

Increasing the casting speed will have the effect of decreasing the time that the strand spends in the mould and spray zones, and also of increasing the depth of the liquid pool. Looking first at the mould, a decrease in the mould dwell time will result in a thinner shell at the bottom of the mould. Since this may increase the danger of break-outs, an increase in the mould length should be considered. Here the mathematical model can assist us since it can calculate the shell thickness for different casting speeds and mould lengths.

Halfway or midway cracks are the result of reheating of the surface of the strand due to a sudden reduction in the rate of surface heat extraction as the strand moves into the secondary cooling zone. So, if the spray system is to be altered to avoid midway cracks, reheating of the surface of the strand must be minimized as much as is practicable. How can this be achieved? A mathematical model can give part of the answer. For example, if the surface temperature distribution to be maintained through the sprays is specified, the mathematical model can provide the spray heat-flux distribution that is required to achieve it. The following basic assumptions were made during the formulation of the mathematical model:

- ❖ The continuous casting process is steady state.
- ❖ A round billet is considered and radial symmetry assumed.
- ❖ Energy dissipation due to internal friction in the liquid state is neglected.
- ❖ The melt free surface is assumed to be covered with a protective slag layer, through which negligible heat is assumed to be lost.

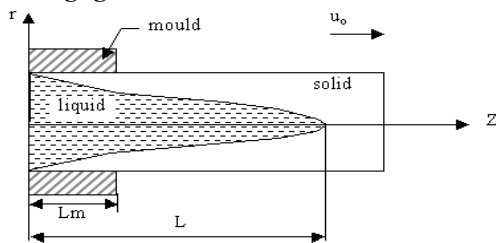


Figure 3. R-Z coordinates attached to mould

The governing equation for the heat transfer analysis of continuous casting is:

$$\rho c \left(\frac{\partial T}{\partial t} + V \cdot \nabla T \right) = \nabla \cdot (k \nabla T) \quad (1)$$

Taking the above assumptions into account, the governing equation will be reduced to:

$$\rho c u \frac{\partial T}{\partial z} = \frac{\partial}{\partial z} \left(k \frac{\partial T}{\partial z} \right) + \frac{1}{r} \frac{\partial}{\partial r} \left(kr \frac{\partial T}{\partial r} \right) \quad (2)$$

The axial heat conduction is negligible compared to that convected due to the bulk motion of the moving

strand. Thus, heat conduction is important solely in the radial direction. Under this condition the governing equation becomes:

$$\rho c u \frac{\partial T}{\partial z} = \frac{1}{r} \frac{\partial}{\partial r} \left(kr \frac{\partial T}{\partial r} \right) \quad (3)$$

The boundary conditions are:

$$\text{At the meniscus/free surface } (z = 0, 0 < r < R), T = T_p \quad (4)$$

At the billet surface:

$$q_s = -k \frac{\partial T}{\partial r} \quad \text{or} \quad h(T - T_\infty) = -k \frac{\partial T}{\partial r} \quad (5)$$

At the center due to axis symmetry ($r = 0$ and $0 \leq z \leq L$):

$$\frac{\partial T}{\partial r} = 0 \quad (6)$$

At the liquid-solid interface ($r = r_i$ and $0 \leq z \leq L$): $T = T_m$;

$$\left(k \frac{\partial T}{\partial r} \right)_l + \left(k \frac{\partial T}{\partial r} \right)_s = \rho Q_L \frac{dr_i}{dt} \quad (7)$$

4. CONCLUSIONS

A one dimensional solidification problem was solved for a slab-like region of water with initial temperature of 10 °C when a temperature of -20 °C is applied on the outer surface shown in

Figure 4. The slab was modeled by using 20 two-node linear elements, 10 for the liquid part and 10 for the solid part. As solidification progresses, the mesh on the water is compressed and on the ice side is expanded;

The continuous casting process is introduced. One and two dimensional heat transfer analyses of the process are discussed. Results showed that such mathematical analysis of the process can help to control and optimize the process and to investigate the consequences of parameter changes without the safety and cost limitations of in-plant experiments.

The proposed algorithm can be used for the analysis of both stationary and moving solidification problems in which phase change occurs at a specific temperature.

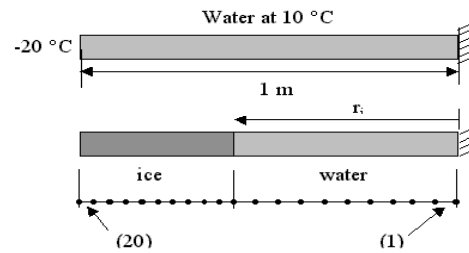


Figure 4. Modeling of the one dimensional problem

REFERENCES

- [1.] Choudhary, K. and Mazumdar, Dipak, "Mathematical modeling of fluid flow, heat transfer and solidification phenomena in continuous casting of steel", Steel Research, 66, No. 5, 1995
- [2.] Popa, E., Kiss I., Danciu A. "Research and experiments the influence of casting parameters upon the surface temperature of the continuous cast semi-products", Annals of the Oradea University, România 2005
- [3.] Popa, E., Mihuț G. "Simulation of the continuously cast semi-products in the case of introduction of consumable microcoolers, KOD 2008 Conference, Novi Sad, Serbia



HEAT LOSS FLUXES FROM STEEL MELT TO DIFFERENT BOUNDARY REGIONS OF A LADLE

¹⁻³ UNIVERSITY “POLITEHNICA” TIMIȘOARA, FACULTY OF ENGINEERING OF HUNEDOARA, ROMANIA

ABSTRACT:

One of the important outputs of the heat conduction model is the heat loss flux from steel melt to different heat transfer regions of a ladle. These papers present examples of the predicted heat loss fluxes to different heat transfer regions of mid-aged 105-tonne steel ladles lined with alumina and spinel as working refractory in walls. The heat loss fluxes to different ladle heat transfer regions, except for the top free surface, generally exhibit exponential decay with time.

KEYWORDS:

steel ladle, numerical simulation, CFD, fluid flow, heat loss

1. GENERAL CONSIDERATIONS

In modern steelmaking throughout the world, continuous casting (CC) is the dominating process for producing semi-finished steel products (billets, blooms and slabs). However, the CC process requires a strict control on the temperature of liquid steel in the tundish. Further, the tundish temperature is influenced considerably by the temperature of teeming steel streams coming from the ladles. Therefore, it would be of practical importance to predict the teeming stream temperature as a parameter for further prediction and control of the steel temperature in tundishes.

Three numerical models were developed. Firstly, a one-dimensional (1D) numerical model for simulating heat conduction in ladle wall, bottom and top slag layer for the whole ladle operation cycle was established. This model was used for predicting steel ladle heat loss fluxes. Secondly, using the predicted heat loss fluxes as thermal boundary conditions, a two-dimensional (2D) CFD numerical model was developed for simulating natural convection flow in steel ladles during holding. Thirdly, a three-dimensional (3D) CFD model was also developed for simulating fluid dynamics in steel ladles with drainage flows during teeming. The 3D CFD model was used for predicting the teeming stream temperatures.

In the present parameter numerical experiments, two types of 105-tonne steel ladles were investigated: the one lined with alumina as working refractory in wall, the other lined with spinel as the working refractory in wall. Other lining materials were the same for both types of ladles. Totally 18 simulation cases are performed for the two types of steel ladles lined with alumina and spinel, respectively. Table 1 gives the parameter of numerical experiments.

Table 1. Parameter of numerical experiments

Simulation case No. *	Hot-face temperature [°C]	Slag thickness ** [mm]	Holding time [min]	Teeming rate*** [t/min]	
A1	S1	1000	83	30	2,816
A2	S2	1000	55	20	2,488
A3	S3	1000	28	10	2,229
A4	S4	800	55	30	2,229
A5	S5	800	28	20	2,816
A6	S6	800	83	10	2,488
A7	S7	600	28	30	2,488
A8	S8	600	83	20	2,229
A9	S9	600	55	10	2,816

* “A” refers to alumina ladles and “S” refers to spinel ladles

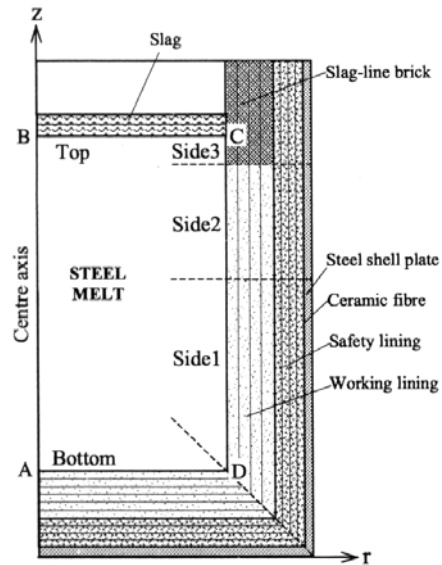
** The slag thickness of 28, 55 and 83 mm corresponds, respectively, to 500, 1000 and 1500 kg slag

*** The teeming rates are calculated based on 105 tonne liquid steel drained for 38, 43 and 48 minutes, respectively.

2. SIMULATION METHODS

The mathematical models used in this work for carrying out numerical experiments were established in two computer software environments. The one is a special-purpose computer program, TEMPSIM [1], for only simulating heat transfer in steel ladles. The other is a general-purpose CFD modelling computer code, ADINA-F (Automatic Dynamic Incremental Nonlinear Analysis). The former numerically solves the heat conduction equation for ladle wall, bottom and top slag layer, while the latter numerically solves the Navier-Stokes type momentum, energy and turbulence equation group for the steel melt bounded by ladle wall, bottom and top slag layer.

TEMPSIM assumes the heat conduction is either in radial direction through ladle wall or in axial direction through ladle bottom and top slag layer. Accordingly, it was used to establish the 1D heat conduction model described previously (Fig. 1). This heat conduction numerical model was applied in this work for predicting heat loss fluxes. Figure 2a schematically illustrates the computation domain with grid lines defined by the heat conduction model. Note that the computation domain used by the model excludes the region marked with "ABCD" standing for the steel bath. Moreover, in this computation domain, five heat transfer regions named as "Bottom", "Top", "Side1", "Side2" and "Side3" are further defined, (Fig. 2a). The region "Bottom" is the interface between steel melt and bottom lining; the region "Top" is the interface between steel melt and top slag layer; the regions "Side1", "Side2" and "Side3" are, respectively, the interfaces between steel melt and sidewall lining at different levels.



(a) 1D heat conduction model

Fig.1. Computation domains defined in the numerical models

With all these numerical models available, a three-step modelling strategy was employed in the present work in which,

- the 1D heat conduction model was first implemented to the wall, bottom and top slag layer in steel ladles to provide the thermal boundary conditions (e.g., heat loss fluxes) to the 2D and 3D CFD models; then,
- the 2D CFD model was applied to simulate natural convection in the ladles and to provide the initial conditions (velocity and temperature profiles) to the 3D CFD model; and, finally,
- the 3D CFD model was executed to simulate fluid flow and heat transfer in the ladles with drainage flows during teeming and to predict the teeming stream temperatures. This three-step modelling methodology was applied to each simulation case listed in Table 1.

Table 2. Thermal-physical properties of lining materials used in numerical simulations [2]

Lining material	Density [kg/m ³]	Heat conductivity [W/m °C]					Heat capacity [J/kg °C]				
		200 °C	600 °C	1000 °C	1400 °C	1600 °C	200 °C	600 °C	1000 °C	1400 °C	1600 °C
Ceramic fibre	80	0,02	0,03	0,04	0,04	0,04	850	1000	1100	1200	1200
Chamotte	2100	1,56	1,65	1,76	1,87	1,87	860	977	1084	1200	1200
Slag line brick	3110	4,00	2,60	2,09	2,00	2,00	1010	1194	1280	1368	1419
80%Al ₂ O ₃	2900	2,15	2,00	1,84	1,74	1,65	850	1030	1125	1180	1200
Spinel (10 % C)	3000	7,40	7,40	7,40	7,40	7,40	850	1030	1125	1180	1200
Bottom mass	2750	1,00	1,30	1,50	1,70	1,80	850	1030	1125	1180	1200
Slag scull	3648	3,91	3,46	3,41	3,08	2,99	840	993	1073	1120	1137

3. SIMULATION CONDITION

In steel plant, the steel ladles are operated in the following cycle: tapping (from electric furnace EBT) → ladle furnace LF → continuous casting CC → ladle maintenance → transfer to EBT or to preheating station → tapping. The liquid steel held in ladles goes through LF treatment where

the steel is homogenized by argon bubbling and its temperature is adjusted to 1570 - 1590°C. After that, the liquid steel is transported to the CC station and cast into slabs. The time lapse between the end of LF treatment and the start of teeming is around 10-30 minutes, which is defined as the holding time in this work.

Since the ladles to be simulated are mid-aged, which means that they have normally been in operation for more than 30 heats, quasi-steady thermal states have more likely been reached in the ladle linings.

Numerical experiment cases are executed under the following conditions (Table 1):

- ❖ after the end of teeming, all the ladles without preheating are directly transported to the EBT and prepared for tapping;
- ❖ just before the start of tapping, the average hot-face temperatures, weighted by the areas of heat transfer regions (Fig. 2a), are set at 600°C, 800°C and 1000°C, respectively, by manipulating the cooling time of the ladles after teeming and before receiving the next heat;
- ❖ all heats of liquid steel (105 tonne) together with different amounts of slag (500 kg, 1000 kg and 1500 kg) are tapped from EBT into the ladles during 5 minutes and have the same tap-end temperature of 1675°C;
- ❖ 25 minutes after tapping, the ladles are covered with a refractory lid for 30 minutes corresponding to the period of LF treatment;
- ❖ at the end of LF treatment, all heats of liquid steel are homogeneous and have the same temperature, 1580°C;
- ❖ the holding periods, i.e., the duration of steel melt held in the ladles after LF treatment/homogenization and before the start of teeming, are 10 min, 20 min and 30 min, respectively; and, finally,
- ❖ the teeming time is designed to be 38 min, 43 min and 48 min corresponding to teeming rates of 2.816 tonne/min, 2.488 tonne/min and 2.229 tonne/min, respectively.

In addition, the conditions (5) to (7) are also used in CFD simulations of the same ladles during holding and teeming periods.

4. SIMULATION RESULT

One of the important outputs of the heat conduction model is the heat loss flux from steel melt to different heat transfer regions of a ladle. Figures 2 and 3 illustrate, respectively, examples of the predicted heat loss fluxes to different heat transfer regions (Fig. 1) of mid-aged 105-tonne steel ladles lined with alumina and spinel as working refractory in walls. The simulation conditions follow cases No. A5 and S5 in Table 1 for both types of steel ladles. It can be seen from both figures that the heat loss fluxes to different ladle heat transfer regions, except for the top free surface, generally exhibit exponential decay with time. A comparison between the two figures shows that the alumina ladle loses more heat per unit area and time to the top region of the wall (Side3), which is slag-line brick having greater heat conductivity than alumina, (Fig. 2a and Table 2); while the spinel ladle loses most heat per unit area and time to the lower regions (Side1 and Side2) of the wall. This difference is not surprising, because spinel (mixed with 10% graphite) is much more conductive than alumina and slag-line brick (Table 2).

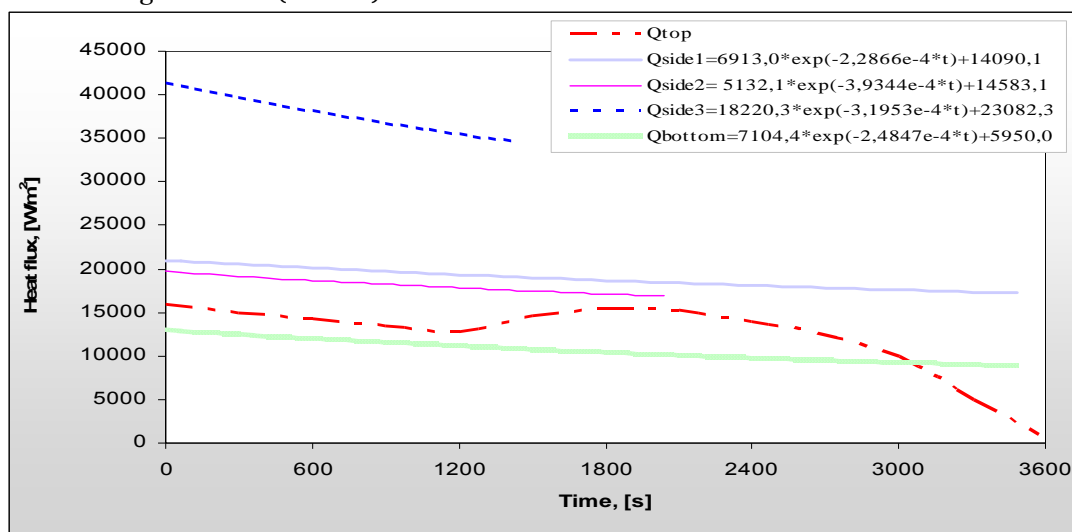


Fig.2. Predicted heat loss fluxes to different region of a mid-aged 105-tone steel ladle with alumina as working refractory in wall

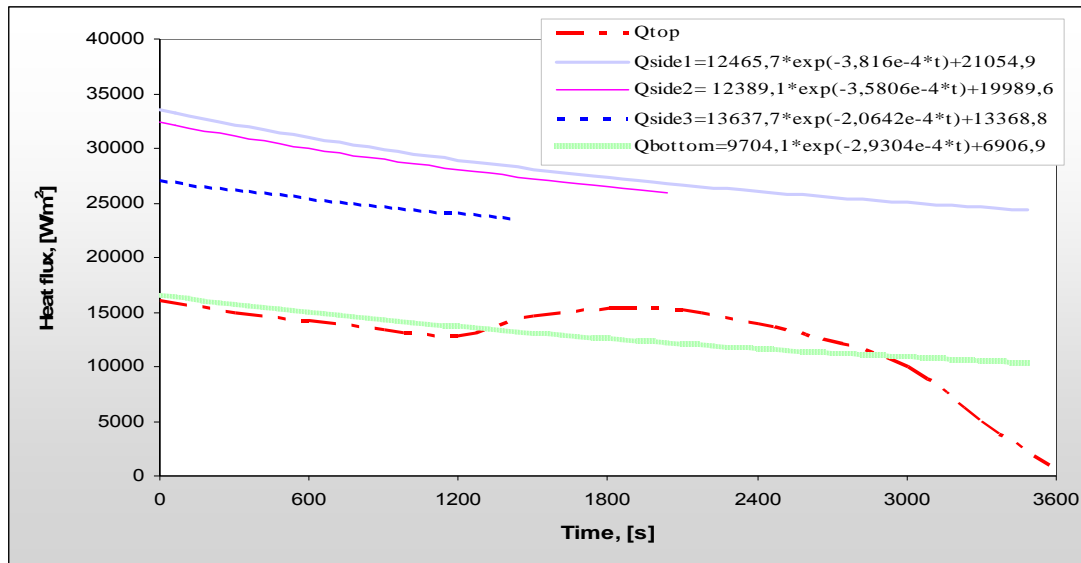


Fig.3. Predicted heat loss fluxes to different region of a mid-aged 105-tonne steel ladle with spinel as working refractory in wall

6. CONCLUSIONS

The influences of some important parameters on fluid flow and heat transfer in steel ladles during holding and teeming, which are normally inconvenient or impossible to examine directly using experimental methods, have been studied by means of mathematical modelling through performing numerical experiments. In this work, a three-step modelling strategy for the numerical experiments has been adopted. Two types of mid-aged 105-tonne production steel ladles, lined with alumina and spinel in walls, have been investigated, respectively. The following conclusions can be drawn from the present parameter numerical simulation studies.

It can be deduced that local heat losses from top and bottom regions of the steel bath to nearby boundaries will play a decisive role in affecting the top and bottom temperatures (hence the extent of thermal stratification). Generally, for the same bulk-cooling rate, larger heat fluxes to ladle bottom and lower section of sidewall (resulting in further lowered bottom temperatures) will lead to a greater extent of thermal stratification than uniformly distributed heat fluxes; while larger heat fluxes to top slag layer and upper section of sidewall (resulting in lowered top temperatures) may lead to smaller extent of thermal stratification than uniformly distributed heat fluxes.

REFERENCES:

- [1] Fredman T. P., Scand. J. Metall., Vol. 29, 2000, pp. 232-258.
- [2] Kitamura M., Kawasaki S., Kawai S., Kawai K. and Miyake K., Trans. Iron Steel Inst. Jpn., Vol.23,1983,pp. B165.
- [3] Minion R. L. and Leckie C. F., Steelmaking Conference Proceedings, Vol. 69, 1986, Iron and Steel Society, Washington, U.S.A., pp. 335-343.
- [4.] Olika Bekele, "Simulation of Ladle Lining and Steel Temperature in Secondary Steelmaking", Licentiate Thesis, 1992, Lulea University of Technology, Sweden.





¹ Peter KOŠTÁL, ² Andrea MUDRIKOVÁ

USE OF E-LEARNING AND VIRTUAL LABORATORY TO AUTOMATION TEACHING

¹⁻² SLOVAK UNIVERSITY OF TECHNOLOGY, FACULTY OF MATERIALS SCIENCE AND TECHNOLOGY,
INSTITUTE OF PRODUCTION SYSTEMS AND APPLIED MECHANICS, TRNAVA, SLOVAKIA

ABSTRACT:

In this paper is described the main ideas of national project "KEGA 3/7131/09 – Laboratory of production system program control". This project is focused to build of virtual laboratory and supplemental e-learning documents for several studying subject at our institute. This virtual laboratory serve for teaching automatic control principles and programming in flexible production via various control modes often used in the technical practice. In this laboratory there are applied real elements of control systems. By means of these laboratory students as future graduates of technical university can acquire and improve occupational competences demanded by actual labor market.

KEYWORDS:

virtual laboratory, e-learning, production system, automation

1. INTRODUCTION

Within the grant project KEGA being solved in the Institute of Production Systems and Applied Mechanics, STU Bratislava, in years 2009-2011, we endeavor to acquire and improve abilities and skills which employers expect graduates of technical universities to have in present circumstances.

Intent of this project is to create a laboratory for program control of production systems by pneumatics and a suitable teaching system supporting key and occupational competencies, abilities and skills of technical university students which at the same time would reveal strong point's and weak spots of their preparation for practice. In this paper we wish to present targets of this grant mission and its expected merit.

To achieve project goals it is necessary to revise curriculum and to use such teaching forms and methods that enable to exceed the scope of cognitive knowledge of scientific disciplines and professions that means to develop key competencies of students. These gain extraordinary significance not only for the personal development but also in term of lifelong education and employability of technical university graduates.

The present time brings along the need of superior education providing for:

- ❖ Ability to make decisions,
- ❖ Solve problems,
- ❖ Work with information,
- ❖ Ability to learn – lifelong education,
- ❖ Computer literacy,
- ❖ Communicative skills even in foreign languages,
- ❖ Self-activity and self-responsibility

Rapid changes put higher and higher demands on people nowadays. Obtained professional knowledge is out of date after a shorter and shorter time. Professional knowledge includes areas of „general basic knowledge and knowledge specific for particular major“.

This one is usually obtained cognitively and stored in the left brain hemisphere. However, in the area of electronics and technology, changes will be more frequent.

Key competencies should help us deal with professional knowledge with aim to solve the problems. Competencies with focus on one particular situation are quickly out of date or totally useless.

„Key competencies have longer lifetime than professional qualification. That’s why these are the basis for the next learning“

Key competencies can be understood as a complex of universal abilities exceeding the boundaries of specific professional knowledge and abilities. They express abilities of people to behave adequately to a specific situation.

Working in virtual laboratory will develop and strengthen computer literacy, so important on the present and even more important in future as we presume and last but not least will absolutely support acquisition of other key and occupational competencies of our university graduates.

Graduates will acquire the needed skills, experience and knowledge of production system controlling design methodology. They can simulate functions of designed devices. For simulation a specialized software will be installed on our intranet. By this software we can supervise every part of the designed control system. This control system includes only real industrial parts (PLC, stepper driver, servo driver, sensors, etc.).

By object-lessons and connection with practice we want to increase value of our graduates at the labour market.

2. PROJECT TARGET AND IMPLEMENTATION

The Project target includes building of virtual laboratory for program control systems. That laboratory is instrumental to teaching architecture principles of pneumatic and electro-pneumatic and program control systems and to verification of these systems’ functions by simulations.

Students gain experience of working with real industrial parts and the learning process is more effective. The goal is to make the pedagogical process more attractive for students in several studying subjects e.g. :

- ❖ Automation and mechanization,
- ❖ Theory of automates,
- ❖ Production systems,
- ❖ Production systems operation,
- ❖ Production and manipulation devices programming,

Students learning in this planned laboratory will acquire necessary skills and will acquaint themselves with generation methodology of several systems (pneumatic, electro-pneumatic, and electric ones) what will markedly increase their value at the labour market. The Fig. 1 presents the mentioned virtual laboratory.

Creation of virtual pneumatic or electro-pneumatic program control systems requires both individual work and decision making and cooperation including discussion on simulation of the proposed control circuit (Fig. 2).



Fig. 1: View to virtual laboratory

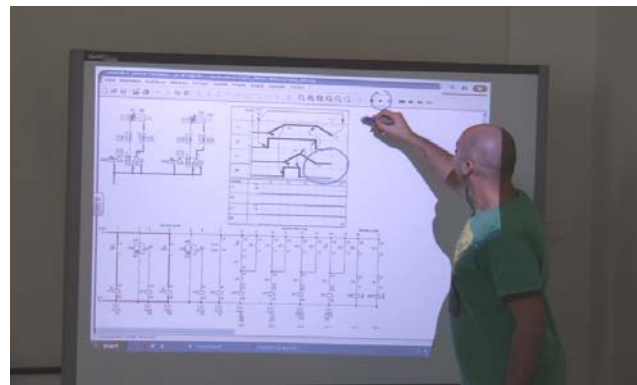


Fig. 2: Discussion about an electro-pneumatic scheme

By this laboratory students will obtain an opportunity to prepare assignments and projects of various subjects applying pneumatic and electro-pneumatic control systems and get ready for the real problem solving in practice. Thereby they also get a practice so important for employers. It widely develops and strengthens their technical occupational competencies and also their key competencies.

Within the project there will be developed study e-learning materials (manuals, methods, examples,...) and made available on Internet which will enable effective working in the laboratory and serve as a basis for further development of knowledge and skills of our students.

3. E-LEARNING

Traditional learning design is indicative of the learning field's reluctance to change. In spite of advances in neuroscience, collaborative technology, and globalized business climate, learning is still largely based on design theories created during the early 1900's to 1960's. The environment in which we are immersed has changed. Media and technology has changed. The social environment has been altered. The world has become networked and connected. In this environment of colossal change, the design methodologies used to foster learning remain strangely outdated – created for a time and need which no longer exist. Learning Development Cycle (LDC) is a learning design model to bridge the gap between design approaches and knowledge needs of academic and corporate learners.

Much of LDC is rooted in more traditional design structures. We are currently still in the beginning stages of societal and technological alterations. The model is intended to simply open doors to new design approaches, while maintaining aspects from previous models that still serve learners. More developed (connectivist-centric models) will be required as we move forward. LDC is a transitory design approach, bridging traditional design and beginning to embrace internet-era design.

Different types of learning exist. Learning happens in a variety of ways – from courses, conversations, life experiences, personal thought, or working on a project. Each different type of learning requires a different design process (as the object of the design differs depending on learning type). LDC presents four broad learning categories: transmission, acquisition, emergence, and accretion. These categories will be discussed in greater detail in this paper.

Learning today has moved beyond courses (courses serve a static knowledge field). As a result, course-based ID is not as useful for designing alternative modes of learning. The more rapidly knowledge and information climates change, the greater the need for responsive dynamic models.

E-Learning – phenomena of education of the 21st century. It is astounding by its extensiveness, attracts by huge amounts of technical resources, and affects nearly all areas of human gnosis. The reason is time and change velocity in daily life of all of us. One option is to apply electronic education – e-Learning in our lifelong education. Education is one of the most important life priorities for us but also for the modern society.

Electronic learning or e-learning (sometimes written as elearning) has various definitions. E-learning is facilitated and supported via information and communications technology (ICT).

The American Society for Training and Development (ASTD) defines e-learning as a broad set of applications and processes which include web-based learning, computer-based learning, virtual classrooms, and digital. Much of this is delivered via the Internet, intranets, audio- and videotape, satellite broadcast, interactive TV, and CD-ROM. The definition of e-learning varies depending on the organization and how it is used but basically it involves electronic means of communication, education, and training.

Many terms have been used to define e-learning in the past. For example web-based training, computer-based training or web-based learning, and online learning are a few synonymous terms that have over the last few years been labelled as e-learning. Each of this implies a "just-in-time" instructional and learning approach.

Regardless of the definition you chose to use, designers, developers, and implementers make or break the instructional courses and tools. E-learning is simply a medium for delivering learning and like any other medium, it has its advantages and disadvantages. E-learning covers a wide array of activities from supported learning, to blended or hybrid learning (the combination of traditional and e-learning practices), to learning that occurs 100% online.

Sound e-learning is founded on instructional design principles, pedagogical elements that take into account learning theories. Given its nature, online distance education is well matched with e-learning and flexible learning but is also used for in-class teaching and blended learning.

4. E-LEARNING IN VIRTUAL LABORATORY

If we look at e-learning as at efficient utilization of information technologies in educational process then it actually means new opportunities that can be used in education.

E-learning is a solution designed for education, however education conceived in full context. It is not limited to education of students only but is in a broad sense a method of information sharing and passing within lifelong education that is a necessity especially for technicians.

In contrast to classical information systems dealing especially with information sharing and a possibility to find information necessary in proper time; e-learning lays a big stress on method of representation. Nowadays it is not enough only to acquire correct information in due time but it

also is necessary to understand it fully and see it in context. And just e-learning supports these abilities.

E-education as a progressive teaching form opens many new opportunities. This form can be used in all formal education grades and also in lifelong education

E-Learning effectively measures every course by means of testing objects and control systems. It enables to set up desired goals without prejudice (e.g. student must answer correctly to test questions verifying his/her actual knowledge of studied subject after taking in the course). E-Learning gives immediately available information on individual students, how many points they achieved, how much time they spent in individual course parts, how they answered questions. Equally simply E-Learning evaluates statistically fruitfulness of individual courses and thereby identifies courses to be revised. Likewise E-Learning brings new forms of communication and cooperation among students and between students and lectors which would be inconceivable without using information technologies.

E-Learning turns teaching into an addressed, individual, interactive and interesting process integrated with daily life of students.

E-learning means a process which describes and solves creation, distribution, managing and feedback realization of the pedagogical process by computers and network. These applications contain simulations, multimedia, combinations of text and graphics, audio, video and electronically testing of students. Every student can choose individual form of study that is suitable for him. E-learning is a high quality extension of existing possibilities of study.

The virtual laboratory applies a combination of classical way of teaching and e-Learning courses.

E-Learning turns teaching into an addressed, individual, interactive and interesting process integrated with daily life of students.

For working in the virtual laboratory of pneumatics and electro-pneumatics we use software environment FluidSIM that is one of many software enabling to set up various pneumatic and electro-pneumatic control circuits as well as to verify their function by simulation of these control circuits. Fig. 3

Software FluidSIM was compiled by the company FESTO and serves the purpose of control simulation of pneumatic and electro-pneumatic circuits.

Step by step students learn creation principle of pneumatic and electro-pneumatic control circuits by means of e-Learning materials and with participation of a lector. On the basis of e-Learning courses they pass step by step through creation principles of control circuits at first, thereafter through verification by simulation of control circuit function. Control circuit diagram can be seen in Fig. 4.

Work of students in the virtual laboratory is a part of e-Learning courses where they can create their own pneumatic and electro-pneumatic control circuits for control of specific equipment and thereafter verify its reliable function via simulation.

5. CONCLUSIONS

We have “learning centers” and “training departments” – treating learning as if it were a compartment or corporate activity in which we sometimes engage, rather than a constant, ongoing process – a thread through the fabric of daily activities. Learning is a thread that runs through all of life. We do not belong only in corporate training rooms. The act of learning is ongoing and constant.

An organization’s ability to adapt is important to ongoing survival (even innovation, if you will). But the adaptation must be of a particular type. It must be progressive, ongoing, punctuated with periodic bursts (the transformation), but many about a progressive, but not overly reactionary trends to what is going on in the larger learning landscape. Few organizations will be positioned to

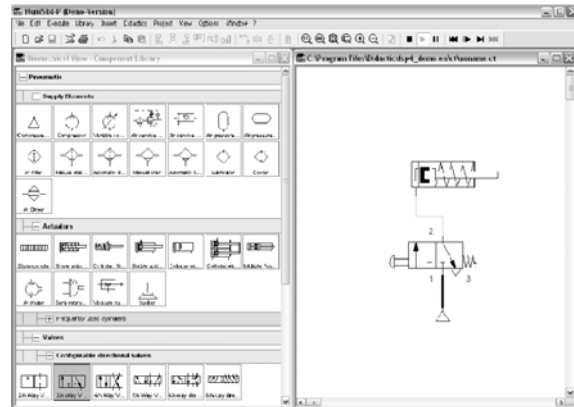


Fig. 3: FluidSIM workbench

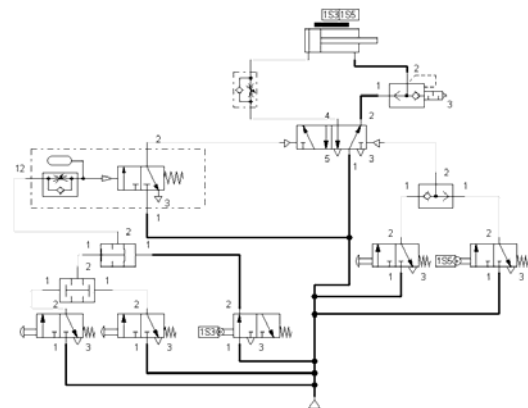


Fig. 4: Circuit scheme in FluidSIM

adopt wholesales the ideas I've presented. To do so would damage many elements of the system continuing to work well. But to survive, all organizations need to embrace experimentation – an ongoing “blood in the corporate veins” type of experimentation. Policy-induced change can be effective, but most often, if we follow the lessons of evolving organisms, developing corporate competence progressively is the best approach for long-term sustained change.

The needs of continual learning, often tightly linked to work, required a new approach and model. LDC has been designed to create an alternative, less-linear view of learning. Learning is the intent of any development activity – communities, courses, networks, or ecology. Selecting the most appropriate design approach will assure greater a more positive and valuable experience for the learner.

ACKNOWLEDGMENT

This paper was created thanks to the national grant KEGA 3/7131/09 – Laboratory of production system program control

REFERENCES

- [1] Rusková, Dagmar, Cagaňová, Dagmar 1997, Needs analysis, In: IATEFL. Proceedings of the Teacher Training Symposium. Teacher Training in a Climate of Change. – Bratislava, Univerzita Komenského v Bratislave., - ISBN 80-88901-08-1. - S. 87-94
- [2] Mudriková, Andrea - Charbulová, Marcela: Virtual laboratory for pneumatic and electropneumatic as a tool for increasing efficiency of teaching technical academic fields. In: AMO 2008 : 8th international conference on advanced manufacturing operations. Bulgaria, Kranevo, 18-20 June 2008. - Sofia : DMT Product, 2008. - S. 115-118
- [3] Holubek, Radovan - Horváth, Štefan - Velíšek, Karol: Increased effective education pneumatic and electropneumatic at virtual laboratory. In: Annals of DAAAM and Proceedings of DAAAM Symposium. - ISSN 1726-9679. - Vol. 20, No. 1 Annals of DAAAM for 2009 & Proceedings of the 20th international DAAAM symposium "Intelligent manufacturing & automation: Focus on theory, practice and education" 25 - 28th November 2009, Vienna, Austria. - Vienna : DAAAM International Vienna, 2009. - ISBN 978-3-901509-70-4, s. 0193-0194
- [4] Matúšová, Miriam - Hrušková, Erika - Košťál, Peter: Spatial arrangement of information and power flows in pneumatics and electro pneumatics laboratory. In: Annals of MTeM for 2009 & Proceedings of the 9th International Conference Modern Technologies in Manufacturing : 8th - 10th October 2009, Cluj-Napoca, Romania. - Cluj-Napoca : Technical University of Cluj-Napoca, 2009. - ISBN 973-7937-07-04. - S. 169-172
- [5] Bílik, Jozef - Kapustová, Mária - Košťálová, Miroslava: Zvýšenie teoretickej a praktickej pripravenosti absolventov študijného programu tvárnenie pre súčasnú prax. (Increasing of theoretical and practical readiness of graduates in studying subject forming for today praxis) In: Inovatívne postupy výučby výrobných technológií na univerzitnom stupni štúdia: Zborník vedeckých príspevkov, vydaný pri príležitosti ukončenia projektu KEGA 3/5209/07 s názvom "Podpora výučby výrobných technológií formou virtuálnych exkurzií". - Zvolen : Technická univerzita vo Zvolene, 2009. - ISBN 978-80-228-2050-9. - S. 7-10
- [6] Mudriková, Andrea - Košťál, Peter - Matúšová, Miriam: Building of a production system program control laboratory. In: Annals of DAAAM and Proceedings of DAAAM Symposium. - ISSN 1726-9679. - Vol. 20, No. 1 Annals of DAAAM for 2009 & Proceedings of the 20th international DAAAM symposium "Intelligent manufacturing & automation: Focus on theory, practice and education" 25 - 28th November 2009, Vienna, Austria. - Vienna : DAAAM International Vienna, 2009. - ISBN 978-3-901509-70-4, s. 0603-0604





¹. Štefan NIŽNÍK, ². Ondrej MILKOVIČ, Svätoboj LONGAUER

METALLURGICAL TWO-STEP PRODUCING METHOD OF FE NANOPARTICLES

¹. TECHNICAL UNIVERSITY OF KOŠICE, FACULTY OF METALLURGY, KOŠICE, SLOVAKIA

ABSTRACT:

Submitted paper is dealt with preparation of iron based nanoparticles and marginally also cobalt nanoparticles through precipitation from solid solution of age-hardenable alloys and their subsequent insulation by electrochemical or chemical resolution of matrix. The simplest system is Cu-matrix in which Fe resp. Co as elements are precipitated in form of coherent particles γ -Fe,Co. These particles are changed at plastic deformation or at extraction and insulation by martensitic transformation on α -Fe, Co. For purposes of nanoparticles precipitation from solid solution there is performed the targeted heat treatment consisting of solution annealing, quenching and precipitation annealing. The size of nanoparticles is regulated by heat treatment of chosen material according to the required procedure. The volume of separated nanoparticles is proportional to the time of dissolution and to the potentiostatic mode according to applied potential-dynamic curves. The quality and material characteristics of nanoparticles was controlled by the methods of TEM, x - ray analysis and measurement of magnetic properties.

KEYWORDS:

Fe nanoparticles, precipitation, electrochemical dissolution, characteristics

1. INTRODUCTION

At present time the nanoparticles are produced by intricate sophisticated techniques e.g. laser-induced pyrolysis, laser evaporation and condensation, plasma torch synthesis, deposition from colloidal solutions, reduction from aqueous solutions, crystallization from amorphous solid phase, etc. from which neither one reckons with precipitation of nanoparticles from crystalline solid phase. At the same time almost each of the appointed technologies is complicated and from views of investment and also operating cost is considerably demanding. When techniques producing free metallic nanoparticles are used, the particles are usually covered by oxides with thickness depending on technique [1,2].

Method for nanoparticles preparation presented in this work consists of the aimed heat treatment of basic material where nanoparticles are formed by controlling precipitation from solid solution and the production is reposed on insulation or extraction of nanoparticles by electrochemical eventually chemical way. So, the largeness of nanoparticles in the range 3 – 1000 nm is intentionally regulated by metallurgical heat treatment of chosen material according to the required procedure. Quantity of separated nanoparticles is straight-proportioned to the time of solution and to the potentiostatic mode. According to [3] the amount of Fe nanoparticles electrochemically separated from Cu matrix is 0,024 μ g from the plane 0,5 cm² within 30 min and are stored in n-hexane. Besides, preliminary experiments with Cu-Fe material system show that extracted Fe particles are either oxidless or only with small not dangerous oxide layer.

It is a matter-of-course, the supposed method allow to production also of nanowires by creating their shape through the thermo-mechanical treatment or through the separation of regular rod-shaped Fe particles from eutectoid or eutectic alloys. The idea as well as the procedure of nanoparticles separation are safekeeping by two patents [4,5]. As a very significant factor from the point of view of exploitability of nanoparticles prepared by „metallurgical“ method there is high

quality of particles appreciated by size and shape homogeneity as well as their structure. It's utilizable in the medical applications [6-7].

Electrochemical isolation consists of the matrix solution in the selected solvent during which the nanoparticles are at least ~ 100 mV more ingenuous and their corrosion potential is more positive towards the metal potential of the basal matrix. During the solution process of the matrix, the particles hold their stability and keep their consistency in solution. In some alloyed systems it is sufficient to use a chemical solution of the matrix for favourable insulation of particles, so as not to come to attacking of the particles [3].

2. EXPERIMENTAL METHODS

For the operation of presented method of nanoparticles preparation the model alloy system Cu-Fe was chosen, which marks out max solubility of Fe in Cu solid solution $\varepsilon 4\%$ at 1096°C . With decreasing temperature the solubility of iron in solid solution is falling down to zero at room temperature.

Copper wire with diameter 10 mm and chemical composition 1,88 % Fe, 0,015 % P, 0,08 % Zn a 0,05 % B was submitted to the dissolving annealing at $1000^\circ\text{C} / 12$ hod and was quenched into cold water. In order to precipitate the spheroid Fe nanoparticles, the samples were annealed at the temperature of $600^\circ\text{C} / 30$ min, 1, 12 and 24 hours, and quenched into cold water.

Producing of Fe nanoparticles was design by electrochemical dissolution of copper matrix in aqueous solution as well as etching solution by potentiostatic mode. Labor technique was followed: Pt electrode as auxiliary; SCE (saturated calomel electrode) as reference; specimen as anode. Computer controls the potentiostat fixed on a defined value. The dissolving conditions are appropriate at the potentiostatic mode of -250 mV (SCE) in ammonia solution.

The morphology and distribution of particles and the state of substructure and interphase boundary were monitored by optical and transmission electron microscopy TEM by electronic microscope JEM 2000 FX and JSM 35 CF with microanalytical Link 860. Results of electron-microscopic observation will be evaluated by statistical methods.

3. RESULTS AND DISCUSSION

Morphology and distribution of the Fe particles were studied by means of carbon replica technique by TEM. After precipitation annealing, soft precipitate consisting of regular globular particles was found within the samples. The information about its control is very important for obtaining the specific dimension of particles by consumer order especially for medical applications. The distribution function is time invariant during the steady-state precipitation annealing. This reason is a good condition for preparing the smaller (one domain) particles, because the smaller precipitates are assigned the smaller dispersion.

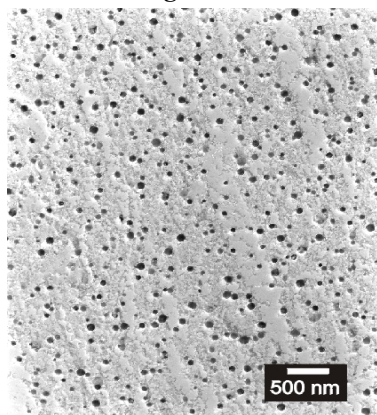


Fig. 1 Extracted Fe precipitates from Cu matrix

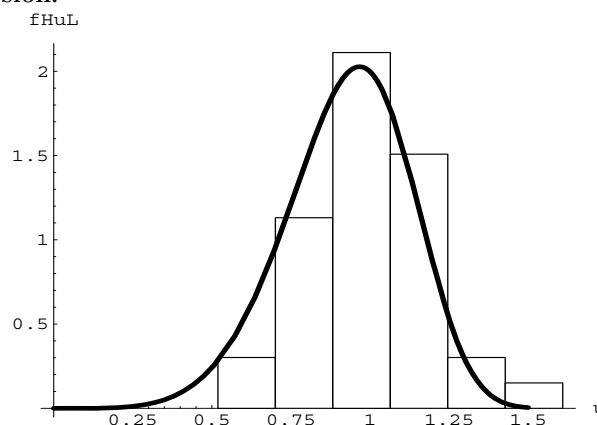


Fig. 2 The size distribution of Fe precipitates aged at 973 K for $86,4\text{ ks}$

The regular spherical particles with extraordinary homogeneous distribution can be observed in the Fig. 1. According to the expectation, the increase of annealing time resulted in growth of particles. The range size of particles after annealing 12 hours moves between $18 - 22$ nm. Fe particles after 24 hrs of annealing had the dimension $\approx 26 - 32$ nm. In all cases, the distribution of particles was statistically equable in whole volume of samples and the particles had globular shape [8].

Quantity of isolated nanoparticles is directly proportional to time of dissolution in potentiostatic mode. The amount of 0,024 mg Fe spherical nanoparticles were separated from the surface 0,5 cm² in 20 ml electrolyte at potentiostatic mode -250 mV (SCE) for 30 min.

Characterization of Fe nanoparticles after their insulation from Cu matrix is documented in Fig. 3. Measuring of the nanoparticles radiuses was shown a good agreement with the mean precipitate radius after precipitation annealing. This confirms that precipitates are not dissolution in the electrolyte.

TEM micrograph of nanoparticles diffraction is shown in Fig. 4. The core-shell structure can be shown with the dark core end the light shell. Shel thickness is around 3 – 4 nm at mean diameter of nanoparticles 10 – 21 nm. Fig. 5 presents the selection electron diffraction. The straight pattern of α -Fe phase and two diffusive rings corresponding to 2 line ferrihydrite.

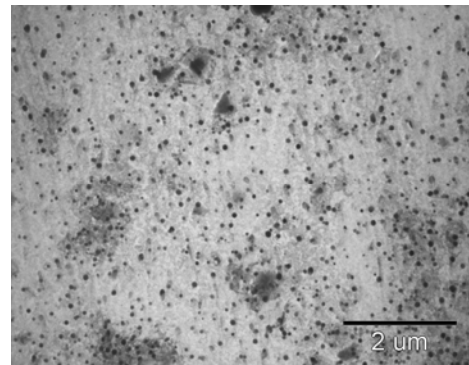


Fig. 3 Insulated nanoparticles after matrix dissolution

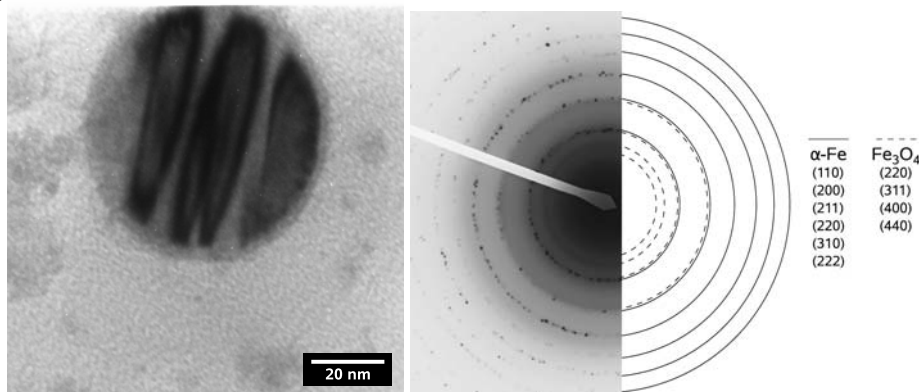


Fig. 4 TEM micrograph of insulated Fe nanoparticles

Fig. 5 Selection electron diffraction of nanoparticles

Characteristics of the magnetic properties of nanoparticles was determined by measuring the temperature dependence of magnetization in the magnetic field (FC) and without magnetic field (ZFC) and also from measurements of magnetic hysteresis loops at different temperatures.

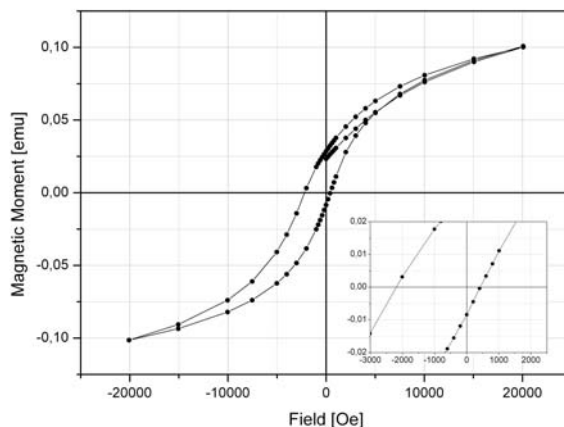


Fig. 5 Magnetic hysteresis loop at 2 K

4. CONCLUSIONS

1. After choosing experimental treatment of precipitation annealing at 600 °C/0,5, 1, 12, 24 hours, the statistically regular distribution of precipitate was obtained in the volume of samples. There were the particles with globular shape, which dimensions grew by annealing time from 4,5 to 32 nm.

Measurements of magnetic properties of Fe nanoparticles with a mean radius of 27.7 nm from the dependence of magnetic moment on the temperature not confirmed the superparamagnetic behavior of these particles. At produced nanoparticles with mean radius of 10 nm was found the blocking temperature ($T_b = 65$ K), which characterizes the behavior of superparamagnetic particles above this temperature. This justifies the fact that the presented method of nanoparticles production can be used for applications which require phenomenon of superparamagnetism (medicine: magnetic resonance imaging, medicament carrier).

2. The advantages of this method consists of possibilities to control the size and shape of nanoparticles in a narrow range tolerance with relative accuracy 5 nm by heat treatment at min financial costs of the production facilities.
3. The amount of Fe nanoparticles separated from the surface of 0,5 cm² for 30 min is 0,024 mg. The particles are not dissolved during the dissolution process of the matrix and the particles don't change their chemical composition.
4. Nanoparticles with mean radius of 10 nm have the blocking temperature (T_b = 65 K), which characterizes the behavior of superparamagnetic properties above this temperature, what can be used for applications in medicine.

ACKNOWLEDGEMENTS

The autors would like to acknowledge the support of Scientific Grant Agency of the Ministry of Education of the Slovak Republic for its financial contribution to the project No.1/4138/07 „Magnetic nanopartricles for medical and technical applications“.

LITERATURE

- [1] Schmid, G.: Nanoparticles, Wihley-VCH Verlag GmbH & Co. KgaA, 2004.
- [2] Jönsson, B., J., at al.: Oxidation states and magnetism of Fe nanoparticles prepared by a laser evaporation technique. In: Journal of Application Physics, 1996, č. 79.
- [3] Milkovič, O., Halama, M., Longauer, S., Nižník, Š.:Preparation mode of Fe nanoparticles, Acta Met. Slovaca, 13, 2007, 694.
- [4] Milkovič, O., Halama, M., Nižník, Š.: Spôsob výroby feromagnetických Fe nanočastic elektrochemickou separáciou, Zn. spisu: PP 0087 – 2005, zaregistrovaná 29.7.2005,
- [5] Longauer, S., Nižník, Š.: Spôsob prípravy a izolácie nanočastic z tuhej fázy, Zn.spisu: PP0088 – 2005, zaregistrovaná 29.7.2005
- [6] Wang, Y., C., et al.: The preparation, surface modification, and characterization of mettalic γ -Fe nanoparticles. In: Material science and engineering B, 1999, č. 60, s. 223- 226.
- [7] Salata, O.V.: Applications of Nanoparticles in biology and medicine, Journal of Nanobiotechnology, 2, 2004.
- [8] Hirata, V. M. L. et al.: Ostwald ripening of γ -Fe precipitates in Cu-1,5 at. % Fe alloy. In Scripta Metallurgia et Materialia, č. 31, 1994, s. 2.
- [9] Timko, M., et al.: Czechoslovak Journal of Physics 54, Part 2 Suppl. D., 2004, s. 599-606.
- [10] Bansmann, J., et al.: Materials Science and Engineering C 19, 2002, s. 305-310.
- [11] Martin, J., I., et al.: Journal of Magnetism and Magnetic Materials 256, 2003, s. 449-501.
- [12] Konerecká, M., et al.: Journal of Magnetism and Magnetic Materials 293, 2005, s. 271-276.



RESEARCH REGARDING THE EFFECT OF ALLOYS VIBRATION ON MICRO- AND MACROBLISTER FROM CASTED PARTS

¹⁻² UNIVERSITY POLITEHNICA BUCHAREST, ROMANIA

³ TECHNICAL COLLEGE "MEDIA" BUCHAREST, ROMANIA

ABSTRACT:

Compacting casted parts and reducing the blister on the solidification of alloys are equally interests in improving the quality, characteristics and reducing manufacturing costs by increasing the removal result index from blister compaction.

Theoretical and experimental research conducted by the authors has lead to obtain beneficial results in this respect. This paper presents the results and conclusions drawn from this research.

KEYWORDS:

Alloys, quality, manufacturing costs

1. INTRODUCTION

The structure and physical-mechanical characteristics of a casted metal material are influenced by its density and compactness.

At the alloys solidification it can occur discontinuities, due to the shrinkage phenomenon, characteristic of most alloys and to the pronounced decrease in solubility of gases in the melt, at crystallization temperature.

2. THE STUDY

Obtaining a compact metal material is provided if the v speed of the alloy penetration into capillary channels of the biphasic zone is equal to the contraction speed v_{contr} . [1]

$$v_{\text{contr}} = \alpha \cdot m \cdot R \quad [\text{m/s}] \quad (1)$$

where: α - contraction coefficient of the alloy at solidification;

m - ratio between the liquid mass volume from the biphasic zone and this zone's volume;

R - rate of occurrence of solid phase [m/s].

In ordinary conditions, the v speed is expressed as such:

$$v = \frac{r^2}{8\eta} \cdot \frac{P_e + P_m - P_g + \frac{2\sigma}{r} \cos \theta}{l}, \quad [\text{m/s}] \quad (2)$$

where: r - radius of the capillary channel [m]; P_e - external pressure [Pa]; P_m - metalostatic pressure [Pa]; P_g - channel gases pressure [Pa]; σ - superficial tension of the alloy [N/m]; θ - wetting angle [rad]; η - dynamic viscosity of the alloy [Pa·s]; l - length of penetration of the alloy in capillary channels [m].

From the equality of the two speeds $v=v_{\text{contr}}$ results:

$$\frac{r^2}{8\eta} \cdot \frac{P_e + P_m - P_g + \frac{2\sigma}{r} \cdot \cos \theta}{l} = \alpha \cdot m \cdot R \quad (3)$$

from where:

$$l = \frac{r^2 \left(P_e + P_m - P_g + \frac{2\sigma}{r} \cdot \cos \theta \right)}{8\eta \cdot \alpha \cdot m \cdot R} \quad (4)$$

Mechanical oscillations decreases the superficial tension σ at the liquid-solid interface wetting angle θ and imprints the alloy a maximum initial speed $v_i = A\omega$.

Mechanical vibrations action produces in the biphasic zone a dendrite fragmentation, reducing the length of capillary channels to be covered by the liquid alloy to fill the gaps caused by shrinkage and increase the speed of the liquid alloy flow in these areas, improving supply conditions in micro-cavities.

Also, vibrations determine a macro-blister concentration and a reduction of the porosity in the hot spots, an effect explained by increasing the melt flow.

Mechanical vibrations applied in liquid metal alloys introduce new forces that determine changes in the macrostructure and macro-blister of the casted parts.

The size, shape and position of micro-blister can be determined theoretically by plotting isotherms of solidification in the walls of the casted parts.

Macro-blister is located in those areas of the wall where the liquid alloy solidifies last and alone. Macro-blister consists of one or more concentrated cavities in clearly defined areas, they result from the solidification of large volumes of liquid alloy. Macro-blisters are called as well concentrated blisters. [2]The alloy layers that isolate the blisters between them and cover them in the top part are called decks.

The main macro-blister is found in the upper part to the casted part compared with the casting position, while the secondary macro-blister is found in the lower part or in hot spots in the thermal axis zone.

Macro-blister is determined using technological evidence, while micro-blister by applying methods of flaw (X or gamma rays) or by determining the density of samples cut from the casted part wall.

The volume, shape and position of the macro-blister and micro-blister in the walls of the casted parts are influenced by several factors which at their turn depend on the technological nature of the alloy, the nature of the mold, the casting conditions and the casted part geometry.

The total volume of the blister is:

$$V_r = V_{MR} + V_{mr} \quad (5)$$

in which: V_{MR} - the macro-blister volume; V_{mr} - micro-blister volume.

The factors which influence the blister are the following:

- ❖ alloy's nature;
- ❖ form's nature;
- ❖ casted part geometry;
- ❖ casting conditions.[3]

Avoiding the process of developing a micro-blister is impossible, but the routing of the contraction process in order to obtain a macro-blister with as smaller as possible volume and with an optimum distribution in the part's wall is possible.

3. ANALISES, DISCUSIONS, APPROACHES and INTERPRETATIONS

The development of the alloy was made in a crucible furnace, heated by burning a natural gas flame. After melting, the temperature was increased and maintained at 800°C.

For casting and solidification of the samples were used metal forms.



Fig. 1. Alloy's solidification



Fig. 2 Extraction of vibrated samples from the mold

Among physical properties, density is directly related to the development process and represent the unit volume's mass.

From the performed measurements performed we can remember the following:

- ❖ sample casted from non-vibrated alloy, solidified in outdoor air; (O)
- ❖ sample casted in non-vibrated alloy, solidified under the influence of vibration after casting until solidification; (V)
- ❖ sample casted from alloy vibrated in pot, solidified without vibration (O')
- ❖ sample casted from alloy vibrated in pot, solidified under the influence of vibration after casting until solidification. (VV)[4]

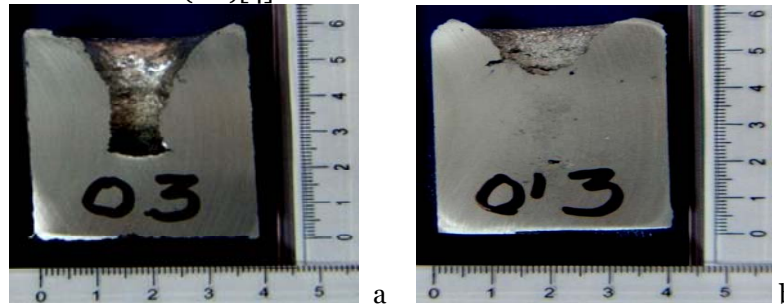


Fig. 3 Blister aspect for different situations
 a- non-vibrated; b- the vibration of melted alloy (only in pot, before casting)

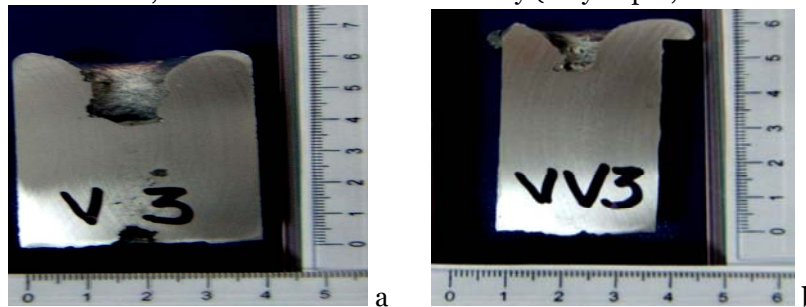


Fig. 4 Examples of section blisters
 a- solidified under the influence of vibration after casting until solidification; b- vibrating the alloy in the pot and during casting until solidification.

Vibrations determine macro-blister concentration, a decrease of porosity from the liquid alloy, to manage the formation processes and structure compacting with small crystals which present the best physical and mechanical characteristics, including increased density of casted alloys with those advantages. Measurement results are presented in Table 1 for an aluminum alloy type ATSi12.5 Mg0.25.

Table 1. The measurements results on non-vibrated, vibrated samples

No.	Sample	Sample mass [g]	Volume [cm ³]	Density [g/cm ³]	Density increase thought vibrating [%]
1	O	30,9044	11,6	2,66	-
2	V	31,9044	11,4	2,79	4,88
3	VV	30,8544	10,9	2,83	6,39

Mechanical properties are also determined by the macrostructure because of the existence of chemical heterogeneity, crystalline or mechanical or discontinuities that play the role of power and micro-concentrators, by size, crystal form, nature and morphology of structural constituents.

Table 2 shows the values obtained by carrying out systematic evidence of resistance to fracture, yield, and elongation at break for the four types of casting:

- ❖ casting in gravitational field (O);
- ❖ casting after the liquid alloy vibrating in the mold (O');
- ❖ vibrating after casting in the mold until solidification (V);
- ❖ sample from the liquid alloy vibrated in the pot casted in the mold and vibrated until solidification (VV). [4]

Following research which refers to treating metal melts with mechanical vibrations, highlighting the fact that they have positively influenced the structure obtained after solidification and on mechanical properties, in the sense that it improves them. The values obtained are much higher than those obtained in the classical variant.

Table 2. Values for tensile strength, yield, elongation, weakening the fracture toughness for the cast alloy AlSi12.5Mg0.25 of samples realized during research

No.	Sample type	R _m [MPa]	R _{p0.2} [MPa]	A _u [%]	Z [%]	HB [MPa]	Observations
R1	O1	170	102	3,5	2	87,5	Un-worked sample
R2	O2	176	101	3	2,04	88,6	The split inclusions 0.5 mm
R3	O3	175	103	3,2	2,2	87,3	
R4	O/1	185	111	4,2	5,8	89,3	Un-worked sample inclusions in the area from feeder
R5	O/2	93,8	-	-	-	-	Defect in structure, blister with a diameter of 1.5 mm
R6	O/3	186	112	5	-	90,6	
R7	V1	295	162	4,4	3	105	
R8	V2	296	162	4	2,7	104,3	
R9	V3	295	160	3,9	2,7	106,3	
R10	V4	294	170	3,9	-	103,1	
R11	V5	294	165			103,2	
R12	VV1	150	-	-	-	-	Defect in structure
R13	VV2	295	147	5,6	3	99,3	
R14	VV3	294	145	4,2	1,5	98,6	
R15	VV4	290	150	2,1	2,1	97,2	
R16	VV5	285	151	4	2,8	97,3	Turning diameter of 50 mm, sample in the thermal axis

The mechanisms by which these vibrations act on the liquid phase during solidification and melting are complex. [5] Explanation and understanding of these mechanisms is of great theoretical and especially practical importance, allowing us to define appropriate technology for treatment of melt with vibrations.

Figure 5 shows the variation of the degassed alloy hardness under the influence of vibration (50Hz) in the casting pot. It is noted that though gas elimination was achieved a material compaction, evidenced by increasing the hardness by about 5 percent compared with the gross alloy.[6]

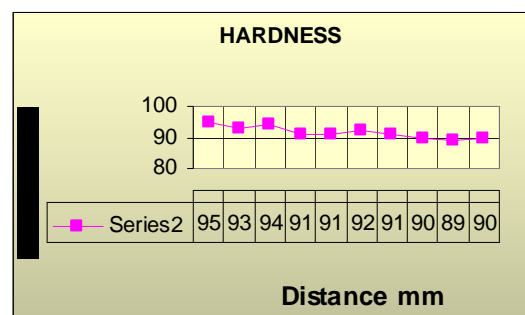


Fig. 5 HB-hardness variation on the radius for alloy AlSiMg vibrating pot, gravitational casting for the φ 20mm disc, sample O'2

4. CONCLUSIONS

The contour analysis of the contraction gap leads to the conclusion that under the natural action of vibration is reduced the blister depth and its lower part is rounded.

For the alloys with high contraction, prone to cracking, it was observed that due to mechanical vibrations the micro-blisters decrease reducing axial porosity.

Under the influence of mechanical vibration decreases the total volume of macro-blister and focuses on the superior side, reducing the volume of liquid alloy for feeders.

The main favorable technological effects obtained by applying physical-mechanical treatments, consisting of increasing compactness and improving the structure of castes parts.

It also finds a sharp increase in hardness values by 25 percent compared to a gravity cast alloy (static), a slight decrease in the hardness towards the thermal axe, at the same diameters or different diameters of the samples a longer vibrating time leads to chopped microstructures and higher hardness values.

REFERENCES

- [1.] BAUM B.A., TIAGUNOV G. B. - Protessa litiia, Moskova 1992
- [2.] CĂMUI C. - Studii și cercetări privind efectul acțiunilor fizice ale energiei vibrațiilor de joasă frecvență asupra cuprului în momentul turnării și solidificării în semifabricate; lucrare de absolvire cursurii post universitare, București 1991
- [3.] MĂRGINEAN I., VELICU Șt. - Procedee speciale și neconvenționale în turnătorii, vol. I și II. Ed. BREN, București 2002
- [4.] PĂRVULESCU C.-Cercetări privind influența vibrației asupra solidificării aliajelor turnate în piese; Teză de doctorat, UPB 2010
- [5.] POP M.A.-Cercetări asupra tehnologiilor și materialelor moderne pentru confecționarea garniturilor de model; Teza de doctorat, UT Brașov 2009
- [6.] ȘUȘU C.-Contribuții la îmbunătățirea calității topiturilor unor aliaje de aluminiu destinate turnării pieselor; Teză de doctorat, UT Cluj-Napoca 2008.



¹Eugen Mihai CRIȘAN, ²Teodor HEPUT

INFLUENCE OF BASIC ADDITIVE ON THE QUALITY OF PELLETS

¹ UNIVERSITY "POLITEHNICA" TIMIȘOARA, FACULTY OF ENGINEERING HUNEDOARA, ROMANIA

ABSTRACT:

Besides the humidity, the granulometric composition and the specific surface of the pelleted material, the compressive strength of the pellets is also influenced by some additions with binding proprieties (bentonite, lime, limestone, dolomite, etc.). During the hardening process, these additions form a resistant slag that contributes to the binding of the granules of ferrous raw materials and, finally, to the increasing of the compressive strength of the pellets.

To determine the influence of the addition of lime and dolomite on the compressive strength of pellets, we performed a series of experiments in the laboratory phase, consisting of the production of pellets based on various recipes, by adding bentonite & lime or bentonite & dolomite.

During the research, we aimed to establish correlations between the compressive strength of pellets and the additions of water, bentonite, lime or dolomite. The data obtained in the experiments were processed in MATLAB programs, resulting simple or multiple correlation equations. Based on these equations, we could establish the optimum addition of materials with basic character.

KEYWORDS:

pellet, compressive strength, lime, dolomite, iron oxide, calcium oxide

1. INTRODUCTION

Besides the humidity, the granulometric composition and the specific surface of the pelleted material, the compressive strength of the pellets is also influenced by some additions with binding proprieties (bentonite, lime, limestone, dolomite, etc.). During the hardening process, these additions form a resistant slag that contributes to the binding of the granules of ferrous raw materials and, finally, to the increasing of the compressive strength of the pellets.

When using the lime as additive, simultaneously with the hardening process can appear various chemical combinations between the iron oxide and the calcium oxide, obtaining calcium ferrites, or between the iron oxide, silica and lime, obtaining calcium and iron silicates. In case of CaO additive in excess and basicity ration up to 1.8, we obtain calcium diferrite, $2\text{CaO}\cdot\text{Fe}_2\text{O}_3$, which becomes friable in case of reduction at low temperatures.

When using dolomite as basic additive, the formation of calcium diferrite is avoided mostly due to the reduction of the CaO content. From the reaction between CaO and SiO_2 that takes place in the gangue of the pelleted raw material, it results calcium silicates of CaOSiO_2 or 2CaOSiO_2 types, which ensure a good binding of the material during the low temperature reduction process.

The use of additives for increasing the resistance of the pellets should be made respecting an optimal proportion, this being the subject of the present research.

2. LABORATORY EXPERIMENTS

The experiments regarding the producing of pellets were performed in the laboratory "Energy and raw material base in industry", at the Engineering Faculty of Hunedoara. This laboratory is endowed with the installations required for producing pellets (volumetric ranking device, mixing drum, pellet making machine and hardening installation). The compression resistance has been determined by using the tension-compression test machine found in the "Strength of materials" laboratory of the faculty. The raw material used to produce pellets consisted

of steel plant dust and red mud (resulted from alumina production). The compositions are presented in Table 1. We produced two sets of pellets, each set consisting of 3 lots.

Table 1

Set	Lot	Set	Lot	Remarks
A	A1 with 1% lime	B	B1 with 1.5% dolomite	In each set, the addition of bentonite ranged between 0 and 1% (i.e. 0%; 0.5% and 1%), and the addition of water ranged between 7.5 and 11.5%, (i.e. 7.5%, 9.5% and 11.5%)
	A2 with 3% lime		B2 with 3.5 dolomite	
	A3 with 5% lime		B3 with 5% dolomite	

The weight of the pellet batch was 2 kg (ferrous raw material, bentonite, lime/dolomite). The hardening of the pellets respected the combustion diagram of hematite ferrous materials. From each batch, we selected three pellets to determine their compression resistance. To establish the correlations, we took into account the average value.

3. RESULTS OBTAINED FROM PROCESSING THE EXPERIMENTAL DATA

By processing the data obtained in the laboratory phase, we obtained equations of correlation between the binder additives & water (considered as independent parameters) and the pellet compression resistance (considered as dependent parameter). The data were processed in MATLAB programs, the results being presented hereunder, in graphical and analytical forms.

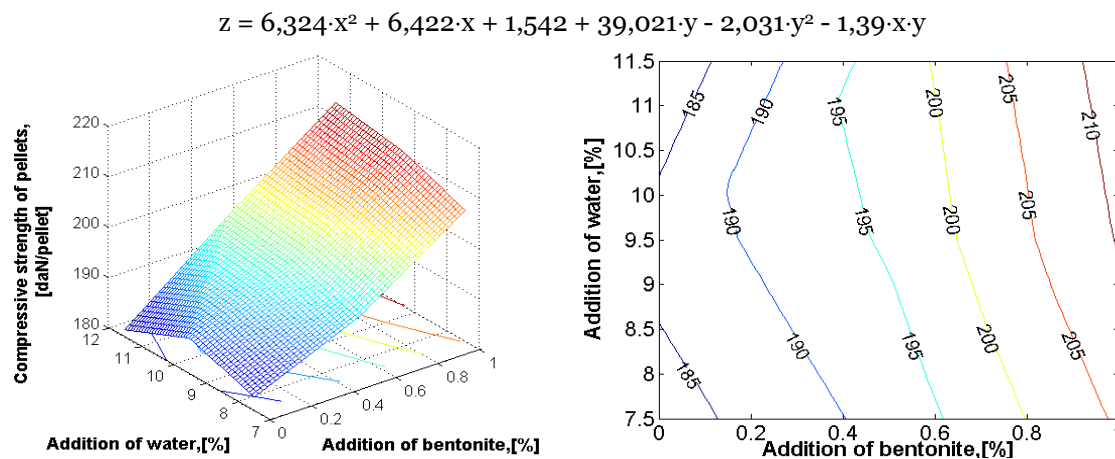


Fig.1. Variation of compressive strength of pellets to a concentration of 1% lime
 (x- addition of bentonite [%], y- addition of water [%],
 z- compressive strength of pellets, [daN/ pellet])

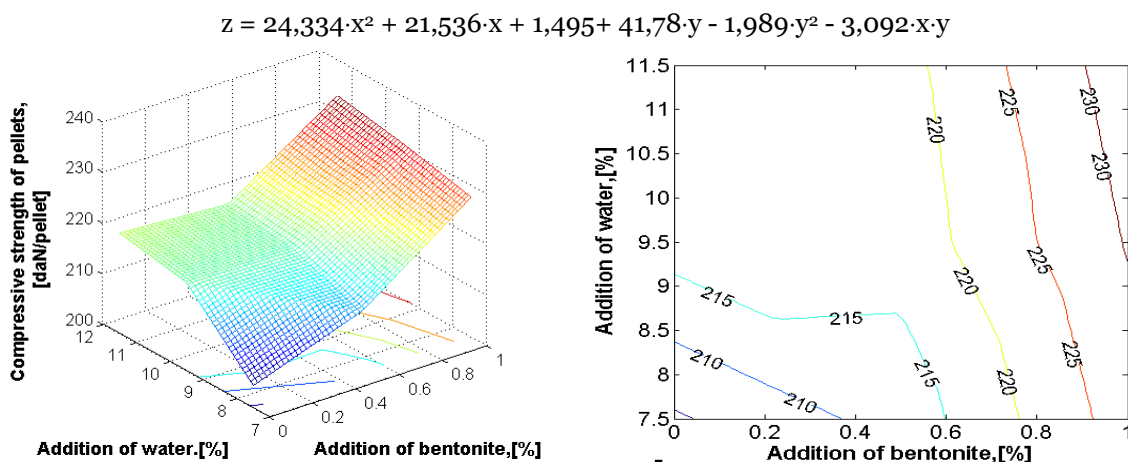


Fig.2. Variation of compressive strength of pellets to a concentration of 3% lime
 (x- addition of bentonite [%], y- addition of water [%],
 z- compressive strength of pellets, [daN/ pellet])

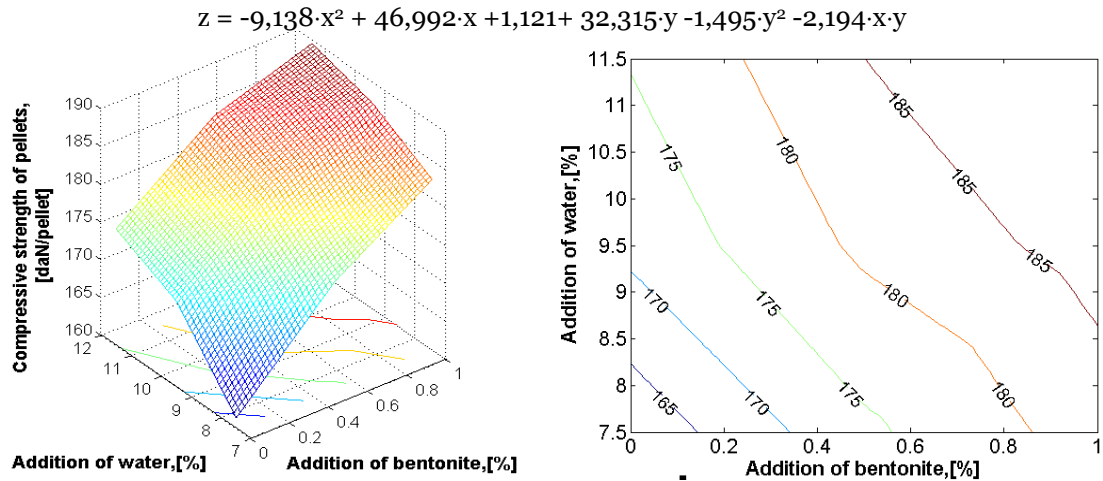


Fig.3. Variation of compressive strength of pellets to a concentration of 5% lime
 (x- addition of bentonite [%], y- addition of water [%],
 z- compressive strength of pellets, [daN/ pellet])

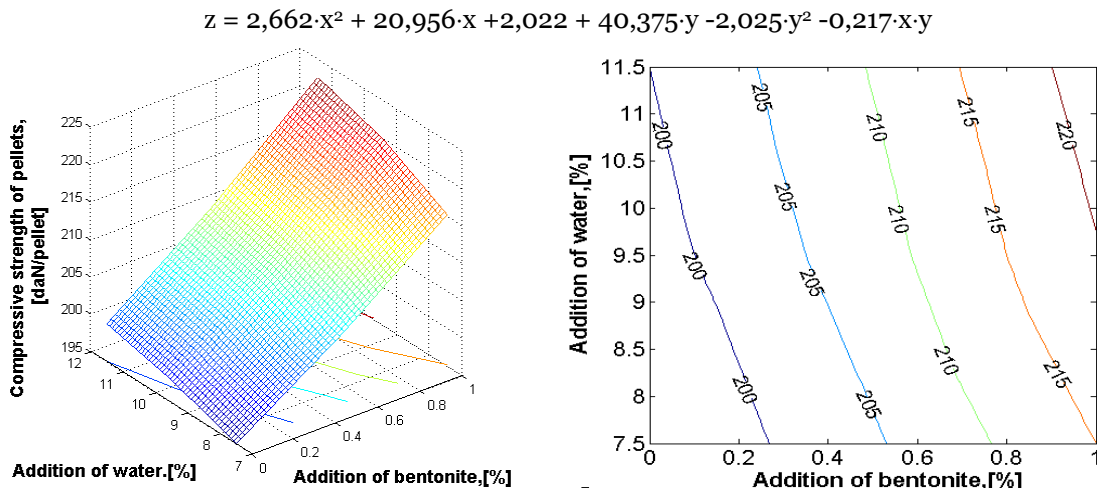


Fig.4. Variation of compressive strength of pellets to a concentration of 1.5% dolomite
 (x- addition of bentonite [%], y- addition of water [%],
 z- compressive strength of pellets, [daN/ pellet])

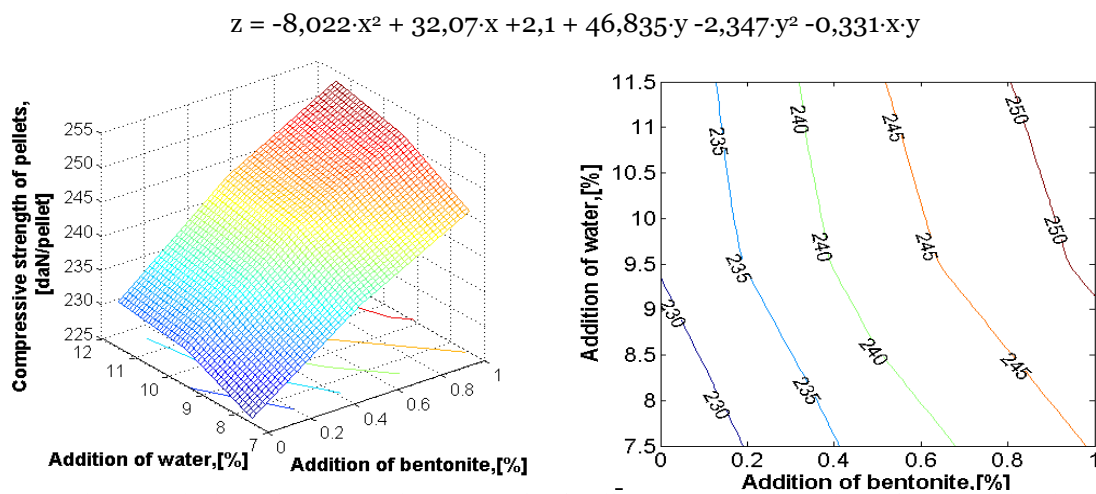


Fig.5. Variation of compressive strength of pellets to a concentration of 3.5% dolomite
 (x- addition of bentonite [%], y- addition of water [%],
 z- compressive strength of pellets, [daN/ pellet])

$$z = -8,756 \cdot x^2 + 45,475 \cdot x + 1,402 + 37,567 \cdot y - 1,765 \cdot y^2 - 2,305 \cdot x \cdot y$$

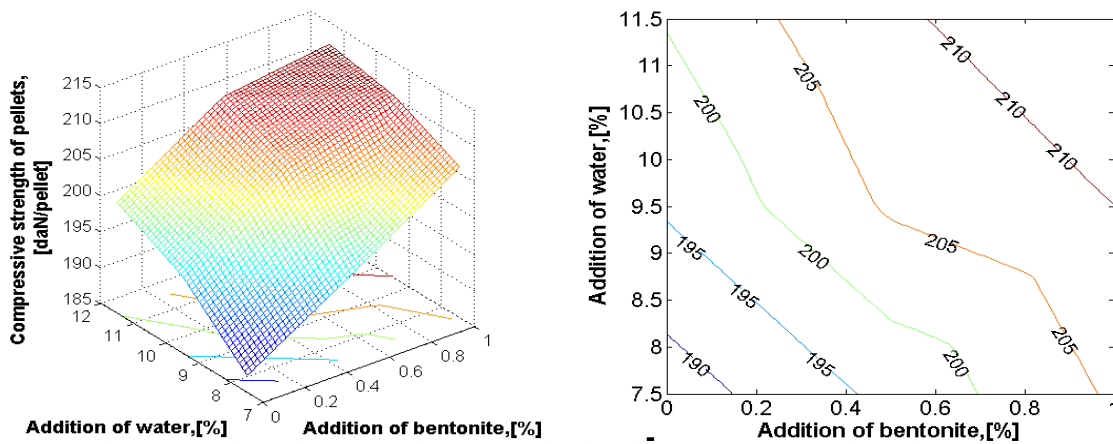


Fig.6. Variation of compressive strength of pellets to a concentration of 6% dolomite
 (x- addition of bentonite [%], y- addition of water [%],
 z- compressive strength of pellets, [daN/ pellet])

Analysing these correlations, we could establish the optimum domains for the flux, bentonite and water additions, in order to obtain higher pellet compression resistance values in case of flux addition.

4. CONCLUSIONS

Based on the experiments, on the results obtained from data processing and on the technical analysis of these data, the following conclusions resulted, in a nutshell:

- ❖ the two types of ferrous wastes (steel plant dust and red mud), both resulted from metallurgical processes, can be processed through pelleting. This means they can be used in the iron & steel industry;
- ❖ it is advisable to add 1% bentonite and 10-11% water, the upper limit corresponding to the higher limit of the added flux;
- ❖ by processing these wastes and transforming them in pellets fit to be used as raw or auxiliary materials in the iron & steel industry, the areas currently covered by them can be given back to nature, contributing in this way to the greening of the environment.

BIBLIOGRAPHY

- [1.] Project nr.31-098/2007 with title Prevention and fighting pollution in the steelmaking, energetic and mining industrial areas through the recycling of small-size and powdery wastes, Program 4 "Parteneriate in domeniul prioritare" 2007-2013.
- [2.] Heput Teodor, Constantin Nicolae, Socalici Ana, Ardelean Marius, Ardelean Erika, Researchs regarding recycling of small-size and powdery ferrous wastes existing in Hunedoara area, Symposium Generation, prevention and processing of pollutant emissions in industrial environment, Bucuresti, 12-13 iunie 2009.
- [3.] Ardelean Erika, Ardelean Marius, Socalici Ana, Heput Teodor, Josan Ana, Researches in laboratory phases regarding to capitalization of ferrous pulverous waste in pellets, International Conference of Metallurgy and Materials Science, Bucuresti, 2008.
- [4.] Heput Teodor, Socalici Ana, Ardelean Erika, Ardelean Marius, Environment ecological process in Hunedoara area through reinsertion in economic circuit of scrap and pulverous waste, Annals of the Faculty of Engineering Hunedoara - Journal of Engineering, VII(3), pp. 293-298, 2009





MACRO-MICRO-NANO COMPOSITE MATERIALS

¹⁻³. POLITEHNICA UNIVERSITY OF BUCHAREST, ROMANIA

⁴. TECHNICAL UNIVERSITY OF CLUJ NAPOCA, ROMANIA

ABSTRACT:

Metal or ceramic composites with reinforced metal or ceramic materials consist the future for material class. The paper proposes to present the results and the conclusions of a few researches in this field.

KEYWORDS:

composite, nano-composite, metallic materials

1. INTRODUCTION

Mixture of several components, whose properties complement each other, resulting in a material with properties superior to those specific to each component part, defines the composite material.

Delineate the difficulties arising in composite materials based on the idea (often used as an objection) that, practically, almost any material is a composite material are extremely rare because no impurities, no defects, alloying elements or not impregnated, coated, treated superficially covered. The distinction is harder to do if their material is taken into account the atomic and molecular scale.

Depending on the structure of materials can be classified as :

- a) crystalline materials:
 - ❖ polycrystalline (ferrous and nonferrous alloys);
 - ❖ crystal (metals, oxides, carbides, nitrides, semiconductor and optoelectronics)
 - ❖ Microcrystalline (alloys subjected to heat treatment such as hardening);
- b) semicrystalline (polymer);
- c) amorphous and glassy materials (metallic and nonmetallic);
- d) composite materials:
 - ❖ Each component dispersed;
 - ❖ Pressed powder aggregate;
 - ❖ Associated material, obtained by surface coating with metallic or nonmetallic substances;
 - ❖ Layered (obtained by assembling successive or simultaneous).

The superiority of composite materials compared to conventional materials, resulting in Figure 1.1, which is the ratio of tensile strength and density with temperature.

As shown, metal matrix composites are superior to conventional ones, but with lower properties of ceramic composites.

Resistance-temperature composite materials, corrosion or oxidation is determined primarily by the nature of the matrix. In general, the matrix is deformable composite material, having a lower strength than the composite material. Matrix choice is based on the purpose and the possibility of producing composites. Components operating at high temperatures should not occur expansion differences between the matrix and dispersed component (if metal or alloy cermet). In case of major mechanical stress, modulus reinforcement material must be greater than the matrix material to provide load transfer between components. A very strong adhesion between the composite constituents favor this transfer, leading to increased fragility.

Concerns about the world in terms of technology, have led to technologies shaping next generation of ceramic-metal composite materials:

- ❖ by polyphasic sintering process (or cosinterizare) under load or no load;
- ❖ by impregnating the porous ceramic with molten metal mass;
- ❖ by deposit of very fine particles (nano) on various supports (metal, ceramic composite were even) by electrodeposition method, the adsorption, diffusion, thermochemical treatments, etc.. In-depth analysis of processes, it is found that any of the methods used to manufacture composite aggregates and other processes specific phenomena. The result is a composite manufacturing process engineer pluricomplex with specific physical, chemical, thermal, electrical.

In theory composites seem to be two basic models, namely, model Naidich Weyl respectively. Principle schemes for the two models are presented in figures 1.2 and 1.3. Due to the high polarizabilității of oxygen anions and their large size compared with metal cations, can be considered in accordance with Weyl's model that the surface oxide layer is a double-anion, figure 1.2.

In the absence of oxygen in the bath metal compound $Me^{2+}O^{2-}$ formation involves the deployment of a reaction:

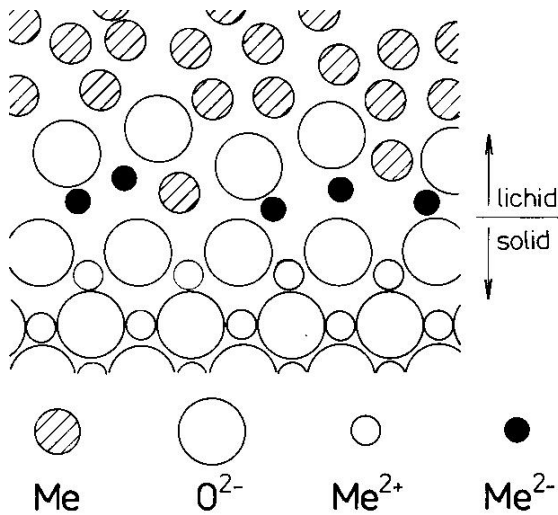
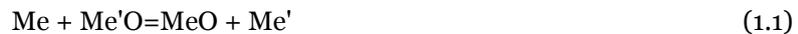


Fig. 1.3 Naidich's model for liquid metal-oxide ceramic interface

The increased metal affinity for oxygen, the solubility of the compound $Me^{2+}O^{2-}$ drops and activity at the interface increases. For sufficiently high oxygen content in the melt formed a continuous layer of metal oxide to the substrate surface. Adhesion energy is approximately equal to the energy required to destroy the ionic bonds between the two oxides.

Active metals forming strong links with ceramic materials, making them usable for metal or alloy elements. Customize these models for making ceramic-metal composite is presented in figures 1.4 and 1.5.

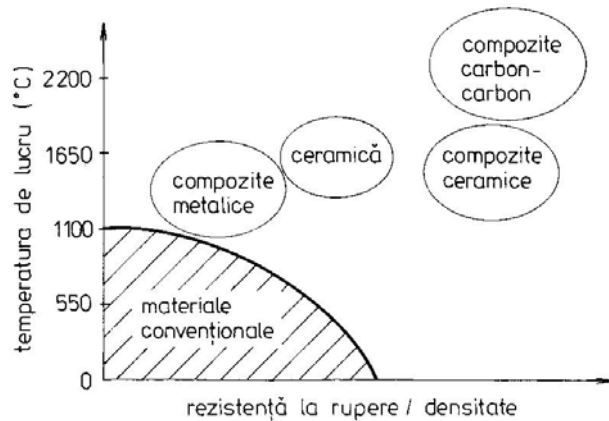


Fig. 1.1 The place they occupy between the composites materials resistant to high temperatures

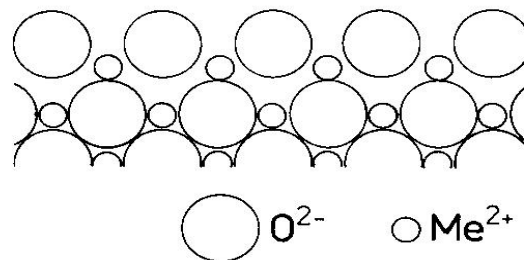


Fig. 1.2 The surface structure of the Weyl phase ceramic-metal oxides

Chemical interaction contribution to the adhesion energy increases with increased production of free energy of reaction (1.1), thus increasing the liquid metal affinity for oxygen. Naidich's model - Fig. 1.3, on the situation in which the metal bath is dissolved oxygen. It forms a compound with the metal surrounding $Me^{2+}O^{2-}$, which is adsorbed at the interface due to electrostatic attraction forces of Me^{2+} cation and the anion layer, the surface oxide paticle.

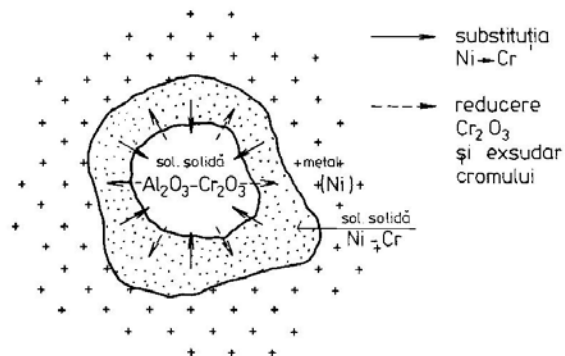


Fig. 1.4 The scheme links the formation mechanism of solid solution

Figure 1.4 is represented schematically by the solid solution formation of connections, Cr_2O_3 , reduction occurs, followed by the appearance of metallic chromium exudate, or substitution unoxidised metal chromium and chromium metal-forming solution (in this example nickel-chromium).

Another link between the formation mechanism involves the formation of a cermet components spinels intermediate phases, as in the case of cermet (Fe, Ni, Co) - Al_2O_3 .

Figure 1.5 is represented schematically by the phase spinels link formation mechanism.

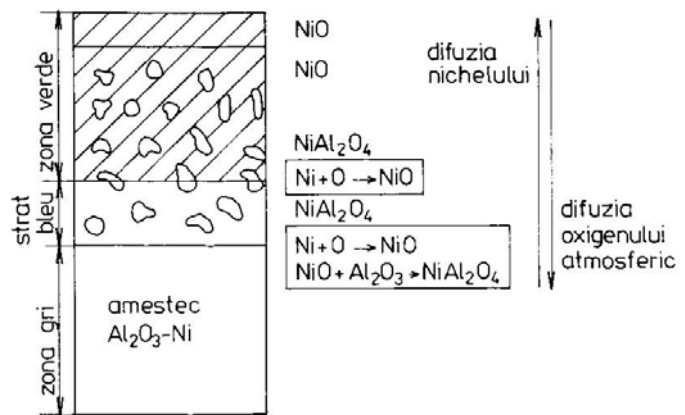


Fig. 1.5 Formation mechanism of the phase diagram link spinels

2. EXPERIMENTAL RESEARCH RESULTS

Distribution of aluminum in the ceramic composite made by impregnating aluminum can highlight thin section due to metal opacity, it appeared black on photomicrography.

Aluminum content throughout the ceramic wall thickness is not uniform. Entering the ceramic mass takes place only until a certain depth, and its amount decreases from the periphery inwards (fig. 1.6, 1.7, 1.8).

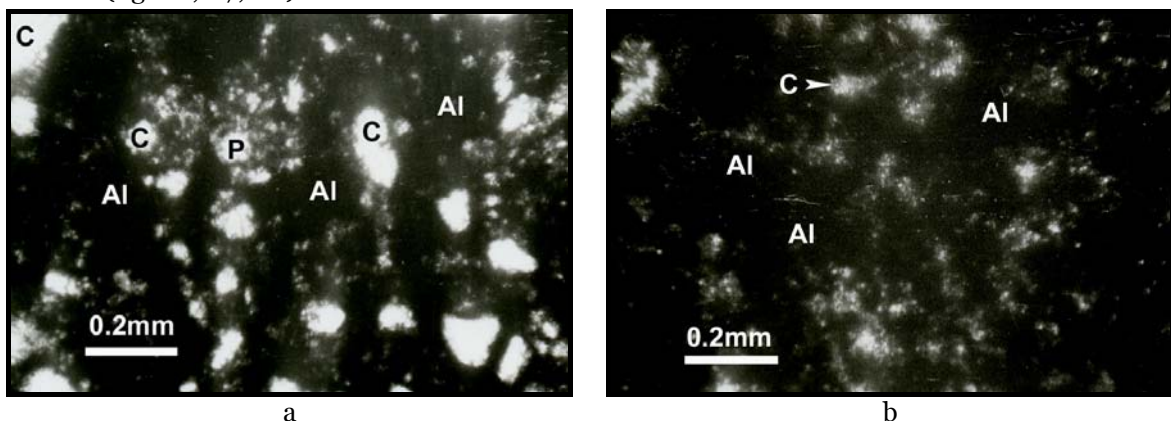


Fig. 1.6. Composite - ceramic-aluminum product R1 + Al (transmission polarizing microscopy). Microcrystalline structure consisting of an opaque metal mass (Al) ceramic relics occur \pm matrix composed of tiny pores (P) (see b). Most clastelor are represented by corundum (C). The texture is compact. a) The exterior of the composite - 1N; b) central area of the composite - 1N

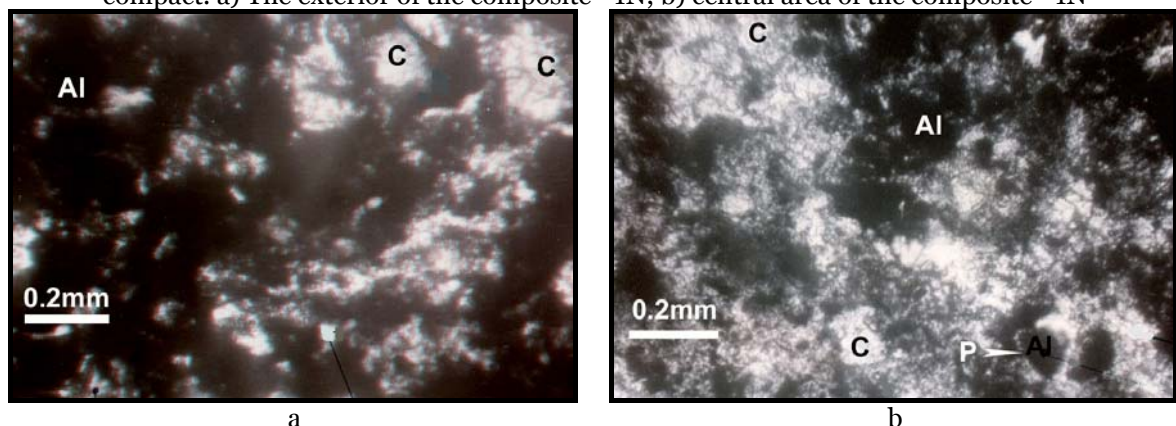


Fig. 1.7. Composite - ceramic-aluminum product R2 + Al (transmission polarizing microscopy). Microcrystalline structure consisting of an opaque metal mass (Al) occur relict crystals formed ceramic matrix \pm sometimes with pores (P) (see b). Most clastelor are represented by corundum (C). The texture is compact. a) The exterior of the composite - 1N; b) intermediate zone of the composite - 1N

Microscopically the mass is noted ceramic aluminum penetration through the pores open and total or partial substitution of mineral phases that contain silicon (mull, quartz, vitreous mass).

Marginal area of the composite structure is microcrystalline, consisting of an opaque mass, a uniform, which contains rare relics of corundum (Fig. 1.6a, 1.7a).

Composition, the interior wall mass content is remarkable decrease opaque (metal) and ceramic mass relics increase the structure and composition can be recognized (Fig. 1.6b, 1.7b, 1.8, and b).

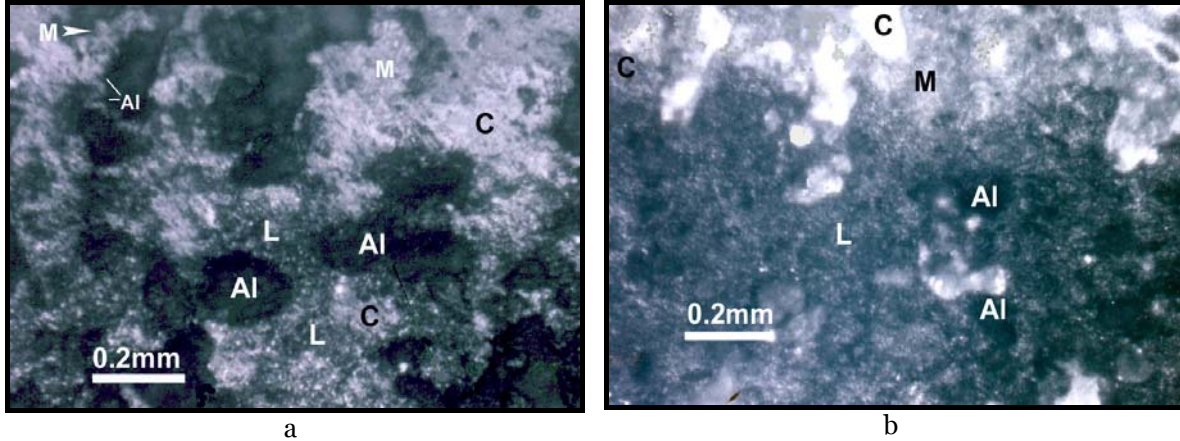


Fig. 1.8. Composite - ceramic-aluminum product R2 + Al (transmission polarizing microscopy).

Microcrystalline structure consisting of an opaque metal mass (Al) ceramic relics occur in aggregates of crystals formed and the matrix (L). Most clastelors are represented by corundum (C), reporting to mull (M). The texture is compact. a) The term close to the center. Observe the unit mull corrosion by aluminum (top left) - 1N; b) central area of the composite - 1N

Metallographic microscopy study of the structure allowed the predominantly metallic phases. Metallographic preparations were made from all sorts of evidence: impregnated with aluminum, nickel and copper. Microphotographs were conducted on samples and free of damage caused by chemical attack (Fig. 1.9 and 1.10)

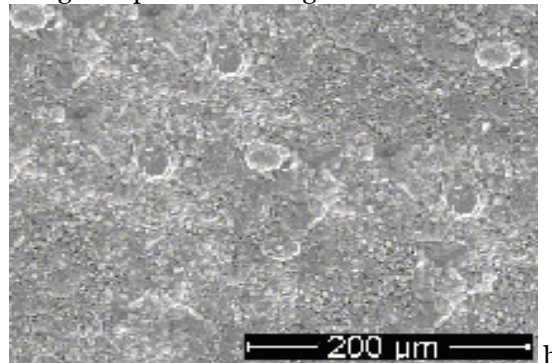
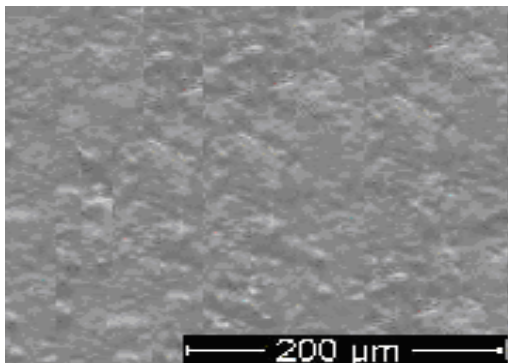


Fig. 1.9. Table R1 ceramic impregnated with copper zone of transition between the coated and impregnated; 250X



Fig. 1.10. Sample appeal $FeCl_3+HCl$ chemical mass-R1 ceramic impregnated with Cu, marginal zone; 250X

SEM microstructures surface for Cu- Mo coatings are presented in fig.1.11.



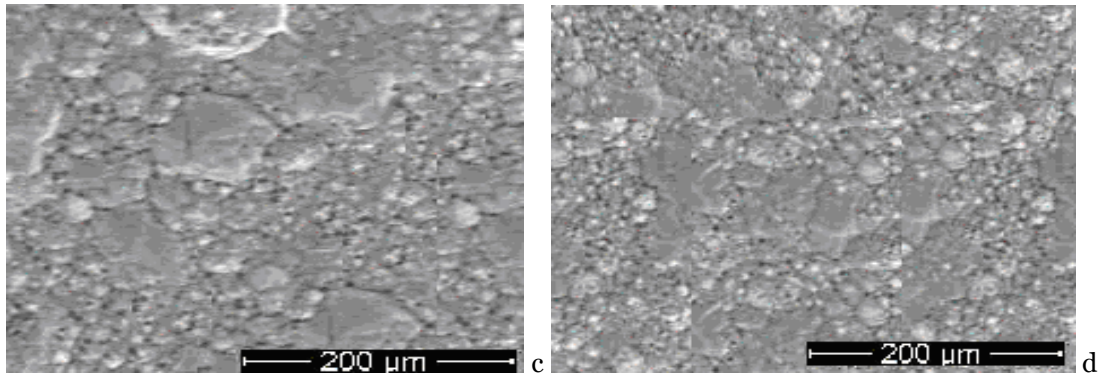


Fig. 1.11. SEM surface microstructures for Cu-Mo coatings size $3\mu\text{m}$, 90min, 500rpm, $i=1,5\text{ A/dm}^2$: a) pure b) Cu-Mo, 20g / L, c) Cu-Mo 40g / L, d) Cu-Mo, 60g / L, magnification x 500

3. CONCLUSIONS

From the figure for nano-composites made by electro-deposition, our analysis reveals their fine structure.

Metallographic microscopy study of the structure allowed the predominantly metallic phases highlighting the fact that metal has penetrated into the pores of the ceramic material.

REFERENCES

- [1.] Banea, Valentina, Surdeanu, T., Turos, Maria, Noi tendințe de utilizare a ceramicii tehnice în industria românească, *Lucrări ale Conferinței de Știința și Ingineria Materialelor CONSILOX – VII, Vol.I, 11-13 sep. 1996, p.116-122.*
- [2.] Iancau, V. *Materiale metalice compozite si tratamentele lor termice*, Ed. Dacia Cluj-Napoca, ISBN 973-35-07-96-2, 1999.
- [3.] Marginean L. *Studii și cercetări privitoare la realizarea unor compozite ceramo-metalice*. Teză de doctorat, Universitatea Tehnică din Cluj-Napoca, 2007.
- [4.] Pop Alin-Mihai. *Cercetări asupra tehnologiilor și materialelor moderne pentru confecționarea garniturilor de model*. Teză de doctorat, Universitatea TRANSILVANIA din Brașov , 2009.
- [5.] Fodor Liliana. *Cercetări privind realizarea unor depuneri de straturi superficiale compozite armate cu nanoparticule*. Teză de doctorat, Universitatea Tehnică din Cluj-Napoca, 2010.
- [6.] Orac Lucica. *Materiale compozite cu proprietăți speciale*. Universitatea „Dunărea de Jos” din Galați, România; Univesitatea de Arhitectură și Construcții Kiev, Ucraina, 2009.



¹Ana JOSAN

THE ANALYSIS OF CASTING DEFECTS RECORDED IN THE METALLURGICAL ENTERPRISES

¹ UNIVERSITY POLITEHNICA OF TIMISOARA, FACULTY OF ENGINEERING FROM HUNEDOARA, ROMANIA

ABSTRACT:

This paper presents the range of types and sizes of castings in a foundry, that The Foundry Criscior Brad. Are presented percentage, the types of defects recorded in technological practice (in elaboration, moulding, casting), and the possibilities of preventing their occurrence.

KEYWORDS:

Casting, defects, foundry, casting pieces

1. INTRODUCTION

The Foundry Crişcior Brad is a foundry small and medium-sized pieces. In this foundry, it casting a wide range of pieces, both in terms of material and dimensions of (fig.1).

Thus, in terms of material casted are obtained castings of:

- ❖ austenitic manganese steel
- ❖ carbon steel
- ❖ Low-alloy steel with manganese and chromium
- ❖ Grey iron
- ❖ Non-ferrous alloys.

Foundry typo-dimensional range includes castings such as presented in Table 1.

Table 1.

- swing hammers	- 4,5 kg
- wear plates	- 6,5 kg
- grills	- 7,3 ...9,7 kg
- Wheels Drive	- 25 kg
- Wheels shaft	- 30 kg
- cylinders	- 70 kg
- racks	- 100 kg
- roller support	- 18 kg
- Train bandages	- 270 kg
- pump housings	- 100...150 kg
- rotor	- 120 kg



Figure 1. Castings from Foundry Criscior Brad.

2. METHODOLOGY AND DISCUSSION

Performed the qualitative analysis of a batch of steel castings in Foundries Criscior Brad, be found that of 360 castings, 47 pcs. had casting defects (fig. 2).

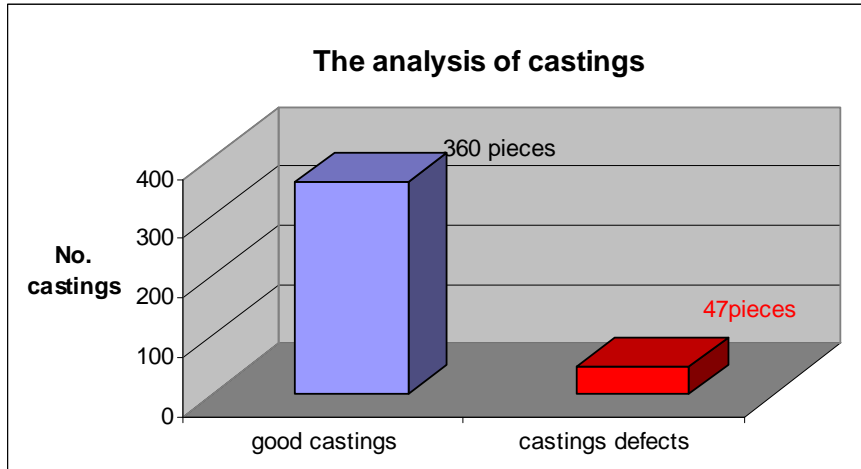


Figure 2. The analysis of castings.

Given the casting technology, and the statements made in industrial practice, can state that most common defects (of all defect castings) leading to the rejecting of them are [1, 2, 3]:

- inclusions (G 131) și adherences (D 221) rate of 7,74%; in fig. 3 are presented types of adherences appeared in steel casts;



Figure 3. Castings presenting non-metallic inclusions and adherences. Cavities, micro-cavities and pores (B 311) appeared at a rate of 3,59%;



Figure 4. Casting presenting micro-cavities and pores.

- fissures or cracks (C 221) rate of 1,67%;



Figure 5. Castings presenting fissures.

- Inadequate chemical composition - is a defect which, because standards stipulated in the chemical composition leads, definitely, to the rejecting of castings;
- Inadequate hardness – is a defect which, because the elaborating technology is not respected leads, definitely, to the rejecting of castings.

3. CONCLUSIONS

The share of defects registered in the period that were analyzed is shown in fig. 6

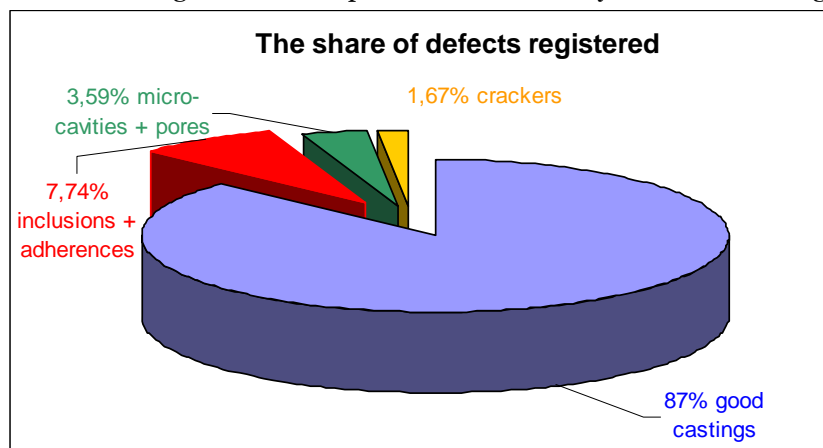


Figure 6. The share of defects registered in industrial practice.

Preventing the occurrence of failures presented in this paper, can be done only through strict compliance of their manufacturing technology, as well as by a good disciplined technology. Thus, for the avoidance of defects described above, should be taken following measures [3, 4]:

- ❖ strictly respecting their elaborating technology of the liquid alloy;
- ❖ correct Choosing choice of moulding technology;
- ❖ correct Choosing of moulding materials (sand, binders);
- ❖ correct execution of moulds;
- ❖ respecting the alloy casting parameters;
- ❖ respecting the thermal treatment diagrams applied castings;
- ❖ correct rapping of moulds.

REFERENCES

- [1.] Ștefănescu, C., Tehnologii de executare a pieselor prin turnare, Ed. Tehnică, București, 1981.
- [2.] Istrate, C., Toboc, P., Controlul de calitate și remanierea defectelor pieselor turnate, București, E.D.P., 1981.
- [3.] * * *, Atlas internațional al defectelor de turnare, Ed. Tehnică, București, 1977;
- [4.] Josan, A., Tehnologia formării și turnării aliajelor, Ed. Politehnica, Timișoara, 2002.





¹ Gabriela MIHUȚ, ² Erika POPA

ANALYSIS UPON INFLUENCE OF THE ALLOY ELEMENTS OVER THE MECHANICAL CHARACTERISTICS OF THE HIGH RESISTENT STEEL WITH HELP OF MATHEMATICAL MODELS

¹⁻² UNIVERSITY "POLITEHNICA" TIMIȘOARA, ENGINEERING FACULTY FROM HUNEDOARA, ROMANIA

ABSTRACT:

In this paper we suggest a mathematical shaping of the influence of the main alloy elements over the mechanical characteristics of steel type 15VMoCr14X. It has been noticed that the alloy elements increase the tensile strength, but differently: Cr, Mo and V increase the resistance of ferrite less than Si, Mn and Ni. Si, Mn and Mo very much decrease the resilience of ferrite, more than Ni and Cr do. The increase of the alloy content over 1.2% leads to a sudden fall of the resilience. The exception of this rule is nickel that both increases the resilience of ferrite and decreases the transition temperature.

KEYWORDS:

alloyed steels, tensile strength, mathematical shaping

1. INTRODUCTION

In the alloyed industrial steels, the alloy elements are to be found under many forms: solid solutions (dissolved in ferrite), chemical compounds (carbides) as alloyed cementite and special carbides, inter-metallic compounds with iron or with each other, sulfides and other non-metal inclusions, in free state, under the form of dispersed particles in the steel.

Many alloy elements, holding higher affinity with carbon than iron, dissolve in cementite, being capable of forming both alloyed cementite and special carbides. The elements situated at the left of iron in the periodical system of elements (Cr, Mn, Mo, V, etc.) form carbides. The elements that hold higher affinity with oxygen than iron form oxides. When processing steel, as a result of the oxidation process, the oxides Al_2O_3 , V_2O_5 and SiO_2 can be formed. The alloy elements that hold higher affinity with sulphur than iron form sulphides (MnS, etc.). The alloy elements increase the tensile strength, but differently: Cr, Mo and V increase the resistance of ferrite less than Si, Mn and Ni. Si, Mn and Mo very much decrease the resilience of ferrite, more than Ni and Cr do.

Chromium is an alpha favouring element that, when over 12%, determines the disappearance of the γ - α range. It dissolves both Fe_α and Fe_γ , forming especially simple and double carbides, when the carbon content is sufficient. The chromium-based carbides have a higher thermal stability and it is necessary for the austenitic transformation to be made at high temperatures, as well as a long maintenance so that hardening can be possible. The hypoeutectic chromium alloyed steel types have a reduced hardenability because they always contain a bigger quantity of proeutectic ferrite.

Chromium is characterized by high temper and by the fact that it forms stable carbides that give steel high resistance to wear and makes it suitable for steel cutting. The hardening of alloyed steel is accompanied by a certain loss of its resilience and elongation per unit length. For increasing the resilience and the elongation per unit without decreasing the temper too much, nickel is added in the chemical composition of steel.

Chromium determines an increase in the steel hardening, being the third most used element, after manganese and silicon, the most used chromium alloyed steel types being the perlitic ones. We can say that:

- ❖ a chromium content lower than 1% favours the steel hardening;
- ❖ a chromium content of 1-3% increases the resistance to hydrogen under pressure and favours the nitrification process;
- ❖ as the chromium content increases, the steel becomes more and more resistant to oxidation and corrosion;
- ❖ a chromium content higher than 30% determines steel to become infusible;
- ❖ chromium increases the temper and the resistance to wear but decreases the resilience (tenacity).

Molybdenum is an alpha-favouring element, just like chromium, but weaker than silicon. The austenite range of steel is restrained in the presence of molybdenum, becoming closed at concentrations higher than 2% Mo, raising the eutectic transformation temperature and moving it when the carbon content is lower. Dissolved in ferrite, molybdenum hardens it and increases its resistance to creep.

Molybdenum is twice more carbide-favouring than wolfram and its diffusion speed in austenite is four times higher. This property, that determines a better homogeneity when in hot condition, determines a better machinability and tenacity of medium-carbon steel and high-carbon steel but also a higher sensitivity to the thermal treatment and decarburization. Molybdenum very much lowers the martensitic transformation temperature (M_s), to 1.5% Mo, and decreases the softening tendency when tempering of the hardened steel types, even when the Mo content is only 0.2%.

When tempering the molybdenum alloyed steel types, it takes place a finely dispersed precipitation of some constituents similar to carbides that cancel the tempering brittleness effect, the steel types with 0.5% Mo content not having this effect anymore. Usually, molybdenum is used as an alloy element along with other elements, at processing the alloyed steel types.

2. THE RESULTS OF THE EXPERIMENTS

The chemical composition of type 15VMoCr14X steel is shown in Table no.1 and the requested values of the mechanical characteristics, compared to those obtained as a result of laboratory tests, are shown in Table no. 2.

Table 1

Chemical composition, %	C	Si	Mn	P	S	Cr	Mo	V	Cu	Ni
Requested	0.12- 0.18	Max. 0.20	0.8- 1.10	Max. 0.02	Max. 0.015	1.25- 1.50	0.80-1.00	0.20-0.30	Max. 0.16	Max. 0.30
Obtained	0.18	0.09	0.86	0.006	0.015	1.50	0.92	0.30	Max. 0.16	-

Table 2

Mechanical characteristics	$R_{p0.2}$ N/mm ²	R_m N/mm ²	A_5 %	WU_5 J	KCU_5 J/cm ²	$R_1 \cdot 10^{-7}$ N/mm ²
Requested	930	1080-1280	10	39	80	500
Longitudinally	1153-1170	1240-1238	17.5-15	54.8-55.8	140-152	550
Transversally	1148-1152	1230-1240	15.75-17.5	47.1-48.1	72-50	510

For the statistical and mathematical analysis, there were used 50 industrial batches.

The average values and the average square aberration of the variables are:

C	0.16385	0.022374
Cr	1.4554	0.076195
Mo	0.86115	0.014365
R_m	1173.1	57.189

Next, there are shown the results of the multidimensional processing of experimental data. For that purpose, we searched for a method of moulding the dependent variables depending on the independent variables x, y, z :

$$u = c_1 \cdot x^2 + c_2 \cdot y^2 + c_3 \cdot z^2 + c_4 \cdot x \cdot y + c_5 \cdot y \cdot z + c_6 \cdot z \cdot x + c_7 \cdot x + c_8 \cdot y + c_9 \cdot z + c_{10} \quad (1)$$

The optimal form of moulding, studied on a sample of 50 batches is given by the equations:

$$R_m = -1.73e + 004 \cdot C - 4511 \cdot Cr^2 - 4.07e + 004 \cdot Mo^2 + 1.078e + 004 \cdot C \cdot Cr + 2.113e + 004 \cdot Cr \cdot Mo - 4.668e + 004 \cdot Mo \cdot C + 3.063e + 004 \cdot C - 7307 \cdot Cr + 4.691e + 004 \cdot Mo - 1.582e + 004 \quad (2)$$

where the correlation coefficient is: $r = 0.75898492451823$ (3)

and the aberration from the regression surface is: $s = 37.23642463369599$ (4)

This surface from the four dimensional space allows a maximum point having the following co-ordinates:

$$C = 0.2592; Cr = 1.277; Mo = 0.7591; R_m = 1281 \quad (5)$$

3. CONCLUSIONS

The behaviour of these hypersurfaces in the vicinity of the point where three independent variables take their average value can be studied only tabular (for example, table no.3), by attributing values to the independent variables on spheres concentric to the studied point. Because this surface cannot be represented in the three-dimensional space, the independent variables were successively replaced with their average values.

Table 3

No.	Chemical composition [%]			The tensile strength Rm, [N/mm ²]
	Cr	Mo	C	
1.	1.51	0.86	0.14	1160
2.	1.48	0.87	0.15	1235
3.	1.48	0.88	0.16	1203
4.	1.48	0.86	0.17	1204
5.	1.35	0.86	0.18	1200

This is how the following equations were obtained.

$$Rm_{Cmed} = -4511 \cdot Cr^2 - 4.07e + 004 \cdot Mo^2 + 2.113e + 004 \cdot Cr \cdot Mo - 554 \cdot Cr + 3.926e + 004 \cdot Mo - 1.127e + 004 \quad (6)$$

$$Rm_{Crmed} = -4.07e + 004 \cdot Mo^2 - 1.73e + 004 \cdot C^2 - 4.668e + 004 \cdot Mo \cdot C + 7.765e + 004 \cdot Mo + 4.632e + 004 \cdot C - 3.601e + 004 \quad (7)$$

$$Rm_{Momed} = -1.73e + 004 \cdot C^2 - 4511 \cdot Cr^2 + 1.078e + 004 \cdot C \cdot Cr - 9573 \cdot C + 1.089e + 004 \cdot Cr - 5614 \quad (8)$$

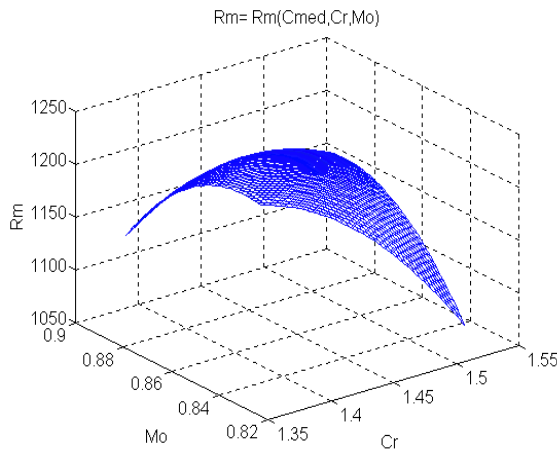


Figure 1. The surface
 $Rm = Rm(C_{med}, Cr, Mo)$

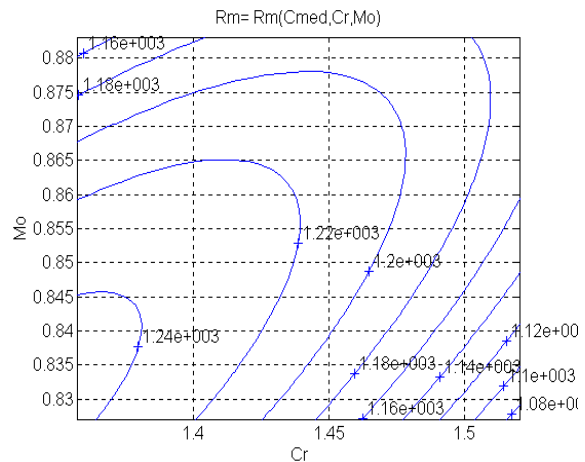


Figure 2. The level curves of distribution
 $Rm = Rm(C_{med}, Cr, Mo)$

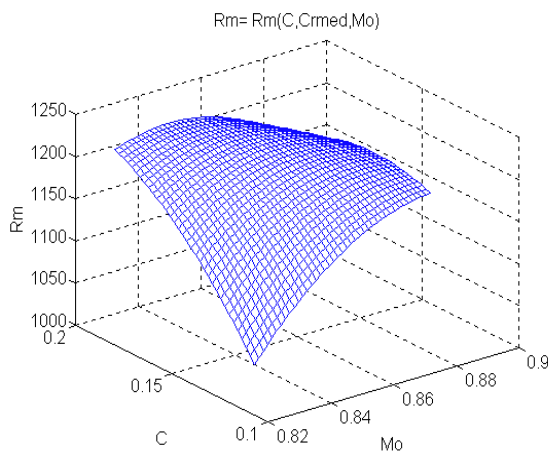


Figure 3. The surface
 $Rm = Rm(C, Cr_{med}, Mo)$

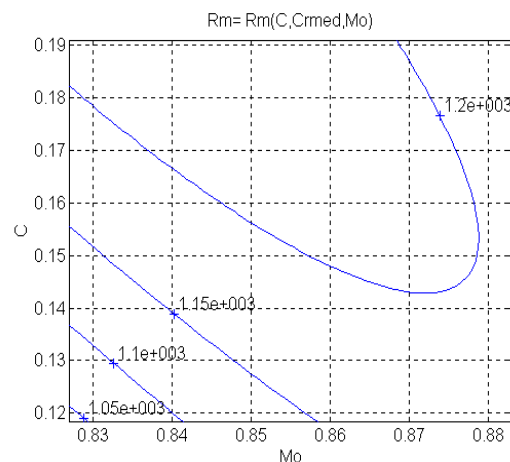


Figure 4. The level curves of distribution
 $Rm = Rm(C, Cr_{med}, Mo)$

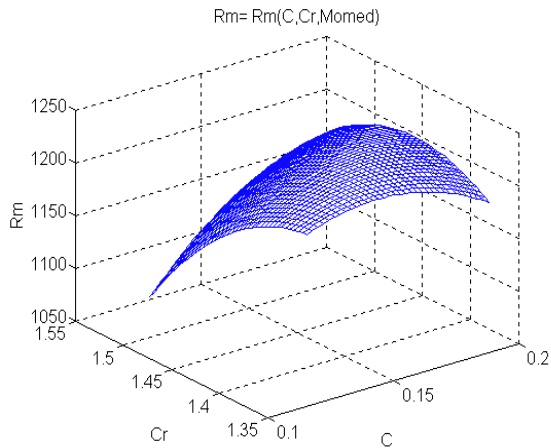


Figure 5. The surface $R_m = R_m(C, Cr, Mo_{med})$

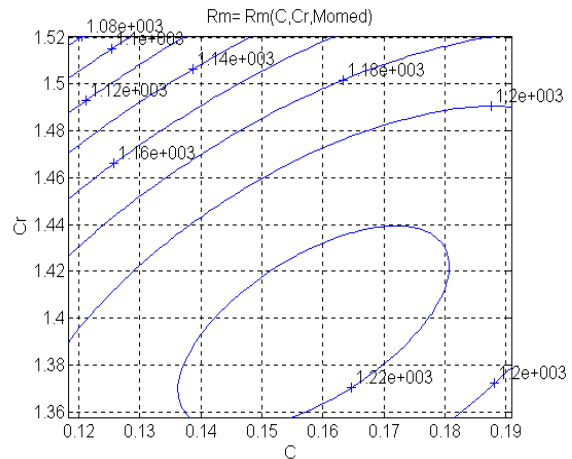


Figure 6. The level curves of distribution $R_m = R_m(C, Cr, Mo_{med})$

These surfaces, belonging to the three-dimensional space, can be represented and, therefore, interpreted by technologists. The surfaces are represented in fig. 1, 3 and 5. For a more correct quantitative analysis, in fig. 2, 4 and 6, there were represented the corresponding level lines, resulting the following conclusions: in the case of $C = C_{med}$, R_m allows a maximum for $Mo = 0.86\%$ and $Cr = 1.5\%$, and minimum values for $Mo = 0.84\%$ and a maximum Cr ; in the case of $Cr = Cr_{med}$, a maximum can be noticed in the area where $Mo = 0.84\%$ and $C = 0.14\%$; when $Mo = Mo_{med}$, there can be noticed a maximum of R_m for $Cr = 1.47\%$ and C is maximum, the minimum value being reached when Cr is maximum and $C = 0.13\%$.

Knowing these level curves allows the correlation of the values of the two independent variables so that R_m be obtained in between the requested limits.

REFERENCES

- [1.] Taloy - Optimizarea proceselor metalurgice, E.D.P. București, 1982.
- [2.] Maksay, Șt. - Matematici speciale, Editura „Politehnica” Timișoara, 2001.
- [3.] Vacu, S., ș.a. - Elaborarea oțelurilor aliate, vol.I, E.T. București, 1980





¹ Lucia VÎLCEANU

THE INFLUENCE OF THE LOCAL COMPRESSION EFFECT ABOUT THE WORKING LIFE OF THE COMPONENT WIRES IN A WIRE-ROPE

¹ FACULTY OF ENGINEERING HUNEDOARA, ROMANIA

ABSTRACT:

Steel ropes are important elements for the functioning of the machineries and of the equipment for transportation: mineral-drawing installations, boring plants, cranes, elevators, excavators, funiculars. Examining the wires of an out-of work steel rope, they noticed that the local compression stress in between the wires had such high values that it produced an impression on the wire in the contact area. The contact stress appears between the wires of the same rope strand, of two adjacent rope strands and between the wires and the rope take-up roller.

The paper shows the research regarding the induced and deforming stress at the moment of contact between wires and the traction cable take-up roller. The results will be used to calculate the fatigue crack propagation and to estimate the steel rope working life.

KEYWORDS:

contact pressure, working life, finite element method, stress-strain state, numerical analysis

1. INTRODUCTION

The wire ropes' durability, equated with the service life of the wire ropes, is determined to some extent by their appropriate choice and their rational exploitation. Using the best types of steel ropes, in different industrial areas, finding better ways for improving their quality and their exploitation conditions, will lead to the increase of their durability, the safety of the exploitation and to the achieving of great savings for the industry. These savings may come from the reduction of the rope consumption, thus from the reduction of quality steel consumption and from the cutting of break times in production, necessary for replacement of used ropes. During operation we encounter a supervised behaviour of the ropes because terms for replacing used ropes are always followed and the quality of the wire components is periodically checked. Withdrawing the rope from exploitation is operated when one or more of the following conditions are fulfilled:

- ❖ ropes reaching their service life, evaluated in tones-kilometres or kilometres- time in connection with the weight per meter of cable.
- ❖ reaching a certain number of broken wires per cable pace.
- ❖ the decrease of the safety coefficient of the cable at a certain value, the decrease of the real laceration force of the cable and diminishing of the number of bents until the breaking of the wires settles at the regular control testing. If during one of these current tests 25% of the wire components do not fit the standards, the cable is quashed.
- ❖ if during a macroscopic examination the deterioration of a strand is found, the breaking of the wires on a certain section is accelerating or an accentuated wear is found in one of its areas due to rust and corrosion.

During the examination of the wires that make up an out of order cable, evidence was found that the request of local compression between wires had such high values that a print appeared on the wire on the contact area. Contact requests appear among wires of the same strand, among wires belonging to bordered strands and among wires and the cable winding reel. The parameters involved in the evaluation of the voltage state and wear, belonging to wires in contact, may refer to: the geometry of contact elements, the statistic and tribology of the contact, mechanical

characteristics of the materials, operating factors. These parameters possess a simultaneously influence during contact, conditioning and influencing each other, which leads to a mingling of the result of their action.

2. METHODOLOGY

The estimation of the real stresses in the cross-section of the wire rope is very difficult because the wires are placed under different angles reported to the axes. There are subjected not only to traction, but also to bending and torsion. So, the state of stress in the wires is very sophisticated after the wiring manufacturing process. According to the hypothesis which fundament the strength calculus, the mechanical loads in the wires of a wire rope are considered as statically loads type Saint-Venant: traction, bending and secondary bending because of the support of a wire to other two adjacent wires, respectively the static contact loading type Hertz or Steuermann. *The classical contact theory between elastic bodies proposed by Hertz* (Fig.1), which did not take into account the non-linear aspects of every contact problem, is comparatively presented with *Steuermann's and Panton's theories* for the contact under a straight common line, typically for the contact between an external and an internal cylinder surfaces.

A comparison between the results obtained by Steuermann and Hertz (Fig.2) leads to the following conclusion: when the ratio $\frac{q}{E(R_2 - R_1)}$ increase, the difference between the results (according to the above mentioned theories) also increases. Anyway, there is a relative good agreement between the results for contact angles less than 20°.

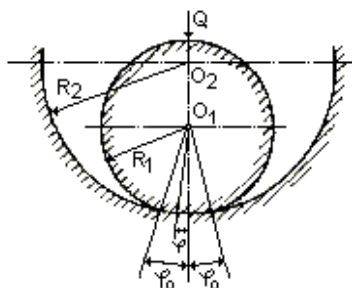


Fig.1. Contact between a cylinder and a cylinder cavity

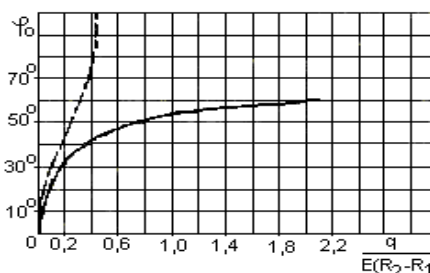


Fig.2. Comparison between Steuermann's and Hertz's results

For the particular case when the two cylinders are manufactured from the same material, E. Panton proposed the following approximate formula:

$$Q(\varphi) = \frac{Q}{R_1 (\sin \varphi_0 \cos \varphi_0 + \varphi_0)} \cos \varphi \quad (1)$$

There is presented in Fig.3 the distribution $Q(\varphi)$ for three values of the contact angle: $\varphi_0 = 30^\circ$, 50° and 60° according to Panton's (non-continuous line) and Steuermann's theories (continuous line). It may be observed in Fig.3 that the results according to the above mentioned two theories are in a perfect agreement when increasing the contact angle φ_0 .

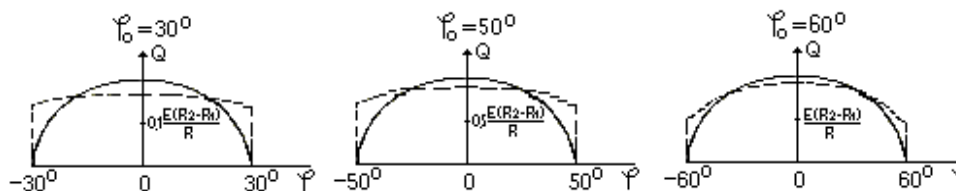


Fig.3. The distribution $Q(\varphi)$ according to Panton's (non-continuous line) and Steuermann's theories (continuous line)

The purpose of the *experimental research by photoelasticity* about the state of stress in the component wires of a wire rope consist in the estimation of the percentage deviations of the contact stress calculated values according with Hertz's, Panton's and Steuermann's theories in comparison with the real values of the stresses. This type of experimental research would ease the choice of the best relation depending on the size of the contact angle φ_0 . In terms of contact problems, the location of the maximum tangential stresses is associated with the initiation and propagation points of several cracks, which require the accurately determining of the voltage spectrum in the immediate vicinity of the contact area.

In view of the photoelastic analysis were made two discs having the diameters of 15 and 20 mm and concave surfaces with beams of 26; 20,1 and 15,15 mm. They were made out of optical

active and translucent materials. For the achieving of the isochrones photos an installation with two polaroids was used. The polaroids consisted of \varnothing 150 mm of monochromatic light produced by a bulb with downloads of sodium vapours. This installation is part of the endowment of The Laboratory of Strength of Materials from the Mechanical Engineering Faculty belonging to Polytechnic University of Timisoara (Fig.4).

A specimen was made for the calibration of the photoelastic material. This specimen was tested during a pure bending thus determining the photoelastic constant of the material $\sigma_0 = 2,65$ MPa, with a 6 mm thickness. During the tests the goal was not to induce contact requests which could lead to plastically strains. The tests ensured the reproductively of the results, reproductively checked by the lack of residual stress state in the parts after the download, a fact easy found in polarized light.



Fig. 4. The isochrones photos for $R_1/R_2 = 0,58$ at $q=74,21$ N/mm, the higher level of isochrone $n=8$ φ_0

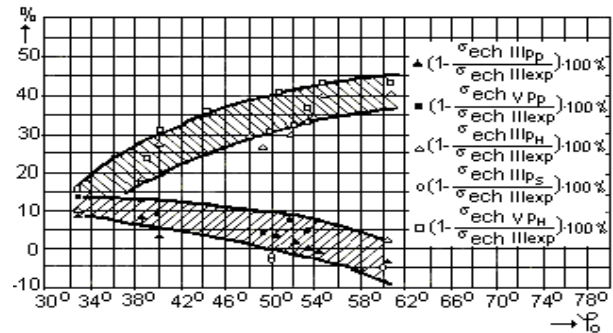


Fig.5. The deviation variation of theoretical results from the experimental tests depending on the contact angle for two contacts $R_1/R_2 = 0,58$ and $R_1/R_2 = 0,75$

The Fig.5 diagram represents the deviation variation of results from the experimental ones depending on the contact angle φ_0 for the two contacts $R_1/R_2 = 0,58$ and $R_1/R_2 = 0,75$ where Hertz's hypothesis is not valid.

From this representation results the fact that the values σ_{ech} calculated after Panton and Steuermann are grouped in an area of deviation of (+10%...-5%), while when using Hertz's formulas they leads to deviations of approximately (+15%) at $\varphi_0 = 33^\circ$ up to approximately (+40%) at $\varphi_0 = 60,5^\circ$.

This percentage error of the results decreases with the rising of the application and with the rising of the maximum order of the isochrones, up to a stresses value of approximately 10 MPa. This leads to an increase due to the value of variation of the elasticity modulus reaching an error of 10% at 20 MPa. This error is introduced by the asymmetry request wich couldn't be completely eradicated. The error is compensated by the average between the readings of the isochrone's order from the two edges of the contact area.

The *fatigue alternant loading* is the main reason of the degradation of the wire ropes. The results of the compression contact fatigue tests, performed on the Nădășan-Boleanțu testing machine placed in the Laboratory of Strength of Materials from the Mechanical Engineering Faculty, are plotted in a diagram (Fig.6) which expresses the dependence between the life-time of a wire with a 1 mm diameter versus the compression contact stress.

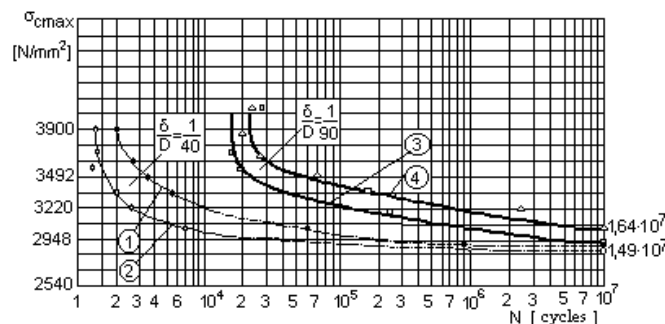


Fig.6. The results of wires fatigue testing on NB machine

A statistical analysis according to the log-normal distribution law has been performed.

The value of the life-time of the wires belonging to a traction wire rope obtained after the linearization of the distribution curve is in a perfect agreement with the life-times indicated in the special references when the wire rope considered as an element with a restricted life-time because of the typical working conditions.

The *finite element numerical analysis about the local compression effect* is the solution for the contact problem between two wires with different or same diameters in contact. Also the contact problem between an external and an internal cylinder shape bodies (Fig.7) has been analyzed by

using a hybrid technique considering the contact without friction for all the cases which have been presented above.

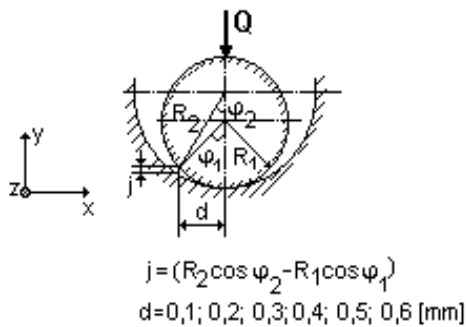


Fig. 7. The objective geometry

From the analysis of the graphical processing of the results we can reach the following conclusions:

- ❖ The equivalent von Mises stress σ_{VM} [N/mm²] has a maximum value in the center of the contact surface, decreasing to its extremities;
- ❖ The tangential stress τ_{xy} [N/mm²] is zero in the center of the contact surface, where the triaxial compression appears [1]. The maximum value of the tangential stress corresponds to the value of the half-breadth of the contact surface $b = 0,0545$ mm, decreasing to its extremities;
- ❖ The vertical movement is greatest possible in the middle of the contact surface, situation that can be visualized by representing the deforming state by bands of equal movement on the deformed position of the cylinder (Fig.9).

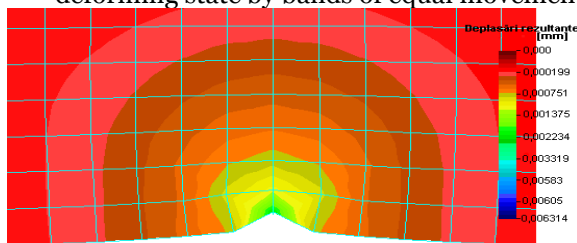


Fig. 9. The resultant displacements [mm] for the cylinder of radius $R_1 = 0,625$ mm, case of loading $Q = 45$ N

phenomenon because of the maximum σ_y stresses which are perpendicular on the contact area has been analyzed after the loading fatigue block (Fig.10) has been imposed ($\sigma_{y_{max}}$ - in function of the number of cycles). After the running on of the software, the cumulative degradation coefficient for every loading step and the total cumulative degradation coefficient have been performed.

During this program the fatigue limit curve (Fig.6-curve 1) for an alternative-symmetrical loading cycle of a non-torsion wire, bent on a segment lacking a channel and with the diameter of 40 mm, was used.

The calculus performs the link between state of stress in wires produced by the request of contact compression and of the wires' working life belonging to the steel wire ropes which are subjected to multiple and different requests encountered during the functioning of the operating wire ropes.

At first the meshing of two wires with same diameters in contact and the calculus model has been performed. After the running on of the software, all the components of stress and deformation tensors have been performed for 9 equal representation steps in function of the maximum and the minimum variation limits of stresses and deformations (Fig.8). Results are presented as special tables and diagrams about the stress and deformation fields. It can be observed that the state of stress and deformation is similar for every two adjacent wires in contact.

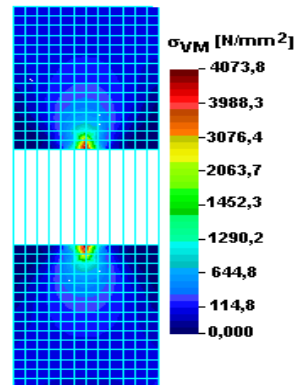


Fig. 8. The equivalent von Mises stress σ_{VM} [N/mm²] for the considered stress model, case of loading $Q = 45$ N

deforming state by bands of equal movement on the deformed position of the cylinder (Fig.9).

The analysis about the life-time of the component wires of a steel wire rope by finite element numerical analysis presents the opportunities to use dedicated software, which is typical for the analysis of the behavior of wires under variable loading as well for the life-time estimation. The finite element numerical analysis of the degradation of the wires because of an alternant loading has been performed for the contact between two wires with same diameters of 1,25 mm, for 9 loading cases. The fatigue

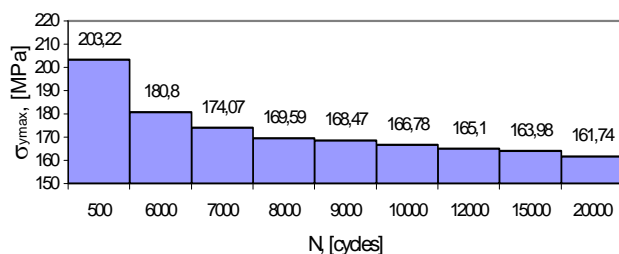


Fig.10. Loading fatigue block $\sigma_{y_{max}} - N$

3. CONCLUSIONS

The static processing of the results coming from the fatigue attempt along with the contact compression of wires on the NB testing machine, accepting a normal distribution of life-time, provided that the values of wire's life-time obtained after the lining of the distribution right are fitting in the range of accredited values by specialists in the market.

The paper also presents the numerical modeling with the finite elements of the contact request between a cylindrical surface and a concave one, achieved in order to visualize the state of displacements and stresses.

The finite elements numerical analysis of degradations which appear inside the steel wire ropes because they are subjected at variable loading was performed in order to obtain the cumulative degradation coefficient for every loading step.

REFERENCES

- [1.] Babeu, T. – The Basic Theory for Resistance of Materials, Mirton Publishing House, Timisoara, 1998
- [2.] Faur, N., Dumitru, I. – Finite differences and finite elements in resistance of materials, Mirton Publishing House, Timisoara, 1997
- [3.] Ghita, E. – Resistance and working life at solid bodies' contact, Mirton Publishing House, Timisoara, 2000
- [4.] Tudor, A. – The real contact of friction surfaces, Romanian Academy Publishing House, Bucharest, 1990
- [5.] Vilceanu, L. – Resistance and working life at steel wire ropes in contact, Mirton Publishing House, Timisoara, 2003





¹Sorina Gabriela ȘERBAN, ²Maria Laura STRUGARIU

DETERMINATION OF PARAMETERS INVOLVED IN TRANSFORMING THE IDEAL GAS, USING MICROSOFT ACCESS

¹⁻² UNIVERSITY POLITEHNICA OF TIMISOARA, FACULTY OF ENGINEERING FROM HUNEDOARA, ROMANIA

ABSTRACT:

A transformation is a sequence of states through which a thermodynamic system when its parameters vary from baseline values to those in the final state. All thermodynamic properties at a time system is the system state. State parameters are all measurable physical quantities that characterize the unique thermodynamic state of the system. A substance is characterized, as we know, the state variables: pressure, volume, temperature, etc.. At a certain amount of substance, these three variables are a well established interdependence of thermal equation of state.

To ease the study of gases have made some considerations that lead to a relatively simple model study. These so-called ideal gas, the molecules are considered material points, and the interaction forces between molecules are void. It is obvious that this case can not be met in practice, but the considerations made on this system can be extended with some corrections and within certain limits, the real gas.

The application is done using Microsoft Access and was made for students to be able to easily own knowledge about the transformations simple ideal gas of this gas. Students can calculate and make conclusions can be drawn, however this program is not meant to replace the teacher but to offer a tool to study in classes, the theory that parties are not very many. The menu is affordable, intuitive and helpful. For a better understanding of the application is structured in four parts.

KEYWORDS:

transformation isobar, izocoră transformation, isothermal transformation, the parameters of state, Microsoft Access

1. INTRODUCTION

Following the experiences with the constant volume gas thermometer was found that at very low pressures, tending to zero, all gases tend to behave the same way. Based on these considerations the notion of ideal gas.

Ideal gas is a homogeneous and isotropic gas whose molecules have their own volume and between them there is no interaction forces.

Ideal gas is a theoretical concept, it does not actually exist, but all gases tend to behave as the ideal gas (using the same law) when their pressure tends towards zero, as in this case, the volume of gas is very busy compared with the volume of the molecules (which becomes negligible), and greatly increase the distances between molecules and the forces of interaction between them also become negligible.

In 1661 Boyle Mariotte discovered in 1679 and experimentally verified and confirmed exactly that for an ideal gas in all possible states of an isothermal, the product of pressure and volume is constant, ie:

$$(p \cdot V)_{T=const} = const.$$

For any two states 1 and 2 of the same isotherm:

$$(p_1 \cdot V_1)_{T=const} = (p_2 \cdot V_2)_{T=const}.$$

In 1790 Charles found experimentally that if a given amount m of ideal gas occupies a constant volume when the pressure is proportional to the temperature, so their ratio is constant:

$$\left(\frac{P}{T}\right)_{V=const} = const$$

For any two states that occupy the same volume of gas:

$$\left(\frac{P_1}{T_1}\right)_{V=const} = \left(\frac{P_2}{T_2}\right)_{V=const} = const$$

In 1802 Gay-Lussac has shown that the volume of an ideal gas maintained at constant pressure varies linearly with temperature:

$$V = V_0 + V_0 \cdot \gamma \cdot (t - t_0)$$

where: $\gamma [1/^\circ C]$ = volumetric expansion coefficient of ideal gas;

$V_0 [m^3]$ = gas volume at the reference temperature t_0 .

$$\gamma = \frac{1}{273,15} \left[\frac{m^3}{m^3 \cdot ^\circ C} \right] \text{ or } \left[\frac{1}{^\circ C} \right]$$

For any two states 1 and 2 volume ratio is:

$$\left(\frac{V_1}{T_1}\right)_{p=const} = \left(\frac{V_2}{T_2}\right)_{p=const}$$

2. DESIGN AND IMPLEMENT APPLICATION

Data was stored in an Access database type, called ChimUniv. As an Access database type it includes all the items needed for the application: data tables, forms, query requests, reports, macros, modules.

Today there are applications that do not have a graphical interface through which to access the program options. Therefore, it was developed and implemented a main interface that allows accessing various options of the application, using the mouse and keyboard. The main interface has the following layout:



Fig.1. Main Menu

It is noted that there are several command buttons, labeled, to be used to select various options of the program. The main menu contains a summary of this application, and skills that they need to learn the student until the end of time.

For a better understanding of the application is structured in four parts, each with several components:

- ❖ Isothermal transformation: definition, graphical representation,
- ❖ Isobar transformation: definition, graphical representation,
- ❖ Transforming izocoră: definition, graphical representation,
- ❖ Ideal gas law applied problems.

Figure 2 is the transformation of the isotherm shape and includes a summary of Boyle-Mariotte law and is made in the same way as the other two forms (Fig.3 and Fig.4).

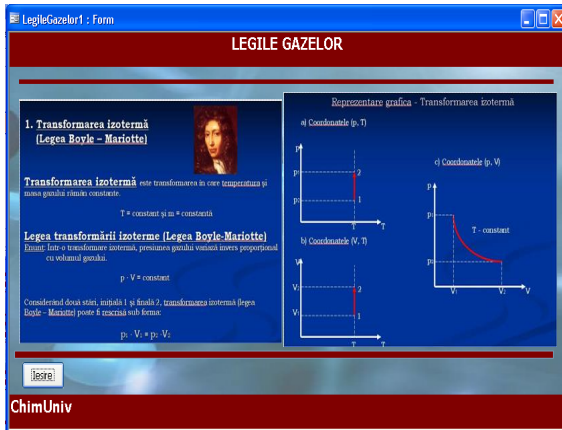


Fig.2. Isothermal transformation

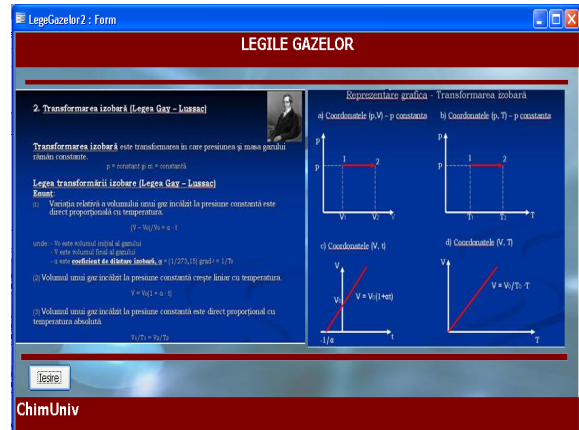


Fig.3. Transforming isobar

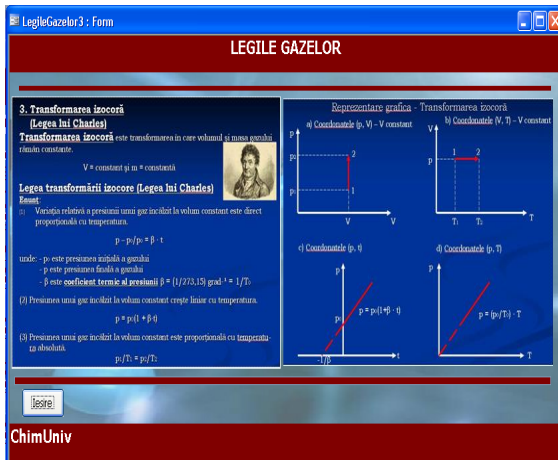


Fig.3. Transforming izocoră

Gas Laws form includes all three transformations, and moreover appears Van der Waals equation and the Clapeyron-Mendelev equation. By activating buttons , will open the forms that will present an example of application to each law separately. Clapeyron-Mendelev equation in the case is five examples of problems.

Each application / problem has boxes where the student will enter data in the problem statement will be executed transformations and the application will calculate what the problem is required. Each form has a pressing „Clear” button that will clear the boxes and other data can be entered and a button”to exit” out of the application.

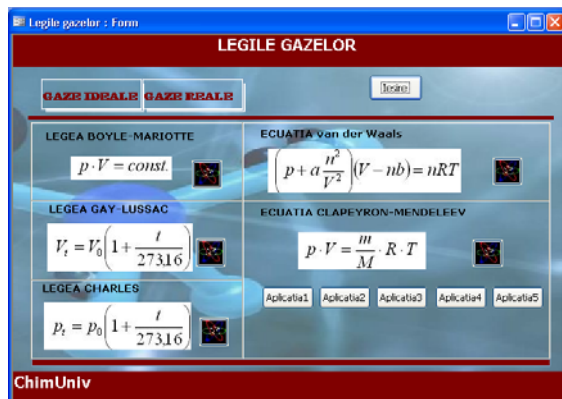


Fig.4. Forma_ Gas Laws

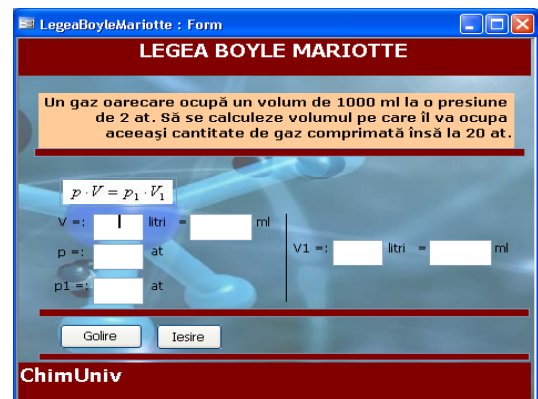


Fig.5. Application _ Boyle Mariotte Law

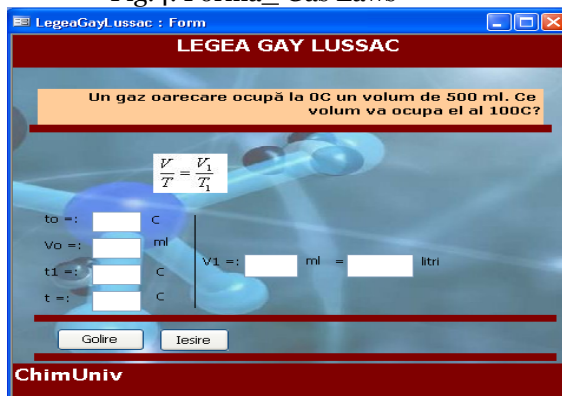


Fig.6. Application _ Gay Lussac Law

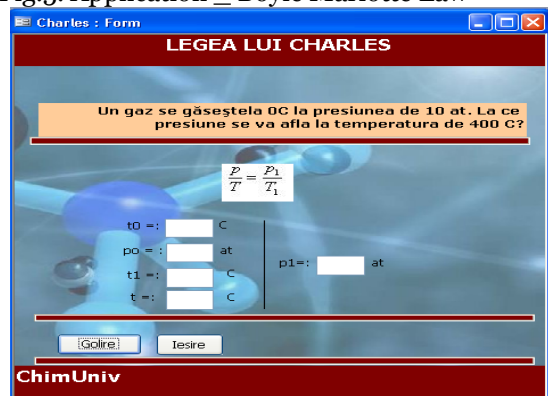


Fig.7. Application _ Charles Law

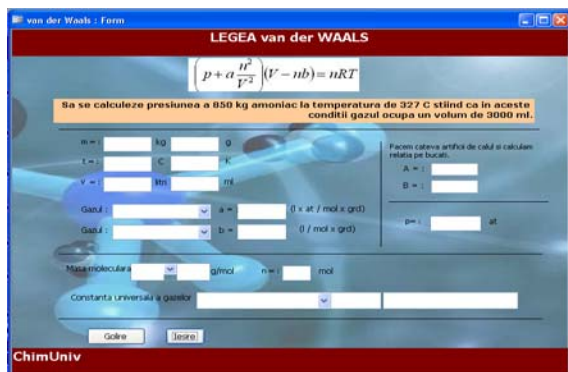


Fig.8. Application _ van der Waals Law

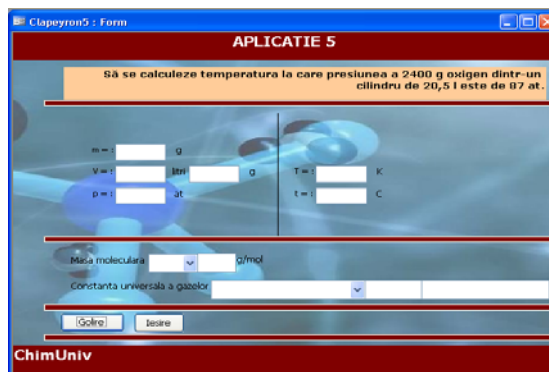


Fig.9. Application _ Mendeleev Clapeyron Equation

Submitted application can run on the following conditions: - the existence of a computing system, Pentium I 200 MHz at least 32 MRAM available - there is a Windows operating system and Office 2003 package.

It can be converted and Office 97, if this software is available.

Experimental data processing by computer is faster, more complete, attractive and can help increase motivation and interest of students to study Chemistry.

4. CONCLUSION

Feedback provided by participants (pupils, students), underlines the strong impact that the use of educational software can play in teaching and learning chemistry. Such applications are considered as an alternative to the real experiment and a means to improve understanding by learners of abstract concepts.

They may increase the motivation of students to learn and to engage their interest in making science topics. Clearly, the attractiveness is enhanced lessons, the teacher is the best choice in joining the virtual real experiment.

Using educational software will increase the competence and creativity, increasing the average educational attainment and higher to increase the knowledge base of students, and generally to increase the use of information technologies in various fields activity.

Development of educational software, with the pupils / students is one way to attract those who are less interested in Chemistry.

I must mention that this application is part of my doctoral thesis (still unfinished at this point), which includes a number of such applications developed with Microsoft Access and others.

ChimUniv system development aimed at creating an easy to use for both learners, but perhaps especially for teachers, given that a very large extent, success depends on the availability of this in a manner that Such educational programs more attractive. Feedback is always assured.

The point at which we started in implementing this system was that the information could greatly facilitate the study of chemistry in school and university, this is because, using the computer can accumulate knowledge in a more intuitive and more attractive.

Bibliography

- [1.] Eleonora Neacșu, Bazele termotehnicii, Litografia Institutului Politehnic „Traian Vuia”, Timișoara 1990
- [2.] Mădărășan, T, Bălan, M., Termodinamică tehnică – Editura Sincron, Cluj Napoca 1999.
- [3.] Atkins P.W., Trapp C.A., Exerciții și probleme rezolvate de chimie-fizică, Editura Tehnică, București 1997
- [4.] Florescu Vasile, Baze de date – fundamente teoretice și practice Editura Infomega, București 2002
- [5.] Eduard Koller, Monica Roșculeț, Programare în Access 97 ,Teora, București 2002
- [6.] Sorina Șerban, Referat Nr.3 - Stadiul actual și tendințe în cercetările privind sistemele de instruire asistată de calculator, Universitatea “Politehnica” Timișoara,2006



¹ Ana JOSAN, ² Vasile PUȚAN, ³ Sorin RAȚIU

THE OPTIMIZATION OF MANUFACTURING PROCESS OF A PART CAST STEEL FOR QUALITY ASSURANCE

¹⁻³. UNIVERSITY POLITEHNICA OF TIMISOARA, FACULTY OF ENGINEERING FROM HUNEDOARA, ROMANIA

ABSTRACT:

This paper presents a critical analysis of a part manufacturing technology low alloy steel castings T35Mn14. Technology deficiencies are presented and the measures in order to optimize the technology.

KEYWORDS:

Castings, defects, foundry, armors, molding

1. INTRODUCTION

Generally, the admitted rejectings registered for castings in a foundry should be within the range 4 ... 5%.

A particular case of castings obtained at The Foundry Criscior Brad and which particular aspects is the casting called *Armor* (fig. 1).

This armor is a steel casting T35Mn14 (low alloy steel castings) and represents the active part of a large spiral classifier ($\phi 2000 \times 6000$ mm), used in mining, the classifying of materials.

The spiral classifier has two propellers, and for each propeller is need 120 pcs. armor, so that an order of a classifier is needed the casting of 240 armors.

This piece is relatively small scale, i.e. 800 x 180 mm, , weighing 19 kg and low alloy cast steel castings, *T35M14*, whose chemical composition is as follows: C = 0,33...3,38%; Mn = 1,30...1,50%; Si = 0,30...0,50%; Cr = 0,50...0,70%; P = max 0,035%; S = max 0,035% [1].

2. METHODOLOGY AND DISCUSSION

Industrial practice has shown that, for casting analyzed, registered rejecting for the 120 armors is about 11%, respectively 13 rejecting castings (fig. 2, 3).

Following the critical analysis of the molding-casting technology of casting *Armor* and to decrease the percentage of rejecting registered in industrial practice, is necessary to optimize the manufacturing process of casting under study.

Thus, the current molding-casting technologies were identified these deficiencies:

- ❖ Use wooden models lead to material consumption lead to a higher consumption of material.
- ❖ High manual labour the processing of inner holes
- ❖ Appearance of the defect called *corner blister* (*B 122*) in the interior angles [3]
- ❖ High percentage of rejects due to improper use molding batch.

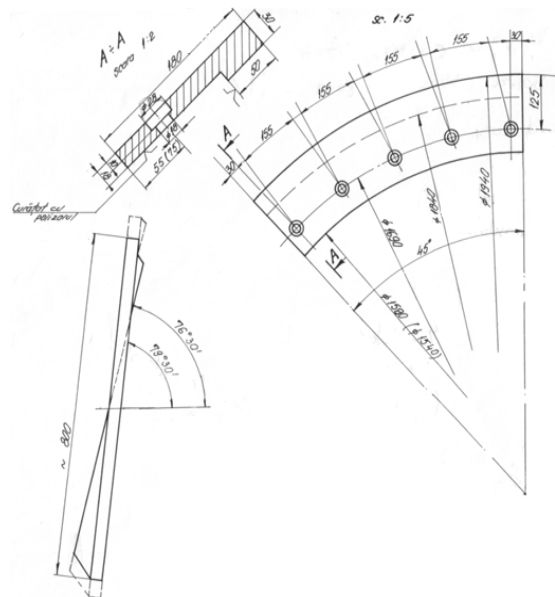


Figure 1. The armor - finished piece design

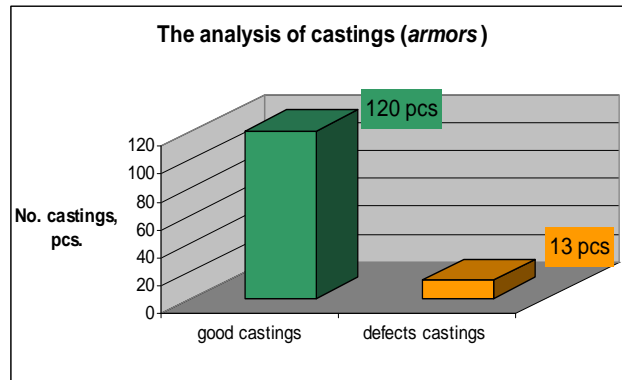


Figure 2. The analysis of castings

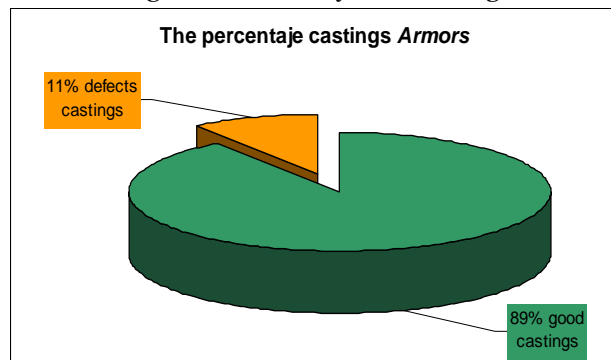


Figure 3. The share of defects registered at casting for casting studied



Figure 4. The metal model of casting *Armor*

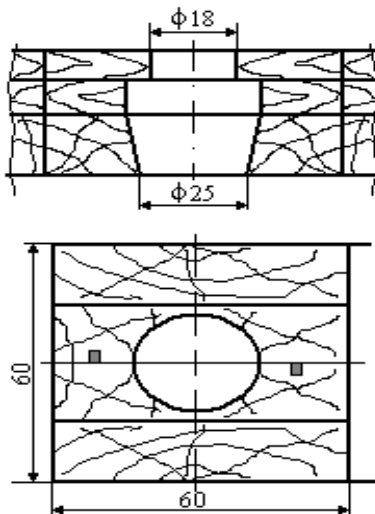


Figure 5. Core boxes.

In order to optimization the obtaining technology of casting studied (armored) shall take the following measures [2, 3, 4, 5, 6]:

1. replacing wooden model of a metal model (model is chosen for making aluminum alloy) (fig.4):
2. Obtaining molded cores in core boxes (Core boxes are made of wood and will produce five cores while). Core dimensions are made in core boxes are presented in Fig. 5, 6.



Figure 6. Mould cores made to obtain the holes of the casting *Armor* and fitting them into the mold.

- using the interior cooler and proper execution of the connections to the joint walls at right angles; the cooler for the casting studied (fig. 7), are made of same material as the alloy that is casting and has the form of a bar, with dimensions 20x10 mm.

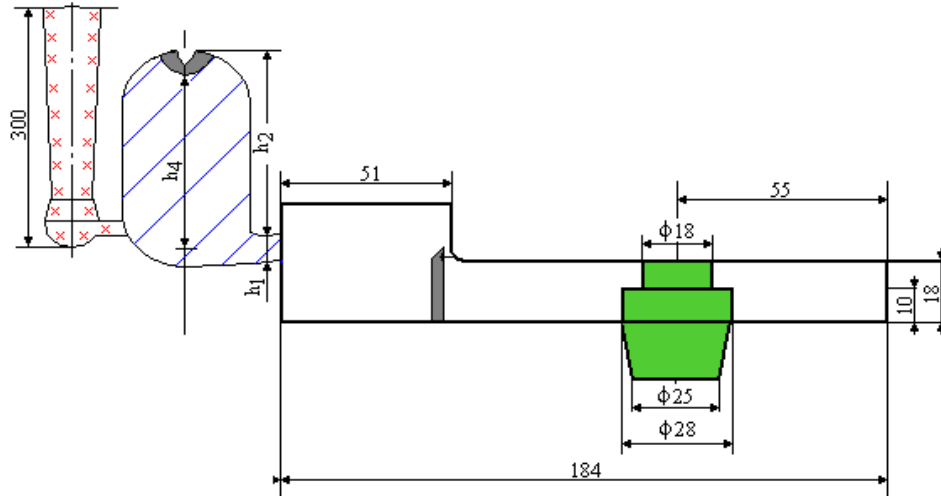


Figure 7. Apply the cooler interior and outline the connection radius.

- changing the moulding technology with two types of moulding batch (filling and model) and adoption of molding technology based with a mixture of sodium silicate.

The best method of prevention of the occurrence of defects registered at moulding is to ensure a high quality of moulding mixture for steel castings, because much of the defects is due to the way of realization of the mould.

Thus, by examining the 13 rejecting castings, results the following (fig. 8):

- ❖ 6 pcs. presented a large amount of nonmetallic inclusions and adherences, because inadequate quality of the moulding batch ;
- ❖ 4 pcs. presented a internal holes, both intercrystalline and intracrystalline (shrink pores, blisters, corner blisters, micro-shrinkages hole);
- ❖ 3 pcs. presented the cracks, crusts.

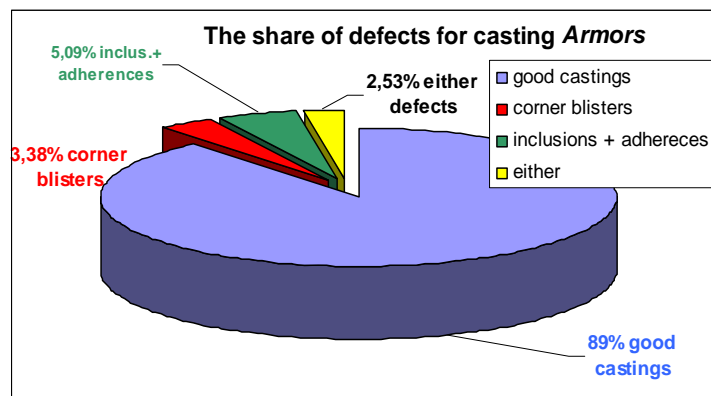


Figure 8. The share of defects registered for casting *Armor*.

3. CONCLUSIONS

The two mould parts, before assembly, are presented fig. 9 and the casting studied, mounted on spiral classifier is presented in figure fig. 10.



Figure 9. The mould parts (upper and lower), before assembly for casting.



Figure 10. The armor mounted on spiral classifier

Change the current moulding-casting technology a landmark analysis involves changing costs of obtaining its.

Thus:

- ❖ The total value of materials used in elaborating-moulding, a labour and a production price for the two technologies are presented in fig. 11.
- ❖ Even if the consumption of materials has increased significantly (12%), the following diagram is noted that, in improved technology, the price has dropped by approx. 7%

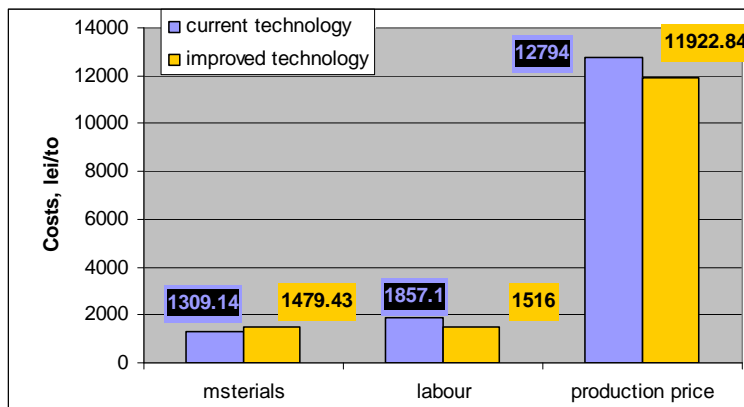


Figure 11.

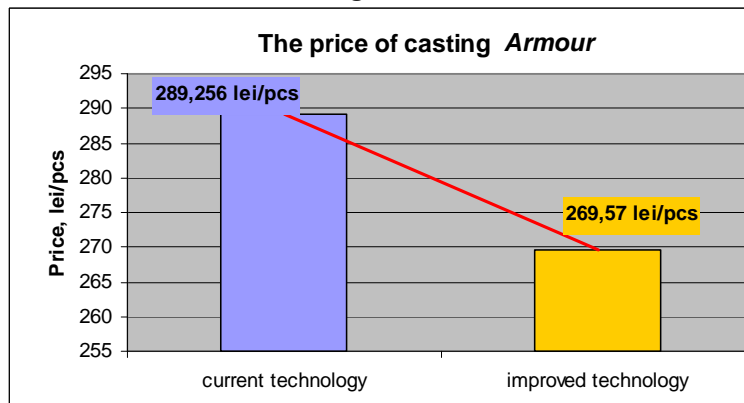


Figure 12.

- ❖ percentage of reject has decrease after the application of new technology with 5,5%
- ❖ the durability of the metal model is about 10 times higher than the wood, and dimensional accuracy is ensured when using metal models.

REFERENCES

- [1.] STAS 1773-76, Oțeluri slab aliate, turnate în piese.
- [2.] Ștefănescu, C., Tehnologii de executare a pieselor prin turnare, Ed. Tehnică, București, 1981
- [3.] * * * Atlas internațional al defectelor de turnare, Ed. Tehnică, București, 1977.
- [4.] Ștefănescu, Cl, Cosneanu, C., Sisteme de amestecuri de formare pentru turnătorii, București, Ed. Tehnică, 1989
- [5.] Josan, A., Tehnologia formării și turnării aliajelor, Ed. Politehnica, Timișoara, 2002.
- [6.] Socalici, A., Ardelean, E., Ardelean, M., Hepuț T., Josan, A. – Turnarea și solidificarea oțelului, Ed. Cerami, Iași, 2007

EXPERIMENTS AND RESULTS REGARDING THE USE OF FOAMED SLAGS AT THE STEEL ELABORATION IN ELECTRIC ARC FURNACES

¹⁻⁴UNIV. POLITEHNICA OF TIMISOARA, FACULTY OF ENGINEERING – HUNEDOARA, ROMANIA

ABSTRACT:

In paper is presented a synthesis of results obtained of authors regarding to reinsertion in the economic circuit of scrap and pulverous waste existing in Hunedoara area.

Through these capitalization of wastes in the iron and steel industry I done substantial economies in cost-price of final product, on aside, and but the other side are in progress an ecological process of environment Hunedoara area through give back of occupied surfaces with these waste to the natural frame.

KEYWORDS: Pulverous wastes, briquette, steel plant dust, agglomeration-blast furnace sludge, lime dust

1. INTRODUCTION

Use of steelworks dust from steel production or as a mechanical mixture or as micropellets (even pellets) as a slag foaming agent to believe that technology is the optimal solution for the use of these wastes. Simultaneous processing of waste containing iron powder and waste containing carbon powder to obtain a product suitable for use in various stages of technological flux led to the development process of obtaining a product called CARBOFER ®.

Data from literature and those obtained from their experiments, CARBOFER recommended as a substitute for the official site of slag foaming in electric arc furnaces, no influence chemical composition of steel and slag.

2. THE STUDY

In order to achieve phase laboratory experiments, we collected samples from several sections powdery waste of ArcelorMittal steel platform and storage ponds, being collected representative samples of the following types of waste: electric steelworks dust; - scale and dump the dross; the agglomeration, blast furnace dust (sludge agglomeration-blast); lime powder. Each waste sample was subjected to the operation of mixing (the homogenization was processed drum). Evaluating the quality of waste powder, determinations were made of physicochemical characteristics, namely: chemical composition and size. Experiments on the production site CARBOFER were conducted in the laboratory energy and raw materials base of the Faculty of Engineering of Hunedoara.

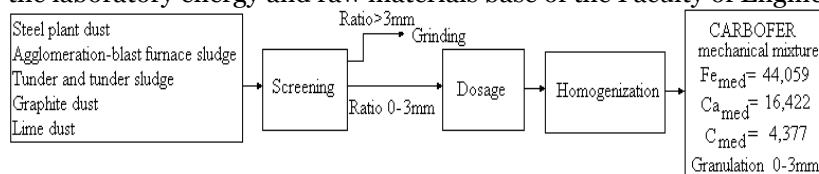


Fig.1. CARBOFER mechanical mixture flux

CARBOFER production powdery mixture flux, processing took place after the technological shown in Figure 1, Figure 2 is presented in such a recipe. I experienced a total of 10 recipes with chemical composition in Table 1. Also, for those recipes we determined size composition, presented in tabular and graphic tab.2 in fig.3



Fig.2. Example CARBOFER mechanical mixture

Tab.1. The chemical composition of the mixture mechanically CARBOFER

Recipes no.	The chemical composition, [%]										
	SiO ₂	FeO	Fe ₂ O ₃	P ₂ O ₅	S	C	Al ₂ O ₃	CaO	MgO	MnO	other oxide
R1	4,65	4,88	39,93	0,10	0,56	23,55	3,72	9,13	1,11	1,22	11,14
R2	4,25	4,97	43,82	0,09	0,50	22,67	3,36	7,75	1,00	1,24	10,36
R3	3,86	5,05	47,70	0,09	0,44	21,78	3,00	6,36	0,88	1,26	9,58
R4	3,47	4,96	51,74	0,09	0,39	17,96	2,64	7,87	0,81	1,40	8,66
R5	3,07	5,04	55,67	0,09	0,33	17,07	2,28	6,49	0,70	1,43	7,84
R6	2,67	5,13	59,57	0,08	0,28	16,19	1,92	5,11	0,58	1,45	7,04
R7	2,29	5,10	63,51	0,08	0,22	13,34	1,56	5,65	0,50	1,54	6,21
R8	1,89	5,18	67,44	0,08	0,17	12,46	1,20	4,27	0,38	1,57	5,39
R9	1,50	5,14	71,44	0,08	0,11	9,61	0,84	4,81	0,29	1,67	4,51
R10	1,50	5,22	72,30	0,08	0,11	9,61	0,83	3,85	0,28	1,67	4,55

Tab.2. Product classification CARBOFER granulometric class.

Recipes nr.	Granulometric class, [mm] / Share, [%]						
	3,0-1,0	1,0-0,75	0,75-0,45	0,45-0,315	0,315-0,25	0,25-0,18	0,18-0
R1	6,325	39,975	24,93	14,75	6,135	4,25	3,635
R2	10,625	37,2	24,433	14,083	6,031	4,221	3,407
R3	14,925	34,425	23,936	13,416	5,927	4,192	3,179
R4	14,7	30,795	24,485	15,807	6,358	4,485	3,37
R5	17,22	28,23	24,65	15,96	6,252	4,52	3,168
R6	20,63	25,56	24,484	15,703	6,147	4,523	2,953
R7	23,99	21,97	23,912	16,118	6,402	4,634	2,974
R8	26,51	19,405	24,077	16,271	6,296	4,669	2,772
R9	27,2	16,13	24,498	17,916	6,548	4,876	2,832
R10	28,09	16,175	24,325	17,239	6,54	4,865	2,766

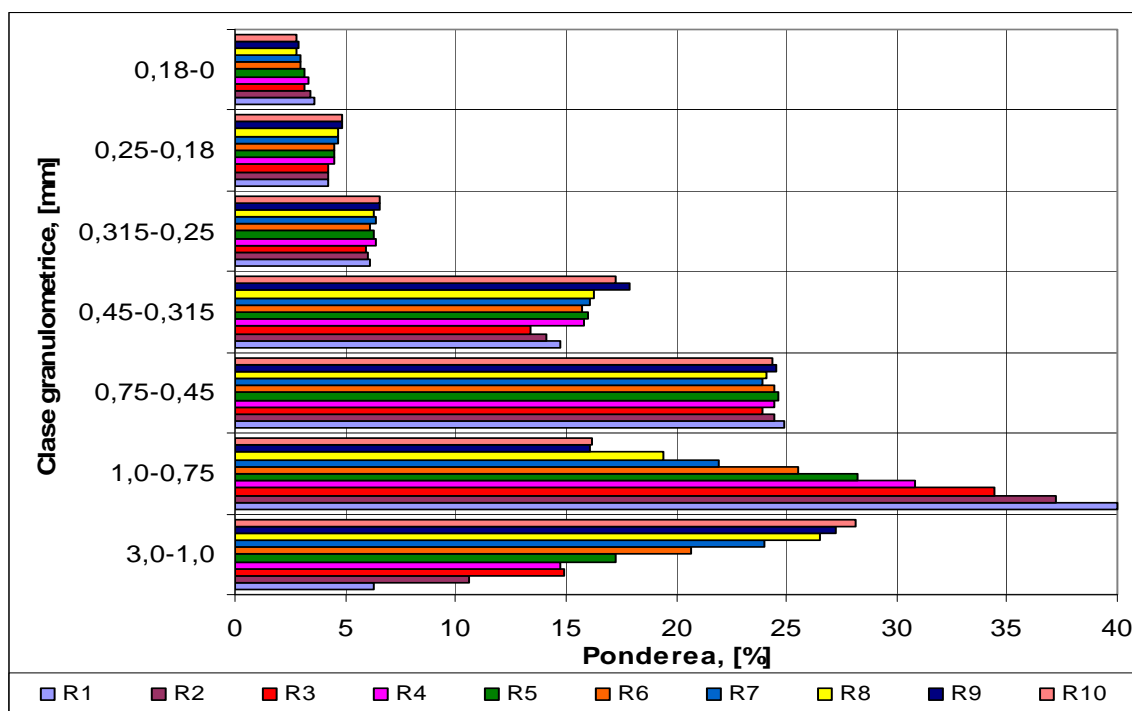


Fig.3. Product classification CARBOFER granulometric class.

3. DISCUSSIONS

CARBOFER product - mix engineer, the first stage, we sampled from the 10 recipes tested in laboratory conditions, samples were analyzed at SC CCPPR SA Alba Iulia.

For each recipe there was a quantity of 2kg of powdered mechanical mixture, which was melted in an induction furnace melts Metal fitted Laboratory of the Faculty of Engineering of Hunedoara. After having analyzed the behavior of each recipe were chosen as representative recipes R1 and R5 (to continue industrial experiments), obtained by using various waste materials both ferrous and addition chemistry of recipes (calculated and determined) is tab.3 presented.

Bulk density was determined only for the two recipes are selected for subsequent experiments, results are presented in tab.4

Tab.3. Chemical composition of tested recipes industrial.

Recipea nr.	Chemical composition, [%]										
	SiO ₂	FeO	Fe ₂ O ₃	P ₂ O ₅	S	C	Al ₂ O ₃	CaO	MgO	MnO	alți oxizi
calculated											
R1	4,65	4,88	39,93	0,10	0,56	23,55	3,72	9,13	1,11	1,22	11,14
R5	3,07	5,04	55,67	0,09	0,33	17,07	2,28	6,49	0,70	1,43	7,84
determined											
R1	4,72	-	40,07	-	-	-	3,81	9,52	1,23	-	16,43
R5	3,22	-	52,68	-	-	-	2,67	7,14	0,71	-	15,7

Tab.4. CARBOFER product bulk density, mechanical mixture.

Density, [kg/dm ³]	Recipe no.	
	R1	R5
	0,8854	1,1150

To determine the foaming capacity, slag samples taken were investigated in terms of macroscopic and microscopic appearance.

The analysis was done by examining the macroscopic appearance of virtual samples and conducting clay-sized photographs (Fig. 4 and 5), all recipes slag formed is uniform porosity and the pores are smaller (especially in cases where the height of the slag foaming was smaller and less intense) respectively standard slag (fig.6).

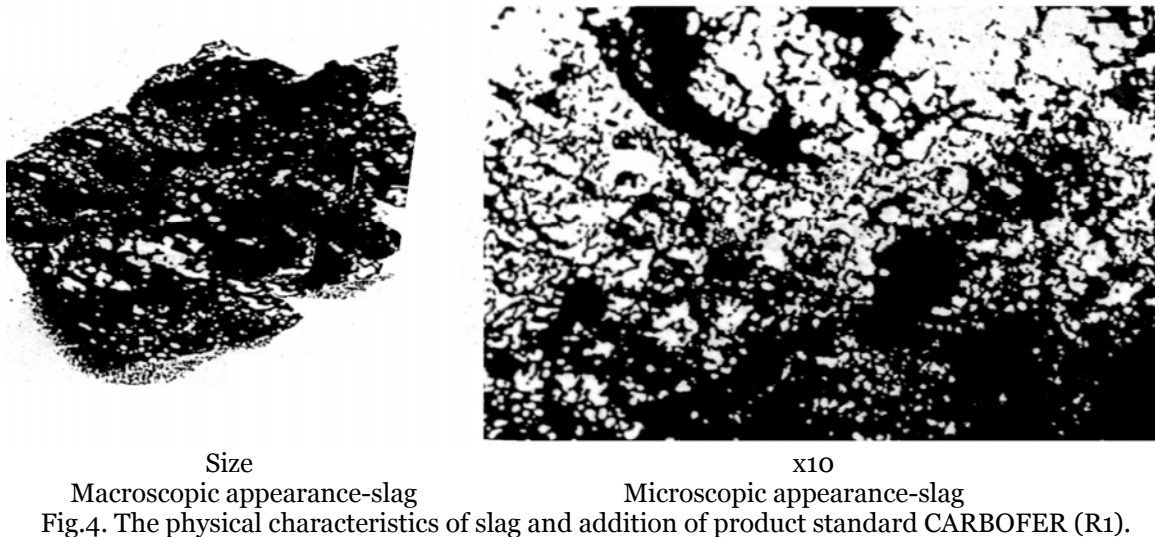


Fig.4. The physical characteristics of slag and addition of product standard CARBOFER (R1).

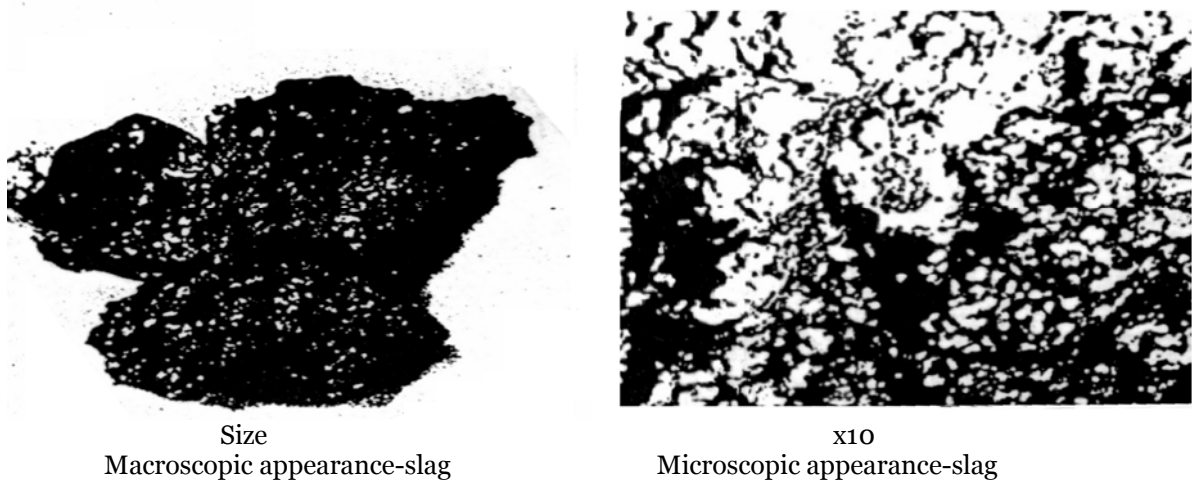
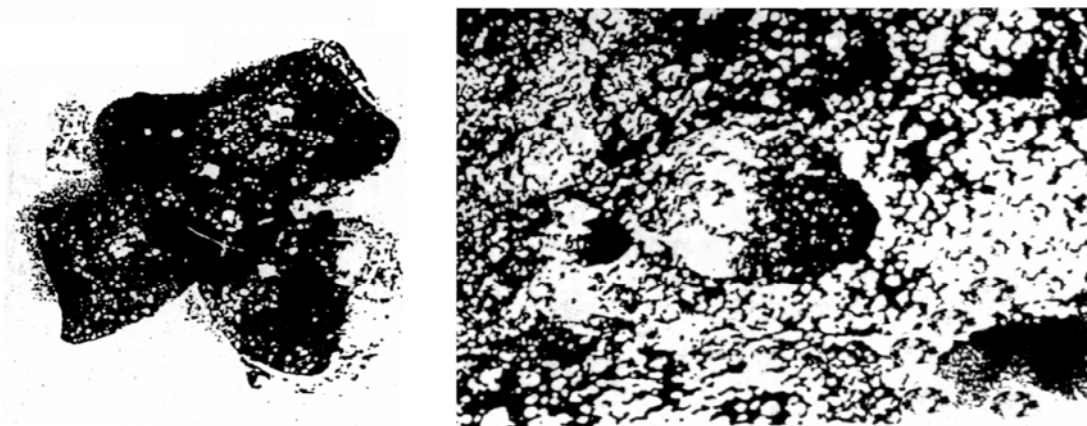


Fig. 5. The physical characteristics of slag and addition of product standard CARBOFER (R5).



Size
Macroscopic appearance-slag
x10
Microscopic appearance-slag
Fig. 6. The physical characteristics of standard slag

4. CONCLUSIONS

Experiments performed revealed that the product CARBOFER added a foaming slag with good capacity, leading to foaming phenomenon. There was a difference in the intensity of the two products CARBOFER frothing; foaming is more intensive use after the first prescription product.

Product CARBOFER use as a substitute for the usual agents of slag foaming in electric arc furnace has both an environmental benefit and economic one. Environmental benefits are shown by a significant reduction in environmental pollution, namely by increasing recovery of waste powder and reducing these waste storage facilities. The economic advantage is the immediate transfer of costs for waste disposal in the UK which are between £ 30-57 / t waste stored to other destinations.

ACKNOWLEDGMENT

The researches do the object of Research Project no.31-098/2007, with title Prevention and fighting pollution in the steelmaking, energetic and mining industrial areas through the recycling of small-size and powdery wastes, financed by National Center of Program Management, project managed by Prof.dr.ing. Teodor Hepuț.

REFERENCES

- [1.] Nicolae, M., ș.a., Dezvoltare durabilă în siderurgie prin valorificarea materialelor secundare, Ed. Printech, București, 2004.
- [2.] Constantin, N., Procedee neconvenționale de obținere a materialelor feroase, Editura Printech București, 2002.
- [3.] Dobrovici, D., Hățărascu, O., Șoit-Vizante I., Intensificarea proceselor din furnal, Ed. Tehnică, București, 1983
- [4.] Ilie, A., Cercetări privind valorificarea superioară a materialelor pulverulente din siderurgie, Teză de doctorat, Conducător științific: Prof.dr.ing. Dragomir I., București, 1999.
- [5.] Borza, I., Popoiu, Ghe., Coican A., Tehnologia elaborării fontei, Litografia Timișoara, 1983.
- [6.] Hepuț, T., ș.a., Prevenirea și combaterea poluării în zonele industriale siderurgice, energetice și miniere prin reciclarea deșeurilor mărunte și pulverulente, Contract de cercetare nr.31-098/2007, beneficiar: CNMP, parteneri: CEMS București, SC CCPPR SA Alba Iulia





ESTABLISHING THE MAIN TECHNOLOGICAL PARAMETERS OF INDUCTION SURFACE HARDENING FOR SHAFT PARTS TYPE

¹ UNIV.POLITEHNICA OF TIMISOARA, FACULTY OF ENGINEERING FROM HUNEDOARA, ROMANIA

ABSTRACT:

Induction heating is a particular process which uses electromagnetic fields for heating conductive materials (steel, copper, brass, aluminium).

The main difference from a traditional heating process is the location of heat sources which are distributed inside the work-piece. For this reason the induction heating process is very fast and controllable. Depending on the frequency used the heating can be superficial (induction surface hardening) or deep in the piece (forging, heat treatment etc.).

The main advantages of this technology are: high production rate due to the high specific power delivered to the work-piece, high automation of the process, precise repeatability of treated pieces, in-line installation, low floor space needed, controllability of temperature with high precision, avoiding of deformation of pieces especially in surface hardening, primary energy saving, safe and clean work ambient for employees.

There are a lot of applications where induction heating is used in different industries: melting of metals, heat treatments (hardening, tempering, annealing), forging, hot rolling, surface hardening, cold crucible melting, welding, pre-heating, dry-coating, special applications. All these applications get benefits from the suitable characteristics of this technology.

In this paper is presented the determination of the technological parameters for superficial hardening of axel pieces type made from 41Cr4 and 54CrMo4 steel. This technological parameters is optimum heating temperature, heating time and adequate cooling method for obtains a higher hardness.

KEYWORDS:

induction heating, hardness, heating temperature

1. INTRODUCTION

Surface hardening is a local heat treatment, which is applied to obtain a martensitic structure on the surface of pieces, to the depths between tenths of a millimetres up to 5-10 mm. Surface hardening is done by heating at high speed of the surface layer of products to a temperature in the austenitic range, shortly maintain and rapid cooling at rates higher than the critical quenching speed.

After applying surface hardening results duplex pieces, with hardened outer layer, resistant to wear and fatigue with plastic and tenacious core, resistant to other types of service loads: bending, shock, twisting. In addition, the compressive stress in the hardened layer increases resistance than alternating loads. However, for the combination of features, surface hardening must be applied to semi-hard steel with carbon content between 0.3% and 0.65%.

Given the specific heating conditions, heating temperature decreases rapidly from the surface to the center of product. As a result, only a very thin layer over the surface are heating upper the A_{c3} point and presents after the rapid cooling a complete quenching structure (martensitic), but with different degrees of overheating. Next layer heated between A_{c1} and A_{c3} , becomes an incomplete hardened layer, which makes the transition to the initial structure (feature the core).

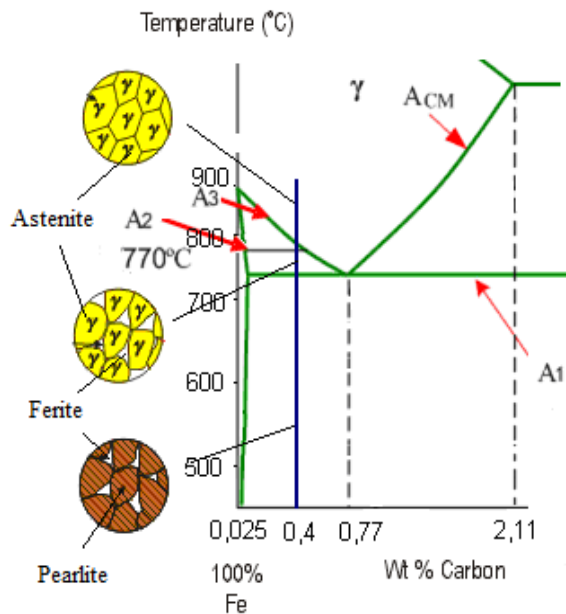


Fig.1. Fe-Fe₃C diagram, steel area

This change occurs because the magnetic permeability decreases suddenly at reach and overcome the Curie point temperature (770° C). In figure 2 is presented some pieces with different hardening depth.

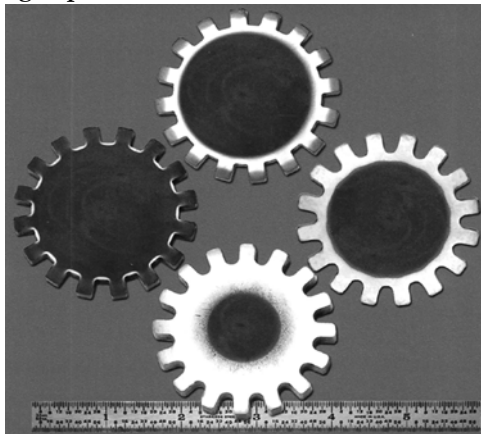


Fig. 2. Some pieces with different hardening depth depending of generator power, frequency and maintained time in inductor

2. THE STUDY

For practice work of this surface hardening process is requires the following steps: - choosing the power and frequency AC generator;

- ❖ choose the method of heating and cooling;
- ❖ the choice of working parameters.

Special attention is given to steel. The charge is made that preliminary tests, should be possible have the average chemical composition presented in standard and and have average hardenability to lower limit of the hardenability band.

Current charge used in the production process must then be reasonably restricted in terms of chemical composition, purity, austenitic grain and hardenability, otherwise there is risk of deviations in treatment results from batch to batch of products.

Of particular importance for the results of inductive quench and subsequent their reproducibility is the initial structure, namely heat treatment earlier surface hardening. Ferrito-pearlitic structures (rolling, annealing and normalizing) give a good response to induction surface hardening, with uniform and smooth as possible condition.

In conclusion, for high frequency current heating, the initial structure of the problem assumes a special importance because it usually is accompanied by an extremely high heating rate

The final thickness of hardened layer depends not only completely during heating, but also the time of the finish action of heat source and start cooling, period during which the temperature distribution changes in the product section.

Depth current penetration in the superficial layer and finally hardened layer depth depends on frequency of induced current is determined by the relation:

$$\delta = 5,03 \cdot 10^3 \sqrt{\frac{\rho}{\mu \cdot f}}, [\text{cm}]$$

where: ρ - receptivity of steel, cm;
 μ – relative magnetic permeability of steel;
 f - current frequency, Hz.

For steel the current penetration depth is determined by the formula:

$$\delta = \frac{14,1}{\sqrt{f}}, [\text{cm}] \text{ at } 15^\circ\text{C}$$

$$\delta = \frac{200}{\sqrt{f}}, [\text{cm}] \text{ at } 800^\circ\text{C}.$$

and, accordingly, change phase and diffusion processes are limited here within extremely small. The greater dispersion of steel structural components, the solid solution is formed faster and faster the diffusion process completes, which contributes to the uniformity of composition. In figure 3 and 4 is presented a microstructure of steel pieces before and after the induction surface hardening.

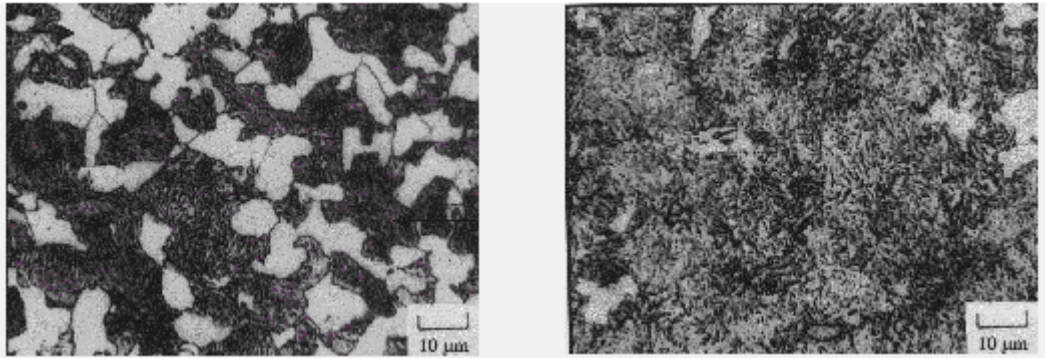


Fig.3. Steel microstructure 1C45 (AISI 1045) before and after the induction surface hardening

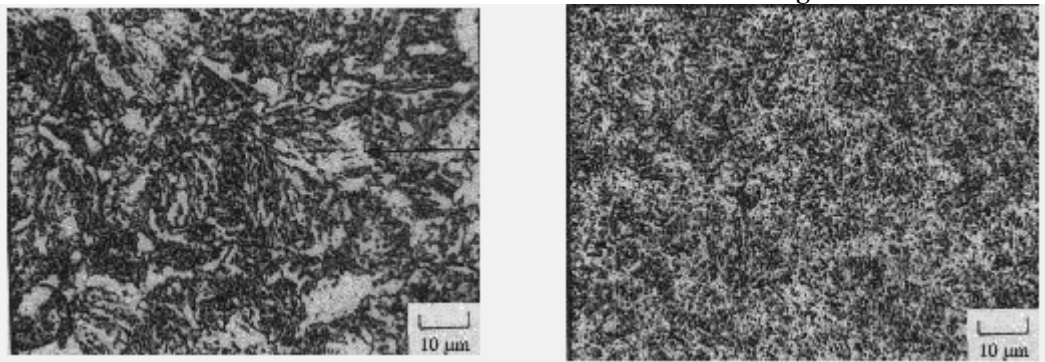


Fig.4. Steel microstructure 42CrMo4 (AISI 4140) before and after the induction surface hardening

It appears that the induction heating is desirable that the initial structure to be sorbite or perlite, where results the different quench depths:

- ❖ steel microstructure dependent mostly on temperature and speed of induction heating, the higher the heating rate is higher, the layer structure of hardened steel will be fine;
- ❖ it is desirable that the initial structure of steel is therefore required to provide good properties for core, i.e. resistance;
- ❖ initial structure should favours changes in solid state and there lead to a favourable state and to eliminate the soft layer (ferrite network and transition layer).

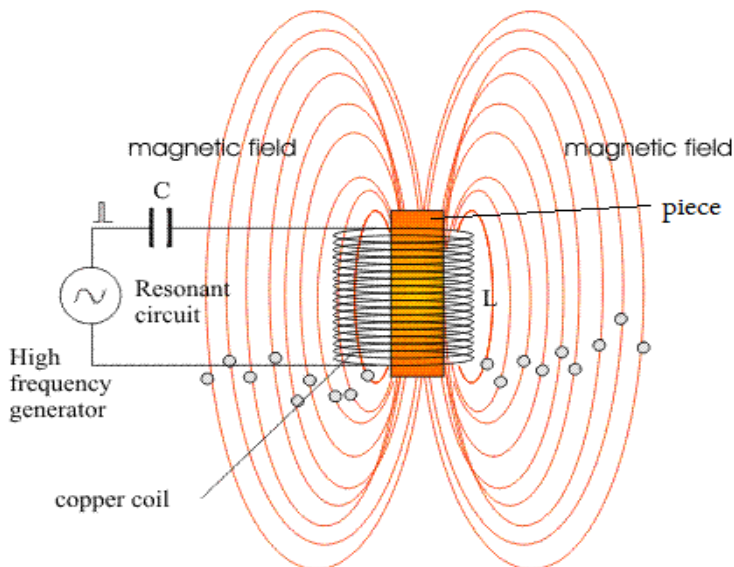


Fig.5 Work principle for induction heating

A surface hardening equipment, fig.5 is composed of high-frequency generator and tempering machine, whose construction depends on the geometry of surface hardening of parts subject. Also in this picture is presented work principle for induction heating.

3. DISCUSSIONS

Experiments were conducted in the laboratories of the Faculty of Engineering Hunedoara. For experiments have been used a specialized facility for surface induction hardening (type CTC100K15 compact frequency converter), T200 FLIR thermal imager, a

radiation pyrometer ST88 PLUS and a metallographic microscope type Krüss Optronic. Medium frequency power converter converts the medium frequency power used of induction heating. All parts of converter, both as external power is cooled with water. It is recommended for reducing the cost of cooling water, the water recirculation and cooling in a heat exchanger.

Power circuit of converter is a parallel resonant LC circuit provided with of inductive and capacitive compensation composed from inductor and hot work pieces. Power circuit includes tempering transformer, shown in the figure below, and also is presented the inductor who are used in experiments.



Fig.6 . Tempering transformer and inductor

Quenching transformer is shown in figure 6, is provided with multiple entries, depending on the inductor used. If heating is not correct (too long heating time) is needed to move to other transformer connections tempering ($\Phi 30$ mm inductor, transformer coupled 4:1; piece $\Phi 19$ mm diameter).

For a better control of temperature as was preferred measurements of temperature using thermographic cameras that allows real-time continuous measurement of pieces temperature in inductor with sufficiently high precision. The following figure shows how the pieces temperature was measured.

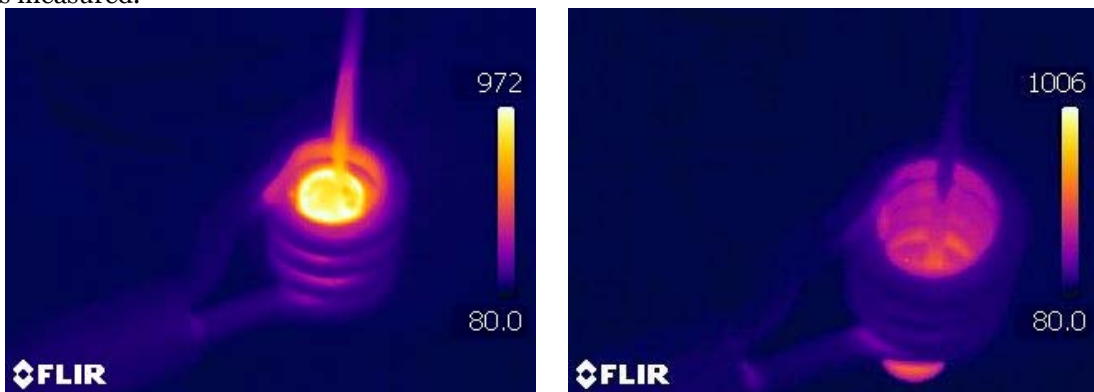


Fig. 7. Temperature of pieces measured with thermographic cameras

For experiments we used two sets pieces, consisting of 4 pieces made of steel 41Cr4 improvement, and 6 pieces of steel made from 34CrMo4. The specimens have dimensions $\Phi 19$ mm diameter, length 26 m

In order to conduct experiments, it was measured the sample temperature maintained in the inductor, while the power generator was kept constant at 60% and 70% of rated generator power. Please note that attempts to measure temperature and using a radiation pyrometer, but measurement errors occurred because of how the piece is heated (inside the ring inductor with multiple coil). All the pieces were quenched in water, and the hardness was measured in several points on the surface.

4. CONCLUSIONS

Since the experiments were conducted using the methodology described above, were measured hardness at three points on the surface of samples by Rockwell method, and the values obtained are presented in the following tables.

Tab.1 Hardness for pieces from 34CrMo4 steel

Pieces	Temperature	Hardness			Time	Power
	°C	HRC	HRC	HRC	s	%
1	910	52,5	50	52	9,1	70
2	920	53	55	50	11,3	60
3	880	49	46	48,5	10,2	60
4	1002	54	55	51	10,5	70
5	980	57	54	54	9,2	70
6	930	49,5	50	50	11,5	60

Tab.2 Hardness for piceses from 41Cr4 steel

Pieces	Temperature	Hardness			Time	Power
	°C	HRC	HRC	HRC	s	%
1	840	53	54	47	9,8	60
2	1010	65	61	61,5	10,7	70
3	972	59	60,5	65	9,1	70
4	980	56,5	59	60,5	12,3	60

In the first phase, a macroscopic analysis of surface was studied of the two cut samples in order to reveal the penetration depth of the hardened layer. These samples are presented in the following figures on the right is highlighted hardened layer, for 41Cr4 steel.



Fig. 8 Microstructure for pieces made from 41Cr4 steel

Hardened layer depth, is about 4 mm for specimens of steel and approximately 3.5 mm for specimens of steel. Are normal differences between hardened layer depth and hardness differences because steel 41Cr4 steel has a greater hardenability as 34CrMo4 steel (higher carbon content and boron contains increases hardenability).

The sample thus prepared was studied with metallographic microscope, as shown in the following figures some of the photos microstructures obtained. It just shows the microstructure of the steel sample 41Cr4 with different orders of magnitude.

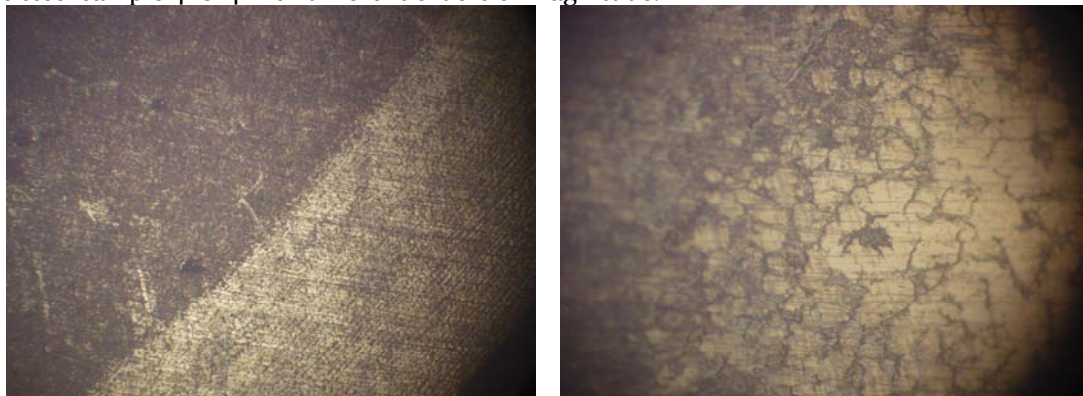


Fig.9 Microstructure of transition zone hardned-unhardned at magnitude 140x – left and 350x – right, for 41Cr4 steel

In figure 10 and 11 is presented dependences between hardness of pieces and heating temperature for booth of steel quality.

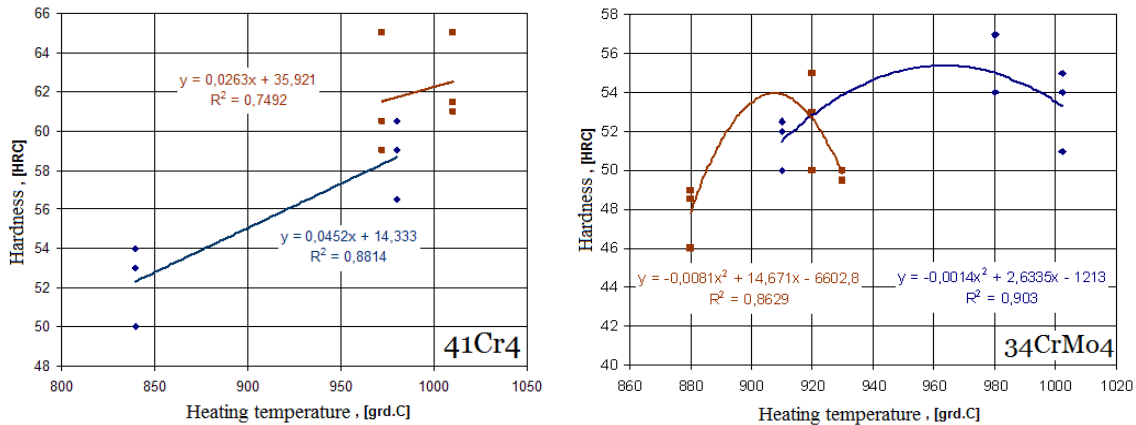


Fig.10 Hardness variation for pieces in case of 60% and 70% nominal power of generator.

In the case of 34CrMo4 steel data (which are in greater number) can be traced and a spatial dependence, in this case the hardness depending on temperature and time heating. This kind of variance of hardness is built in the statistical analysis program.

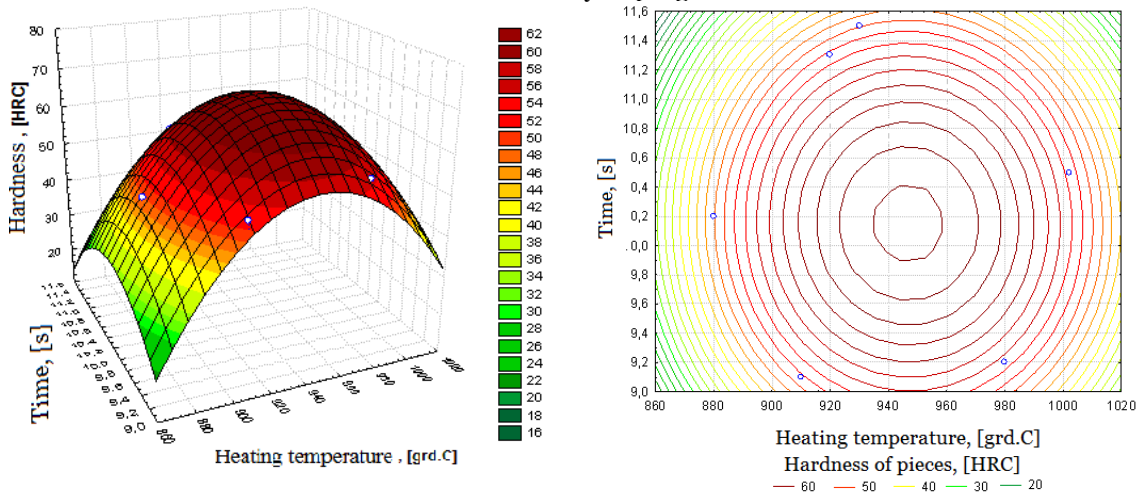


Fig.11. Hardness variation for pieces made from 34CrMo4 steel, cumulative value

In figure 11 is added also the contour graph which provide more suggestive of dependence that exists between the three parameters.

Thus, studying the previous charts are recommended for heating the steel 41Cr4 temperature range 950...1000°C to obtain a hardness of about 58... 62 HRC, while the equipment is above to 60-70% of maximum power (9 ... 10.5 kW).

For steel 34CrMo4, we recommend heating at 940 ... 980°C to obtain hardness values of 52...56 HRC, under the same power condition. In addition, in this case it may recommend duration of heating time to be 9.8 ... 10.6 seconds.

In both cases it is noted that the heating temperature for quenching is recommended to be much higher, with 120 ... 150 °C than classical austenitic temperature (which for these two steels is 840 ... 860 °C), due to this high-speed heating.

REFERENCES

- [1.] Carțis I. Gh., - Tratamente termice, Editura Facla, Timișoara, 1982.
- [2.] Ardelean M., Prejban I., Mihut G. - Tratamente termice, calcule tehnologice, Editura Cermi, Iași, 2007.
- [3.] Anghel F. - Metode și procedee tehnologice, volumul II - Tehnologii moderne, Editura Printech, Bucuresti 2006.
- [4.] *** Documentație tehnică instalație compactă de încălzire prin inducție tip CTC 100K15, AAGES Targu Mures.



¹Daniela MILOȘTEAN, ¹Mihaela FLORI

AN OVERVIEW ON THE SEMISOLID STATE PROCESSING OF STEEL

¹ FACULTY OF ENGINEERING HUNEDOARA, UNIVERSITY "POLITEHNICA" TIMISOARA, ROMANIA

ABSTRACT:

The high melting point alloys such as steels are difficult to process in semisolid state due to high temperature needed for processing. Owing to the obvious advantages of this new technology comparative with the conventional manufacturing technologies, many studies try to resolve the technological problems and to offer the possibility of a profitable commercial exploitation.

This article emphasizes the importance of solid fraction in semisolid state processing technology and exposes the main steel grades investigated and presented in the literature. Also are presented the methods to obtain precursory material for thixoforming and the materials used for die manufacturing needed in this new process.

KEYWORDS: steel, semisolid state, solid fraction, thixoforming, die material

1. INTRODUCTION

Topics as decreasing manufacturing costs and increasing the quality of the final products draw attention to many production engineers. Thus, the development of new technologies as *semisolid state processing* (known as SSP) becomes necessary.

Semisolid processing of alloys was initiated at the beginning of the 70's at MIT (Massachusetts Institute of Technology) [1,2]. At the basis of this new technology are the experiments realized by David Spencer *et al.* on Sn-15Pb alloy where he obtained a semisolid suspension with thixotropic characteristics by mechanical stirring [3].

Semisolid metal forming is realized at temperatures between liquidus and solidus lines, when in the alloy exist about 40-60% solid fraction [4]. In this range, if the microstructure of the alloy is globular it manifests a property named thixotropy. This term was introduced by Peterfi in 1927 to define the property of slurry which become fluid when is agitated and to thicken when resting [5]. Thus, this interesting property of semisolid alloys with globular structure made possible the invention of a new technology that offers several advantages over the conventional casting, forging, etc, such as porosity reduction, lower forming temperatures, improved flow properties, reduced process force, near net shape forming, better mechanical properties, etc. [6]. The most known SSP technologies are: *thixoforming* and *rheocasting* used for aluminum and other alloys, respectively *thixomolding* and *rheomolding* especially for magnesium alloys [7]. Thixoforming consist in obtaining parts in final shape from semisolid slurries with globular structure achieved by heating the semi-finished product with non-dendritical structure. If the shaping takes place in an open die the process is called thixocasting and if the shaping is realized in a close die, is called thixoforging. Rheocasting is actually the process of forming in the semisolid state direct from cooling melt, without the need for using of a globular structure semi-finish product [3].

This article presents an overview on the most studied steels processed in semisolid state; it also refers on the methods used to obtain precursor material for thixoforming and on the most suitable materials for die manufacturing.

2. THE IMPORTANCE OF SOLID FRACTION IN SSP

The solid fraction is one of the most important parameters that affect principally the viscosity of the semisolid slurry. It can be calculated using a simple phase diagram (fig.1) and level rule. In

fig. 1 is presented the phase diagram of a binary alloy, together with microstructures obtained by casting (fig.1.a) and by thixoforming (fig.1.b) of X210CrW12 steel. So, for simple binary eutectic alloys that melt and solidify under equilibrium condition (assuming that the liquidus and solidus line are linear), the weight of solid fraction f_s at a given processing temperature T is given by [8,9]:

$$f_S^{ech} = \frac{(T_M - T) - m_L \cdot c_0}{(T_M - T) \cdot (1 - k)} \quad (1)$$

where T_M is the melting point of the pure solvent, m_L is the slope of the liquidus line, c_0 is the alloy composition and k is the partition coefficient of the alloy.

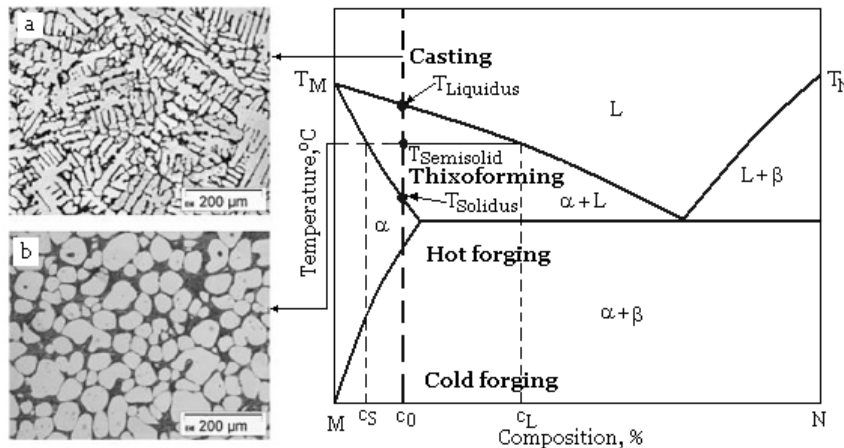


Fig.1. Schematic representation of the thixoforming area in a simple phase diagram and the corresponding microstructure (a-dendritic, b-globular) for X210CrW12 steel [10]

Under fast solidification condition, when occurs a complete diffusion in the liquid and no diffusion in the solid phase (maximum microsegregation) the weight of solid fraction f_s at a given processing temperature T is given by Scheil equation [8,9]:

$$f_S^{Sch} = 1 - \left(\frac{T_M - T}{T_M - T_L} \right)^{\frac{1}{1-k}} \quad (2)$$

where T_L is the liquidus temperature of the alloy.

The steel grades processed in semisolid state are selected according to few criteria:

- ❖ the material must have a wide solidification range ($T_L - T_S$). Usually the methods used to determine the semisolid range are Differential Thermal Analysis-DTA (fig.2), Differential Scanning Calorimetry-DSC and thermodynamic data [9];
- ❖ the temperature processing interval when in the alloy exist 40-60% solid fraction f_s must be sufficiently large;
- ❖ the volume of solid fraction must not be sensitive to temperature variations specially in the range with 40-60% solid fraction [4,8].

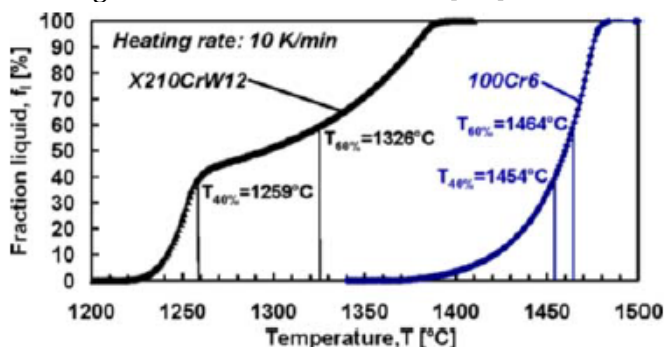


Fig.2. The variation of the liquid fraction versus temperature obtained by DTA [11]

It can be seen in fig.2 that the X210CrW12 steel has a temperature processing range (40-60% f_s) of 67°C while for 100Cr6 steel the interval is only of 10°C. Hence for the second steel grade it is necessary a very strict temperature control [11].

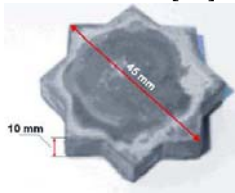
So, the slurry temperature influences the solid fraction with direct consequences on the viscosity which indicate the capability of a material to fill a mold and determines the force necessary for deformation and flow of materials [2].

3. STEEL GRADE SELECTED FOR THE SSP

It should be noted that semi-solid processing bases were established by studying low melting point alloys such as aluminum and magnesium alloys used for the most parts that are now

commercialized. So far, the SSP technology was not applied on industrial scale for high melting point alloys such as steels [12-14], but over time have been done researches on several steel grades that are more likely to be processed by this new technology (tab.1).

Table 1. An overview on the steel grades processed in semisolid state

	<p>Process – Thixocasting Year - 2004 Reference – [15]</p>  <p>Thixocasted steel part</p>	<p>Process –Thixo-extrusion Year – 2009 Reference – [16]</p>  <p>Extruded bars</p>
X210CrW12 (AISI D6)	<p>Process –Thixo-extrusion Year – 2009 Reference –[17]</p>  <p>Extruded bars. Left: view of a cut segment, right: cross-section</p>	<p>Process – Thixocasting Year - 2009 Reference – [18]</p>  <p>Thixocast sample</p>
	<p>Process – Rheoforging Year – 2005 Reference – [11]</p>  <p>Part obtain through rheoforging</p>	<p>Process – Thixocasting Year – 2010 Reference – [19]</p>  <p>Thixocast samples</p>
100Cr6	<p>Process - Thixoforging Year – 2010 Reference – [20]</p>  <p>Part obtain through thixoforging</p>	
	<p>Process – Thixoforging Year – 1993 Reference – [1]</p>  <p>M2 tool steel thixoforged parts</p>	<p>Process – Thixoforging Year – 2010 Reference – [14]</p>
M2		
	<p>Process - Rheo-rolling Year – 2003 Reference – [21]</p>	<p>Process - Rheo-rolling Year – 2008 Reference – [6]</p>
60Si2Mn		
	<p>Process - Rheo-rolling Year – 2003 Reference – [22]</p>	<p>Process - Rheo-rolling Year – 2008 Reference – [6]</p>
1Cr18Ni9Ti		
	<p>Process – Rheo-rolling Year – 2005 Reference – [23]</p>  <p>Rheo-rolled product</p>	
T12		

UHCS

Process - Rheocasting

Year – 2006

Reference – [24]

Process - Thixoforging

Year – 2005

HP9/4/30 Reference – [25]



Thixoforged fingers from a slug

At the University of Science and Technology Beijing, China, a research group have focused the studies on the rheo-rolling process and developed a device for semisolid steel preparation and rolling. The steel grades used in their investigation are principally: 60Si2Mn, 1Cr18Ni9Ti and T12 [6,21-23,26]. Results showed that semi-solid slurry obtained through electromagnetic stirring, of the steel grades 60Si2Mn and 1Cr18Ni9Ti, can be rolled successfully. They observed that for 1Cr18Ni9Ti stainless steel the strength of the plate rheo-rolled is increased compared to that of the conventionally repeated hot-rolled plate, but the elongation is decreased [22]. For 60Si2Mn spring steel rheo-rolled the rupture strength and elongation are lower than that of traditionally repeated hot-rolled plate [21]. Also, through rheo-rolling at different solid fraction, with increasing the solid fraction the mechanical properties (rupture strength and elongation) of semisolid rolled products become better [6]. T12 high carbon steel (1,2%C) was investigated only in terms of microstructure [23].

The Institute of Metal Forming, RWTH Aachen University of Technology, from Germany is another research center interested of the SSP technology. G. Hirt and his team investigated two different process routes for semi-solid precursor material preparation subsequently forged in semisolid state. The 100Cr6 steel grade was chosen for investigation because of the various application possibilities, and the X210CrW12 steel for his good suitability for microstructure studies. They concluded that the preliminary semisolid forging and rheoforging trials for both steels grade predict the high potential of the process [11].

The study realized by W. Püttgen et al. on the two steel grades mentioned above, describe the phase formation during rapid cooling from semisolid state. They have shown that the microstructure in the as-quenched state does not reflect the condition from semisolid state, and therefore is not possible a metallographic evaluation of the liquid fraction [12].

In the work carried out at the University of Sheffield a research group has demonstrated the feasibility of HP9/4/30 steel thixoforging having prior microsegregated microstructure [25].

The steel grades M2 [14], X210CrW12 [18] and 100Cr6 [19] are also investigated at the Institute of Metallurgy and Materials Science of the Polish Academy of Science, Krakow.

Even if semisolid forming of steel is more difficult to be realized compared with that of low melting point alloys there is a progress made so far in this domain and exists the possibility of industrial scale implementation.

4. METHODS USED TO OBTAIN SEMISOLID PRECURSORY MATERIAL

A successful thixoforging process requires precursory material with a unique microstructure in which the solid particles are spheroidal. This material has a thixotropic behavior in semisolid state and it can be obtained in several ways as were published in the literature [7,27].

The usual routes used to produce the steel feedstock material for thixoforging are: electromagnetic stirring (fig.3), spray forming-Osprey (fig.4) and SIMA-Strain Induced Melt Activated. For low melting point alloys besides the above mentioned methods there are other techniques of obtaining raw material for thixoforging as: mechanical stirring [28], casting at liquidus temperature (the UBE new rheocasting process is based on this principle) [27], the new MIT process [27], etc.

The *electromagnetic stirring* process was developed in the USA and consists in breaking the dendrites during solidification due to the rotating electromagnetic fields within the continuous casting crystalliser and in forming of an alloy with a nondendritic structure under the shape of a rosette [7,29]. This method is used both in the semisolid processing of low and high melting point alloys (60Si2Mn, 1CrNi9Ti [6,21,22]).

In the *SIMA process* the alloy which has been previously hot-worked is heated so recrystallisation take place before partial melting; so the liquid penetrates the grain boundaries and leads to a fine globular microstructure [27,30].

In the *OSPRAY process* the melted metal passes through a nozzle and encounters an inert gas at a high pressure. The liquid metal is sprayed by the high pressure gas as micrometric drops which

cool down with a high speed while being in the air. While the bigger drops remain intact and the smaller ones are solidified during spraying, those having intermediary dimensions become semisolid (fig.4). Liquid and semisolid drops with a high liquid fraction spread upon impact, while the solid and semisolid drops with a high solid fraction get fragmented. So the resulted structure contains fine and spherical grains [27].

In 1993 Kapranos and his colleagues [1] have investigated two distinct routes (RAP and Ospray) used to produce the feedstock for M2 tool steel thixoforging. Both methods have proved to be viable for production of precursory material for tool steel thixoforging.

Recently feedstock material (M2 tool steel) obtained by Ospray method was thixoformed and the results show that the hardness value recorded a significant increase [14].

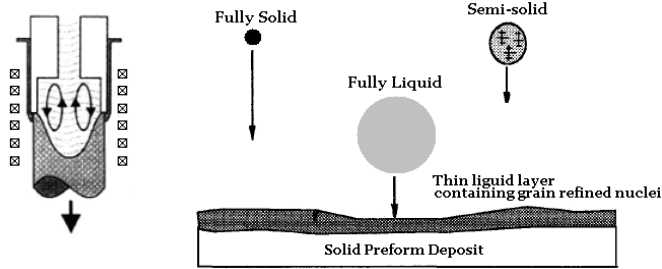


Fig.3. Electromagnetic stirring [29] Fig.4. The Osprey process [1]

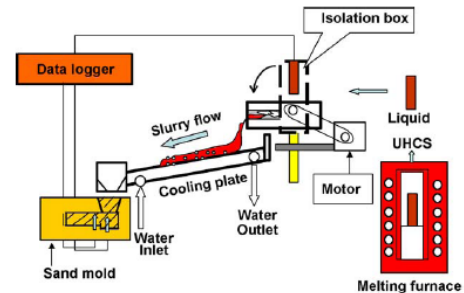


Fig.5. The cooling plate technique [24]

The “rheo” routes (rheocasting, rheoforging, rheo-rolling, rheoextrusion) does not require semi-finished products with globular structure, because in this type of process the melted material is subjected to different techniques (electromagnetic stirring [21-23], mechanical vibration [31], cooling slope technique - fig.5 - [24,32], etc.) in order to obtain in the semisolid interval a globular solid fraction in a liquid matrix.

Ultra-high carbon steel (UHCS) with 1,49%C processed in semisolid state by the cooling plate technique gave good results in terms of the mechanical properties compared with the conventional casting [24].

Because the rheo-route does not require a semi-finished product with a globular structure as a starting material there are lower energy costs and thus from this point of view this route is preferable.

5. DIE MATERIALS

One of the biggest problems which appear at the semisolid state processing of steel is finding an appropriate die material. This is due to the high temperature at which the process takes place. The searched material must have properties like: resistance at high temperatures, thermal shock resistance, good wear and corrosion resistance [33], durability in exploitation, low coefficient of thermal expansion [34], etc. In this condition the materials appropriated for thixoforming die are principally dense ceramic materials, laser treated steels or others alloys (Inconel 617, Satellite 6, CrNiCo).

Recently, S. Muenstermann et al. developed a self-heating ceramic tool for the semi-solid extrusion of steel (X210CrW12) under near-isothermal conditions. The ceramic material used for the die is high-purity alumina (Al_2O_3). Results showed that this new concept allows isothermal thixoextrusion of the steel. Also they investigated the behavior of the alumina die regarding wear and corrosion resistance. The conclusion was that by applying the self-heating tool concept the ceramic dies have excellent corrosion and wear resistance, and regarding the chemical interaction between tool and the work material, alumina dies are not decomposed in the steel thixoextrusion process, leaving the work piece unaffected [17,33].

Another potential tool material for steel semisolid forming is silicone nitride (Si_3N_4) thanks to its high strength and excellent thermal shock resistance at 300-400°C [35]. The non-oxide ceramics materials (Si_3N_4) are susceptible to oxidation and corrosion while oxide ceramics (Al_2O_3) exhibit significant lower mechanical properties and poor thermal shock resistance [35]. Despite these properties unfavorable for a die material used in semisolid processing of steel, S. Muenstermann and R. Telle developed two new tool concept strategies based on the benefits of the both materials (high strength of non-oxide ceramics materials and excellent corrosion resistance of oxide ceramics) [35]. A schematic view of the tool concept strategies for thixoforming dies is given in fig.6.

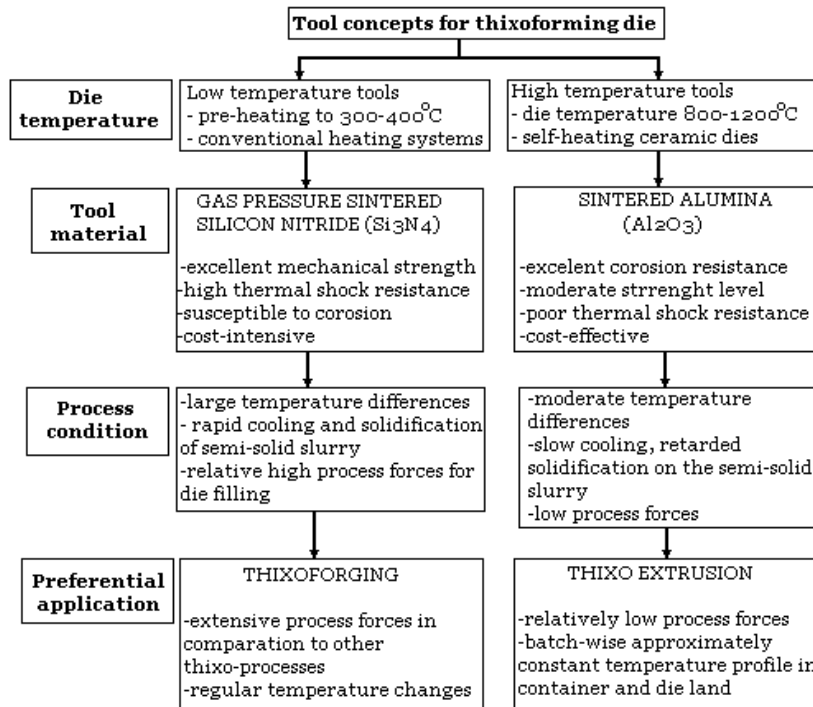


Fig.6. Tool concept strategies for steel thixoforming die [35]

These two strategies developed by S. Muenstermann and R. Telle for the thixoforging and thixoextrusion of steel using silicon nitride and respectively alumina die were experimented and the results were promising.

Regarding the die final price, it was concluded that the alumina tool costs (raw material, production and investment costs) are lower compared with the non-oxide ceramics [33].

Y. Birol [34] tested the CrNiCo die material alloy and used it in the steel thixoforming process. By comparing the thermophysical properties and the thermal fatigue behavior of CrNiCo alloy with the X38CrMoV5 steel used in manufacture of conventional forging dies, it was concluded that the first one can be a viable die material.

Other alloys (Inconel 617, Satellite 6) were investigated as die materials and subjected to high temperature abrasive wear testing and compared to the X32CrMoV33 hot work tool steel (used in conventional hot forging of steel parts). At 625°C, the wear resistance (represented by weight loss) and the surface hardness of the tool steel is better compared to the alloys, while at 750°C the results are superior for the alloys [36]. From the point of view of service life, Inconel 617 and Satellite 6 alloys presented few and shallow cracks after 5000 thermal cycling while X32CrMoV33 steel resisted only 1500 cycles [37].

Also, by laser glazing of tool steel (AISI H13) dies, the initial results showed a large increase in hardness value for the surface layer, but the temperature working limit was only of ~600°C. So the results are unsatisfactory for thixoforming of steel (where the die cavity surface reaches 700-750°C only for a few seconds [34,38]) and this steel could be used as die material for non-ferrous semisolid forming [39,40].

The investigations realized so far on die materials are encouraging, but just now it wasn't found a material that meets all requirements necessary for large scale use.

6. CONCLUSIONS

Analyzing the literature studies it may be concluded that the semisolid processing has many advantages over traditional technologies and has already been applied to industrial production of magnesium and aluminum alloys. In recent years, steel semisolid processing also drew attention, the results on applying this technology being encouraging with high melting point alloys. Also finding an appropriate die material with a good durability in exploitation is yet under investigation, but the research made so far are promising.

REFERENCES

- [1.] P. Kapranos, D.H. Kirkwood and C.M. Sellars, Semi-solid processing of tool steel, *Journal de Physique IV, Colloque C7, supplement au Journal de Physique III*, Vol. 3 (1993)
- [2.] O. Lashkari, R. Ghomashchi, The implication of rheology in semi-solid metal processes: An overview, *Journal of Materials Processing Technology*, Vol. 182 (2007) 229–240
- [3.] M.C. Flemings, Semi-solid forming: the process and the path forward, *Metallurgical Science and Technology*, Vol. 18 (2) (2000)
- [4.] D.I. Ulenhaut et al., Structure and properties of a hypoeutectic chromium steel processed in the semi-solid state, *Acta Materialia*, Vol. 54 (2006) 2727-2734
- [5.] F. Czerwinski, The Basics of Modern Semi-Solid Metal Processing, *JOM*, Vol. 58 (6) (2006) 17-20
- [6.] R. Song, Y. Kang and A. Zhao, Semi-solid rolling process of steel strip, *Journal of Materials Processing Technology* Vol. 198 (2008) 291-299
- [7.] Z. Fan, Semisolid metal processing, *International Materials Reviews*, Vol. 47 (2) (2002)
- [8.] E. Tzimas, A. Zavaliangos, *Materials Selection for Semisolid Processing*, *Materials and Manufacturing Processes*, Vol.14 (1999)
- [9.] E. Tzimas, A. Zavaliangos, Evaluation of volume fraction of solid in alloys formed by semisolid processing, *Journal of Materials Science*, Vol. 35 (2000) 5319-5329
- [10.] H. Stankova et al., Influence of thixoforming on structure development of the tool steel, 12th International Research/Expert Conference “Trends in the Development of Machinery and Associated Technology” TMT 2008, Istanbul, Turkey
- [11.] G. Hirt et al., Semi-Solid Forging of 100Cr6 and X210CrW12 Steel, *CIRP Annals – Manufacturing Technology*, Vol. 54, Issue 1 (2005) 257-260
- [12.] W. Püttgen et al., On the microstructure formation in chromium steels rapidly cooled from the semisolid state, *Acta Materialia*, Vol. 55 (2007) 1033-1042
- [13.] R. Kopp et al., Forming and joining of commercial steel grades in the semi-solid state, *Journal of Materials Processing Technology* 130-131 (2002) 562–568
- [14.] J. Dutkiewicz et al., Thixoforming of spray formed M2 tool steel, *International Journal of Material Forming* Vol. 3, Suppl.1 (2010) 755 – 758, DOI 10.1007/s12289-010-0880-3
- [15.] H. Bramann et al., Casting of a cold work steel alloy in semi-solid state, *Journal of Materials Processing Technology* 155-156 (2004) 1357-1364
- [16.] F. Knauf, R. Baadjou and G. Hirt, Analysis of semi-solid extrusion products made of steel alloy X210CrW12, *International Journal of Material Forming*, Vol. 2, Suppl. 1 (2009) 733-736 DOI 10.1007/s12289-009-0426-8
- [17.] S. Muenstermann et al., Semi-solid extrusion of steel grade X210CrW12 under isothermal conditions using ceramic dies, *Journal of Materials Processing Technology* 209 (2009) 3640–3649
- [18.] J. Dutkiewicz et al., Thixoforming technology of high carbon X210CrW12 steel, *International Journal of Material Forming* Vol. 2, Suppl. 1: 753 – 756 (2009), DOI 10.1007/s12289-009-0558-x
- [19.] L. Rogal et al., Characteristics of 100Cr6 bearing steel after thixoforming process performed with prototype device, *Trans. Nonferrous Met. Soc. China* 20 (2010) 1033-1036
- [20.] K. P. Solek et al., Characterization of thixoforming process of 100Cr6 steel, *Trans. Nonferrous Met. Soc. China* 20 (2010) 916-920
- [21.] W. Mao et al., Slurry Preparation and Rolling of Semi-Solid 60Si2Mn Spring Steel, *Journal of Material Science and Technology*, Vol. 19, No. 6 (2003)
- [22.] W. Mao et al., Semi-solid slurry preparation and rolling of 1Cr18Ni9Ti stainless steel, *Journal of University of Science and Technology Beijing*, Vol. 10, No.6 (2003)
- [23.] J.G. Li et al., Microstructural morphology of the semi-solid high carbon steel T12 before and after rheo-rolling, *Journal of University of Science and Technology Beijing*, Vol. 12, No. 2 (2005)
- [24.] M. Ramadan et al., Semi-solid processing of ultrahigh-carbon steel castings, *Material Science and Engineering A* 430 (2006) 285-291
- [25.] M.Z. Omar et al., Thixoforming of a high performance HP9/4/30 steel, *Materials Science and Engineering A* 395 (2005) 53-61
- [26.] R. Song et al., Investigation of the Microstructure of Rolled Semi-Solid Steel, *Journal of Materials Sciences and Technology*, Vol. 18, No. 3, (2002)
- [27.] H.V. Atkinson, Modelling the semisolid processing of metallic alloys, *Progress in Materials Science*, No. 50 (2005) 341-412
- [28.] M. Modigell, J. Koke, Time-Dependent Rheological Properties of Semisolid Metal Alloys, *Mechanics of Time-Dependent Materials* 3 (1999) 15-30

- [29.] D. Stoica, I. Ilca, Reflection regarding the obtaining of precursor material at semisolid state processing, Scientific Bulletin of the „Politehnica” University of Timisoara, Transaction of Mechanics, Editura Politehnica, Timișoara, ISSN 1224-6077, Tom 52(66), Fasc. 8, (2007) 43-48
- [30.] J.-Y. Li et al., Microstructural evolution and flow stress of semi-solid type 304 stainless steel, Journal of Materials Processing Technology, 161 (2005) 396-406
- [31.] D. Miloștean, M. Flori, Experimental research in pilot phase regarding the semisolid state processing of steel, Annals of the Faculty of Engineering Hunedoara, Mirton Publishing House, Timisoara, ISSN 1584-2673, Tome VII, Fascicule 3, (2009) 383-385
- [32.] B. Amin-Ahmadi, H. Aashuri, Semisolid structure for M2 high speed steel prepared by cooling slope, Journal of Materials Processing Technology, 210 (2010) 1632-1635
- [33.] S. Muenstermann, R. Telle, Wear and corrosion resistance of alumina dies for isothermal semi-solid processing of steel, Wear 267 (2009) 1566–1573
- [34.] Y. Birol, Testing of a novel CrNiCo alloy for tooling application in semi-solid processing of steel, International Journal of Material Forming (2010) 3:65–70, DOI 10.1007/s12289-009-0418-8
- [35.] S. Muenstermann, R. Telle, Ceramic tool concepts for the semi-solid processing of steel alloys, Mat.-wiss. u. Werkstofftech., Vol. 37, No. 4 (2006)
- [36.] Y. Birol, High-temperature abrasive wear testing of potential tool materials for thixoforming of steel, Tribology International 43 (2010) 2222-2230
- [37.] Y. Birol, Ni- and Co-based superalloys as potential tool materials for thixoforming of steel, International Journal of Material Forming, Vol. 3, Suppl. 1 (2010) 739-742
- [38.] A. Rassili et al., X38CrMoV5 hot-work tool steel as tool material for thixoforming of steel: Numerical and experimental evaluation, Trans. Nonferrous Met. Soc. China 20 (2010) 713-718
- [39.] D. Brabazon et al., Glazing of tool dies for semi-solid steel forming, International Journal of Material Forming, Vol. 2, Suppl. 1 (2008) 985-988, DOI 10.1007/s12289-008-0223-9
- [40.] S.N. Aqida et al., Thermal stability of laser treated die material for semi-solid material forming, International Journal of Material Forming, Vol. 2, Suppl. 1 (2009) 761-764





¹ Adrian GĂVĂNESCU

REFINING OF STEEL BY USING SYNTHETIC SLAG

¹ UNIVERSITY POLITEHNICA OF TIMISOARA, FACULTY OF ENGINEERING FROM HUNEDOARA, ROMANIA

ABSTRACT:

Treating the liquid steel with synthetic slag in the casting ladle is an efficient and relatively cheap method of reducing the non-metal inclusion content by reducing the sulphur and oxygen content. The synthetic slag used in the experiments corresponds to the CaO - Al₂O₃ system, which ensures, by their composition, the extraction of sulphur and oxygen from the liquid steel, based on Nernst's repartition law. The method also has the advantage of being applicable in all the processing technologies. The paper presents the results and conclusions of the laboratory experiments regarding treatment of steel with various composition synthetic slags.

KEYWORDS:

synthetic slag, steel, desulphurization, deoxidation

1. INTRODUCTION

The essence of the process of using synthetic slag consists in making a contact on a large surface between the melted steel and a slag having a composition selected to ensure an advanced steel deoxidation and desulphurization.

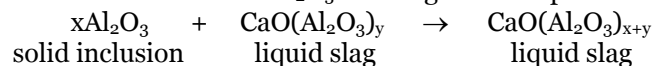
The disadvantages of diffusion (extraction) deoxidation are removed by this procedure as it is made by emulsifying the steel with the slag (which does not contain CaC₂) and the process is very fast (10 to 12 minutes) [1].

The admixture represents 2 – 4 % of the liquid steel quantity in case of using solid synthetic slag and 3 – 6% in case of using melted slag.

It was proved by practice that the most effective slag are the ones from the systems CaO – Al₂O₃, CaO – Al₂O₃ – CaF₂, CaO – Al₂O₃ – CaF₂ + NaF.

Compositions of some slag on the market are presented in Table 1 [2]. The composition of these slag can be modified according to the requirements of the users in the metallurgic industry.

The used calcium-aluminate synthetic slag are liquid at work temperature and they participate not only in the deoxidation process (by oxygen diffusion), but also in the removal of inclusions they come in contact with. When solid Al₂O₃ inclusions come into contact with CaO – Al₂O₃ liquid slag, the alumina inclusions are absorbed and form liquid calcium-aluminates which are richer in Al₂O₃. The reaction between Al₂O₃ and slag can be represented as follows:



Beside the deoxidation effect, the synthetic slag, mainly the ones with a high content of CaO, due to their increased basic capacity and fluidity, high dispersion and contact surface increase capacity ensure favourable conditions for advanced desulphurization of steel.

Table 1. Synthetic slag available on the market

	CaO(%)	Al ₂ O ₃ (%)	SiO ₂ (%)	CaF ₂ (%)	MgO(%)	Na ₂ O(%)	FeO(%)
1.	72-77	0-2	19-24	2-4	-	0,5-1,5	-
2.	75-80	12-15	0,7-1,5	4-6	-	-	-
3.	17-20	63-68	< 4	-	7-10	-	-
4.	70	15	0,9	-	2,5	-	0,5
5.	50	42	2	-	1,5	-	1,5

2. DISCUSSIONS

Laboratory experiments were conducted to verify the efficiency of synthetic slag deoxidation and desulphurization capacity. Experiments consisted in melting in a Tamann furnace steel samples with the next composition (Table 2)

Table 2. Compositions of steel before the treatment

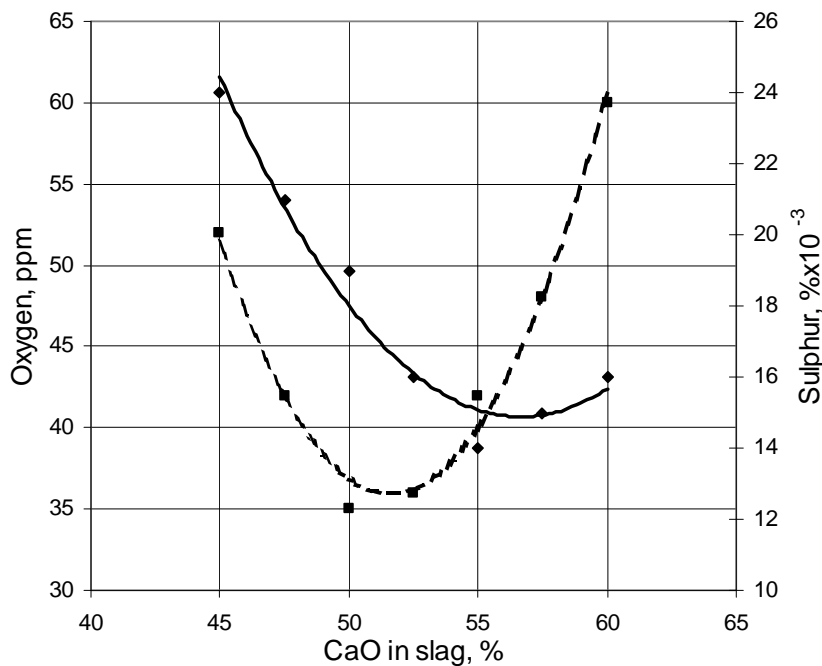
C [%]	Mn [%]	Si [%]	P [%]	S [%]	O _{total} [p.p.m.]
0.34	0.56	0.28	0.031	0.030	78

A quantity of 4 kg of steel was melted for each determination of oxygen and sulphur content after a treatment under 80 grams synthetic slag for 10 minutes. The compositions of the synthetic slag and the results of the oxygen and sulphur content measurements after treatment are shown in Table 3 and in Figure 1.

The dependence between slag compositions and oxygen and sulphur contents of steel after treatment is:

$$[O] = 0,3524 \cdot (CaO)^2 - 36,386 \cdot (CaO) + 975,19 \quad R^2 = 0,98 \quad (1)$$

$$[S] = 0,0705 \cdot (CaO)^2 - 7,9857 \cdot (CaO) + 241,1 \quad R^2 = 0,96 \quad (2)$$



oxygen (---■---) and sulphur (—◆—) after treatment

Fig. 1. Influence of slag compositions to oxygen and sulphur contents of steel

Table 3. Contents of oxygen and sulphur before and after treatment

	Slag compositions[%]		Oxygen [ppm]		Sulphur [%x10 ⁻³]	
	CaO	Al ₂ O ₃	before	after	before	after
1	45,0	55,0	30	24	78	52
2	47,5	52,5	30	21	78	42
3	50,0	50,0	30	19	78	35
4	52,5	47,5	30	16	78	36
5	55,0	45,0	30	14	78	42
6	57,5	42,5	30	15	78	48
7	60,0	40,0	30	16	78	60

In conclusion, calcium-aluminate solid synthetic slag, with a content of CaO between 51 ... 56% will ensure a removal of about half of initial quantity of sulphur and oxygen from treated steel.

For establishing the regression equations between the quantities of synthetic slag and final contents of oxygen and sulphur were made experiments using different quantities of slag, with a duration of 10 minutes.

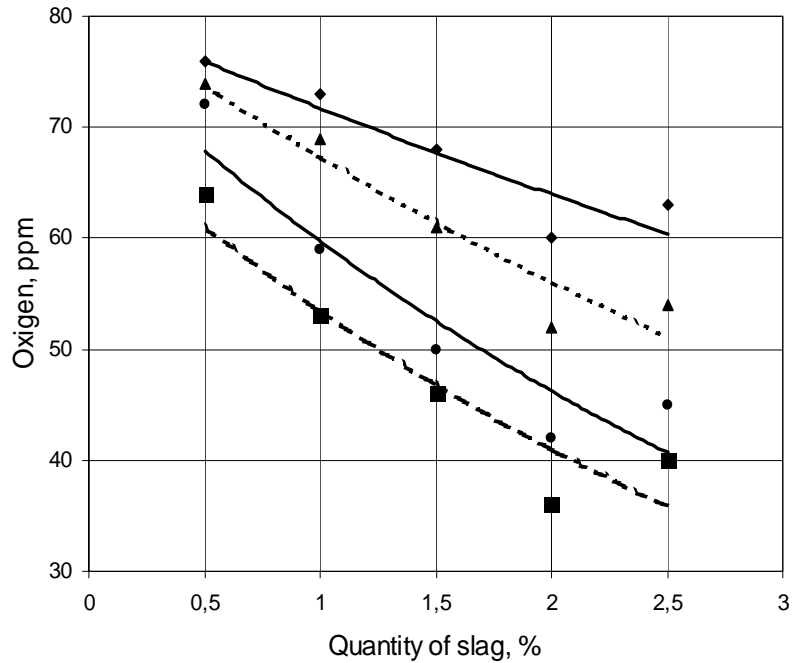
Dependence between the oxygen and sulphur contents of steel after treatment and the quantity of synthetic slag is:

$$[O] = a \cdot e^{-bQ} \quad (3)$$

$$[S] = c \cdot e^{-dQ} \quad (4)$$

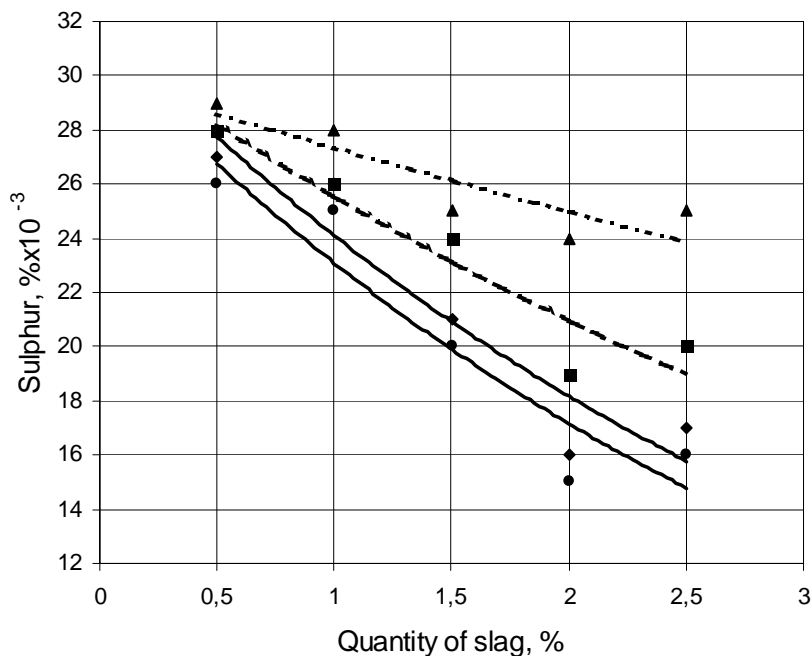
and is presented in table 4 and in figures 2 and 3.

Quantity of synthetic slag Q is in percent from the quantity of steel and the high values of correlation coefficient shows tide interdependency between the oxygen and sulphur contents of steel, after treatment and the quantity of synthetic slag.



CaO-Al₂O₂ slag with: — ▲ — 45% CaO — ■ — 50% CaO — ● — 55% CaO — ◆ — 60% CaO

Fig. 2. Influence of slag quantity to oxygen contents of steel



CaO-Al₂O₂ slag with: — ▲ — 45% CaO — ■ — 50% CaO — ● — 55% CaO — ◆ — 60% CaO

Fig.3. Influence of slag quantity to sulphur contents of steel

Table 4. Dependence between the oxygen and sulphur contents of steel after treatment and the quantity of synthetic slag - Q [% from steel quantity]

Slag composition		Oxygene [ppm]			Sulphur [%x10 ⁻³]		
CaO [%]	MgO [%]	Coefficient of ecuation		Coeff. of correlation R ²	Coefficient of ecuation		Coeff. of correlation R ²
		a	b		c	d	
45	55	80,783	0,1826	0,9002	29,915	0,0902	0,7596
50	50	69,961	0,2654	0,8495	31,115	0,1973	0,8739
55	45	76,786	0,9141	0,9141	30,797	0,3027	0,9229
60	40	80,401	0,1143	0,8406	31,947	0,2822	0,8756

For establishing the regression equations between the duration of treatment τ and final contents of oxygen and sulphur were made experiments using 80 grams of synthetic slag (representing 2% from the steel quantity) with different contents.

Dependence between the oxygen and sulphur contents of steel after treatment and the duration of treatment is:

$$[O] = a \cdot e^{-b\tau} \quad (5)$$

$$[S] = c \cdot e^{-d\tau} \quad (6)$$

and is presented in table 5 and in figures 4 and 5.

Table 5. Dependence between the oxygen and sulphur contents of steel after treatment and the duration of treatment with synthetic slag - τ [minutes]

Slag composition		Oxygene [ppm]			Sulphur [%x10 ⁻³]		
CaO [%]	MgO [%]	Coefficient of ecuation		Coefficient of correlation R ²	Coefficient of ecuation		Coefficient of correlation R ²
		a	b		c	d	
45	55	70,088	0,0272	0,8974	30,152	0,0183	0,8647
50	50	60,625	0,0477	0,8219	28,031	0,0340	0,8084
55	45	70,335	0,0518	0,8539	27,492	0,0582	0,8450
60	40	70,469	0,0140	0,9043	28,237	0,0490	0,8937

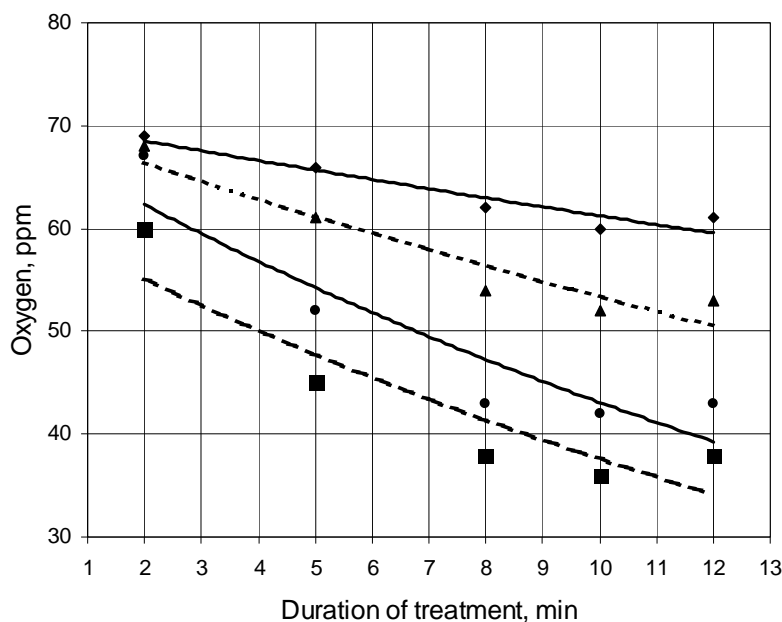


Fig.4. Influence of treatment duration to oxygen contents of steel

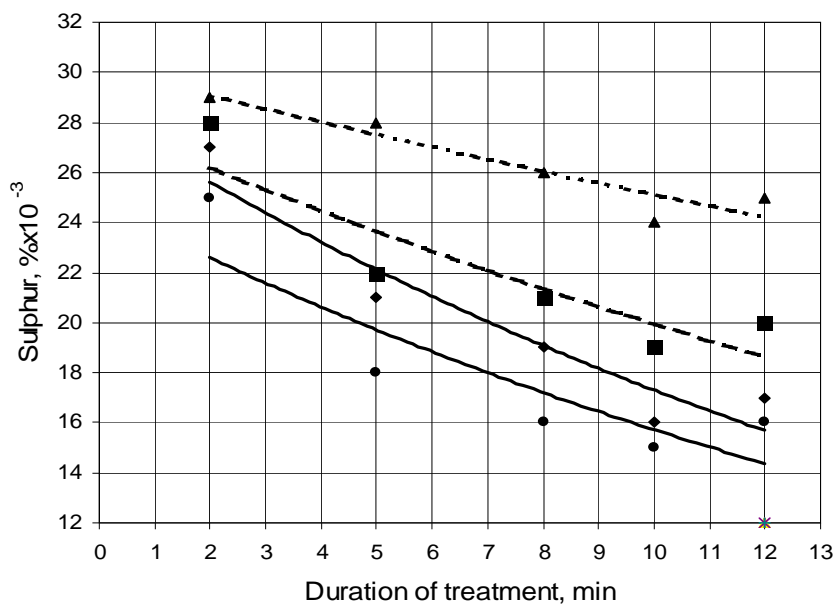


Fig.5. Influence of treatment duration to sulphur contents of steel

CaO-Al₂O₃ slag with:

—▲— 45% CaO ; —■— 50% CaO ; —●— 55% CaO ;—◆— 60% CaO

The equations which describe the dependency between the oxygen and sulphur contents of steel, after treatment and duration of treatment are either exponential or lineal, but both ensure the increasing of the deoxidation and desulphurization process, through increasing treatment duration (τ is in minutes).

3. CONCLUSIONS

The following conclusions can be drawn regarding the deoxidation and desulphurization effect of synthetic slag:

- ❖ the optimal contents of CaO from calcium – aluminate slag is situated between 50 ... 55%, richer in CaO ensuring a better desulphurization of steel;
- ❖ the contents of oxygen and sulphur are decreasing exponentially with increasing of slag quantity, a quantity of solid slag representing 1,5 ... 2 % from steel is optimal, using a bigger quantity is not justified because it raise melting problems;
- ❖ the optimal duration of treatment is 8 ... 10 min., an increasing is not justified because it causes an excessive coldness of liquid steel;
- ❖ the steel treatment with synthetic slag can be considered as the most accessible and safe method to effectively improve the qualities of regular steels, having positive economic effects by reducing the duration of furnace processing and decreasing the ferro-alloy consumption.

REFERENCES

- [1.] I.Dragomir, Teoria proceselor siderurgice, Editura didactică și pedagogică, București, 1985.
- [2.] A.Cubero, J. Molinero, C. Bertrand, Secondary steelmaking synthetic slags for ultra clean steel production, in Proceedings of the 5th International Conference on clean steel, Balatonfured, Ungaria, June 1997, pp. 140-150
- [3.] A. Găvănescu, Effects of synthetic slag steel treatment, in Proceedings of the National Conference on metallurgy and materials science, București, Sept. 2001, pp. 96-101
- [4.] A. Găvănescu, G. Nica, Experiments and results regarding the refining of steel by synthetic slag treatment, in Proceedings – Istrazivanja i razvoj mašinskih elementa i sistema IRMES – Jahorina Sarajevo, Sept. 2002, pp. 409-414





EFFICIENCY OF MAINTENANCE IN STEEL MAKING INDUSTRY

¹⁻³. BADISCHE STHAL ENGINEERING GMBH, GERMANY

⁴. MEMBER OF ROMANIAN SCIENCE AND TECHNIQUE ACADEMY, FACULTY OF ENGINEERING HUNEDOARA, ROMANIA

ABSTRACT:

Efficient maintenance brings efficient energy consumption and efficient environmental work of the steel making equipments. Maintenance is a real partner for profit.

BSE – Badische Stahl Engineering - “Best practice” tools give to the Steel Making Companies, the possibility to know where their “maintenance efficiency” is located compared to others in the industry.

KEYWORDS:

Maintenance; Effectiveness; Efficiency; Best practice; Steel making industry.

1. INTRODUCTION

The steel making industry, steel represent in Romania a very important part of GDP. In this industry branch the crisis appear to be at the final. In August 2010 as compared to August 2009 gross industrial production index increased by 5.7% due to the production increase in electricity, gas, steam and air conditioning supply sector (+8.5%) and in manufacturing (+6.2%). The industrial branches which especially determinate the increases of the manufacturing gross index were: Metallurgy (+27.0%).

Steel production in Romania belongs to the international owners – more than 95 % and the international trend of the steel making industry is also apprehend in Romania.

In steel making industry the volume and the costs of production are very important for a profitable activity. It is important to see the whole picture to make the right decisions and to follow the right strategy. In our conception there are two options:

Focus on direct costs:

- ❖ Limited market
- ❖ Low sales prices
- ❖ Low contribution margin per ton
- ❖ Cost saving (expenditures) is crucial
- ❖ Indirect costs are in this situation not that important because additional output would only increase stock level and bind capital
- ❖ In this case it is possible to increase the risk of delays, while less money is spent for maintenance activities

Focus on indirect costs:

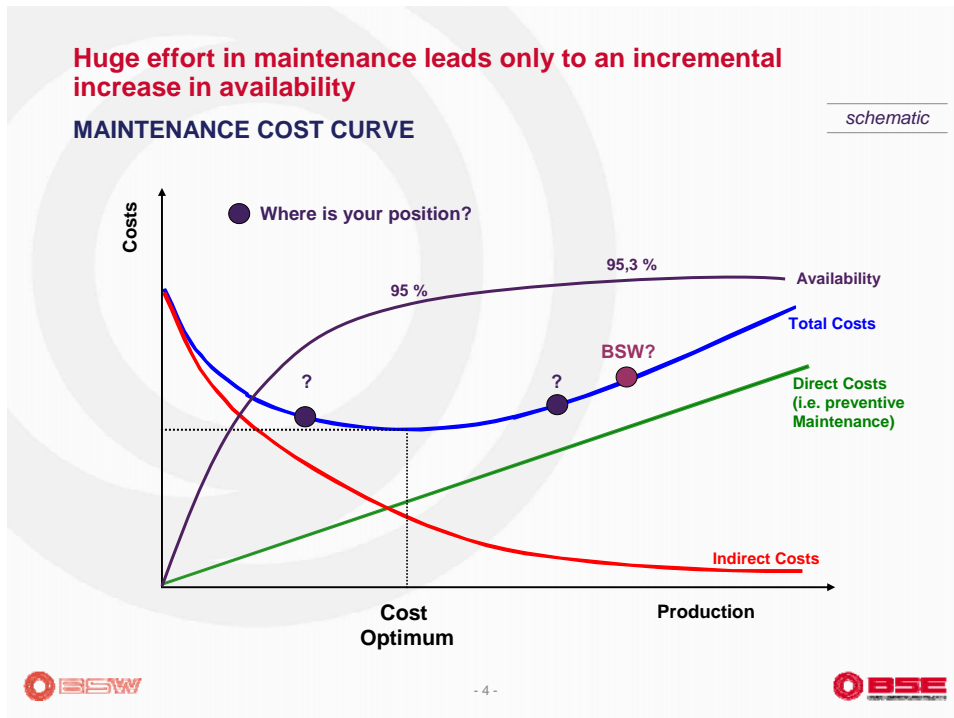
- ❖ Strong market demand
- ❖ Attractive sales prices
- ❖ High contribution margin per ton
- ❖ High availability and operation time required to meet market demand
- ❖ Focus on time, spend more for direct maintenance cost in order to reduce indirect cost
- ❖ Achieved additional contribution margin is higher, than expenditure for maintenance

Maintenance is operational partner for efficiency; especial in Steel making industry, operational should recognize the benefits of working together with maintenance, as a supportive team to reduce unplanned breakdowns, to increase equipment effectiveness, and to reduce overall maintenance costs.

The future capable company has a firm understanding of physical asset management and maintenance process and its important role. It recognizes the contribution of maintenance to total operations' success and profitability. Effective maintenance and physical asset management are closely linked to success and profitability.

The Steel making Companies must analyze and find the most efficient maintenance process.

BSE developed a concept named "Best practice". Best Practice Study covers very important aspects of successful steel operations and the main indicator is "Total operational efficiency". Maintenance efficiency is one of the component, analyze by us in this paper. Maintenance is forever.



2. MCM – MAINTENANCE COST MANAGEMENT

BSW – Badische Stahlwerke GmbH, is one of the most productive Mini Mill in the world; few years before the maintenance cost start to increase continuously, like contra-measure BSW communicate this issue to BSE specialists and after proper researches in the plant come MCM concept. Was analyze all the components of Maintenance costs: Material costs, contractors, own maintenance, etc. Was also analyzing the saving possibilities, risk estimation and major issues concerning maintenance at BSW in a full year (2005).

	Site issues	Results
Integration of production team	<ul style="list-style-type: none"> -Too little integration of production team into maintenance processes -Lower responsibility and less care for equipment by operator -Unconscious handling -Strong wear 	High costs for maintenance and spares parts
Capacity balance	<ul style="list-style-type: none"> -Strong separation between the sectors, although the activities are not that different -The need of employees were counted for each sector -Free capacities between the ranges are not used -Experiences of sectors are not exchanged 	More contracting
Shift work	<ul style="list-style-type: none"> -70 % of the BSW maintenance employees work in the 5-shift-System (112 of 162) -Shift work is primarily risk insurance. -The effectiveness of standard works is smaller. -No comprehensive job planning -Only absolutely necessary work is done, other jobs shifted to dayshift or shutdown day 	More contracting

Results three points to starting from:

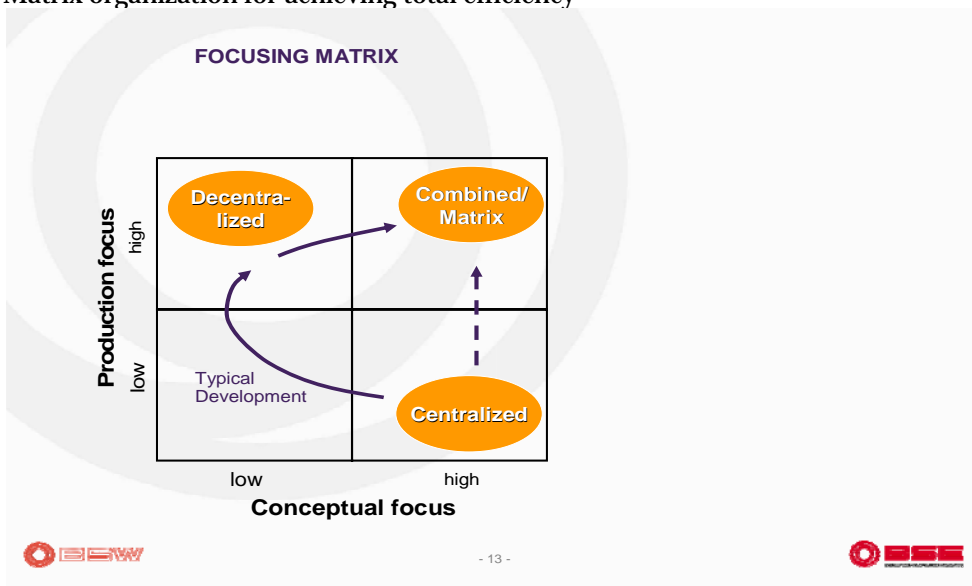
- ❖ Material costs
- ❖ Contractors
- ❖ Own maintenance

Possible solutions of the maintenance optimisation can be represented by side condition for solution:

- ❖ Adapt the maintenance to the changed conditions
- ❖ Engage the production stronger
- ❖ Improve the work scheduling
- ❖ Create capacities in the own maintenance
- ❖ Make a comprehensive common strategy possible
- ❖ Reduce contracting significantly
- ❖ Offer a high work quality and improvement potential with spare part repairs

An optimum maintenance organization must be adapted to the individual situation of a mini mill

- ❖ Centralized maintenance for building up skills and knowledge
- ❖ Decentralized maintenance for pushing productivity
- ❖ Matrix organization for achieving total efficiency



Action plan:

1. Appropriate maintenance strategy to be establish

In general three different maintenance strategies exist

- **Breakdown strategy (run to failure)**
- **Condition based preventive maintenance (exchange after inspection)**
- **Time based preventive maintenance (exchange after fixed period of time)**

Depending on the impact on production, an appropriate strategy needs to be applied, together with other important tools: 5 “S” – House quipping and Continuous improvement concept.

2. Detailed down day planning and appropriate coordination during execution are factors for efficiency

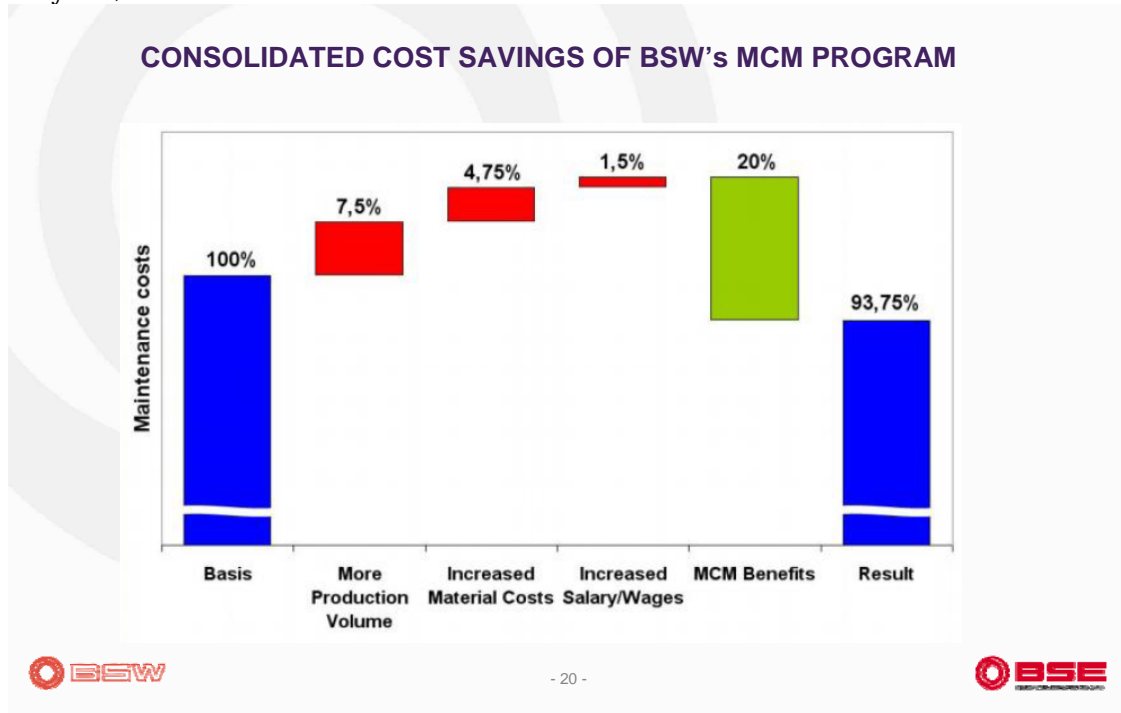
3. A detailed and comprehensive delay reporting is the base for continuous optimization

PROCESS MONITORING – DELAY REPORTING

- Reporting covers the
 - recording of production delays (production loss)
 - recording of equipment problems (no production loss)
- Equipment problems must not be identical with production delays.
- Not every equipment problem causes a production delay.
- Therefore it is important to analyze the combination of production records and maintenance records.
- Production and maintenance reports should be computerized and should use a code system based on a common categorization of equipment. This allows quick evaluation.

3. RESULTS OF MCM

After MCM implementation at BSW, considerable savings could already be realized within three years,



Can maintenance efficiency be measured?

The tool name: “Best practice” was developing by BSE.

The BSE Best Practice Study covers every important aspect of steel making and helps to determine the Company position in the industry.

a). Background Best Practice Study

- The Best Practice Study compares steel plants and rolling mills from all over the world in order to find the best performers, e.g. per region or steel quality.
- It is possible to carry out an overall benchmark, and also to study the details and compare consumption figures or cost on a detailed level (e.g. kWh per ton...).
- Our customers can position themselves within this framework in order to benchmark their performance with the industry and also to identify potentials for future improvement.
- Selected Key Performance Indicators (KPI's) are used for the comparison

b). Holistic approach through four different areas:

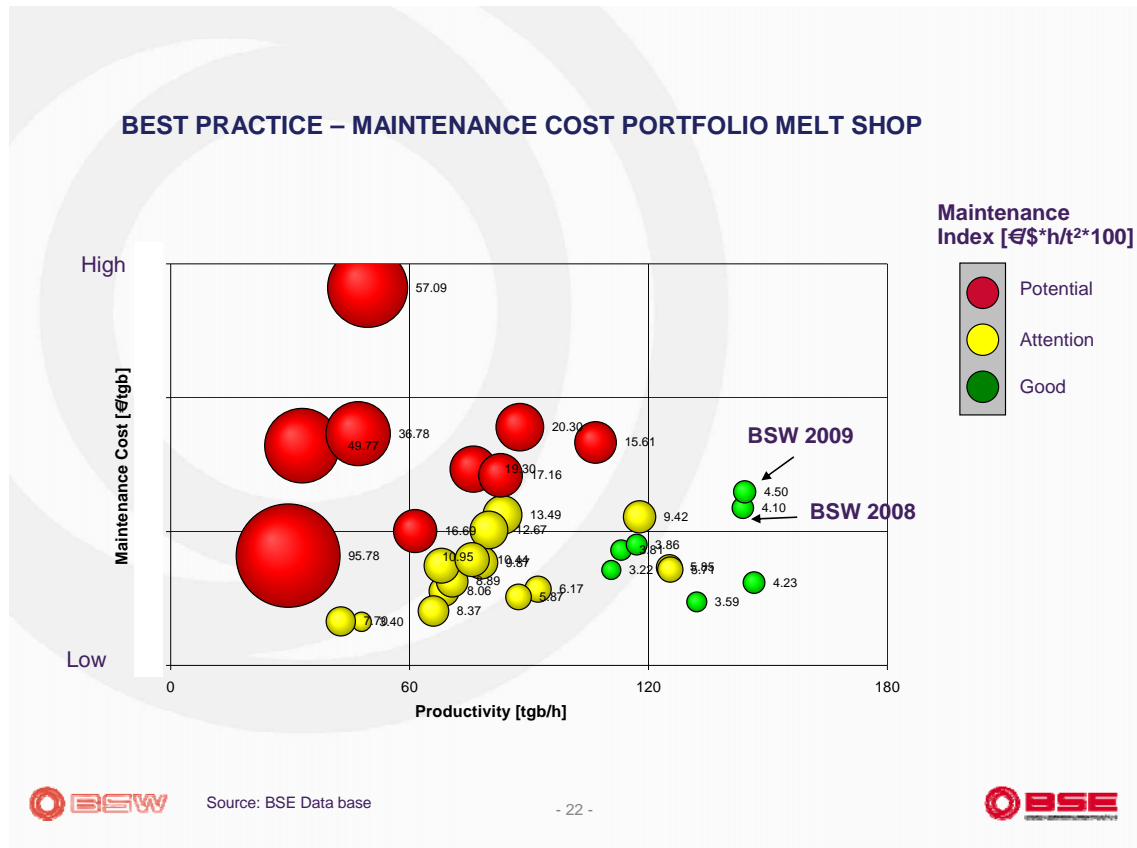
- Productivity Management
- Cost Management
- People Management
- Environmental Management

c). Identification of Best Performers per grade or region

d). Determination of position within industry and identification of potentials for further improvement

In our case, to measure and compare the maintenance efficiency and effectiveness, we try to find a correlation between the maintenance efforts by means of money and the productivity in tones per hour. The size of the bubbles represents the maintenance index itself. Green bubbles are good, red bubbles are bad.

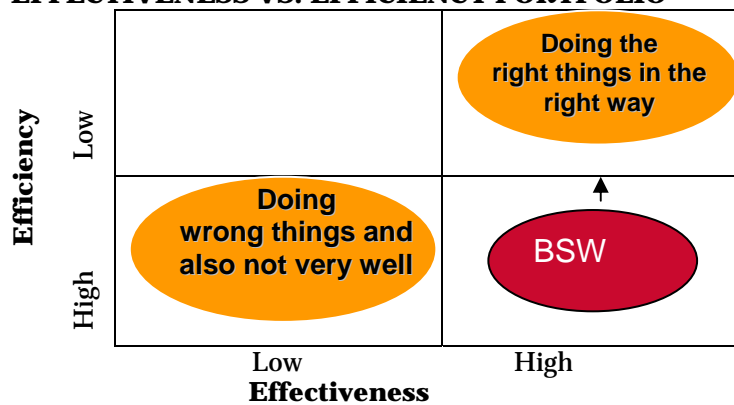
Efficient maintenance is represented by low costs and high output. But high output also allows higher absolute maintenance costs. This graph should give the customer an indication where his own maintenance efficiency is located compared to others in the industry.



4. CONCLUSIONS

Effectiveness comes before efficiency, but the goal is “doing the right things in the right way”

EFFECTIVENESS VS. EFFICIENCY PORTFOLIO



If you want to know where your position in the industry is, you can apply to Best practice, free of charge – “bestpractice@bse-kehl.de”

REFERENCES

1. Reiner Hageman - Efficiency in maintenance - 4” International Mini-Mill symposium “We SEE the future” April 25 to April 28, 2010 in Schluchsee / Germany.
2. *** The future Capable Company – Maintenance Life Cycle Engineering Inc. 2002.
3. BSE – Best practice in the steel industry, framework for Mini Mills - 2010
4. www.bse-kehl.de





¹Iulian RIPOSAN, ²Mihai CHISAMERA, ³Stelian STAN

GRAPHITE NUCLEATION IN GREY CAST IRON – A REVIEW

¹⁻³.POLITEHNICA UNIVERSITY OF BUCHAREST, BUCHAREST, ROMANIA

ABSTRACT:

A three-stage model for the nucleation of graphite in grey irons has been proposed. Stage 1 involves formation of small oxide-based sites (usually less than 2.0 μm) in the melt. Stage 2 involved precipitation of complex (Mn,X)S compounds (usually less than 5.0 μm) nucleated by stage 1 micro-inclusions. Finally in stage 3 graphite nucleates on the sides of the (Mn,X)S compounds which have low crystallographic misfit with graphite. Three groups of elements are important to sustain this sequence for effective graphite nucleation. These are strong deoxidizing elements, such as Al and Zr, to form a high count of very small stage 1 micro-inclusions; Mn and S to sustain MnS type sulphide formation; and inoculating elements which act in the first stage and/or in the second stage of the graphite nucleation sequence. Inoculating elements improve the capability of (Mn,X)S compounds to nucleate graphite. In inoculated irons the (Mn,X)S compounds are more complex. They have a lower Mn/S ratio and higher capability to nucleate graphite, especially when preconditioning/inoculating elements contribute with a high count of effective stage 1 particles.

KEYWORDS:

Grey iron; Graphite nuclei; Graphite nucleation model; Inoculation; Preconditioning; Oxides; Sulphides





¹I. HULKA, ²D. UȚU, ³V.A. ȘERBAN

MICRO-SCALE SLIDING WEAR BEHAVIOR OF HVOF SPRAYED WC-Co(Cr)

¹⁻³DEPARTMENT OF MATERIALS AND WELDING SCIENCE, "POLITEHNICA" UNIVERSITY OF TIMIȘOARA, ROMANIA

ABSTRACT:

The paper presents the investigations of the sliding wear behavior of two different thermal sprayed cermet coatings. WC-Co and WC-CoCr powders were HVOF sprayed on a C45 steel substrate using an ID Cool Flow gun. Scanning electron microscopy (SEM) and X-Ray Diffraction (XRD) were performed in order to investigate the coatings morphology as well as the phase modification achieved through the HVOF spraying process. Tribological tests concerning the sliding wear behavior of the tested materials were performed using the pin-on-disk method.

KEYWORDS: sliding wear behavior, thermal sprayed cermet coatings

1. INTRODUCTION

In industries, mechanical components have to operate under severe conditions such as high load, speed or temperature and hostile chemical environments. Usually, various surface treatments have been used in order to improve the surface characteristics. Such treatments are: ion implantation, laser nitriding alloying, physical vapor and thermal spraying deposition etc [1].

Thermal spray coatings are becoming increasingly used as surface engineering option to resist corrosive and sliding wear and as thermal barriers in many industries [2]. Thermal spraying involves projection of powders particles into a high temperature flame, produced by igniting hydrogen, oxygen and kerosene, where they are melted and accelerated on the substrate surface. The resulted coatings are formed by the immediate solidification of the molten droplets on the substrate surface of lower temperature where they form splats.

High velocity oxygen fuel (HVOF) is a thermal spraying method which allows spraying of coatings with advanced and often unique properties. Therefore the process has been used in numerous advanced applications and has become very popular over the last two decades [3].

One of the great advantages of the HVOF process is the higher velocity reached by the particles and the low temperatures involved which minimizes any potentially damaging effect to the coating and substrate [4].

Wear protection is an important application field of HVOF sprayed coatings. HVOF technology has improved over the years and now provides coatings with better compaction and low chemical decomposition, especially for WC- based cermet coatings [5].

It is known that high velocity oxy-fuel (HVOF) spraying provides superior results than any other thermal spraying technology by manufacturing cermet coatings, because of the gas velocity and lower flame temperature [6]. A cermet is a composite material composed of ceramic and metallic materials which have the optimal properties as high temperature resistance, high hardness and the ability to undergo plastic deformation.

WC- based coatings are deposited not only on originally manufactured components but also on worn areas of used components for repair purpose. The use of WC based thermal spray coatings has been increasing in several areas due to their potentially high erosion and sliding wear resistance.

The present work investigates the sliding wear behavior of the obtained coatings deposited on C45 specimens using an HVOF gun and as feedstock WC-Co 86 14 and WC-CoCr 86 10 4 micro powders.

2. EXPERIMENTAL PROCEDURE

The substrate used in this study was rectangular C45 still plates with dimensions of 50x50mm which were thoroughly sand-blasted with electrocorindon in order to enhance the binding force between the substrate and the deposited coating. After the grinding process the samples were cleaned with acetone.

The feedstock material used in the study were WC based cermet powders, respectively WC-Co 86 14 and WC-CoCr 86 10 4 micro powders.

The morphology of the powder and of the sprayed samples has been characterized by scanning electron microscopy (SEM) and X-Ray diffraction (XRD) using a $\text{Cu-K}\alpha$ radiation.

The sliding wear resistance was determined using the pin-on-disk method by calculating the variation of the wear track depth with the applied load.

The normal load applied of the ball (WC-Co with a 6 mm diameter) was 10 N, relative velocity between the ball and surface was $v = 20$ cm/s, and the testing distance 1000 m (the trajectory was a circle with a radius of 5.4 mm). The relative humidity was 65 %.

3 RESULTS AND DISCUSSIONS

3.1 Coating morphology

The morphology of the used powder is shown in the SEM micrographs from figure 1. The powder particles are spherical having the size between $-45+15$ μm .

Figure 2 and 3 presents the SEM micrographs of the HVOF sprayed coatings at different magnification (x 500 and x 2000). The thickness of the obtained coatings was about 200 μm .

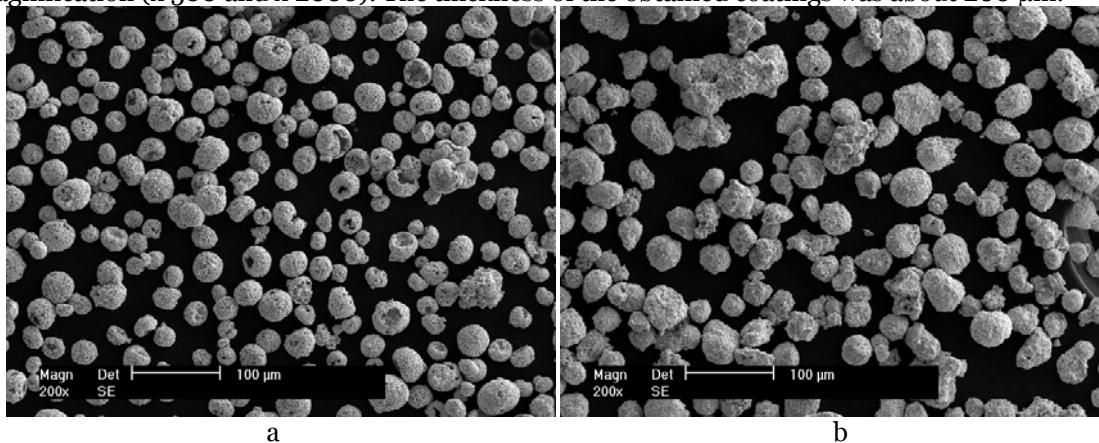


Fig. 1: SEM micrographs of the WC Co (a) and WC CoCr (b) powder

In both cases one may observe a good adhesion between the coating and substrate (Fig.2a and 3a). Comparing the SEM images at higher magnitudes (Fig.2b and 3b) both HVOF sprayed coatings present a certain degree of porosity respectively of internal oxidation.

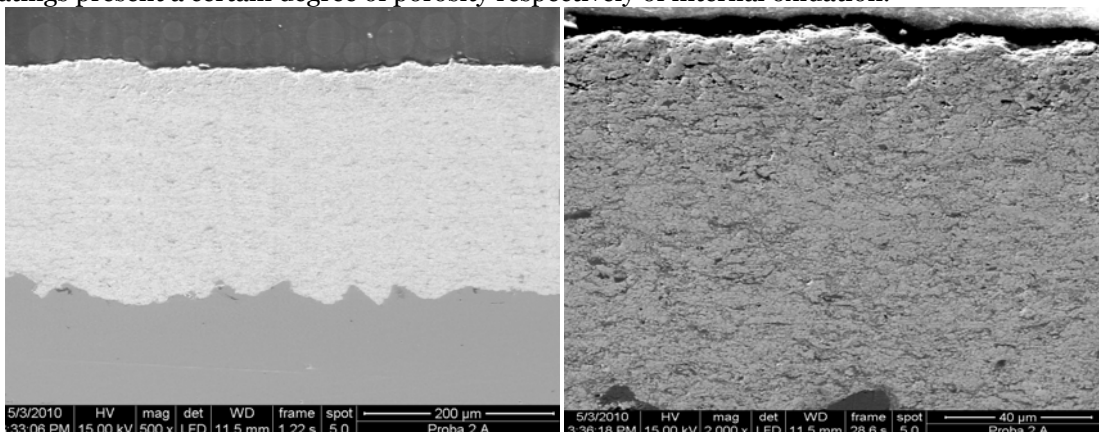


Fig. 2 SEM micrographs of the WC Co coatings

The XRD patterns of the WC-Co(Cr) sprayed coatings are similar, no transformation of the WC-phase into W_2C -phase occurred during the deposition process (figure 4). However one may see a broad signal corresponding to the WC_{1-x} -phase, which indicates a light decarburization of the WC-phase.

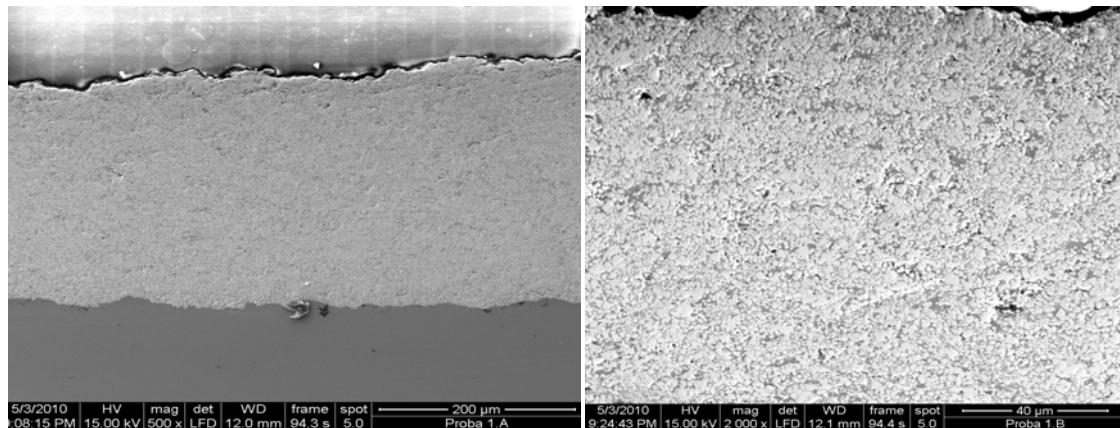


Fig. 3 SEM micrographs of the WC CoCr coatings

The Co- and CoCr-phases corresponding to the metallic matrix were not identified by XRD-measurements due to its low content in the chemical composition.

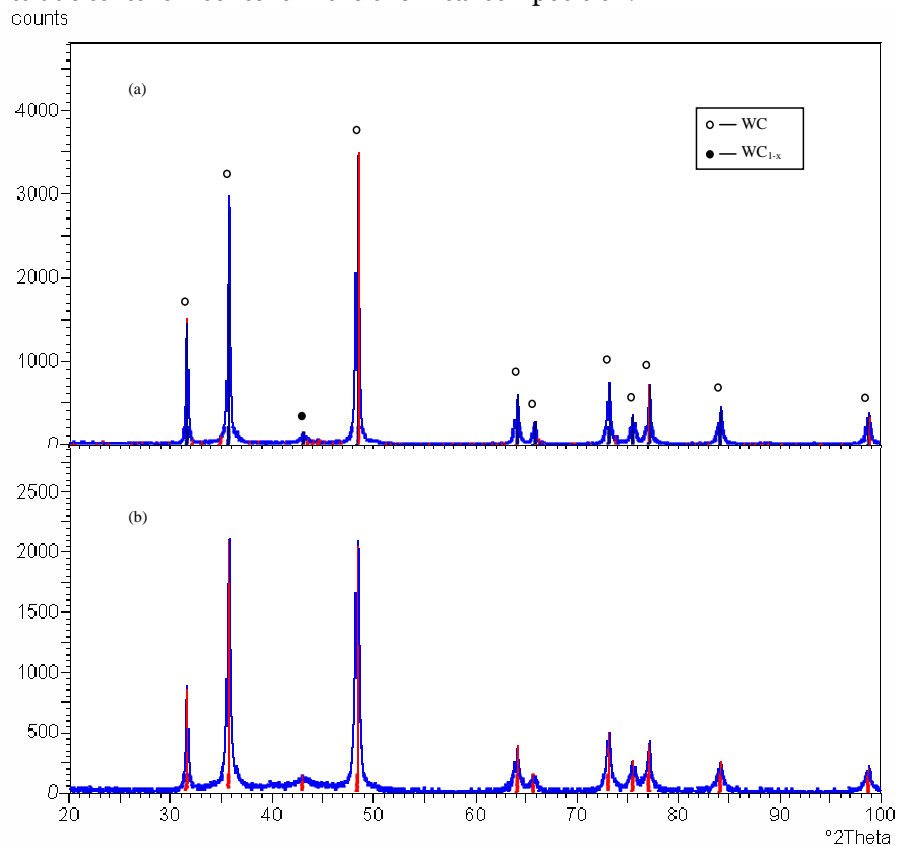


Fig. 4 X-ray diffraction patterns of sprayed coatings (a) WC-Co coating, (b) WC-CoCr coatings

3.2 Wear resistance tests

The pin on disk tests indicated that sliding wear resistance of the deposited coatings was different. The results are summarized in table 1 and the sliding wear rates histograms are shown in figure 5.

Comparing the obtaining result it can be seen that the material loss in case of WC Co was higher in comparison with the WC CoCr coatings. The phenomenon can be explained by the fact that addition of Cr to WC-Co improves binding of the metallic matrix with the WC grains and provides better wear resistant coating.

Table 1 Wear rate of the coatings.

Coating	Wear rate*10 ⁻⁷ [mm ³ /N/m]
WC-Co	51.71
WC-CoCr	39.21

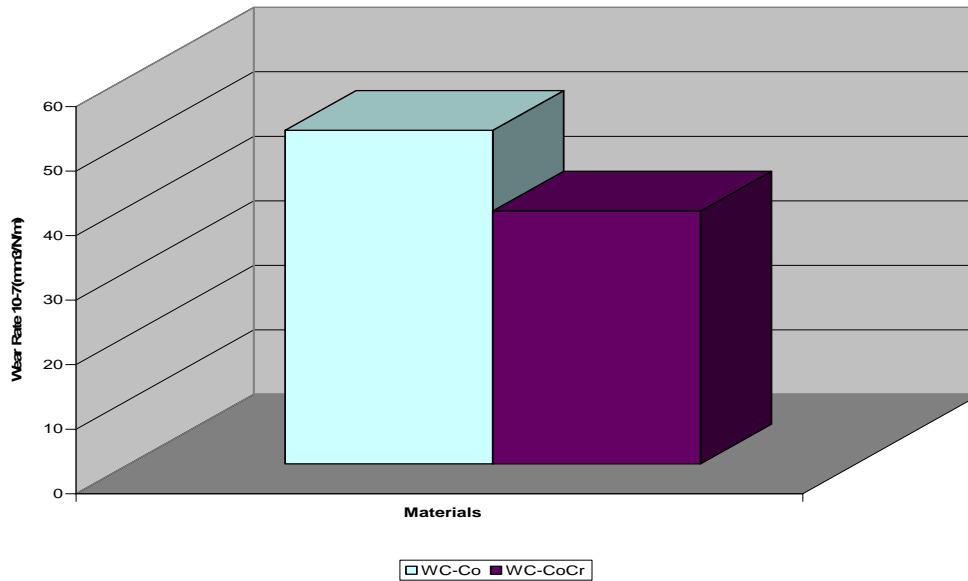


Fig. 5 Sliding wear rates of the tested samples

4. CONCLUSIONS

Different HVOF coatings using WC-Co and WC-CoCr powders have been deposited onto the surface of a C45 steel substrate. The sliding wear resistance of the both coatings was analyzed using the pin on disk method.

Analyzing the obtaining results it was found that WC-Co coating has a higher wear rate in comparison with the WC-CoCr. This phenomenon can be explained by the fact that addition of Cr to WC-Co improves binding of the metallic matrix with the WC grains and provides better wear resistant coating.

In conclusion it can be said that WC-CoCr is considered to be a potential wear resistant coating material as compared to WC-Co coating.

ACKNOWLEDGEMENT

This work was partially supported by the strategic grant POSDRU 2009 project ID 50783 of the Ministry of Labor, Family and Social Protection, Romania, co-financed by the European Social Fund – Investing in People.

REFERENCES

- [1.] Prince M, Gopalakrishnan P, Duraiselvam Muthukannan, More Satish D, Naveen R, Natarajan S. : *Study of Dry Sliding Wear of Plasma Sprayed Mo-Ni/Cr - Ti-6Al-4V Tribo Pair*, European Journal of Scientific Research, ISSN 1450-216X Vol.37 No.1, 2009, pp.41-48;
- [2.] Hodgkiss T, Neville A.: *An analysis of environmental factors affecting corrosion behavior of thermal spray cermet coatings*, Proceedings of the 15th International Thermal Spray Conference, May 2009, Nice, France, pp. 25-29;
- [3.] Klaus E. Schneider, Vladimir Belashchenko, M. Dratwinski, S. Siegmann, Alexander Zagorski: *Thermal Spraying for Power Generation Components*, WILEY-VCH Verlag, GmbH & Co. KGaA, Weinheim, 2006;
- [4.] T. Sudaprasert, P.H. Schipway, D.G. McCartney: *Sliding wear behavior of HVOF sprayed WC-Co coatings deposited with both gas-fuelled and liquid fuelled system*, Wear, Vol. 255, 2003, pp. 943-949;
- [5.] V. A. D. Souza, A. Neville: *Corrosion and synergy in a WC-CoCr HVOF thermal spray coating – understanding their role in erosion-corrosion degradation*, Wear, Vol. 559, pp. 171-190;
- [6.] V.A. Serban, C. Codrean, D. Utu, I. Hulka: *Obtaining of High Performance WC-CoCr CermetCoatings. Alternative Ecological Spraying Methods at Reduced Power Levels*, The 3rd WSEAS International Conference on LANDSCAPE ARCHITECTURE, Timisoara, Romania, October 21-23, 2010;





¹Doina PETRE

THE INFLUENCE OF ELABORATION CONDITIONS UPON THE TENACITY OF SOME ALL PURPOSE STEELS

¹ UNIVERSITY POLITEHNICA OF TIMISOARA, FACULTY OF ENGINEERING FROM HUNEDOARA, ROMANIA

ABSTRACT:

The paper introduces the relationships established between the elaboration conditions (e.i. the chemical composition and the quieting degree) and the level of cold plastic deformation the one part, and the tenacity of some all-purpose steels. The conclusions define the maximum admitted level of deformation in order to preserve an acceptable tenacity of steel, as well as the compulsory content in aluminum left in the steel which can guarantee a minimum level of tenacity.

KEYWORDS:

steel, aluminium, tenacity

1. INTRODUCTION

Since all-purpose steels may be looked for in certain fields and be subject to particular conditions of mechanical shock strains, we did some experiments meant to establish correlations between the chemical composition and the degree of deformation on the one part, and the shock break energy on the other part.

2. EXPERIMENTS

The shock break energy can only be determined on 10mm-side test bars, according to the standards in use. In order to place the notch of the test bar in the least favorable part of the rolled section, respectively in the center, we decided to carry on the experiments on test bars 25 mm long. We considered it important to have the root of the notch in the center of the rolled section, as the central part is most influenced by hardening in the case of round samples deformed between parallel plane surfaces. Structurally, too, the central part is the most segregated one.

In order to establish the influence of the chemical composition and the quieting degree upon tenacity, for steels having a carbon content of up to 0.35%, we tested rolled sections from six steel charges, all of them quieted with silicon, three of them being alloyed with Al (0.027 - 0.05%).

Rolled sections of 35 to 40 mm were turned into samples 25mm diameter, which were subjected to cold plastic deformations.

The tests aimed at determining the dynamic characteristics by shock-bending of U and V-notched test bars.

Since the reference literature mentions as a basic influential factor for steel tenacity the size of the real and inherited austenitic grain, the annealing temperature was 925°C, corresponding to the standard temperature for determining the hereditary austenitic granulation.

After annealing and turning, the samples were kept at room temperature for 72 hours, in order to eliminate all the remnant strains.

The test bars used for determining the shock-break energy were processed to a diameter of 25mm and a length of 60mm, then cold plastic deformed by pressing on 30 kN, 50 kN, 60 kN and 70 kN force generators.

The samples used for shock bending tests were made both of deformed test bars and the blank assay, so that the notch root corresponds to the central area of the rolled section, deformed or not deformed.

The test was performed with a Charpy pendulum hammer, with a direct reading of the break energy in J.

For the identification of the samples and test rods, we established, before the thermal treatment, a marking code based on the steel chemical composition, which was preserved during all tests and which corresponds to a charge and a bar out of which all the samples and test bars with the respective mark have been made. Although the number of tests is reduced by using this procedure, for research purposes it is very efficient, as it eliminates the influence, of temperature, hot deformation, cooling rate after rolling, of area segregation in the ingot, etc.

Table 1 presents the chemical compositions of the charges under analysis.

Table 1. The chemical composition of the charges under analysis

Steel grade	Sample mark	Chemical composition, %								
		C	Mn	Si	P	S	Cr	Ni	Cu	Al
OL321k	1	0.10	0.40	0.25	0.017	0.015	0.05	0.05	0.08	0.005
OL341k	2	0.13	0.34	0.25	0.045	0.014	0.07	0.15	0.30	0.006
OL371k	3	0.17	0.58	0.23	0.042	0.023	0.10	0.07	0.13	0.005
OLC20	4	0.20	0.58	0.34	0.045	0.020	0.16	0.12	0.21	0.030
OLC25	5	0.25	0.70	0.27	0.027	0.016	0.07	0.06	0.09	0.050
OLC30	6	0.33	0.73	0.26	0.040	0.020	0.08	0.06	0.09	0.027

The analysis of the data under question leads to the conclusion that the steels we used belong to the carbon quieted steels, with different contents in aluminum, charges 1-3 with a low aluminum content, which determined a rough austenitic granulation (under 5), and charges 4-6, with a content in aluminum higher than 0.02 %, ensuring a fine austenitic granulation (5-8).

Before the shock break test, we underwent Vickers HV₅ hardness tests, the values obtained on both the blank assay and the deformed samples being given in Table 2.

Table 2. The (HV₅) hardnesses of test rods for shock break tests

Sample mark	% C	HV ₅ hardness				
		Deforming force, x 10 ⁴ N				
		0	30	50	60	70
1	0,10	144	155	151	162	152
2	0,13	146	152	167	-	-
3	0,17	150	158	167	180	174
4	0,20	144	150	165	-	-
5	0,25	152	140	160	178	-
6	0,33	156	158	168	168	-

The table given above presents the results obtained under different deforming forces, for test bars having the same dimensions, namely 25 mm diameter and 60 mm length.

The next table presents the deformation degrees obtained by applying different deforming forces, expressed both by the deformation degree of the section ϵ_s and by the unitary deformation degree ϵ_u .

Table 3. The deformation degree of samples undergoing the shock break test

Sample mark	%C	Deforming force, x 10 ⁴ N							
		30		50		60		70	
		ϵ_s	ϵ_u	ϵ_s	ϵ_u	ϵ_s	ϵ_u	ϵ_s	ϵ_u
1	0,10	3.6	10.5	11.2	21.5	14.5	25.5	18.4	30.0
2	0,13	3.0	9.0	9.7	19.0	-	-	-	-
3	0,17	2.5	7.5	7.9	17.0	11.3	21.6	14.9	26.0
4	0,20	2.6	8.0	7.6	16.5	-	-	-	-
5	0,25	1.4	5.5	6.5	15.1	10.0	20.0	-	-
6	0,33	1.5	5.7	5.5	13.3	9.2	18.7	-	-

The break energy obtained on Charpy V test rods under the pendulum hammer having the energy of 30 daJ is given in table 4.

Table 4. The break energy for the shock bending test

Sample mark	%C	%Al	Compression force, x 10 ⁴ N				
			0	30	50	60	70
1	0,10	0,005	183	22	17	7	10
2	0,13	0,006	138	46	11	-	-
3	0,17	0,005	118	11	9	9	6
4	0,20	0,030	125	135	101	-	-
5	0,25	0,050	127	122	97	97	-
6	0,33	0,027	96	50	98	94	-

It is to be noticed that with shock bending, there is a grouping of the values of the break energy, with respect to the contents in aluminum. Thus:

- ❖ with charges 1 - 3 , where the Al content is 0.005 - 0.006%, the break energy is much below the one in charges 4 - 6 where the Al content is above 0.027%. With charges 1 - 3, the break energy diminishes at a rapid rate even for slight deformation degrees, of 2.5 - 3.0 %, the 15 J brittleness level (accepted for semi-quieted steels) being attained only by the steel with 0.10%C for a deformation of 11%. For the steel with 0.17%C, the brittle fracture is attained even for deformation degrees of 2.5% and for the 0.13%C steel, the deformation should be over 3%;
- ❖ for fine-grained quieted steels, the brittleness level admitted in the reference literature is 29 J and in the case of the steels from charges 4 - 6 , even for deformation degrees of 10 % and contents in carbon of 0.33 % the break energy is above 90 J. With these steels, the decrease in the break energy values is less influenced by the degree of deformation when the content in carbon increases, than in the case of rough austenitic granulation steels.

In order to bring into relief the influence of the connection radius of the notch upon the break energy, we made Charpy U and V test rods out of charge 4. Table 5 presents the comparative results of these tests.

Table 5. Comparative data regarding the values obtained in testing U Charpy and V Charpy tests of the same steel grade

Deformation degree %	Break energy			
	KV J	KU J	KCU J/cm ²	KCU' J/cm ²
0	125	136	170	139
2,6	135	130	163	146
7,6	101	130	163	120

As charge 4 is a steel with fine austenitic granulation, it belongs to the group of high tenacity steels, the values obtained for the break energy ranging within 100 - 136 J, for both the plastic deformed samples and for the non-deformed one.

The break energy of the Charpy V samples show a decrease for the deformation degrees of 7.6 % as compared to the value corresponding to a 2.6% deformation degree, while for the Charpy U samples tenacity is practically maintained at the same level. By comparing the resilience values determined experimentally to those of standard STAS R 10025 - 75 we will find higher real values than those given in table 2 of the above-mentioned standards.

Thus, in order to obtain high tenacities for deformation degrees above 10%, with steels having a carbon content of up to 0.35%, it is compulsory to have an aluminum addition during steel elaboration, so that the rolled sections should preserve an aluminum level of at least 0.025%. In the case of steels with content in aluminum of about 0.005%, the steel is brittle even for low deformation forces, in the range of 3 - 5 %.

3. CONCLUSIONS

- ❖ the break energy for quieted all-purpose construction steels decreases abruptly while cold plastic deforming, the decrease being more accented when the content in carbon is higher. Practically, the quieted steels grade OL 32, OL 34, OL 37 k can not guarantee the tenacity expressed by the break energy of 27J at environment temperature;
- ❖ with steels OL 37 kf, OL 42 kf and OLC 20, OLC 25, OLC 35, with a content in aluminum per product of at least 0.020% the break energy of at least 27J can be guaranteed even for deformation degrees of up to 20 %.

As a conclusion, we suggest as a method of increasing the resistance characteristics by about 30%, the cold plastic deformation by compressing (rolling) to a deformation degree of up to 15%, and if a minimum tenacity level is requested, the steels have to be quieted complementarily, by addition of aluminum, ensuring a minimum aluminum level per product of 0.020 %.

REFERENCES

- [1.] Cazimirovici, E. Teoria deformării plastice, Editura didactică și pedagogică, București, 1981
- [2.] Drăgan, I., Ilca, I., Badea, S., Cazimirovici, E. -Tehnologia de formării plastice, Editura didactică și pedagogică, București, 1979
- [3.] *** Metals Handbook - Proprieties and Selection, Iron and Steel, vol. I ASM, Ohio, 1978
- [4.] Szacinski, A.M., Thompson, P.E. - Comparison of effect on material properties on growth of wrinkles in sheet metal during forming and their removal, Materials Science and Technology, mart. 1991





¹Doina PETRE, ² Adriana PUTAN

THE IMPROVEMENT OF RESISTANCE CHARACTERISTICS OF STEELS THROUGH COLD PLASTIC DEFORMATION

¹⁻². UNIVERSITY POLITEHNICA OF TIMISOARA, FACULTY OF ENGINEERING FROM HUNEDOARA, ROMANIA

ABSTRACT:

The application of a pressing along the generatrix for some steel laminates for general use, with diameters between 6-16 mm, leads to ensuring an important improvement of resistance characteristics, especially the flow limit.

KEYWORDS:

plastic, cold, deformation

1. INTRODUCTION

The following paper shows the results obtained through the application of the mentioned procedure as well as the optimum domain of chemical composition and deformation degrees, in order to get an optimum correlation between the resistance and plastic characteristics of steels. Steels which are the main objective of the presented study, are part of the categories of round wire of laminated steel and concrete steel laminated in heat, with chemical composition like steels for general use for construction (less type OL70), quality carbon steels for heat treatments aimed at machines manufacture and concrete laminated steel at heat with periodical or smooth / fine profile

2. EXPERIMENTS

The utilization characteristics of these steels, and especially flow limit (apparent Re_H or technical $Rp_{0,2}$) and tenacity, are influenced by a complex of factors including the chemical composition and deoxidation practices used for elaboration, the regime of temperatures and the deformation degree in lamination, the width of the products.

Regarding the mechanical characteristics of these products the following mentions must be made:

- the contain of carbon through influencing the pearlite/ferrite proportion and the contain of manganese through the alloying effect of ferrite, are the main controlling factors to reach the guaranteed resistance characteristics. The structure modifications that ensure the improvement of resistance characteristics have adverse effect on plastic characteristics
- the majority of products of general use steel are delivered in hot deformation status. Once the width of the product increases – as an effect of temperature increase at the end of lamination and decrease of cooling speed, at the same chemical composition, the wider products have less resistance characteristics than thinner products.

I chose the concrete irons as a first application of the studied procedure because:

- ❖ they are the steels with a contain of carbon within the limits of the theoretical interval;
- ❖ on of the compulsory characteristics at the reception of these steels is floe limit, on which the pressing by generatrix has an absolute influence;
- ❖ they are not very pretentious form a dimensional point of view;
- ❖ can substantially increase sales value if delivered with higher resistance characteristics;
- ❖ the require restrictions for chemical composition, more precisely the limitation of contains of alloying elements (calculus relations for CE), and thus the value of resistance characteristics cannot be influenced through alloying.

For the research regarding the influence of plastic deformation at cold through the application of force on generators over the resistance characteristics of carbon not-alloyed steels, we used wire samples 6 mm diameter, with lengths between 500 and 1500mm. The wire was taken

from the heart of wire in order to avoid the results be influenced by the way of cooling of wire (eventually not uniform) and in order to ensure very similar conditions at trials.

The samples taken on plastic deformation at cold and determination of characteristics, were used as such, without any preliminary pre-work, in order to reproduce very accurately and application of this process directly on industrial products.

The steel charge that were used for quasi-industrial trials have carbon contains between the limits 0,07-0,14%. The chemical composition of the studies charges is shown in table 1.

Table 1. Chemical compositions of experimental charges

Charge	Chemical composition, %								
	C	Mn	Si	S	P	Cr	Ni	Cu	Al
1	0,07	0,32	0,01	0,030	0,016	0,06	0,07	0,07	-
2	0,11	0,50	0,01	0,045	0,020	0,08	0,06	0,12	-
3	0,09	0,53	0,01	0,028	0,016	0,06	0,09	0,12	-
4	0,07	0,34	0,01	0,030	0,018	0,10	0,10	0,15	-
5	0,14	0,53	0,22	0,030	0,017	0,06	0,06	0,09	0,007
6	0,09	0,37	0,22	0,043	0,015	0,08	0,06	0,09	0,006
7	0,08	0,46	0,01	0,040	0,016	0,07	0,10	0,10	-

Six samples were taken out of each charge, out of which one is the etalon sample (E) and the others (1,2,3,4,5) were exposed to cold deformation on generatrix with different deformation degrees. The deformation degree was determined using the following relation $\varepsilon = \frac{d_0 - d}{d_0} \cdot 100$

in which ε represents the degree of deformation [%], d_0 – the initial diameter of the sample, [mm] and d – the final diameter of the sample [mm].

The study undertaken before, using a deformation through pressing on generatrix for steel products with diameters between 6 and 8 mm, showed the fact that it is possible to obtain a significant growth of resistance characteristics and especially flow limit (proportion $R_{p0,2}/R_m=0,70-0,98$) when relatively small degrees of deformation are applied (table 2).

Table 2. Mechanical characteristics of deforming samples

Nr. crt.	Sample	$\varepsilon, \%$	Mechanical characteristics				Increase $R_{p0,2}, \%$	Increase $R_m, \%$	$R_m/R_{p0,2}$	$R_{p0,2}/R_m$
			Z, %	A, %	$R_{p0,2}, N/mm^2$	$R_m, N/mm^2$				
1.A	E.1	-	74,68	23,3	265	353	-	-	1,33	0,75
	1.1	4,92	68,68	20,5	310	385	16,98	8,96	1,24	0,80
	2.1	18,03	60,89	14,4	440	455	66,03	25,76	1,03	0,96
	3.1	26,23	64,69	15,8	482	493	81,88	39,20	1,02	0,97
	4.1	29,51	65,60	14,8	507	520	91,32	46,76	1,02	0,98
	5.1	34,43	56,54	10,7	528	537	99,24	51,52	1,01	0,99

The aim was to experiment the same procedure on industrial products with bigger diameters.

In order to do this, samples were taken from steels out of the current production, from steel charges with different chemical compositions and different dimensions of the laminated products.

The samples had lengths between 500-1500 mm. the samples used for trials were collected so that the results of the application of deformation not to be influenced by the cooling way and in order to ensure initial conditions as similar as possible.

The samples exposed to plastic cold deformations and determinations of characteristics were used as such, without any preliminary influence, in order to obtain a very accurate reproduction of this procedure directly on industrial products.

After cold deformation on generatrix, from each charge, some samples were taken in order to determine the mechanical characteristics. Samples were debited at 150mm, according to the prescriptions.

The steel charges that were used for the second set of trials have carbon contains between the limits 0.07-0.22%.

After an analysis of the presented data, it comes out that like in the case of wider industrial products, the effect of plastic deformation by pressing on generatrix shows especially on flow limit that registers the higher growth rates till deformation degrees of aprox. 30%, after which the growth rate of, flow limit decreases.

The conclusions that can be drowned from the analysis of the presented data, are:

- ❖ the plastic cold deformation process by pressing on generatrix applied to industrial products of wire with medium diameter between 6-8 mm and laminated products with width between 12-

25 mm, made of steels with less carbon contain, are applied without any difficulty, steels presenting a weak resistance to deformation

- ❖ the influence on resistance characteristics is very strong starting even from low deformation degrees (aprox. 12%)
- ❖ the growth rate of resistance characteristics is high, till deformation degree of cca. 30%, after which the continuing application of deformation on generators does not lead anymore to high growth of resistance.
- ❖ the biggest influence is on flow limit, that registers substantial increases, reaching values similar to those of resistance to breaking for the same type of steels.
- ❖ the proportion $R_{p0,2}/R_m$ increases very much, which constitutes a criteria for determination of steel quality for concrete, which reaches values of cca. 0.99.

In order to set up the technological conditions of the plastic deformation by pressing on generatrix, the data obtained from the experiment in the lab and industrial trials was studied. The analysis of data was based on statistical-mathematical methods, using specific calculus programs.

In order to obtain the correlation between the technological factors that influence the plastic deformation, more precisely the chemical composition of steel and the deformation degree applied, the MATLAB program was used.

We considered 48 sets of data that include the chemical composition of steel, the value of the proportion C/Mn, the value of the reduction degree, applied, as well as determined values flow limit, resistance to breaking, and the calculated value for the proportion $R_{p0,2}/R_m$.

For each correlation the medium values of the parameters, the correlation coefficient, standard exception from the regression area, and the values of the stationary point (minimum, maximum or medium) are presented. In the following lines, based on the analyzed data, the variation areas obtained and the diagrams of level curves, one can set the technological conditions, respectively the chemical composition and deformation degree which leads to the best correlation with the mechanical characteristics of resistance of the deformed products.

During the experiments it was observed that the substantial influence of the deformation by pression on generatrix process is on flow limit that registers very high growth at relatively low deformation degrees. Therefore, in the following lines we present the variation areas of flow limit $R_{p0,2}$, as well as the variations of the proportion $R_{p0,2}/R_m$, function of independent parameters mentioned before.

The analyzed data are $R_{p0,2}$ like an dependent parameter and C, C/Mn, ϵ like independent parameters .

The variation limits of the variables are:

$$C_{\min} = 0,07\% - C_{\max} = 0,22 \%; (C/Mn)_{\min} = 0,17 - (C/Mn)_{\max} = 0,35; \epsilon_{\min} = 0 - \epsilon_{\max} = 38\%;$$

$$R_{p0,2\min} = 255 - R_{p0,2\max} = 623$$

The equation of the hiper-surface of regression is:

$$R_{p0,2} = 5064 * C^2 - 5295 * (C/Mn)^2 - 0,1725 * \epsilon^2 - 5595 * C * C/Mn - 1,945 * C/Mn * \epsilon + 5,866 * \epsilon * C + 3274 * C + 3606 * C/Mn + 13,75 * \epsilon \quad (1)$$

The correlation coefficient for this hypersurface is $r=0,98$, standard exemption from the regression surface is $s=21,13$, and the coordinated of the maximum point are; $C = 0,2319$; $C/Mn = 0,2103$; $\epsilon = 42,62$; $R_{p0,2} = 649,5$.

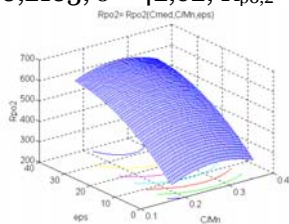


Figure 1. The $R_{p0,2} = R_{p0,2}(C_{med}, C/Mn, \epsilon)$ distribution and level curves

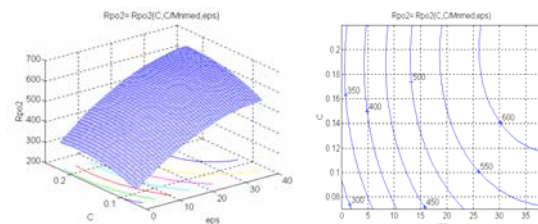


Figure 2. The $R_{p0,2} = R_{p0,2}(C, C/Mn_{med}, \epsilon)$ distribution and level curves

Due to the fact that these hypersurfaces cannot be represented in a tridimensional space, I chose the successive replacement of an independent variable with its medium value, getting to surfaces that can be represented in the tridimensional space and can be interpreted from the technological point of view.

Therefore, we obtain the surfaces that are the object of the following study. Associated to the surfaces we have the level curves for each value of the presented characteristics. Based on these analyses, one can set the maximum level of deformation by pressing on generatrix, that can ensure simultaneously with the increase of resistance of steels and a convenient behavior while processed.

The influence of chemical composition and degree of deformation over the flow limit is highlighted through the regression surface represented by the equation:

$$R_{p0,2} = - 5295 * (C/Mn)^2 - 0,1725 * \varepsilon^2 - 1,945 * C/Mn * \varepsilon + 2858 * C/Mn + 14,54 * \varepsilon - 55,1 \text{ (for } C=C_{med}) \quad (2)$$

The dependency between the value of flow limit, value C/Mn and the degree of reduction if a constant carbon contain and equal with the medium level on charge is considered, presented by figures 1.a and 1.b is the normal one, technological, in the sense that its value increases continuously with the increase of C/Mn and E, on one hand due to the hardness effect of the two elements and on the other, due to hardness induced by the increasing reduction degrees.

3. CONCLUSIONS

The undertaken analysis through mathematical methods of the obtained data, under the conditions of a plastic deformation at cold on generators, with deformation by pressing on generatrix degrees varying between 2- 40%, highlights the fact that in order to obtain increase of resistance, which would not affect the behavior during processing of steels, one must consider a series of measures such as:

- ❖ the carbon contain must be kept under 0,25%, and Mn contain must be kept at the technological limit necessary for carbon not-alloyed steels, respectively under 0,8%.
- ❖ the proportion C/Mn must be kept within the interval 0,2-0,3, so that the value of the flow limit and the proportion $R_{p0,2}/R_m$ can be maintained within the technologically admitted limits.
- ❖ the data shown before highlight the fact that the described process can be applied without any problems directly on industrial products, without a preliminary preparation, getting to important increases of the resistance characteristics.

REFERENCES

- [1.] Petre Doina Elena- Metode de crestere a capacitatii de rezistenta a laminatelor din otel prin modificari microstructurale- Teza de doctorat, Timisoara 2002
- [2.] Dieter, E.G. -Metalurgie mecanica, Editura Tehnica, Bucuresti, 1970





¹Miron BUZDUGA, ²Adriana COMȘA, ³Radu BUZDUGA

RESEARCH IN ORDER TO OBTAIN SPECIAL FIRE BRICK PRODUCTS

¹⁻³FIRE BRIKS RESEARCH, DESIGNING, AND PRODUCTION CENTER, SC CCPPR SA ALBA IULIA, ROMANIA

ABSTRACT:

The purpose of the present paper was obtaining special fire brick products for the metallurgy industry, through a forming and casting method without using clay binder. The laboratory trials have led to finding some compositions used to fire brick products of superior quality from superaluminum chamotte (with over 85 % Al_2O_3) and tabular alumina (with about 98,5 % Al_2O_3).

KEYWORDS:

fire brick products, metallurgy

1. INTRODUCTION

The present theme has imposed itself due to the development and modernizing technologies in ferrous metallurgy and metallurgy in general led to extremely severe demandings on fire brick products used in various equipments and aggregates.

For silicon-aluminum fire brick products (the system SiO_2 - Al_2O_3) the condition for quality increase has meant obtaining products with a high alumina (Al_2O_3).

Initially the silico-aluminum refractory products were made from refractory clay, natural silicates of alumina, with a maximum percentage of 38-40% Al_2O_3 . Later on, there have been made aluminum refractory products with a content of 45-60 % Al_2O_3 , refractory products with 60-75% Al_2O_3 , mullitico-corrundum products with 75-90 % Al_2O_3 and corrundum products with 90-95 % Al_2O_3 . The path to follow was to ennoble the chamottes from refractory clay with incinerated alumina, with higher and higher proportions, together with the alteration of burning parameters (temperature, time etc.). In all the cases though, although the chamotte increased in quality, the binder used in forming remained the same refractory clay, natural raw material with impurities, which did not allow the increasing of Al_2O_3 content in the final product over a certain limit.

To achieve this goal SC CCPPR SA Alba Iulia has studied, produced and patented (BI A/00491), a chemical binder to provide a good binding of the refractory material, but, at the same time, as low as possible impurification of the refractory matrix with foreign, potentially damaging ions.

As testing products in industrial conditions we have chosen the following:

- ❖ special masonry products from the bottom of the casting ladle – ensemble of bubbling inert gases,
- ❖ tubes for the distribution of cast iron in shapes and shells,
- ❖ special holders for the electric resistances of the treatment furnaces,
- ❖ briks and burner bloks for metallurgic industry etc.

2. PRELIMINARY LABORATORY WORK

The raw materials used were high purity tabular alumina and super-alumina chamotte, available on the market. Their properties are presented in Table 1.

The binder used was the one produced by SC CCPPR SA, with the technical characteristics presented in Figure 2.

Tabel 1

Characteristics	Chamotte S68 A	Tabular alumina
Chemical composition :		
Al ₂ O ₃ ,min, %	99.65	70.04
Fe ₂ O ₃ ,max, %	0.04	0.98
Granulometric spectrum		
Residue on the 3,2 mm screen , %	1	
Residue on the 2,5 mm screen, %	14	
Residue on the 1,25 mm screen, %	56	
Residue in the 0,50 mm screen, %	13	
Residue on the 0,50 mm screen, %	16	100

Table 2

Characteristics	Chemical binder
pH	2,5
Density, g/cm ³	1,25

The strenghtner used was magnesium oxide with 98% MgO, chemically detected.

Based on these raw material we made slurries from super-aluminnum chamotte, and, separately, from tabular alumina.

The procedure we used was identical, in both cases, the difference was only in the percentage of solid and liquid materials we used in the production recipe.

2.1. Preparing slurry from aluminum chamotte

There have been prepared two different granulometric recipes to determine the optimum type of packing the chamotte and tabulat alimina in order to get the best omogenity of the casting material, and implicitly the best physico-mechanical characteristics of the end product.

The recipes are as follows, in tables 3 and 4.

Table 3

Receipe	Chamotte SA68A 0-3,2 mm granulation, %	Chamotte SA68A under 0,06 mm granulation, %
R1	55	45
R2	50	50

Table 4

Ingredients	R3	R4
Tabular alumina 8-14	35	
Tabular alumina 14-28	10	
Tabular alumina -325	55	100

The dosage of the ingredients has been gravimetric for the solid materials, and volumetric for the binding solution.

The following recipes have been used:

Table 4

Ingredients	R1	R2	R3	R4
Granulated SA68A chamotte, %	x	y		
Fine SA68A chamotte, %	x	y		
Tabular alumina in granules			z	
Intermediate tabular alumina			z	
Fine tabular alumina			z	w
Chemical binder	x	y	z	w
Strenghtener	x	y	z	w

The casting mix has been prepared in a 10 l ladle with an agitating device with propeller. The order of the preparing steps was as follows:

1. We put the binding solution into the agitating ladle.
2. As wvestarted the agitator the refractory unit, with fine granulation, then the granulated one have been introduced, stirring for about 3 min.
3. After mixing the refractory unit with the binder, the strenghtner has been added, constantly stirring, until the best mix of the casting mass.

4. After the agitator was stopped the slurry was casted in cube shapes, with 80 mm angle sides, and cylinders with 50 mm diameter and 50 mm high.
5. After about 80-90 min. the material was solid enough to allow decasing and manipulation in safe conditions for the test pieces which have been dried and sintered, and physico-mechanically tested.

Without being able to establish precise relationships over various factors, we could see that the coagulation interval, and, respectively of paste hardening within the shapes, is influenced by:

- External parameters:

- ✓ Temperature of the environment
- ✓ Mixing time
- ✓ Agitator speed.

- Internal parameters:

- ✓ Solid material granulation, chiefly the specific contact surface between the solid and the liquid binder.
- ✓ Liquid (binder) concentration and quantity in the mass.

2.2. Characterization of produced compositions

From the casting paste – slurries, cubic test pieces, with 80 mm angle sides, and cylindrical ones, with 50 mm diameter there have been cast.

To shape the test pieces, the shapes have been set on a vibrating table and filled with casting slurry. The vibration carried on during the filling with material, and 60 more seconds after that. Then the shapes have been transferred on a fixed table and let still, so that the material got harden.

After hardening inside the shapes, which took from a few minutes to two hours, depending on the recipe, preparation conditions and environmental factors, the products have been decased and let to dry for 24 hours. After that they have been introduced in the drying stove, at 120°C for another 8 hours.

In all the cases, the dried products have been introduced in the chamber furnace of S.C.CCPR S.A. Alba Iulia on a burning diagram for refractory products of 60A type, for 24 hours at maximum temperature of 1520 - 1550°C.

When out of the furnace the tests have been submitted to various laboratory tests, to determine their quality.

2.3. Characterization of produced compositions

2.3.1. Characterization of compositions from aluminum chamotte

Determinations of porosity and resistance to compression have been performed on the two recipes of slurry from aluminum chamotte SA68A, with different solid granulation. There have also been performed measurements of contraction (after burning) to better appreciate the degree of compacting of products after sintering. The results are as follows, in table 5 and in fig.1-5

Table 5

Determination	Recipe 1	Recipe 2
Contraction, %	1,5-2,2 average 1,7%	1,2-2,1 average 1,65
Ostensible porosity, %	26,5-28	24-25
Absorbion capacity, %	11,0-12,0	10-11
Ostensible density, g/cm ³	2,35	2,30
Resistance to compression, daN/cm ²	343-415 average 385	400-420 average 415

Fig.1.1 Contraction to burning, %

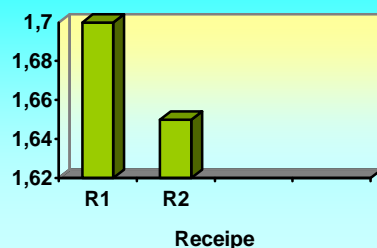
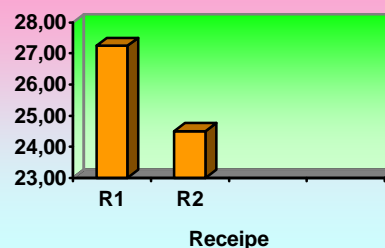
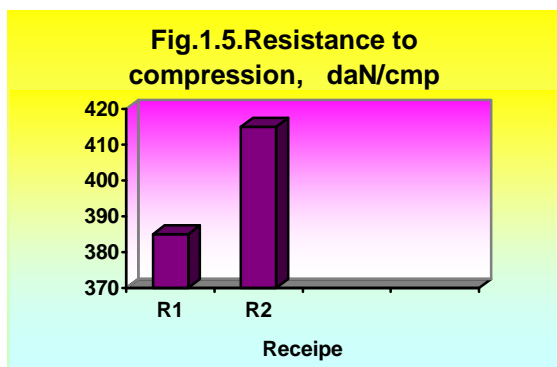
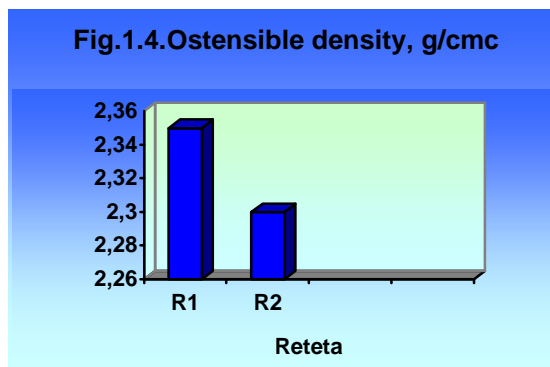
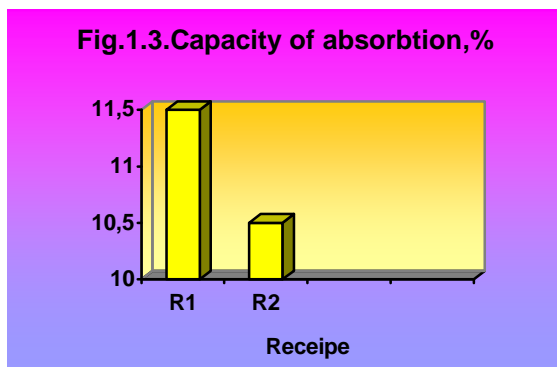


Fig.1.2 Porosity, %





We can see from the results that the two recipes have quite similar final characteristics, with a compaction slightly better for recipe 2, (with finer granulation), which means that both recipes might be used, depending on the dimensions of the pieces we need to produce.

Otherwise, we need to consider the thermo-mechanical and thermo-chemical characteristics of the products for metallurgic industry. Those can be determinantly influenced by the granulation of the refractory material, regardless of its binding manner.

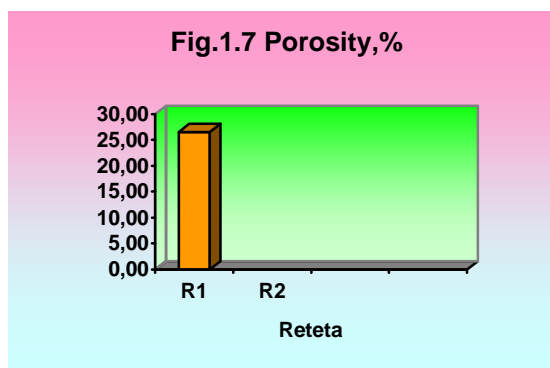
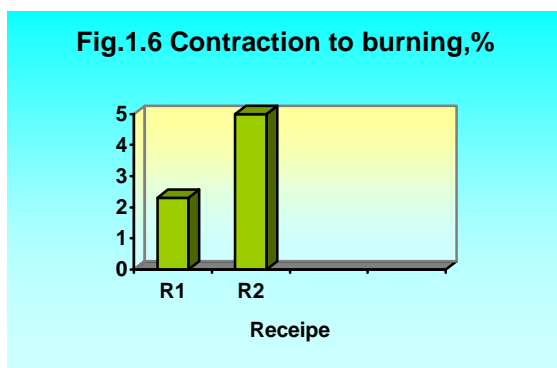
Anyhow, the basic physico-mechanical properties (porosity, resistance to compression, etc.) do not differ from the properties of classical products, shaped by pressing, with clay binder.

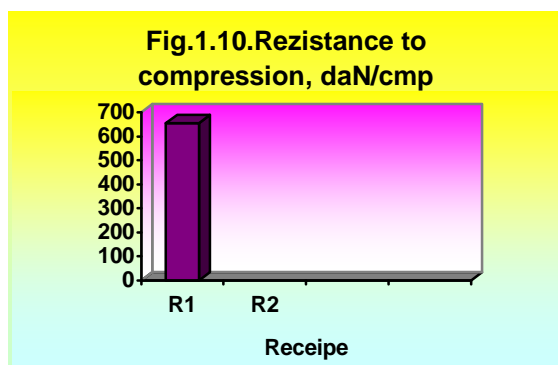
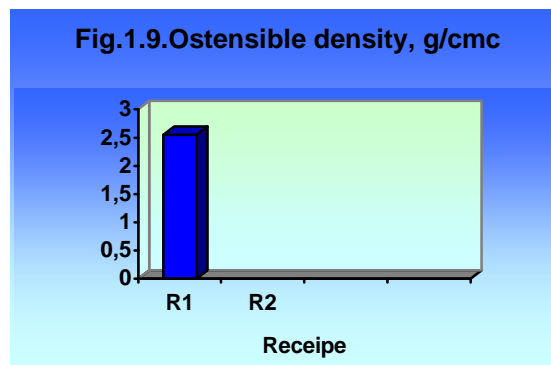
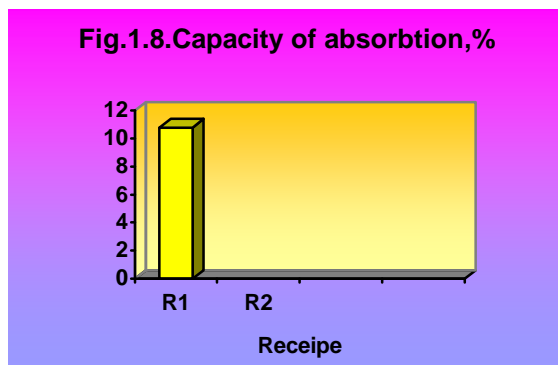
2.3.2. Characterization of compositions from tabular alumina

The results of determinations of contraction to burning, ostensible density, absorption, ostensible porosity and resistance to compression are shown in table 6.

Table 6

Determination	Recipe 3	Recipe 4
Contraction, %	1,9-2,6 average 2,3	4,0-5,8 average 5,0
Ostensible porosity, %	23-28 average 26,5	-
Absorption capacity, %	8,2-11,8 average 10,8	-
Ostensible density, g/cm ³	2,41-2,82 average 2,55	-
Resistance to compression, daN/cm ²	650-666 average 655	-





For the tests in the recipe with 100% fine tabular alumina we did not perform any characteristic determination, because the contractions after burning were much to high, both in their absolute value and variation interval, which led to the conclusion that from this kind of casting paste we can not get refractory products within the dimensional allowed tolerance for metallurgic industry.

The tests from the first recipe, with different tabular alumina granulations have presented acceptable values so that we could recommend their use in various industrial areas of metalurgy.

Considering the results, the laboratory work have proven that there is the possibility of producing cast refractory products without using clay binder in metallurgic industry, products that are able to meet quality requirements for different purposes.

REFERENCES / BIBLIOGRAPHY

- [1.] Goleanu, M. Buzduga, N. Constantin, A. Comsa, M. Butu Effects of Additives on the Sintering Process of Al₂O₃-based Ceramic Materials 2nd International Congress on Ceramics, Verona, 29 iun-4 iul 2008-3-P-38
- [2.] Aurica Goleanu, Miron Buzduga, Adriana Comsa, Radu Buzduga Design of cordierite-mullite refractory material by using recycling grog International Conference B.EN.A - Management and sustainable Marine Development, iul 2008
- [3.] Heput Teodor. Buzduga Miron, Maksay Ștefan, Osaci Mihaela Study on the syntetic flux viscosity used at the continuous casting 11 International Research/Expert Conference Trend in the Development of Machinery and Associated Technologies, TMT 2007, Hammamet, Tunisia ISBN 9958-617-30-7
- [4.] Ștefan Mircea Utilajul și tehnologia produselor refractare și abrazive, Ed.Didactică și Pedagogică -București -1980
- [5.] I.Teoreanu;N.Ciocea Lianți, mase și betoane refractare ,Ed.Tehnică - București - 1977
- [6.] I.Teoreanu și colab Bazele fizico-chimice ale întăririi lianților anorganici, Ed.Didactică și Pedagogică - București - 1972
- [7.] H.C.Emblem,J.R.Walters Barbotină gelificabilă - Patent nr.1546208/23.05.1979-Zirconal Processes Ltd. -Anglia



¹: Adriana COMȘA, ²: Miron BUZDUGA, ³: Radu BUZDUGA

MONOLITIC FIRE BRICK PRODUCTS

¹⁻³: FIRE BRIKS RESEARCH, DESIGNING, AND PRODUCTION CENTER, SC CCPPR SA ALBA IULIA, ROMANIA

ABSTRACT:

The paper comprises data regarding the monolithic fire brick products, the main characteristics of LCC and ULCC concretes, as well as the influence of certain additives on these characteristics and the advantages of using these concretes in metallurgy.

KEYWORDS:

fire brick products, concretes, additives, metallurgy

1. INTRODUCTION

Classification of refractory concretes according to ISO/DIS 1927-1:2008 is as follows presented (Figure 1).

Concluding the above, the content of cement in these concretes is presented in Figure 2.

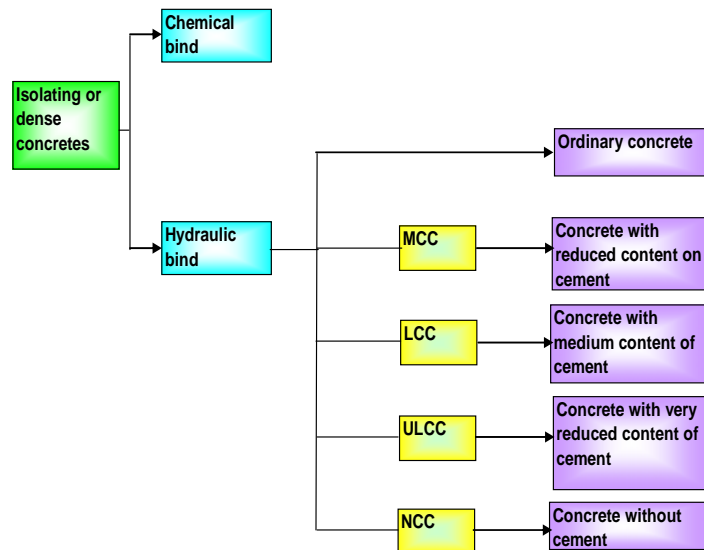
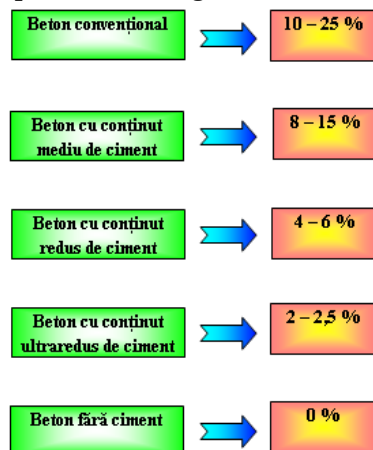


Figure 1. Classification of refractory cements according to ISO/DIS 1927-1:2008

Figure 2. Classification of refractory concretes according to ISO/DIS 1927-1:2008

1.1. Concretes with low and very low content of cement

In Romania, although the low cement concretes have been studied even since 1980, those have not been used in mass production. That is due to the fact that low cement concretes are more demanding and sensitive on first heating.

The production of low cement refractory concretes is based on using additives with advanced grinding gauge, due to the fact that in a casting mix, the density obtained with a classic granulometric distribution is limited to the hollows between the grains, which are filled with excess water during processing.

In figure 3 there is a graphic representation of the dependency of calcium oxide of the cement content, both for an ordinary concrete, and for a reduced cement one.

In Figure 4 there is a graphic representation of the compression resistance on the temperature. As it can be well seen, for an intermediate temperature (800 - 1000°C) the mechanical resistance of ordinary concretes is much lower than that of low cement concretes.

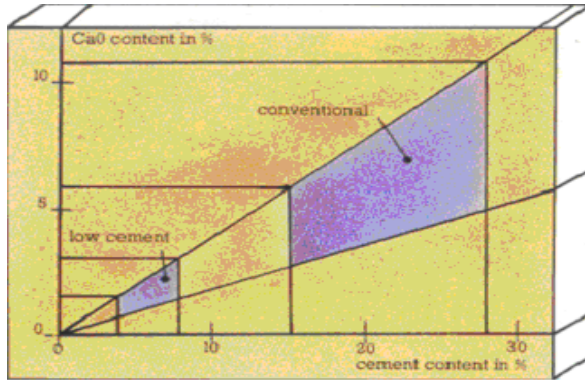


Figure 3. Dependency of CaO on the cement content

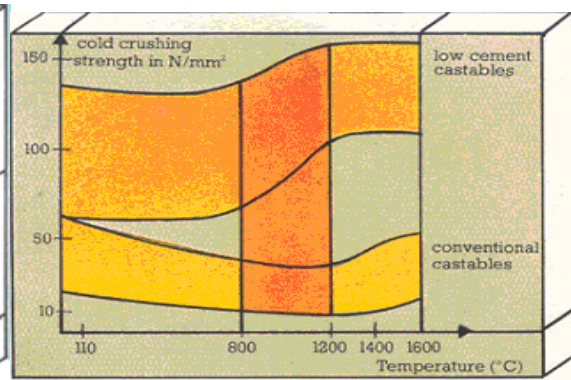


Figure 4. Dependency of temperature resistance on the temperature

The main feature that isolates concretes with low and very low content of hydraulic binder from other types of cement is the presence of very fine components. This very fine material replaces part of the cement content in the conventional concrete.

In table no.1.1 we present the influence of LCC concrete properties varying with its components.

Table 1.

Components of LCC	Properties influence
Refractory aggregate	Capacity of absorption, ostensible density, thermal conductivity, range of temperature of utilization
Super aluminum cement	Rheological properties – capacity of processing by casting, vibration, flowing, mechanical resistance
Dispersing agents	The tixotropy of the mixture
Reactive oxides (Al_2O_3 , SiO_2 , MgO , Cr_2O_3 , TiO_2)	Flowing, volumic stability, ostensible density, resistance to abrasion
Granulometric distribution Relation between grains >1 mm and fine fraction <1 mm	The work: - torcretation – adherence - casting – homogenous flow Homogenous structure

The production of concretes with low content of hydraulic binder is made by casting – vibration, either within the shapes, thus resulting in prefabs, or directly, at the very place used by the beneficiary, using encasements after that being treated until the maximum temperature, following a diagram, according to the quality of the concrete.

1.2. The main characteristics of LCC and ULCC refractory concretes

The classical concretes are generally characterized by the content of Al_2O_3 , which reflects both their refractivity and other physical properties. Regarding the concrete with low content of cement (LCC) and very low content of cement (ULCC) the content of Al_2O_3 is no longer enough for this characterization, other oxides (with smaller percentage of participation) having a great influence on the physico-chemical characteristics.

In table 2 the main oxides in LCC and ULCC concretes are presented, compared to a classical concrete, with the same content of Al_2O_3 and tabular alumina aggregate.

Table 2.

The main oxides	Classical concretes	Concrete with low cement	Concrete with very low cement
The aggregate	Tabular alumina	Tabular alumina	Tabular alumina
Al_2O_3 , %	90	90	88
CaO, %	5	1,1	0,3
SiO_2 , %	2,8	4,0	7,5
Fe_2O_3 , %	1,0	0,15	0,1

The high content of SiO_2 of LCC and ULCC concretes comes, in this case, from the ultrafine powders. In case of using other aggregates (chamotte, bauxite etc.) the content of SiO_2 can be higher to Al_2O_3 content's detriment.

Through the dosage of ultrafine powders an optimum percentage of SiO_2 , can be achieved, which is important because the bending resistance at temperature and the softening temperature of

LCC and ULCC concretes depend of the percentage of anortit formed with calcium aluminates at 1350°C (Figure 5), and the one of ULCC depends on the content of mulit formed with Al₂O₃ at 1300°C (Figure 6).

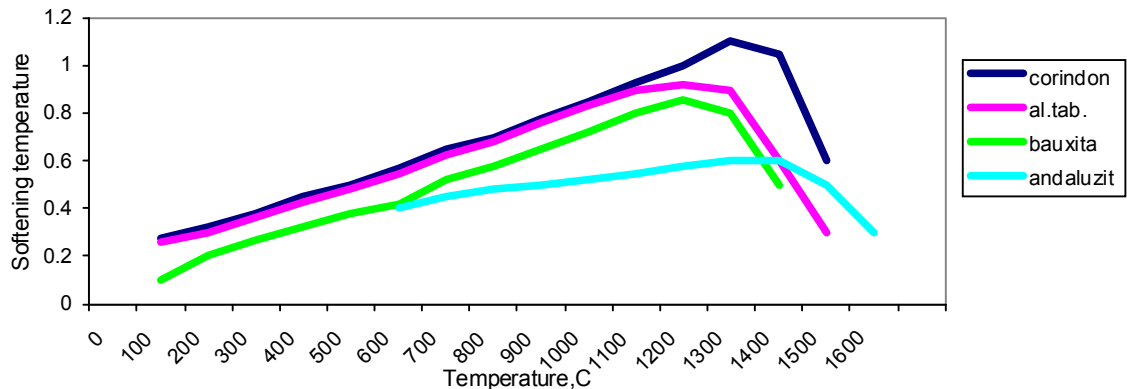


Figure 5. Softening temperature of burned LCC concrete, with various aggregates: 1 – corindon, 2 – 2 tabular alumina, 3 – bauxite, 4 – andalusite

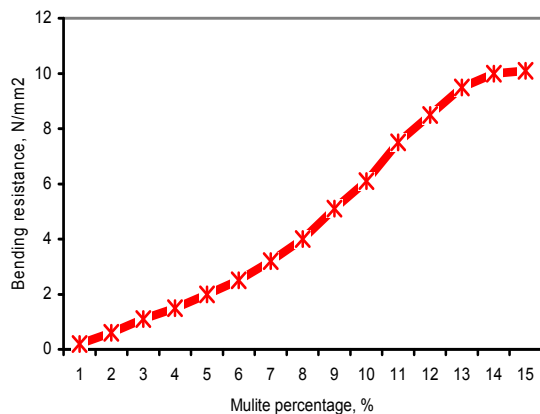


Figure 6. Influence of mulite percentage on the bending resistance at 1500°C of burned ULCC concretes

The ratios of CaO and Fe₂O₃ coming from cement, respectively the impurities of the aggregate, influence the bending resistance and corosion resistance of concretes. Due to the small percentage of CaO and Fe₂O₃, LCC and ULCC concretes have, compared to classical concretes, a higher resistance to chemical corosion, sometimes even better than burned shaped products.

All the classical concretes present, around the critical temperatures, (300 - 1200°C) a drop in mechanical resistance, wich can go up to 75% from the initial resistance, and which is provoked by dehydration of hydroaluminates of calcium, and successive transformations they endure until the beginning of sintering.

In case of LCC and ULCC concretes, instead of this dropping resistance there is a constant increasing, because, due to the presence of tripoliphosphate of aluminum the preponderance of gellic phase is insured, within the compact structure formed by the aggregate and the ultrafine powders, and wich, with the increasing temperature, crystallize forming gibbsit și boehemit. Because of this, the dehydration of crystalline hydrates can not cause, in low temperatures area, up to 500 - 600°C, the policondensation of phosphates coming from the reaction of sodium tripoliphosphate compounds, which fights the drop of resistance due to phase transformations and mentains its values on an ascending curve, until CA și CA₂ appear, when a new increase occurs.

Although at the temperature of 1000°C all the compounds are completly dehydrated, and CA și CA₂ are formed, the increase of mechanical resistance is mentained through the double phosphates of calcium and potasium chrystalization and sodium salts until the beginning of sintering, when the increase of the resistance is high.

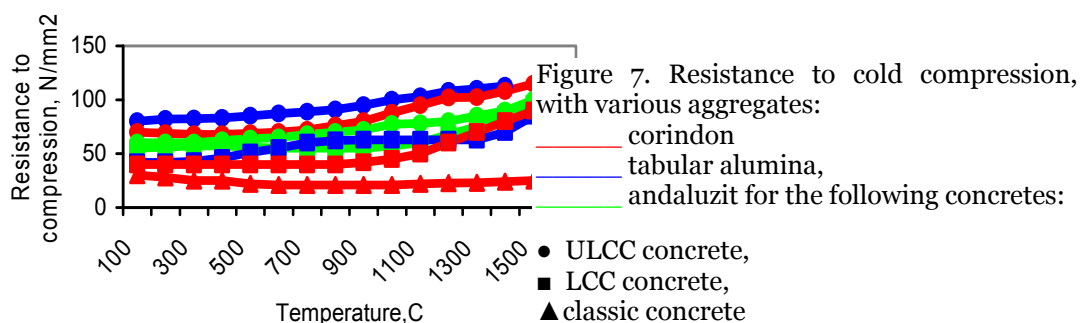


Figure 7. Resistance to cold compression, with various aggregates: corindon, tabular alumina, andaluzit for the following concretes:

● ULCC concrete,
 ■ LCC concrete,
 ▲ classic concrete

The variation of resistance to compression in low temperature after burning at various temperatures, of both classical concrete and LCC și ULCC concretes with various aggregates, is shown in figure 7.

There can be seen that the values of resistance to compression of LCC concrete up to 1300°C are similar to the ones of burned shaped products and far better than in the case of classical concrete. The curves for ULCC concrete show that, regardless of the aggregate, its resistance to compression is much higher than LCC, or classical concretes, or burned shaped products. Resistance to bending in heat is also increased compared to burned shaped products and classical concrete (figure 8).

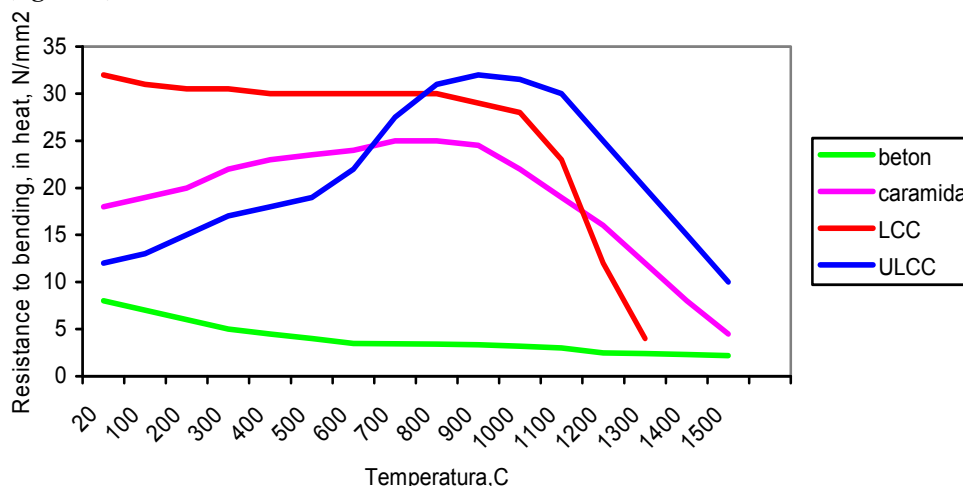


Figure 8. Resistance to bending in heat:

1 – concrete, 2 – brick, 3 – LCC concrete, 4 – ULCC concrete corindonic aggregates

A great influence on heat resistance is due to the mult quantity formed in the process, as well as the drop of CaO percentage in the concrete (Figure 9).

Due to the high values of mechanical resistance, internal tensions and pores distribution, LCC and ULCC concretes have a better impact resistance than classical concretes and burned shaped products, reaching over 50 heading-cooling cycles, when the aggregate is corindonic or tabular alumina.

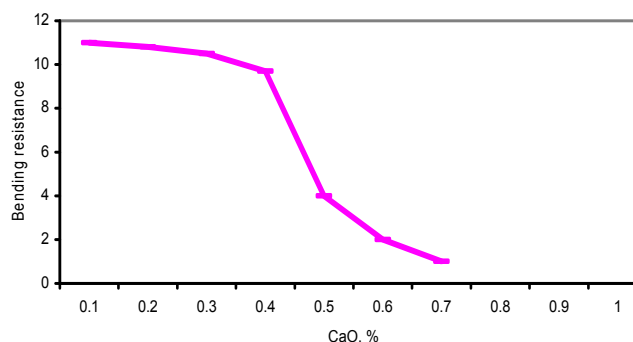


Figure 9. Influence of CaO ratio on the bending resistance at 1500 C, of a burned ULCC concrete

2. GRANULOMETRIC DISTRIBUTION

Producing dense refractory concretes, of high quality, Realizarea unor betoane refractare dense, de calitate superioară este determinată atât de puritatea chimică a componentilor, de dozajul acestora cât și de compoziția granulometrică a amestecului prin care se urmărește să se obțină o compactitate cât mai mare.

By pursuing the granulosity we reach to get as much compactness as possible. This characteristic generally depends both on the distribution, and the shape of the grains. Compounds of aggregates of splintery shape sometimes have a double surface compared to those spheric, thus needing more water to be prepared. To get a high resistance to bending, the rough surfaces of the grains are more advantageous than the smooth ones. The rate of fine aggregate from refractory concretes must be higher than that of ordinary concretes, because they are more profitable to the purpose and provide a relief of sintering process between the aggregate and the cement. The maximum dimension of the aggregate enclosed in refractory concretes is mainly determined by the section of the pieces to be made; it does not have to be bigger than 1/4 - 1/5 from the minimum dimension of the concrete piece. In common practice there are not used aggregates with a higher diameter than 40 mm. In the case of corindon aggregates the maximum dimension reaches just 10 mm.

To obtain maximum capacity of concretes the granulation of the compound needs to approach the ideal curves established by Fuller - Bolomey. In Figure 10 we can see the ideal granulation, in volumes, for the aggregates used for refractory concrete. Establishing the granular distribution according to the maximum section of the concrete piece, the dosages between the aggregate and concrete will be of 3-4,5 volumes of aggregate for a volume of cement.

The maximum dimension of the granules, mm

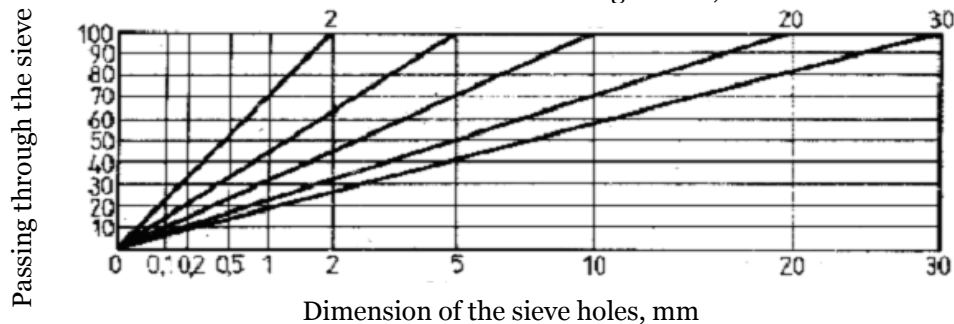


Figure 10. Ideal granularity, in volumes, for refractory aggregates used in refractory concretes

The granulometric distribution of refractory distribution can also be established through the following formulae:

$$y = 100 \cdot \sqrt{d/D} \quad \text{Fuller's formula}$$

$$y = A + (100 - A) \cdot \sqrt{d/D} \quad \text{Bolomey's formula}$$

$$y = 100 \cdot \left(\frac{d}{D}\right)^n \quad \text{Gummel's formula}$$

where: d – dimension of particles

D – maximum dimension dimensiunea of particles

A – coefficient, according to the type of aggregate, A = 8 – 12

n – coefficient, n = 0.2-0.4 – 0.3-0.5. For Gummel n = 0.1 – 1

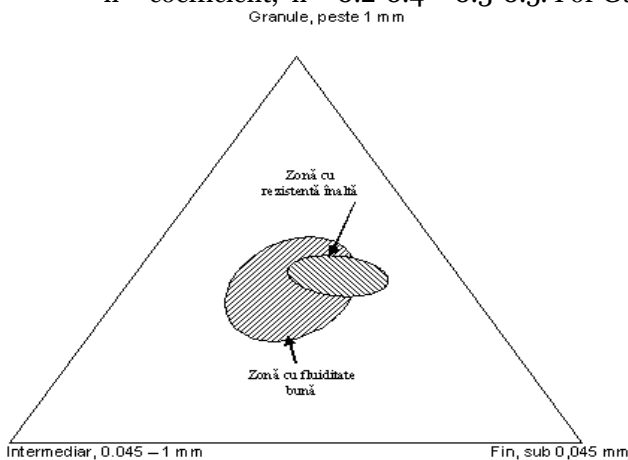


Figure 11. Areas of fluidity of granular compounds

- ❖ 30-45% fine (with no intermediary ratio) lead to good compacticities and low contractions;
- ❖ compositions with 70-80% granules have a good resistance to mechanical impact;
- ❖ compositions with fine ratio, or with granules (provided that the different granular components have the same contraction when burned) lead to a reduced permeability.

3. POROSITY

One of the most important properties of concretes is the ostensible porosity. This gives indications on the resistance to impact, corrosion and infiltration. One of the most important properties of the concretes is the ostensible porosity. This gives indications on the resistance to impact, corrosion and infiltration. According to the place we use the concretes, the ostensible porosity needs to be controlled, to provide the infiltration of melt metal, and, implicitly, the corrosion. The lower ostensible density of tabular alumina is due to the small pores (closed) (<10µm), which do not allow the infiltration of slag, but improve considerably the resistance to impact of the aggregate.

Tabular alumina has a high chemical purity ($Al_2O_3 > 99,4\%$), which improves the resistance to usage for concretes for trenches.

Classic refractory concretes, due to the high content of cement, have, when raw, an ostensible porosity around 9 – 10%. When the content of cement is higher, the ostensible porosity when raw, decreases. This porosity increases during heating, due to dehydration and phase transformations of calcium hydro-silicates, reaching a maximum of 30-35% and dropping then to 23-26% as ceramic conection and sintering occur.

Both LCC and ULCC concretes, although the cement content is reduced, have a reduced porosity, when raw around 6-9%. This is due to filling the intergranular spaces with very fine ratios of powders, the micropores still remained being filled with gelly phase. We have to mention that the ostensible density of LCC and ULCC concretes is high particularly because of that, reaching up to 3-3,2 g/cm³ (according to the nature of the refractory aggregate and temperature). With the increase of temperature LCC and ULCC concretes have a small increase of porosity, compared to ordinary concretes, reaching to max. 14-18% (Figure 14).

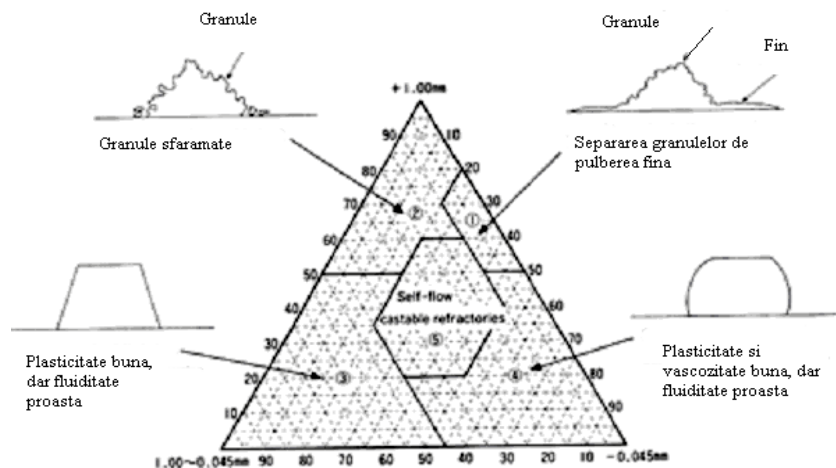


Figure 12. Influence of the dimension of particles on fluidity

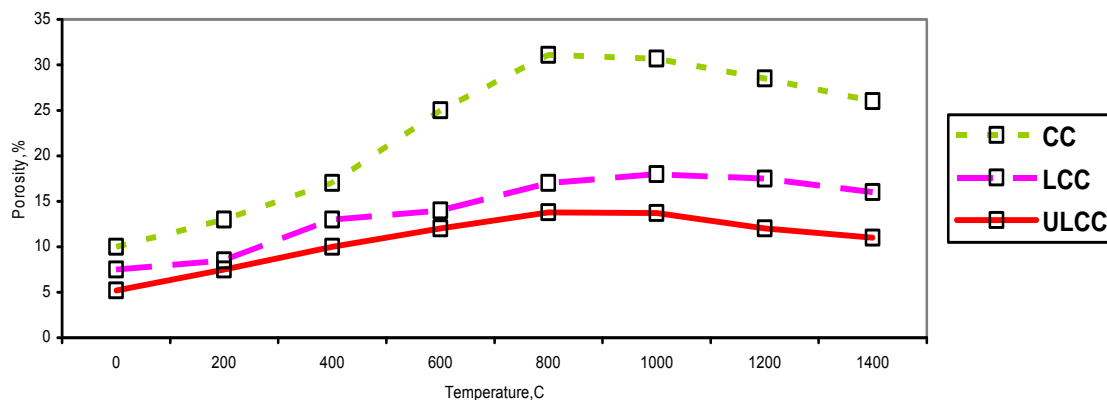


Figure 14. Porosity according to temperature for:

1 – classic concrete, 2 – LCC concrete, 3 – ULCC concrete with tabular alumina aggregate

This is due to the small ratio of hydration water in LCC and ULCC concretes compared to classic concrete, and the preponderance of gellic phase which increases very little the porosity, with the increase of temperature, through the transformations that occur. Thus, LCC concrete has a porosity of 11-14%, which is a far better porosity compared to classical concretes - 25-27%.

The permeability of concretes depends mostly on the size of the pores and less on the total content of pores. In classic concretes, even if after heating the porosity is high until 800°C, the porosity is very low. Over this temperature the permeability increases, due to the increase in crystals, fact that leads to the decrease of internal specific intern surface, and to intern structural changes of dehydrated product of cement.

For temperatures over 1000°C, the permeability of classic concrete reaches the values of other refractory materials. The same thing happens in case of LCC and ULCC concretes, but with smaller values in the area of low temperatures. Over 800°C, the permeability of concretes increases considerably, as at temperatures of 1200-1300°C its value can be compared to a classic concrete.

The low values of permeability to gass of LCC and ULCC concretes, until 800°C lead to the need to carefully choose the heating speed for the vaporization of water, unless special additives are used. Over 800°C the heating speed can be increases without the risk of explosions.

4. EXPANSION – CONTRACTION

During the heating of a classic concrete, especially at first burning, a series of contractions and expansions occur, initially provoked by dehydration and phase changing's of the cement and the expansion – contraction of sinterized cement – aggregate system. Up to 1000°C the expansion of concrete is reversible, the concrete not having yet being made a ceramic connection.

Over 1000°C, and, especially from 1200°C up, due to ceramic conection and sintering of concrete, irreversible changes occur in the dimensions which firstly expand, and when the temperature reaches the refractarity limit of the concrete, or overcomes the temperature of aggregate burning, contract. The contractions occur mainly in chamotte aggregate concretes, when the heating temperature of the concrete reaches and overcomes the burning temperature of the chamotte. The well burned chamotte has, though, small contractions. Unlike the chamotte, the corindonic or tabular alumina aggregates expand continuously almost to the limit of refractarity, when contraction begins.

When cooling, the irreversible expansion or contraction reached at the maximum heating temperature, will contract over or under the initial dimensions, the values ranging between +1,5 and -0,6%. At a new heating, the concrete will reversibly expand to the maximum temperature of the first irreversible heating, which will be the value of maximum expansion for the next heating.

Within LCC and ULCC concretes the contraction determined by the low ratio of cement is compensated by the expansion of ultra-fine powders, making a neutral system for LCC, while for ULCC the trend is towards expansion. Thus, for LCC the variation of dimensions will be given by the expansion-contraction of the aggregate, which, when corindonic or tabular alumina, begins expansion at 1200°C keeping linearly increasing, and when chamotte, will have a reversible expansion, followed, at 1200-1300°C by a contraction (which is partially compensated by the expansion of ultra-fine powders of SiO₂ at the transformation of α-quartz in tridimit around 873°C), reaching, at the maximum temperature of concrete usage (about 1350°C) aproximatively - 0,3%.

Usage of corindonic or tabular alumina aggregates is not justified unless LCC concrete for high temperatures. In this case the concrete will have an almost continuous expansion, until a maximum of +0,8 - -1% .

Unlike the LCC, in ULCC concrete, the tendency to expand occurs regardless of the aggregate we use. When using the chamotte, at a temperature of usage for the ULCC concrete of 1600°C the mulit formed from 1300°C contracts, its contraction giving final expansions of up to +0,4%. For corindonic or tabular alumina aggregates values of expansion of +0,9 ... +1,26% at temperatures of 1600-1700°C occur.

In these conditions, the expansion gaps of LCC concrete clothings must be very carefully dimensioned, taking into consideration the fact that the values presented above are obtained in laboratory where the samples are heated on all their facets. In common practice we must take into consideration values of 70-90% from the theoretical value of expansion. Contraction gaps in the clothings are compulsory, regardless of the concrete or aggregate type.

For LCC concrete with chamotte aggregates these gaps are superficial for low volumes, but for higher values, we need to provide the expansion gaps with dimensions according to the medium reversible expansion factor. This has values ranging from 40·10⁻⁶/°C to 6·10⁻⁶/°C. Even if the concrete contracts under initial dimensions, the contraction occurred after the concrete had expanded.

Similarly, we calculate the expansion gaps for chamotte aggregate ULCC concrete.

Table 4.

Characteristics	Ttype of concrete	Aggregate,%Al ₂ O ₃				
		Chamotte 44-46	Andaluzit 59-61	Chamotte 69-71	Corrindon 91-93	Tabular alumina 98-98,5
Refractoriness	Classic concrete	1460	1500	1670	1820	1850
	LCC concrete	1760	1790	1870	1930	2000
	ULCC concrete	1760	1800	1870	1950	2000
Maximum temperature of use	Classic concrete	1300	1400	1520	1750	1800
	LCC concrete	1550	1560	1600	1800	1900
	ULCC concrete	1600	1650	1650	1800	1900

5. REFRACTORINESS

Using superaluminum cements, the classic refractory concretes will have a variation of refractoriness due not only to the type of aggregate but also to its proportion within the compound.

Both LCC and ULCC concretes, due to their low or very low content of cement and high proportion of aggregate and ultra-fine powders, have higher refractoriness than classic concretes with the same type of aggregate. We need to mention that LCC concrete is refractory just in case of replacing the ultra-fine powders of SiO_2 with Cr_2O_3 or Al_2O_3 . From economic reasons we recommend the use of LCC concrete at temperatures of 1350°C , over this temperature ULCC concrete being the best solution. In table 4 there can be seen the values of refractoriness for different types of concretes.

REFERENCES / BIBLIOGRAPHY

- [1.] Adriana Mioara Comșa, Maria Nicolae, Applications of refractory concretes with low hydraulic binder content, *Metalurgia International*, 8 (2008) 5-7, ISSN 1582 – 2214
- [2.] Adriana Mioara Comșa, Nicolae Avram, Dima Adrian Refractory linings realized from refractory concretes with low hydraulic binder content, *Metalurgia International*, 9 (2008) 9-14, ISSN 1582 – 2214
- [3.] Adriana Mioara Comșa, Buzduga Miron, Constantin Nicolae, Aurica Goleanu, Buzduga Radu, Monolithic refractory for metallurgy, *Metalurgia International*, Special issue nr.3 (2008) 71-72, ISSN 1582 - 2214
- [4.] ISO/DIS 1927-1:2008 Unshaped refractory materials — Part 1:Introduction and classification
- [5.] Drd.ing. Buzduga Miron, Drd.ing. Comșa Adriana , Mase monolitice cu conținut redus de liant hidraulic, *Scientific Bulletin of the Politehnica University of Timișoara*, Tom 52(66), 2007; ISSN 1224-6077
- [6.] Catalog ALCAN 2007
- [7.] Albinas GAILIUS, Dangyras ŽUKAUSKAS Optimisation of the Aggregates Composition in Concrete, ISSN 1392–1320 *Materials Science (MEDŽIAGOTYRA)*. Vol. 12, No. 1. 2006, Lithuania
- [8.] Abilio P. Silva, Ana M. Segadães, Tessaleno C. Devezas Particle Distribution Design in a Self-Flow Alumina Refractory Castable Without Cement *Advances in Science and Technology* Vol. 45 (2006) pp. 2260-2265
- [9.] L Lipan, A Comsa Studiu C 2080 RELANSIN - Tehnologie ecologica de fabricare a betoanelor refractare cu continut redus de liant hidraulic, 2005
- [10.] Myhre, B. Microsilica in Refractory Castables – How Does Microsilica Quality Influence Performance? 9-th Biennial Worldwide Congress on Refractories 2005: pp. 191 – 195.
- [11.] I.Teoreanu, N. Ciontea Tehnologia produselor ceramice si refractare, Vol. II, Editura Tehnica, Bucuresti, 1985, p. 37-49, 125-135.
- [12.] xI. Teoreanu, N. Ciocea, A. Barbulescu, N. Ciontea Tehnologia produselor ceramice si refractare, Vol. I, Editura Tehnica, Bucuresti, 1985, p. 109-117, 121-122
- [13.] N.Deică, Utilizarea rațională a produselor refractare, Editura Tehnică, 1982
- [14.] R. Abramovici Materii prime ceramice, Editura Institutului Politehnic “Traian Vuia”, Timisoara, 1974, p. 369-375.
- [15.] Konopický,K Materiale refractare, Centrul de documentare și publicații tehnice al Industriei Metalurgice, 1970





¹G. E. BADEA, ²P. CRET, ³M. LOLEA, ⁴A. SETEL

STUDIES OF CARBON STEEL CORROSION IN ATMOSPHERIC CONDITIONS

^{1,3}. FACULTY OF ENERGY ENGINEERING, UNIVERSITY OF ORADEA

^{2,4}. CENTER OF TECHNOLOGICAL TRANSFER, UNIVERSITY OF ORADEA

ABSTRACT:

One of the most frequently corrosion type is the atmospheric corrosion. Carbon steel behaviour at atmospheric corrosion is presented on base of the literature data study. This has been reported to account for more failures in terms of cost and tonnage than any other type. About 80% from all degradations produced by corrosion in the metallic constructions are due to the atmospheric corrosion. The atmospheric conditions for corrosion are very complex and the corrosion rates vary in function of geographic zone, of season and daily time. The complexity of the atmosphere, as corrosion environment, results from atmosphere composition and from presence of some factors as pollutants, temperature, humidity, wind speed and direction, etc. These variables make meaningful results from laboratory experiments very difficult to obtain. The object of this work is to outline the principles that govern atmospheric corrosion of the carbon steel – the construction material with the largest application – how is influenced his corrosion rate by the atmospheric variables and that are the corresponding corrosion products

KEYWORDS:

carbon steel, atmospheric corrosion

1. INTRODUCTION

One of the most frequently corrosion type is the atmospheric corrosion. This has been reported to account for more failures in terms of cost and tonnage than any other type. About 80% from all degradations produced by corrosion in the metallic constructions are due to the atmospheric corrosion. The atmospheric conditions for corrosion are very complex and the corrosion rates vary in function of geographic zone, of season and daily time. The complexity of the atmosphere, as corrosion environment, results from atmosphere composition and from presence of some factors as pollutants, temperature, humidity, wind speed and direction, etc. [1]. These variables make meaningful results from laboratory experiments very difficult to obtain.

The atmospheric corrosion is conveniently classified in three [2, 3] types: (1) *dry oxidation*, (2) *damp corrosion* and (3) *wet corrosion*. *Dry oxidation* takes place in the atmosphere with all metals that have a negative free energy of oxide formation. For metals forming non-porous oxides, the films rapidly reach a limiting thickness since ion diffusion through the oxide lattice is extremely slow at ambient temperatures, and at the limiting thickness, the oxide films on metals are invisible. For certain metals and alloys, these films confer remarkable protection on the substrate, e.g. stainless steel, titanium and chromium. *The damp and wet atmospheric corrosion* are characterized by the presence of a thin, invisible film of electrolyte solution on the metal surface (damp type) or by visible deposits of dew, rain, sea-spray etc. (wet type). In these categories may be placed the rusting of iron and steel, 'white rusting' of zinc (wet type) and the formation of patina on copper and its alloys (both types).

The corrosion products may be soluble or insoluble. Usually, those insoluble reduce the corrosion rate by isolating the substrate from the corrosive environment. Less commonly, they may stimulate corrosion by offering little physical protection while retaining moisture in contact with the metal surface for long periods. The soluble products may increase corrosion rates.

The severity of atmospheric corrosion depends on the environment type [4, 5]: *rural, urban, industrial, marine* and *combined*.

The *rural* atmosphere generally the least corrosive and normally does not contains chemical pollutants. The principal corrosive agents are moisture, oxygen and carbon dioxide.

The *urban* atmosphere is similar to the rural type in that there is little industrial activity. Additional contaminants are of the SO_x and NO_x variety, from motor vehicle and domestic fuel emissions.

The *industrial* atmospheres are associated with heavy industrial processing facilities and can contain sulphur dioxide, chlorides, phosphates and nitrate.

The *marine* atmospheres are usually highly corrosive, due to the presence of chlorides, and corrosivity tends to be significantly dependent on wind direction, wind speed and distance from the coast.

The object of this work is to outline the principles that govern atmospheric corrosion of the carbon steel – the construction material with the largest application – how is influenced his corrosion rate by the atmospheric variables and that are the corresponding corrosion products.

2. CORROSION PRINCIPLES OF CARBON STEEL IN ATMOSPHERE

A fundamental requirement for electrochemical corrosion process is the presence of an electrolyte. This film 'invisible' electrolyte tends to form on metallic surfaces under atmospheric exposure conditions after certain critical humidity level is reached. The critical humidity level is not constant and depends on the corroding material, the tendency of corrosion products and surface deposits to adsorb moisture, and the presence of atmospheric pollutants. For iron, the relative critical humidity is 60% in atmosphere free of sulphur dioxide.

In absence of the pollutants, in an atmosphere with relative humidity of least 70%, the carbon steel corrodes with formatting in time of Fe(OH)₂, after the electrochemical mechanism [6], conform to the reactions:

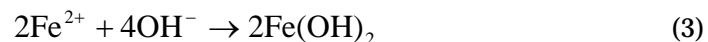
Anodic reaction:



Cathodic reaction:



The products of these reactions combine forming ferrous hydroxide – a compound insoluble at neutral pH – that deposits on the metal surface:



In presence of the oxygen, the ferrous hydroxide oxidizes and forms the rust.

If oxygen from the atmosphere diffuses through the electrolyte film to the metal surface, a diffusion-limiting current density should apply. It has been shown that a diffusion transport mechanism for oxygen is applicable only to an electrolyte-layer of approximately of 30 μm and under strictly isothermal conditions [3]. The predicted theoretical limiting current density of oxygen reduction in an electrolyte-layer of 30 μm significantly exceeds the practical observations on atmospheric corrosion rates. Therefore, the overall rates of the atmospheric corrosion are likely to be controlled not by the cathodic oxygen reduction process, but rather by the anodic reaction(s).

In the presence of gaseous air pollutants, other reduction reactions, involving ozone, sulphur dioxide and nitrogen species have to be considered [7]. It be noted that corrosive contaminant concentrations can reach relatively high values in the thin electrolyte films, especially under conditions of alternate wetting and drying.

2. THE ROLE OF THE IMPORTANT VARIABLES IN ATMOSPHERIC CORROSION OF CRBON STEEL.

Humidity. From the above theory, it should be apparent that presence of electrolyte on the corroding surface (time of wetness) is a key parameter, directly determining the duration of the electrochemical corrosion process. This variable is a complex one, since all the means of formation and evaporation of an electrolyte solution on a metal surface must be considered.

The time of wetness is strongly dependent on the critical relative humidity. The relative humidity of the air varies in large limits, in function of geographic zone, of season and daily time.

Apart from the primary humidity, associated with clean surfaces, secondary and tertiary critical humidity levels may be created by hygroscopic corrosion products and capillary condensation of moisture in corrosion products, respectively. A capillary condensation mechanism may also account for electrolyte formation in microscopic surface cracks and the metal surface-dust

particle interface. Other sources of surface electrolyte include chemical condensation (by chloride, sulphates and carbonates), adsorbed molecular water layers, and direct moisture precipitation (ocean spray, dew, rain).

Temperature. The effect of temperature on the atmospheric corrosion rates is quite complex. An increase in temperature will tend to stimulate corrosive attack by increasing the rate of electrochemical reactions and diffusion processes. For a constant humidity level, the increase in temperature would lead to a higher corrosion rate. However, raising the temperature will, generally, lead to a decrease in relative humidity and more rapid evaporation of the surface electrolyte. When the time of wetness is reduced in this manner, the overall corrosion rate tends to diminish.

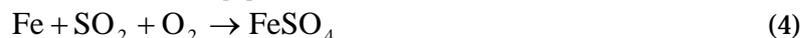
For closed air spaces, it has been pointed out that the increase in relative humidity associated with a drop in temperature has an overriding effect on corrosion rate [8]. This implies that simple air conditioning that decreases the temperature without additional dehumidification will accelerate atmospheric corrosion damage. An important factor in corrosion favouring is the continue oscillations of temperature.

For atmospheric corrosion of metals, the extreme temperatures do not an important role.

Atmospheric contaminants. The electrolyte film that forms on metallic surface contains various compounds resulted from the atmospheric pollutants. Karlson *et al* [9] observed a severe corrosion of steel if in atmosphere there are sulphur dioxide (SO₂) or alkaline chlorides (in principal NaCl).

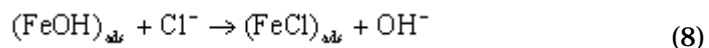
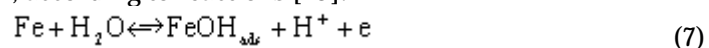
Sulphur dioxide. SO₂, a product of combustion of fossil fuels containing sulphur, play an important role in atmospheric corrosion in urban and industrial atmospheres. For all metals, SO₂ appears to be selectively adsorbed from the atmosphere, less so for aluminium than for other metals, and for rusty steel it is almost quantitatively adsorbed even from dry air at 0°C [2]. Under humid conditions sulphuric acid is formed, the oxidation of SO₂ to SO₃ being catalysed by metals and by metallic oxides.

For non-ferrous metals, SO₂ is consumed in the corrosion reaction whereas in the rusting of iron and steel it is considered [2] that ferrous sulphate is hydrolysed to form oxides and thus the sulphuric acid is regenerated. Sulphur dioxide thus acts as catalyst such that one SO₄²⁻ ion can catalyse the dissolution of more 100 atoms of iron [2]. The reactions can be summarized as follows:



The high solubility of SO₂ (of 1300 times more soluble than O₂ in water) [2] would make it a more effective cathodic reactant than dissolved oxygen even though its concentration in the atmosphere is comparatively small.

Chlorides. The corrosion rates of the carbon steel increase in marine atmosphere due to its salinity [3]. Apart from enhanced surface electrolyte formation by hygroscopic salts such as NaCl and MgCl₂, direct participation of chloride ions in the electrochemical corrosion reactions is also likely. In case of the ferrous metals, chloride anions are known to compete with hydroxyl ions, to combine with ferrous cations produced in the anodic reaction. In the case of hydroxyl ions, stable passivating species tend to be produced. In contrast, iron chloride complexes are soluble, resulting in further stimulation of corrosive attack, according to reactions [10]:



Other atmospheric contaminants, related to industrial emissions in specific microclimates are: hydrogen sulphide, hydrogen chloride, and chlorine that can intensify atmospheric corrosion damage. Hydrogen sulphide is known to be extremely corrosive producing Hydrogen Embrittlement Corrosion of alloys [11]. The corrosive effects of gaseous chlorine and hydrogen chloride in presence of moisture tend to be stronger than those of chloride salts anions because of the acidic character of the former species.

The deposition of solid matter from atmosphere can have a significant effect on atmospheric corrosion rates, particularly in the initial stages. Such deposits can stimulate the atmospheric attack by three mechanisms: (1) reduction in the critical humidity levels by hygroscopic action; (2) the provision of anions, stimulating metal dissolution and (3) microgalvanic effects by deposits more

noble than the corroding metal (carbonaceous deposits deserve special mention in this context) and by different aeration, so it shows in Fig. 1.

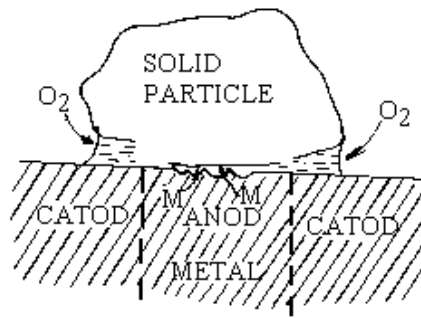


Figure 1 – Corrosion in centre of a surface covered by a solid particle

4. THE CORROSION PRODUCTS FORMED ON CARBON STEEL IN ATMOSPHERIC CORROSION

In presence of oxygen the ferrous hydroxide (reaction 3) oxidizes forming the rust. The iron corrosion products, the rust, have complex composition.

Hiller [12] given a scheme (figure 2) that shows the principal crystalline components of the rust and possible way of their formatting.

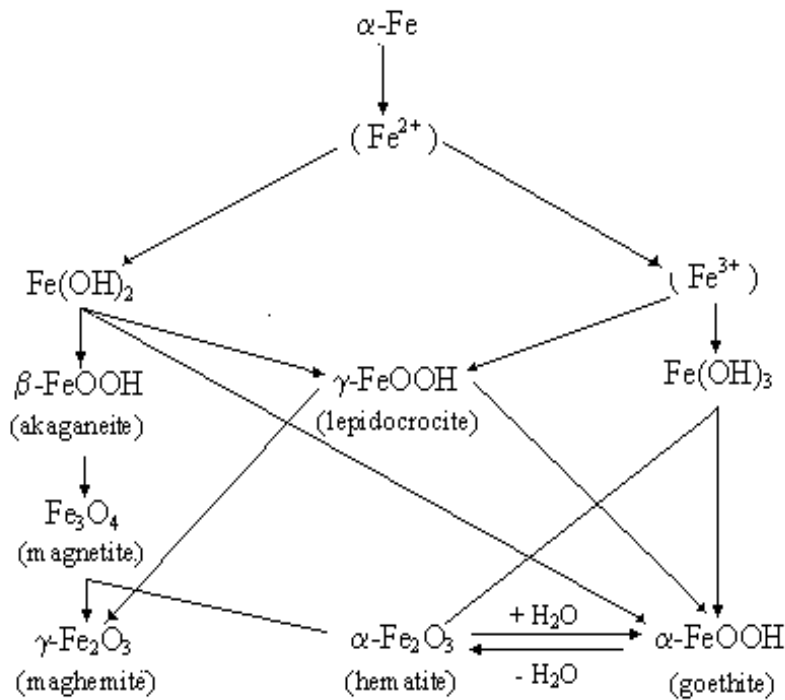
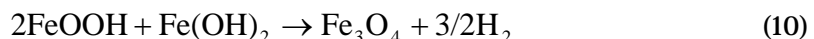


Figure 2 – Hiller scheme for the iron rust compounds [12]

In the first phase of the steel rusting forms $\text{Fe}(\text{OH})_2$, which it oxidizes suddenly forming *lepidocrocite* ($\gamma\text{-FeOOH}$), a crystalline phase with rhombic structure. In function of water presence or absence, this isomerises in *goethite* ($\alpha\text{-FeOOH}$), with rhombic structure also. If the corrosion rate is low, a part of lepidocrocite it transforms in *maghemite* ($\gamma\text{-Fe}_2\text{O}_3$), having a cubic structure.

Akaganeite ($\beta\text{-FeOOH}$), with tetragonal structure, it forms in the environments with high chlorides content. After Keller [13] akaganeite is the most unstable oxihydrate formed at corrosion steel. In humidity conditions this it transforms in *magnetite* (Fe_3O_4), having cubic structure. After Hiller [12] magnetite it forms only in direct contact with metal surface and in presence of a high humidity. This compound does not appear in the incipient phases of rusting; it is a product that forms in time from akaganeite, conform to the reaction:

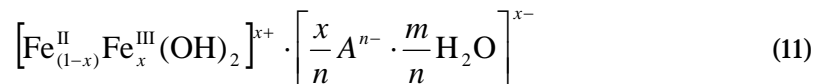


Another oxihydroxide of iron, *crystallite* (δ -FeOOH), having a hexagonal structure, it forms especially in the atmosphere with low humidity [14]. This can find and in the amorphous state – *ferroxite*.

After K.A. van Oecleron [15] the most important compounds of the rust are oxihydroxides of iron and magnetite.

In presence of the pollutants and in the incipient stages of the carbon steel corrosion, sometimes, forms on metal surface the, so called 'green rust' [16-20].

Green rust is a mixture of hydroxide-salts of Fe(II, III) with formulae:



This has a structure in which the iron hydroxide layers with positive charge alternate with negative charged anion layers and with water molecules, leading to a hexagonal symmetry. The green rust is classified [21] in two types:

- ❖ green rust I, in which A^{n-} are anions with planar structure, as Cl^- ;
- ❖ green rust II, in which A^{n-} are anions with three-dimensional structure, as, sulphate, carbonate, etc.

The change in corrosion rate with time varies markedly for different metals due to the differing degrees of protection conferred by the corrosion products. The behaviour of steel is conditioned by the alloying elements present for any given environment. Thus the decrease in corrosion rate with time for carbon steel is very much slower than for low-alloy steel. This can attributed to the much more compact nature of the rust formed on the latter type.

5. CONCLUSIONS

The atmospheric corrosion, the most frequently corrosion type of the carbon steel takes place in presence of the humidity surface layer after the electrochemical corrosion mechanism. The principal parameters that determine the corrosion rate are: humidity temperature and presence of pollutants as sulphur dioxide and chloride ions. The carbon steel corrosion products – the rust – have a complex composition, being formatted of various iron oxides and oxihydroxides types.

REFERENCES

- [1.] X. Naixin, L. Zao, C. Ding, C. Zhang, R.Li and Q. Zhong, *Corrosion Science*, 2002, 44
- [2.] L.L. Shreir, R.A. Jarman and G.T. Burstein (eds), *Corrosion*. Vol. 1: Metal/Environment reactions, Third Edition, Butterworth Heinemann, Oxford, 1994, Reprinted 2000, p. 2.2
- [3.] P.R.Roberge, *Handbooh of Corrosion Engineering*, McGraw-Hill, USA, 1999, p. 58-69.
- [4.] S. Szed, *Emirates Journal for Engineering Research*, 2006, 11 (1), 1-24.
- [5.] J.R. Vilche, F.E. Varela, G. Acuna, E.N. Codaro, B.M. Rosales, A. Fernandez, G. Moreina, *Corrosion Science*, 1995, 37 (7), 941-961.
- [6.] T. Badea, M. Popa, M. Nicola, *Coroziunea și ingineria coroziiunii*, Ed. Academiei Române, 2002, București, p. 101
- [7.] S. Oesch and M. Faller, *Corrosion Science*, 1997, 39 (9), 1505-1530.
- [8.] S. Sharp, *Materials Performance*, 1990, 29 (12), 43-48.
- [9.] A. Karlsson, P.J. Moller and J. Vagn, *Corrosion Science*, 1990, 30 (2, 3), 153-158.
- [10.] N.G. Smart, M. Gamboa, J. O'M. Bockris, J. Aldeco, *Corrosion. Science*, 1993, 34, 759.
- [11.] G.E.Badea, P.Cret, T.Badea, *Proceedings of the 7th International Conference URB-CORR: Study and Control of Corrosion in the Perspective of Sustainable Development of Urban Distribution Grids*, June 25-27, 2008, Baile Felix, Romania, PRINTECH Printhouse Bucharest, 2008, 266-271.
- [12.] J. Hiller, *Werkstoffe und Korrosion*, 1966, 11, p.943-995.
- [13.] P. Keller, idem, 1969, 11, p. 943-950
- [14.] A.M.G. Pacheco, M. Teixeira, M. Ferreira, *British Corrosion Journal*, 1990, 25 (1), 19-25.
- [15.] K.A. van Oecleron, *Korrosionsschutz durch Beschichtungsstoffe*, Carl Hauser Verlag, Munchen, Wien, 1980, Band I, Band II, p. 35-54.
- [16.] Ph. Refait, O. Benali, M. Abdelmoula, J. M. R. Genin, *Corrosion Science*, 2003, 45 (8), p. 2435-2449.
- [17.] L. Legrand, G. Sagon, S. Lecompte, A. Choausse, R. Messina, *Corr. Sci.*, 2001, 43 (9), 1739-1749.
- [18.] Ph. Refait, J.B. Memet, C. Bon, R. Sabot, J.M.R. Genin, *Corr. Sci.*, 2003, 45 (4), 833-845.

- [19.] A. Gehin, C. Ruby, M. Abdelmoula, O. Benali at. Al. Solode State Science, 2002, 4, 61-66.
[20.] C. Ruby, A. Gehin, M. Abdelmoula, J.M.R. Genin, J.P. Jolivet, Solide State Science, 2003, 5, 1055-1062.
[21.] S.H. Drissi, Ph. Refait, M. Abdelmoula, J. M. R. Genin, Corrosion Science, 1995, 37 (12), 2025-2041.

